AD_____
(Leave blank)

Award Number:
W81XWH-06-1-0329

TITLE:
Detection and Evaluation of Early Breast Cancer via Magnetic Resonance Imaging: Studies of Mouse Models and Clinical Implementation

PRINCIPAL INVESTIGATOR:
Sanaz A. Jansen

CONTRACTING ORGANIZATION:
University of Chicago
Chicago, IL 60637

REPORT DATE:
March 2009

TYPE OF REPORT:
Annual Summary

PREPARED FOR: U.S. Army Medical Research and Materiel Command
Fort Detrick, Maryland 21702-5012

DISTRIBUTION STATEMENT: (Check one)

× Approved for public release; distribution unlimited

□ Distribution limited to U.S. Government agencies only; report contains proprietary information

REPORT DOCUMENTATION PAGE

Form Approved
OMB No. 0704-0188

1. REPORT DATE *(DD-MM-YYYY)*	**2. REPORT TYPE**	**3. DATES COVERED** *(From - To)*
05-03-2009	Annual Summary	6 Feb 2006 –5 Feb 2009

4. TITLE AND SUBTITLE
Detection and Evaluation of Early Breast Cancer via Magnetic Resonance Imaging: Studies of mouse models and clinical implementation.

5a. CONTRACT NUMBER
W81XWH-06-1-0329

5b. GRANT NUMBER
BC050329

5c. PROGRAM ELEMENT NUMBER

6. AUTHOR(S)

Sanaz A. Jansen

5d. PROJECT NUMBER

5e. TASK NUMBER

5f. WORK UNIT NUMBER

7. PERFORMING ORGANIZATION NAME(S) AND ADDRESS(ES)

University of Chicago
970 E. 58th Street
Chicago, IL 60637

8. PERFORMING ORGANIZATION REPORT

9. SPONSORING / MONITORING AGENCY NAME(S) AND ADDRESS(ES)
U.S. Army Medical Research and Materiel
Fort Detrick, Maryland 21702-5012

10. SPONSOR/MONITOR'S ACRONYM(S)

11. SPONSOR/MONITOR'S REPORT NUMBER(S)

12. DISTRIBUTION / AVAILABILITY STATEMENT
Approved for public release; distribution unlimited

13. SUPPLEMENTARY NOTES

14. ABSTRACT The early detection of breast cancer is a major prognostic factor in the management of the disease. In particular, detecting breast cancer in its pre-invasive form as ductal carcinoma *in situ* (DCIS) improves prognosis greatly compared with invasive tumors. Although dynamic contrast enhanced MR imaging (DCEMRI) of the breast has demonstrated high sensitivity to invasive breast cancer, there is room for improving the diagnostic accuracy of DCEMRI to DCIS. However, a competing clinical concern is that DCIS is being overdiagnosed and overtreated, as there is evidence to suggest that not all DCIS lesions will progress into invasive cancers. Ideally, improvements in the detection of DCIS would be accompanied by an improved understanding of its natural history—which lesions will progress to invasive cancer, and which will not? The goals of this proposal are to improve sensitivity and specificity of DCEMRI to DCIS by comparing its kinetic and morphologic features with other types of breast lesions, and to use mouse models to probe the progression of DCIS into invasive cancer. Specifically, we have (i) characterized the MR kinetic and morphologic findings of DCIS in women and compared with benign lesions and other malignant cancers, (ii) developed techniques to detect early mammary cancer in mice, and (iii) studied the development and progression of early mammary cancer in mice by performing longitudinal MRI studies of development of DCIS and transition to invasive cancer.
We have developed a novel approach to investigating the natural history of breast cancer by using high resolution MR imaging to image early murine mammary cancer and study the transition from *in situ* to invasive disease *in vivo*.

15. SUBJECT TERMS key words or phrases
early detection, MRI, mouse models, DCIS

16. SECURITY CLASSIFICATION OF:			**17. LIMITATION OF ABSTRACT**	**18. NUMBER**	**19a. NAME OF RESPONSIBLE PERSON**
a. REPORT	**b. ABSTRACT**	**c. THIS PAGE**			**19b. TELEPHONE NUMBER** *(include area code)*
U	U	U	UU	199	

Standard Form 298 (Rev. 8-98)
Prescribed by ANSI Std. Z39.18

Table of Contents

INTRODUCTION

The early detection of breast cancer is a major prognostic factor in the management of the disease. In particular, detecting breast cancer in its pre-invasive form as ductal carcinoma *in situ* (DCIS) improves prognosis greatly compared with invasive tumors. Although dynamic contrast enhanced MR imaging (DCEMRI) of the breast has demonstrated high sensitivity to invasive breast cancer, there is room for improving the diagnostic accuracy of DCEMRI to DCIS. However, a competing clinical concern is that DCIS is being overdiagnosed and overtreated, as there is evidence to suggest that not all DCIS lesions will progress into invasive cancers. Ideally, improvements in the detection early breast cancer would be accompanied by an improved understanding of its natural history, so that as cancers are detected at earlier stages, those that are aggressive and life-threatening can be distinguished from those that are more indolent.

The goals of this project are to improve sensitivity and specificity of DCEMRI to DCIS by comparing its kinetic and morphologic features with other types of breast lesions, and to use mouse models to probe the progression of DCIS into invasive cancer. The specific aims are to: (1) characterize the MR kinetic and morphologic findings of DCIS in women and compare with benign lesions and other malignant cancers, (2) develop techniques to detect early mammary cancer in mice, and (3) study the development and progression of early mammary cancer in mice by performing longitudinal MRI studies of development of DCIS and transition to invasive cancer.

BODY

During the third year of funding of this award, we have continued to work on accomplishing many of the aims of the approved Statement of Work.

Task 1. To evaluate the development of ductal carcinoma *in situ* (DCIS) in mammary glands of a transgenic mouse model via MRI.

a. *Develop in vivo high resolution imaging of mouse mammary glands.*
b. *Perform detailed correlation of MRI with histology to improve understanding of features on MR images.*
c. *Perform serial MRI studies to follow mice while DCIS develops and continue to follow the transition to invasive cancer.*

Task 1a and 1b: We have previously reported that we had developed techniques to image early cancer, including DCIS, in the SV40 Tag transgenic mouse model of breast cancer and had performed a sensitivity and specificity study by making correlations of images with histology. We had performed quantitative analysis of image properties, such as signal-to-noise ratio and contrast-to-noise ratio. We had also assessed murine lesion morphology and found that there were many similarities between human and murine cancers: DCIS lesions presented as nonmass lesions in a ductal shape, while early invasive tumors appeared as round masses. This work was published in October 2008 (see page 32 in the Appendix).

Task 1c: Last year, we had reported some preliminary analysis of a serial imaging study we performed following the progression of DCIS into invasive cancer in 12 SV40 Tag mice. During this past year, we have refined and extended this analysis and have recently submitted a manuscript for publication of this work (please see page 127 for manuscript in Appendix). We were surprised to find that even in these mice that are genetically predisposed to develop invasive carcinoma, DCIS lesions took vastly different progression paths (please see page 162 for Figure in Appendix): (i) 9 lesions progressed to invasive tumors with an average progression time of 4.6 ± 1.9 weeks (ii) 2 lesions regressed, i.e., these lesion were not detected on future images, and (iii) 5 were stable for over 8 weeks, and were identified by a statistical model to represent indolent disease. We investigated whether certain lesions features were predictive of progression, i.e., could distinguish progressing from indolent DCIS. In this small study, we did not find strong evidence for predictive markers. Interestingly, a larger lesion size was not predictive of future invasive transformation, but there was a trend for growth rate to be related to eventual progression (please see page 158 for Table in Appendix).

Task 2. To perform quantitative and qualitative analysis of clinical breast dynamic contrast enhanced magnetic resonance images (DCEMRI).

a. *Maintain research database.*
b. *Quantitative assessment and mathematical modeling of enhancement patterns in lesions of many pathology subtypes.*
c. *Quantitative assessment of parenchymal enhancement patterns in the normal breast.*
d. *Use recently developed imaging methods and develop novel imaging acquisitions.*

Task 2a: We have continued to maintain the research database. It now contains approximately 4500 records, with ~ 1200 histologically proven malignant lesions, ~350 histologically proven benign lesions and over 2000 normal MR exams. We have also spent time this year to integrate this database with another breast cancer database maintained at the University of Chicago developed for the SPORE project. The existing SPORE database collects detailed information on lesion pathology (such as TNM stage, margin status, type of surgery performed), molecular markers (ER, PR, Her2/Neu) and genotyping on over 7000 women. By integrating our imaging findings with this database, we have created a unique research resource for all approved users at the University of Chicago. We are currently performing a study on the imaging characteristics of node positive and node negative T1 (<2cm) breast cancers.

Task 2b: We have also continued to perform quantitative analysis of the contrast enhancement kinetics in several groups of lesions. Lesions are characterized on DCEMRI by both their morphology and contrast media uptake and washout—or kinetic—curves. Kinetic curves have been related to physiological and biological lesion characteristics such as microvessel density, nuclear grade and proliferation indices. Last year we reported on some work we performed comparing kinetic parameters of enhancement in mass vs. nonmass lesions. During this past year our pilot study has been published (please see page 24 for manuscript in Appendix) and we have submitted for publication our semi-quantitative analysis of kinetics in a larger database of lesions (please see page 101 for manuscript in Appendix).

This year we have explored two issues related to standardization of breast DCEMRI examinations. Because quantitative analysis of enhancement patterns of breast lesions is a central theme of this proposal, we began to realize that several key components of breast DCEMRI are not standardized across imaging platforms and institutions. This may compromise the reliability of quantitative kinetic analysis, such as has been performed to date for this proposal. Unlike x-ray mammography, standardization of breast DCEMRI to ensure comparable enhancement patterns in lesions is not widespread at this time. For example, there are no universally applied quality assurance procedures to ensure that as newer technology and systems are implemented that malignant lesions continue to enhance similarly. This was the impetus for our first study, where we compared quantitative kinetic characteristics of 657 breast lesions acquired on three different MR systems. We found that in one system, malignant lesions exhibited considerably lower signal enhancement and a different overall curve shape. We believe this discrepancy may be due to technical issues such as k-space sampling methods or fat suppression techniques. Regardless, this study points to the importance of developing improved standardization procedures for breast DCEMRI acquisitions so that all women undergoing breast MR examinations can be evaluated similarly. This study is now in press (please see page 45 for manuscript in the Appendix).

Our second study was motivated by the fact that despite many years of breast DCEMRI clinical investigations, the appropriate dose of contrast media injected has not been firmly established. In fact, contrast media continues to be employed "off-label" as the FDA has not currently approved any contrast agent for breast MR imaging. We quantified the relationship between dose of contrast administered and contrast kinetics in malignant lesions. Our results suggest that reducing the dose of contrast administered to 0.05 mmol/kg (as has been suggested for patients at risk for developing nephrogenic systemic fibrosis) could compromise the reliable detection of DCIS. We have recently submitted this study for publication (please see page 163 for manuscript in Appendix).

Task 2c: In prior annual summaries, we have reported on the characteristics of normal parenchymal enhancement on DCEMRI of the breast in approximately 200 women (please see page 193 for abstract in Appendix). We are currently in the process of expanding this study to include close to 1000 patients with normal MR images. During this past year, we have also begun to study the imaging characteristics of normal mammary glandular tissue in mice. We found that as in women, normal murine mammary tissue can exhibit contrast uptake, with a 'persistent' curve shape:

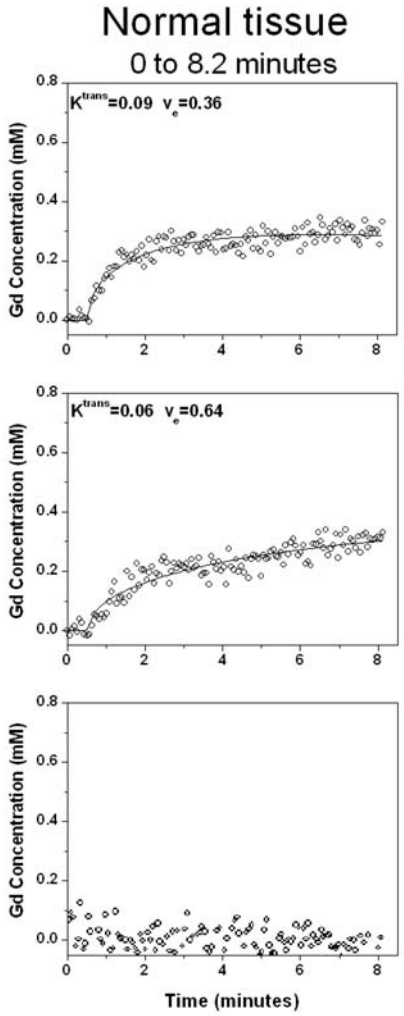

In addition, we have found that normal tissue may exhibit short T2* components, and thus imaging at shorter TE could help improve the visualization of normal tissue in women (please see page 184 for abstract in Appendix).

Task 2d. Our clinical research is geared towards improving the detection of DCIS by DCEMRI. Lesions on DCEMRI are characterized by their morphology and kinetic patterns of enhancement. In our past reports, we have demonstrated that DCIS lesions present typically as nonmass-like enhancement, with a variable kinetic pattern. We have found that kinetic analysis is not very effective for lesions exhibiting nonmass-like enhancement, as is typical for DCIS. This suggests that newer acquisition and analysis techniques need to be developed to reliably identify *in situ* cancers.

During the past year, we have use MR imaging of DCIS in mice to gain insights into potential novel approaches that could be used in women. We have performed detailed measurement of the distribution of gadolinium in murine DCIS, finding that gadolinium penetrates inside ducts distended with DCIS and collects within the duct lumen. This work reveals a new aspect of the physiological basis of contrast uptake of DCIS, and can be used to improve mathematical modeling of contrast kinetics in these lesions and design improved acquisitions. The manuscript for this study was recently submitted for publication and is currently under revisions (please see page 73 for manuscript in Appendix).

In more recent work, we have performed MR relaxometry of early murine mammary cancer. Specifically, we have measured the T1, T2 and T2* of DCIS and early invasive cancers in mice. We found that murine DCIS exhibits short T2* (please see page 184 for manuscript in Appendix). This suggests that imaging at shorter TE improved conspicuity of murine DCIS on clinical MR images.

KEY RESEARCH ACCOMPLISHMENTS: Feb 2008-Feb 2009

- *Progression of murine DCIS:* We have performed a longitudinal imaging experiment tracking the development and progression of murine DCIS in transgenic mice. To our knowledge, this the first time the progression of murine DCIS has been measured *in vivo* and direct evidence that DCIS may be a nonobligate precursor has been obtained (please see page 127 for manuscript in Appendix).
- *Physiological basis of contrast uptake of murine DCIS.* We have used mouse models to provide a new insight into the mechanism of contrast enhancement in DCIS: that Gd enters mouse mammary ducts distended with DCIS and accumulates within the duct lumen (please see pages 73 for manuscript in Appendix).
- *Research database*: We have also continued to maintain the research database, which now contains over 3400 records with ~900 malignant lesions and ~300 benign lesions. We have also integrated this database with a larger breast cancer database, so that

imaging findings can be integrated with detailed pathologic, molecular and genetic information.

- *Standardization of Breast MRI:* We have quantified the relationship between dose of contrast administered and contrast kinetics in malignant lesions. Our results point to the importance of developing a standard dose for contrast enhanced breast MR imaging (please see page 45 for manuscript inn Appendix). In another study, we found that the kinetic curves of malignant lesions did not present consistently across MR systems. This underscores the importance of developing improved standardization procedures to ensure that all women receiving breast DCEMRI are imaged adequately (please see page 163 for manuscript in Appendix).

REPORTABLE OUTCOMES: Feb 2008-Feb 2009

Manuscripts: Full versions can be found in the Appendix

1. Sanaz A. Jansen, Xiaobing Fan, Gregory S. Karczmar, Hiroyuki Abe, Robert A. Schmidt, and Gillian M. Newstead. ”Differentiation between benign and malignant breast lesions detected by bilateral dynamic contrast enhanced MRI: A sensitivity and specificity study.” Magnetic Resonance in Medicine. 2008 Apr; 59(4):747-54.
2. Sanaz A. Jansen, Xiaobing Fan, Gregory S. Karczmar, Hiroyuki Abe, Robert A. Schmidt, Maryellen Giger and Gillian M. Newstead.”DCEMRI of breast lesions: Is kinetic analysis equally effective for both mass and non-mass-like enhancement?” Medical Physics. 2008 July;35(7):3102-3109.
3. Sanaz A. Jansen, Suzanne Conzen, Xiaobing Fan, Thomas Krausz, Marta Zamora, Sean Foxley, Jonathan River, Gillian Newstead and Gregory Karczmar. ”Detection of in situ mammary cancer in a transgenic mouse model:in vitro and in vivo MRI studies demonstrate histopathologic correlation.” Physics in Medicine and Biology. 2008 Oct 7; 53(19): 5481-93.
4. Sanaz A. Jansen, Akiko Shimacuhi, Lindsay Zak, Xiaobing Fan, Abbie M. Wood, Gregory Karczmar and Gillian M Newstead. ”Kinetic curves of malignant lesions are not consistent across MR systems: The need for improved standardization of DCEMRI acquisitions of the breast” (in press, American Journal of Roentgenology)

Abstracts and Presentation: Full versions of these abstracts can be found in the Appendix.

1. Sanaz A. Jansen, Xiaobing Fan, Erica Markiewicz, Gillian Newstead and Gregory S. Karczmar. ”Short T2* components in the normal murine mammary gland and pre-invasive carcinoma may aid in detection of early breast cancer.” in 17th Annual Meeting of the Society for Magnetic Resonance in Medicine, April 2009.

2. Sanaz A. Jansen, Suzanne D. Conzen, Xiaobing Fan, Erica Markiewicz, Gillian Newstead and Gregory S. Karczmar. ”Magnetic resonance imaging reveals the progression, regression and indolence of in situ carcinoma in transgenic mice.” in 17th Annual Meeting of the Society for Magnetic Resonance in Medicine, April 2009.
3. Sanaz A. Jansen, Akiko Shimauchi, Lindsay Zak, Xiaobing Fan, Abbie M. Wood, Gregory S. Karczmar and Gillian M. Newstead. ”Kinetic curves of malignant lesions are not consistent across MR systems: The need for improved standardization of breast DCEMRI acquisitions.” in 17th Annual Meeting of the Society for Magnetic Resonance in Medicine, April 2009.
4. Sanaz A. Jansen, Akiko Shimauchi, Lindsay Zak, Xiaobing Fan, Gregory S. Karczmar and Gillian M. Newstead. ”Different MR systems yield variable kinetic characteristics of breast lesions.” in 31st Annual San Antonio Breast Cancer Symposium, December 2008.
5. Sanaz A. Jansen, Suzanne Conzen, Xiaobing Fan, Gillian M. Newstead, Erica J Markiewicz and Gregory S. Karczmar. ”In vivo magnetic resonance imaging of the progression of murine ductal carcinoma in situ: finding timescales and predictors of future invasion.” in 31st Annual San Antonio Breast Cancer Symposium, December 2008.
6. Sanaz A. Jansen, Tatjana Paunesku, Xiaobing Fan, Gayle Woloschak, Stefan Vogt, Erica J Markiewicz, Suzanne Conzen, Gillian M. Newstead and Gregory S. Karczmar. ”Why does Ductal Carcinoma in situ Enhance on Dynamic Contrast Enhanced MR Imaging of the Breast?” in 94th Annual Meeting of the Radiologic Society of North America, November 2008.
7. Sanaz A. Jansen, Tatjana Paunesku, Xiaobing Fan, Gayle Woloschak, Stefan Vogt, Erica J Marikiewicz, Suzanne Conzen, Gillian M. Newstead and Gregory S. Karczmar. ”Tracking the distribution of gadolinium in early murine breast cancer with x-ray fluorescence microscopy and dynamic contrast enhanced MRI” in Frontiers of Molecular Imaging, Meeting of the Chicago Biomedical Consortium, October 2008.
8. Sanaz A. Jansen. ”Detection and Evaluation of Early Breast Cancer via Magnetic Resonance Imaging: Studies of Mouse Models and Clinical Implementation.” in DOD BCRP Era of Hope Meeting, June 2008.

Informatics: The database (Task 2a) currently contains approximately 4500 records, including ~1200 histologically proven malignant lesions, ~350 histologically proven benign lesions and over 2000 normal MR exams. For each lesion, the MR kinetic and morphologic data acquired is recorded. Then, the subsequent final pathology of the lesion, if available, is also noted. This database is a useful resource that has been used by several collaborators in the departments of Radiology, Hematology/Oncology and Radiation Oncology. In addition, Philips Medical Systems and other outside users license use of the database for testing of CAD algorithms, as well as other product development. In the Fall of 2008 we integrated the breast MRI database with another breast cancer database at the University of Chicago set up as a SPORE funded project that collects pathologic, molecular and genetic information. This integrated database allows for correlation of imaging and molecular findings of lesions, and is a unique resource available to all approved investigators at our institution.

Funding Applied for based on work supported by this award:

1. We are currently in the process of modifying an RO1.
2. DOD Idea award in April 2009.

CONCLUSIONS

In our third year of funding we have performed thorough analysis of 1) a serial imaging experiment of the development and progression of DCIS, 2) the distribution of gadolinium in murine DCIS, and 3) continued to perform detailed quantitative and qualitative analysis of the MR features of malignant and benign lesions. The overall goal of this project is to improve the understanding and detection of early cancer via MRI. On the clinical side, we have continued to use our large database of lesions to compile a rich source of data regarding the enhancement patterns in many groups of patients, lesion subtypes and different MR systems. On the animal side, we have performed the first experiments tracking the development and progression of murine DCIS. To link these two sides together, we have used insights from MR imaging of murine DCIS towards improving clinical detection of DCIS in women.

So what? There are a number of potential implications of this work:

- *Progression of DCIS*: To our knowledge, ours is the first report using MR imaging to probe the development and progression of early murine mammary cancer. This represents the first steps towards probing *in vivo* the characteristics and mechanisms of cancer initiation and progression. We have evaluated potential radiologic markers that could identify aggressive DCIS. This work lays the foundation for future longitudinal studies evaluating the efficacy of therapies at delaying progression of DCIS. In addition, this study and extensions thereof provide detailed empirical measurements of tumorigenesis upon which theoretical models can be developed and evaluated.
- *Improving detection of DCIS*: We used x-ray fluorescence microscopy to demonstrate that MR contrast (Gd-DTPA) was present in mouse mammary ducts distended with DCIS. This new insight can improve mathematical models used to analyze contrast uptake and washout in DCIS, towards ultimately improving its reliable detection. We have also performed preliminary studies suggesting that imaging with shorter echo times could increase conspicuity of DCIS.
- *Standardization of breast MRI:* We found that malignant lesions imaged on different MR systems did not exhibit comparable enhancement characteristics. This study underscores the importance of developing standardization procedures to ensure all women obtaining breast DCEMRI are imaged adequately. Such standardization will be critical if breast DCEMRI is to be used widely. We also studied the relationship between dose of contrast

administered and contrast kinetics, with results suggesting that further study is needed to ascertain a standardized dose of Gd-DTPA for breast imaging. Such studies will be important if contrast administration for breast imaging is to become FDA approved.

REFERENCES: The references are included in each manuscript (see Appendix).

APPENDIX

Manuscripts

Abstracts and Presentations

Differentiation between Benign and Malignant Breast Lesions Detected by Bilateral Dynamic Contrast-Enhanced MRI: A Sensitivity and Specificity Study

Sanaz A. Jansen, Xiaobing Fan, Gregory S. Karczmar, Hiroyuki Abe, Robert A. Schmidt, and Gillian M. Newstead*

The purpose of this study was to apply an empirical mathematical model (EMM) to kinetic data acquired under a clinical protocol to determine if the sensitivity and specificity can be improved compared with qualitative BI-RADS descriptors of kinetics. 3D DCE-MRI data from 100 patients with 34 benign and 79 malignant lesions were selected for review under an Institutional Review Board (IRB)-approved protocol. The sensitivity and specificity of the delayed phase classification were 91% and 18%, respectively. The EMM was able to accurately fit these curves. There was a statistically significant difference between benign and malignant lesions for several model parameters: the uptake rate, initial slope, signal enhancement ratio, and curvature at the peak enhancement (at most P = 0.04). These results demonstrated that EMM analysis provided at least the diagnostic accuracy of the kinetic classifiers described in the BI-RADS lexicon, and offered a few key advantages. It can be used to standardize data from institutions with different dynamic protocols and can provide a more objective classification with continuous variables so that thresholds can be set to achieve desired sensitivity and specificity. This suggests that the EMM may be useful for analysis of routine clinical data. Magn Reson Med 59:747–754, 2008. © 2008 Wiley-Liss, Inc.

Key words: malignant; breast; DCE-MRI; sensitivity

Improvements in breast cancer detection are largely responsible for increasing survival among breast cancer patients (1). Dynamic contrast-enhanced MRI (DCE-MRI) is being used in breast imaging for several purposes, including determining extent of malignant disease and posttreatment evaluation (2,3). DCE-MRI has a high sensitivity to breast cancer, with a lower specificity (4–6). When analyzing DCE-MRI the radiologist assesses both the lesion morphology and kinetics of contrast enhancement. Some studies have suggested that the morphologic information from DCE-MRI is more diagnostically useful than the kinetic information (7,8), implying that there may be room for improvement in extracting more diagnostically relevant information from kinetic data.

Department of Radiology, University of Chicago, Chicago, Illinois.

Grant sponsor: Segal Foundation; Grant sponsor: Biological Sciences Division at the University of Chicago; Grant sponsor: Department of Defense; Grant number: W81XWH-06-1-0329; Grant sponsor: National Institutes of Health (NIH); Grant numbers: R21 CA104774-01A2 and 2 R01 CA078803-05A2.

*Correspondence to: Gillian Newstead, MD, Department of Radiology, University of Chicago, 5841 S. Maryland Ave., MC 2026, Chicago, IL 60637. E-mail: gnewstead@radiology.bsd.uchicago.edu

Received 28 February 2007; revised 29 November 2007; accepted 3 December 2007.

DOI 10.1002/mrm.21530
Published online in Wiley InterScience (www.interscience.wiley.com).

Ideally, DCE-MRI protocols would acquire data with high spatial and high temporal resolution to fully exploit both the morphologic and kinetic information. Unfortunately, with currently available equipment and techniques there is always a trade-off between spatial and temporal resolution in DCE-MRI (7). As a result, the signal intensity versus time—or kinetic—curves typically have only 3–7 data points (9–11) for 3D DCE-MRI, which presents a challenge for differentiating benign from malignant lesions. To simplify analysis of the kinetic curves, radiologists qualitatively assess the initial rise and delayed phase according to the BI-RADS lexicon. Several reports have demonstrated that DCE-MRI data from malignant lesions tend to exhibit "washout" curves, while benign lesions tend to show persistent signal increase with time after contrast injection (12,13). Some groups have performed semiquantitative analysis of these curves—for example, calculating the time to peak enhancement—to better distinguish between the benign and malignant lesions (10). However, semiquantitative parameters have limited use since they are susceptible to errors due to noise, and with varying timing of acquisitions across institutions comparison of these parameters between institutions is problematic.

There have been several studies of pharmacokinetic compartment modeling on breast 3D DCE-MRI data, to relate kinetic curves to the underlying physiology of the lesions (14–18). However, for low time resolution 3D DCE-MRI data the accuracy of physiological parameters obtained from compartmental models is questionable. In addition, these models require an arterial input function (AIF), which is difficult to estimate accurately. As an alternative to these approaches, mathematical equations can be used to fit the kinetic curves. For example, Heiberg et al. (19) used a fifth-order polynomial to fit the kinetic curves (5–7 points), but the coefficients of the polynomial did not show a significant difference between benign and malignant breast lesions. Recently, a five-parameter empirical mathematical model (EMM) was developed to describe contrast uptake and washout behavior (20), and this model successfully distinguishes between benign and malignant lesions. Unfortunately, the EMM was performed with special protocols that allow acquisition of data with high temporal resolution, but are not clinically feasible (15,20). The limited temporal resolution in conventional 3D bilateral DCE-MRI implies that complicated mathematical models cannot be directly applied to kinetic curves to obtain a unique solution.

In this study a modified EMM with only three parameters was used to analyze 3D bilateral DCE-MRI breast data

that was acquired according to clinical protocols, with sparse time resolution of 68 sec. Primary model parameters were determined by fitting the curves to the modified EMM. Secondary diagnostic parameters, such as initial area under curve (AUC_{30}) (21,22), initial slope of enhancement ($Slope_{ini}$) (10,21,23), the time to peak enhancement (T_{peak}) (10), signal enhancement ratio (SER) (11), and enhancement curvature at peak (κ_{peak}) (24) were derived mathematically from the primary parameters after fitting the kinetic curves. The sensitivity and specificity to malignant lesions using these parameters was also evaluated by using receiver operating characteristic (ROC) analysis and was compared to the kinetic curve classification according to the BI-RADS lexicon. In addition to comparing benign versus malignant lesions, the kinetic characteristics of subtypes of benign and malignant lesions were also studied.

MATERIALS AND METHODS

Patients

Diagnostic MR imaging is performed at this institution routinely for several clinical purposes: diagnostic imaging, evaluating extent of known disease, posttreatment, and surgical evaluation and as a screening tool in high-risk women. Bilateral 3D DCE-MRI data from 100 female patients was acquired consecutively between May 2002 and June 2003 and reviewed for study under an Institutional Review Board (IRB)-approved protocol, with informed consent waived and under full HIPAA compliance. The age range of the subjects was 24 to 81 years (mean age = 56.2 ± 13.3 years). Based on the consensus opinion of two experienced pathologists, there were 34 benign and 79 malignant lesions used in this study.

MR Imaging

MR imaging was performed on a 1.5T GE Signa scanner (GE Healthcare, Milwaukee, WI) using a dedicated 4-channel breast coil (Invivo, Orlando, FL) with the patient in the prone position. One pre- and five postcontrast images were acquired in the coronal plane using a 3D T_1-weighted spoiled grass sequence (TR/TE = 7.7/4.2 ms, flip angle = 30°, slice thickness = 3 mm, and in-plane resolution = 1.4 mm) without fat saturation. The first postcontrast acquisition was started 20 sec after contrast injection and the remaining images were acquired every 68 sec. Gadodiamide (Omniscan; Nycomed-Amersham, Princeton, NJ) was injected intravenously at a dose of 0.1 mmol/kg followed by a 20-mL saline flush at the rate of 2.0 mL/sec.

All kinetic analysis was performed by experienced radiologists using coronal and reconstructed axial and sagittal views to assess the lesion. To generate the kinetic curve the radiologist traced a small region of interest (ROI) around what was perceived to be the most enhancing part of the lesion on the first postcontrast image. The average ROI size was 7.1 pixels; thus, the selected ROIs were small and contained the most enhancing contiguous pixels in the lesion as perceived by the radiologist. The plot of signal intensity versus time for this ROI was assessed by the radiologist according to the BI-RADS lexicon, which describes the "initial rise" and "delayed phase" of the kinetic curve. The "initial rise" is classified as rapid, medium, or slow. The "delayed phase" refers to the portion of the kinetic curve after 2 min and is classified as persistent (the signal intensity continues rise), plateau (the signal intensity levels off), and washout (the signal intensity decreases).

Modified EMM

The kinetic curve obtained above was analyzed quantitatively using the modified EMM (24). First, the average DCE-MRI signal intensity as a function of time ($S(t)$) in the selected ROI was calculated. Next, signal changes after contrast injection were calculated as: $\Delta S = (S_n - S_0)/S_0$, where S_0 is the average signal intensity within the ROI in the precontrast scan and S_n is the signal intensity within the ROI at the n^{th} postcontrast timepoint. The following modified EMM was used to describe the lesion contrast uptake and washout and to fit the data:

$$\Delta S(t) = A \cdot (1 - e^{-\alpha t}) \cdot e^{-\beta t}, \quad [1]$$

where A is the upper limit of the signal intensity, α (min^{-1}) is the rate of signal increase, β(min^{-1}) is the rate of the signal decrease during washout. The goodness of fit parameter R^2 was calculated for each lesion. The signal intensity modeled here is dependent on the noncontrast T_1 of the lesions. This is consistent with routine clinical practice, since radiologists typically evaluate changes in signal intensity following contrast injection. Variations in the native tissue T_1 values will affect the measured signal intensity; however, since T_1 values of benign and malignant lesions show considerable overlap (25–28), the results here may not be strongly affected.

Derived Diagnostic Parameters

Semiquantitative diagnostic parameters used commonly in the literature were easily derived from the modified EMM parameters. After some simple mathematical manipulations, we obtained the following derivations for diagnostic parameters: (a) Initial area under curve (AUC_τ): The AUC_τ can be calculated by integration of the kinetic curve, i.e.:

$$AUC_\tau = A \cdot [(1 - e^{-\beta\tau})/\beta + (e^{-(\alpha+\beta)\tau} - 1)/(\alpha + \beta)], \quad [2]$$

where τ is the time over which signal intensity was integrated. In this study we used $\tau = 30$ sec. (b) Initial slope of enhancement ($Slope_{ini}$): The initial slope of the kinetic curve can be calculated by taking the derivative of Eq. [1] at an initial time $t \ll 1$:

$$Slope_{ini} \approx A\alpha. \quad [3]$$

Thus, the initial slope is the product of the uptake rate α and the amplitude of enhancement A. (c) Time to peak of enhancement (T_{peak}): The time at which the kinetic curve reached peak can be solved by setting the derivative of Eq. [1] equal to zero:

$$T_{\text{peak}} = \frac{1}{\alpha}\log\left(1 + \frac{\alpha}{\beta}\right). \quad [4]$$

Please notice that when $\beta \leq 0$ the curves did not reach the peak within the duration of the experiment. In these cases, we used the last point as the peak intensity. (d) Signal enhancement ratio (SER): The signal intensity change at the first timepoint (ΔS_1) relative to the last time point (ΔS_L) was used to calculate the SER using the following formula:

$$SER = \frac{\Delta S_1}{\Delta S_L} = \frac{1 - e^{-\alpha t_1}}{1 - e^{-\alpha t_L}} \cdot e^{(t_L - t_1)\beta}, \quad [5]$$

where t_1 = 60 sec and t_L = 300 sec used in this study. A SER value greater than 1.1 indicates the signal intensity decreases with respect to its value at 60 sec; SER less than 0.9 indicates that signal intensity continues to rise; and SER between 0.9 and 1.1 represents a plateau relative to intensity at 60 sec. (e) Enhancement curvature at peak (κ_{peak}): The curvature at the peak of enhancement was calculated from the definition of curvature formula at time of T_{peak}:

$$\kappa_{peak} \approx -A\alpha\beta. \quad [6]$$

Data Analysis and Statistical Evaluation

For the qualitative evaluation according to the BI-RADS lexicon, distributions of initial rise and delayed phase were determined for benign and malignant lesions. To compare these distributions the chi-square (χ^2) test was used, with $P < 0.05$ indicating statistical significance.

The 3D bilateral DCE-MRI data were processed using software written in IDL (Research Systems, Boulder, CO). The average values of the diagnostic parameters were calculated separately for benign and malignant lesions. In addition, the benign and malignant lesions were further divided into pathologic subtypes. For malignant lesions these subtypes were: invasive ductal carcinoma (IDC), ductal carcinoma in situ (DCIS), invasive lobular carcinoma (ILC), and "other." For benign lesions these subtypes were: fibrocystic change (FCC), fibroadenoma, papilloma, and "other." Two-tailed unequal variance Student's *t*-tests were performed to evaluate which parameters showed significant differences between the benign and malignant breast lesions, with $P < 0.05$ indicating statistical significance.

In order to determine whether modified EMM parameters varied within pathologic subtypes of benign and malignant lesions (for example, if the parameter α varied significantly among DCIS, ILC, and IDC lesions) ANOVA calculations were used, with $P < 0.05$ indicating statistical significance. The ANOVA analysis was performed on the three classified subtypes of malignant lesions (DCIS, ILC, and IDC) and the three classified subtypes of benign lesions (fibroadenoma, papilloma, and FCC). We also performed a multivariate analysis using a stepwise logistic regression algorithm in Matlab (MathWorks, Natick, MA) in order to determine whether a combination of primary and derived EMM parameters could better separate benign from malignant lesions. We used backwise regression (that is, the initial model included all parameters) and the minimum *P* value for removal of 0.1. Receiver operating characteristic (ROC) analysis was performed to compare the diagnostic capability of the parameters derived from the modified EMM with the diagnostic performance of the qualitative BI-RADS categories of initial rise and delayed phase. ROCKIT software (ROCKIT 0.9B Beta Version, Charles E. Metz, University of Chicago (29)) was used to generate the ROC curves and perform statistical comparisons between them via the bivariate and area test.

RESULTS

BI-RADS Classification

The distribution of initial uptake and delayed phase for all lesions as well as the breakdown of benign and malignant lesions into pathology subtypes is shown in Table 1. Malignant and benign lesions did not have statistically significantly different distributions of initial rise, but differed in delayed phase distribution with 65% and 38% showing washout curves, respectively (P = 0.03). Similarly, DCIS and IDC lesions were significantly different in delayed phase, with 50% and 78% showing washout, respectively (P = 0.04). Considering "washout" and "plateau" to be indicative of malignancy (10,13) the sensitivity and spec-

Table 1
Distributions of BI-RADS Categories for the Qualitative Assessment of the Initial Rise and Delayed Phased of Kinetic Curves for Benign and Malignant Lesions

Type of lesions	No. Cases	Initial			Delayed		
		Rapid	Medium	Slow	Washout	Plateau	Persistent
All benign	34	25 (74%)	8 (24%)	1 (3%)	13 (38%)	15 (44%)	6 (18%)
FCC	16	11	4	1	3	11	2
Fibroadenoma	4	2	2	0	2	1	1
Papilloma	7	6	1	0	4	2	1
Others	7	6	1	0	4	1	2
All malignant	79	70 (89%)	7 (9%)	2 (3%)	51 (65%)	21 (27%)	7 (9%)
DCIS	30	26	3	1	15	10	5
IDC	36	33	3	0	28	7	1
ILC	7	6	0	1	4	2	1
Others	6	5	1	0	4	2	0

Numbers in parentheses are percentages.

ificity were 91% (95% confidence interval [CI] 83–96%) and 18% (95% CI 7–35%), respectively. For initial phase criteria, considering "rapid" to be indicative of malignancy, the sensitivity and specificity were 89% (95% CI 79–95%) and 26% (95% CI 13–44%), respectively. In most prior studies of the kinetics of benign and malignant lesions, only IDC lesions were considered (10,13). When considering only the IDC lesions the sensitivity of "washout" and "plateau" as described in the BI-RADS lexicon improved to 97% (95% CI 85–100%), and the sensitivity of "rapid" improved to 92% (95% CI 78–98%).

Modified EMM Parameters

The modified EMM was able to accurately fit the curves, with a goodness of fit parameter R^2 greater than 0.90 for all cases studied here. Some typical examples of the modified EMM fits are shown in Fig. 1 for various benign (top row: FCC, fibroadenoma, and papilloma) and malignant lesions (bottom row: DCIS, IDC, and ILC). The distribution of the primary parameters for all the subcategories of benign and malignant lesions is shown in Fig. 2. Upon visual inspection substantial overlap between benign and malignant lesions was evident for the EMM parameters. After fitting all the kinetic curves the five derived diagnostic parameters were calculated using Eqs. [2–6].

The average values of all primary and derived parameters were calculated and are summarized in Table 2. From calculated averaged parameters it can be seen that malignant lesions had significantly faster contrast uptake (α), steeper initial slope ($Slope_{ini}$), larger enhancement ratio (SER), and sharper curvature (κ_{peak}) than benign lesions. Two-tailed unequal variance *t*-test showed that there was a statistically significant difference between benign and malignant lesions for the parameters of contrast uptake rate α ($P < 0.03$), initial slope $Slope_{ini}$ ($P < 0.04$), signal enhancement ratio SER ($P < 0.0007$), and the curvature at the peak κ_{peak} ($P < 0.02$). To evaluate diagnostic performance ROC curves were generated for all parameters, with calculated A_z values shown in Fig. 3. The parameter A had the smallest area under the ROC curve (A_z), while SER had the largest. The ROC curves for the two parameters (Fig. 4) with the largest A_z values, α (blue line with solid square) and SER (red line with solid circle), are statistically equivalent under the bivariate and area test. From these ROC curves we can see that at a sensitivity of ≈90% the specificity was ≈20–30%, which was within the CI of the specificity achieved with the BI-RADS delayed phase and initial rise descriptors.

It is interesting to study further the kinetic properties of the subtypes of benign and malignant lesions. The calcu-

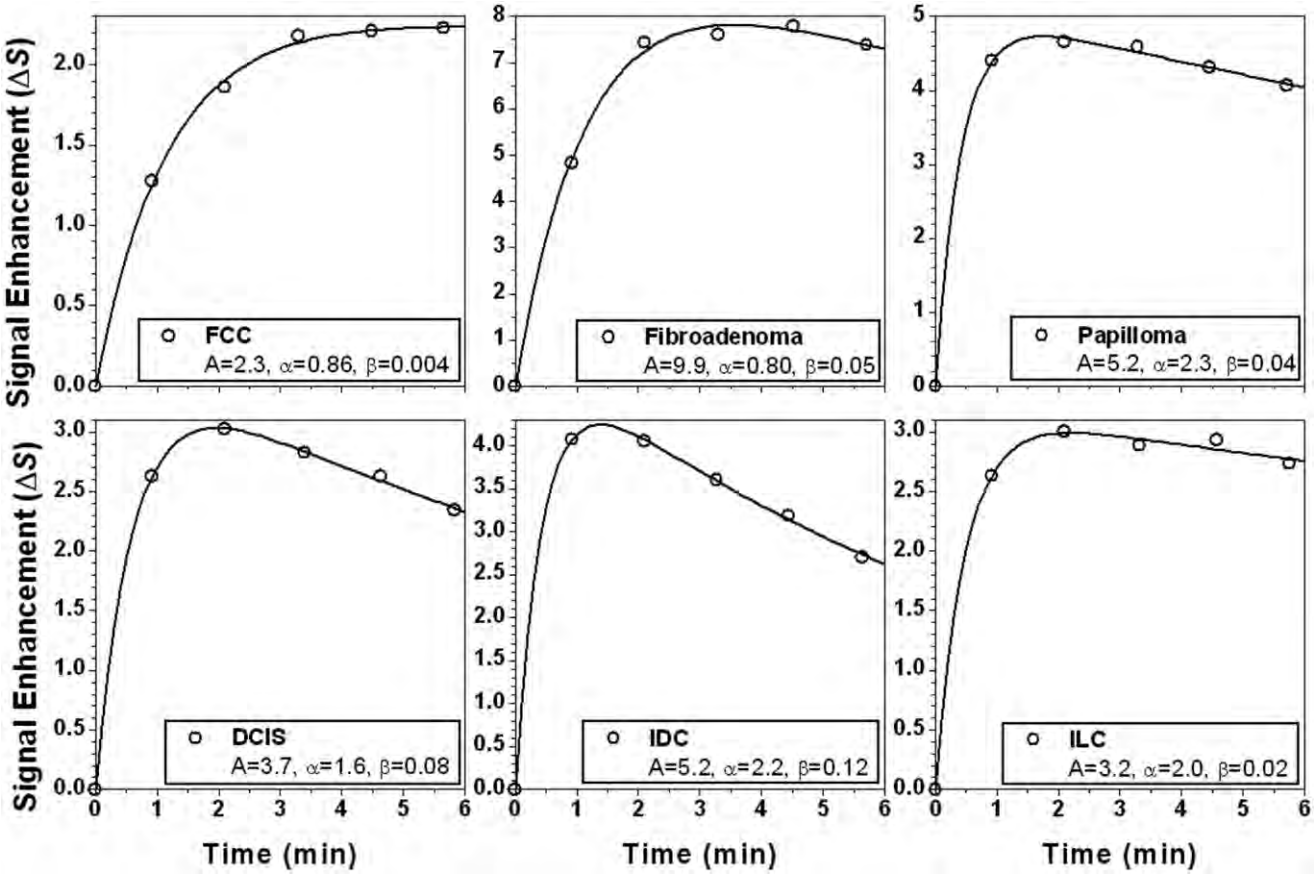

FIG. 1. Examples of MRI signal enhancement versus time curves (open circles) are shown for a variety of lesion types and fitted with the modified EMM (solid lines). The top row consists of benign lesions, from left to right: fibrocystic change (FCC), fibroadenoma, and papilloma. The bottom row consists of malignant lesions, from left to right: ductal carcinoma in situ (DCIS), invasive ductal carcinoma (IDC), and invasive lobular carcinoma (ILC).

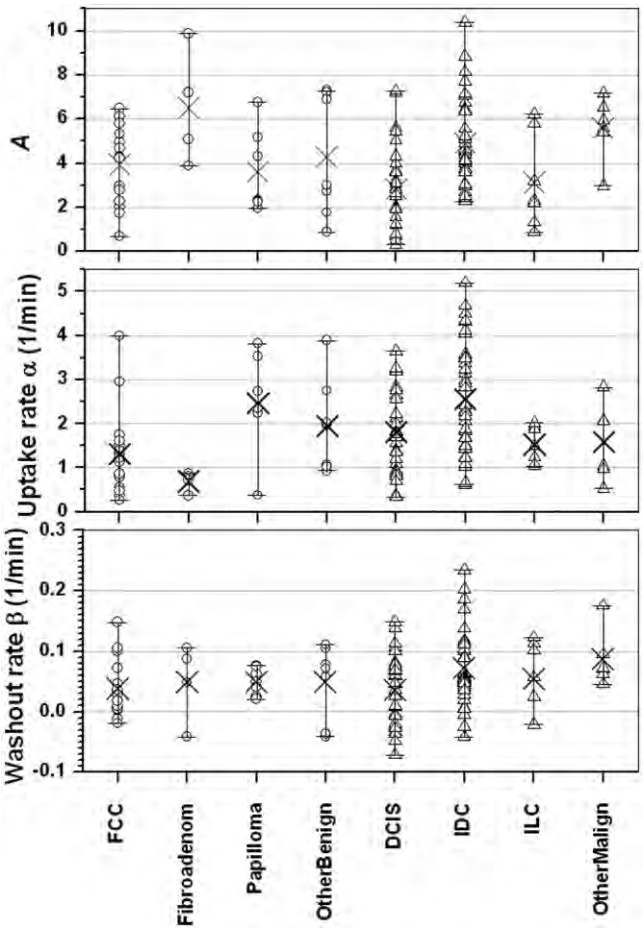

FIG. 2. The distributions of the primary EMM parameters are shown according to lesion type. From top to bottom the primary EMM parameters are the amplitude *A*, the uptake rate α, and the washout rate β. The open circles display the values of the primary EMM parameter for every case in that subtype of benign lesion, and × marks the average value: fibrocystic change (FCC, $n = 16$), fibroadenoma ($n = 4$), papilloma ($n = 7$), and other benign ($n = 7$). Similarly, the open triangles represent the values of each primary EMM parameter for every case in that subtype of malignant lesion, and × marks the average value: ductal carcinoma in situ (DCIS, $n = 30$), invasive ductal carcinoma (IDC, $n = 36$), invasive lobular carcinoma (ILC, $n = 7$), and other malignant ($n = 6$).

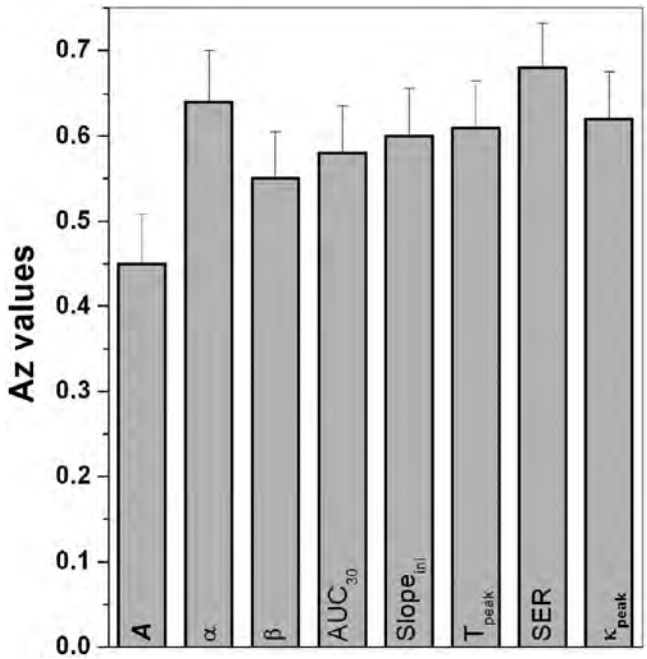

FIG. 3. The bar graph of the area under the ROC curve (A_z) is shown for each EMM primary and derived parameter. The area under an ROC curve (A_z) gives a measure of how well the diagnostic parameter performs; the larger the area under the curve, the better the performance. The A_z values (and corresponding standard error) were determined from the fitted binormal ROC curves generated by the ROCKIT software. The standard errors are almost the same for all the cases.

lated average values showed that the primary as well as diagnostic parameters for FCC were very similar to DCIS, which contributed to the majority of the overlap between the benign and malignant lesions. Performing *t*-test comparisons between these groups (DCIS vs. FCC) yields no statistically significant difference ($P > 0.06$ for all parameters). On the other hand, the contrast uptake and washout rates for IDC were much faster than benign lesions. As a result, IDC lesions had the largest AUC_{30}, deepest $Slope_{ini}$, highest SER, and sharpest κ_{peak}. In addition, for all primary and derived parameters there was a statistically significant difference (at least $P < 0.02$) between IDC and DCIS le-

Table 2
Primary and Secondary Diagnostic Parameters Derived from the EMM in Malignant and Benign Lesions

Type of Lesions	No. Cases	*A*	α (min^{-1})	β (min^{-1})	AUC_{30}	$Slope_{ini}$ (min^{-1})	T_{peak} (min)*	κ_{peak}	SER
All benign	34	4.2 ± 2.2	**1.6 ± 1.1**	0.045 ± 0.047	0.55 ± 0.35	**6.1 ± 4.6**	3.4 ± 1.8	**−0.30 ± 0.49**	**0.88 ± 0.30**
FCC	16	3.9 ± 1.8	1.3 ± 1.0	0.039 ± 0.046	0.48 ± 0.39	5.3 ± 5.5	4.0 ± 1.6	−0.23 ± 0.56	0.78 ± 0.28
Fibroadenoma	4	6.5 ± 2.6	0.69 ± 0.22	0.050 ± 0.066	0.48 ± 0.25	4.4 ± 2.4	4.2 ± 1.4	−0.22 ± 0.25	0.65 ± 0.19
Papilloma	7	3.6 ± 1.9	2.5 ± 1.1	0.050 ± 0.022	0.62 ± 0.28	7.5 ± 3.6	2.0 ± 1.2	−0.33 ± 0.14	1.08 ± 0.7
Others	7	4.3 ± 2.8	2.0 ± 1.1	0.050 ± 0.063	0.66 ± 0.36	7.4 ± 4.4	3.2 ± 2.0	−0.45 ± 0.64	1.04 ± 0.30
All malignant	79	4.0 ± 2.2	**2.1 ± 1.1**	0.058 ± 0.061	0.71 ± 0.54	**8.7 ± 8.3**	2.8 ± 1.9	**−0.67 ± 1.18**	**1.14 ± 0.48**
DCIS	30	2.8 ± 1.9	1.8 ± 0.9	0.037 ± 0.058	0.40 ± 0.23	4.3 ± 2.6	3.6 ± 2.0	−0.18 ± 0.31	0.96 ± 0.35
IDC	36	4.9 ± 2.0	2.6 ± 1.3	0.072 ± 0.062	1.01 ± 0.62	13.1 ± 10.2	2.0 ± 1.5	−1.12 ± 1.57	1.31 ± 0.55
ILC	7	3.1 ± 2.1	1.5 ± 0.4	0.054 ± 0.062	0.44 ± 0.26	4.6 ± 2.7	3.2 ± 2.0	−0.35 ± 0.40	1.04 ± 0.30
Others	6	5.6 ± 1.4	1.6 ± 0.9	0.087 ± 0.046	0.78 ± 0.38	8.5 ± 4.7	2.3 ± 1.0	−0.82 ± 0.89	1.14 ± 0.57

Reported values are mean ± standard deviation for all cases. Numbers in bold indicate that there was a statistically significant difference between benign and malignant lesions.

*For those curves which did not reach a peak within the duration of the experiment, we assumed a time to peak of 5 min.

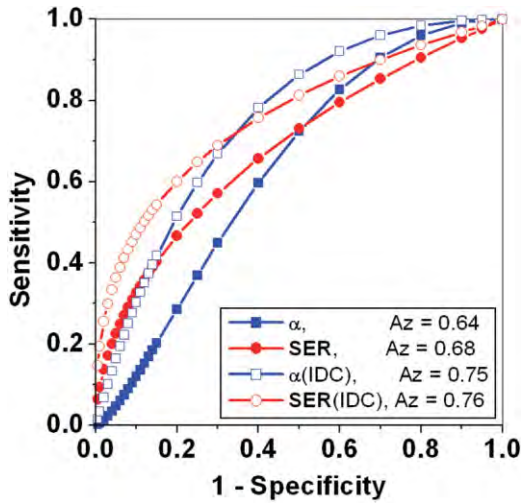

FIG. 4. Fitted binormal ROC curves generated by the ROCKIT software are shown for selected parameters α (blue line with solid squares) and SER (red line with solid circles). The A_z values were improved by comparing benign lesions with IDC lesions only, as shown by the ROC curves for α (blue line with open squares) and SER (red line with open circles).

sions. This suggests that the diagnostic accuracy of the modified EMM parameters may be improved if we consider only IDC lesions. To explore this, Fig. 4 also shows ROC curves (lines with open symbols) for α and SER when testing benign versus IDC lesions only. As shown in the figure, these ROC curves demonstrate considerable improvement in the A_z values compared to their benign versus all malignant lesions counterparts. At a sensitivity of ≈95% the specificity was ≈10–30%, which was within the CI achieved with the BI-RADS classifications.

To test whether a combination of parameters could improve the sensitivity and specificity, multivariate analysis was performed. However, the recommended model selected by backward stepwise regression included only the parameter SER. Based on these results it would seem that combinations of the EMM primary and derived parameters will not improve sensitivity and specificity.

Finally, ANOVA analysis was used to study the variation of the primary and derived parameters within benign and malignant subcategories. Three parameters (α, T_{peak}, SER) varied significantly by subtype for benign lesions ($P < 0.03$ for all), whereas all but one (A, α, T_{peak}, AUC_{30}, $Slope_{ini}$, κ_{peak}, SER) varied significantly for malignant subtypes ($P < 0.007$ for all).

DISCUSSION

In this study we found that 68% of malignant curves exhibited "washout," which is similar to prior reports; however, 38% of benign curves also showed "washout," which is higher than many reports (13). This may be because the benign lesions considered in this study were histologically proven benign—in other words, these lesions were suspicious enough to warrant biopsy. Since most obviously benign lesions have "persistent" type curves and would not be sent to biopsy, this may skew the delayed phase distribution in this study away from the "persistent" curve type. Szabo et al (10) considered only histologically proven benign lesions, and found that 24% of benign lesions showed "washout" type curves, a value closer to the one presented here. Because of the large number of benign lesions with "plateau" and "washout" type curves in this study, using these descriptors from the BI-RADS kinetic classification provided high sensitivity and low specificity in diagnosing malignant lesions.

The results demonstrated that the modified EMM fit the 3D DCE-MRI data very well for all cases. All the secondary diagnostic parameters could be easily calculated from the EMM parameters. Thus, we were able to calculate parameters, such as AUC_{30} and κ_{peak}, which could not be calculated directly from kinetic data comprised of only 6 points. The sensitivity and specificity of the BI-RADS delayed phase and initial rise classifications were 89–91% and 18–26%, respectively. Using the primary model parameter α or the derived parameter SER, at ≈90% sensitivity the specificity was ≈20–30%, which was not statistically different from the corresponding BI-RADS results. However, unlike the BI-RADS classification the EMM can be used to achieve a continuous spectrum of sensitivity and specificity. For example, at a sensitivity of ≈80% the specificity was ≈40%.

The diagnostic accuracy of the model parameters may be compromised by the relatively large number of DCIS and ILC lesions in this study, which showed significant overlap with benign lesions. Indeed, most other studies usually focus only on IDC lesions (10). We found that when considering benign versus IDC lesions only, the plateau and washout descriptors from the BI-RADS lexicon had sensitivity and specificity of 97% and 18%, respectively. Similarly, the rapid descriptor from the BI-RADS lexicon had sensitivity and specificity of 92% and 26%, respectively. The corresponding values for α and SER were comparable to the BI-RADS results. However, at a reasonable sensitivity of ≈80% the specificity of the model parameters improved greatly to ≈60%. The multivariate analysis did not yield a combination of parameters that improved results compared with individual parameters. This may be due to several factors; we have considered a small number of lesions and some parameters may depend on each other mathematically, which in turn may reflect a biological dependence. Further investigation of the relationship that EMM parameters have with each other and with the underlying biology of breast lesions is needed.

We have studied several subtypes of benign and malignant lesions, each having unique underlying biology. Fibroadenomas involve a proliferation of both epithelial and mesenchymal cells, and often present as encapsulated, well-circumscribed masses. Papillomas, on the other hand, grow confined in mammary milk ducts. FCC refers to a variety of benign mammary alterations, which are thought of as exaggerated physiological phenomena rather than diseases. These include proliferative lesions, such as intraductal hyperplasia, as well as fibrocystic disease. Moving to the malignant subtypes of cancer, ILCs involve cancer cells of lobular origin, which have invaded the surrounding stroma in a diffusely infiltrating fashion. IDCs, on the other hand, are cancer cells of ductal origin, which have well-defined but infiltrative margins. DCIS

lesions are also cancer cells of ductal origin that are still confined to the mammary ducts.

The significant overlap of DCIS lesions with benign lesions may be related to similarities in the underlying biology and vasculature (30,31). Because DCIS is the earliest form of malignant breast disease, improving the detection of DCIS is important, and further investigation into the presentation of DCIS would be interesting (32). The ANOVA results in this study indicate that most of the modified EMM parameters varied significantly across the subtypes of DCIS, ILC, and IDC. Uptake and the sharpness and magnitude of washout tended to increase from DCIS to ILC to IDC. DCIS and IDC lesions showed the most difference in all parameters, with DCIS lesions having on average a much longer time to peak enhancement (3.6 min) compared with IDC lesions (2.0 min). On the other hand, only three parameters (SER, T_{peak}, α) showed significant variations among benign lesions; fibroadenomas exhibited a smaller uptake rate and much longer time to peak enhancement than papillomas.

The modified EMM does not make assumptions about the underlying physiology of the lesion. Some assumptions required by two-compartment or multicompartment models (15) can lead to fitting errors and subsequent diagnostic errors. On the other hand, this lack of direct correspondence to identifiable physiologic or anatomic features is also the main disadvantage of the modified EMM approach. This problem can be addressed by deriving equations that connect parameters of the modified EMM to physiologic and anatomic parameters associated with various models (i.e., two or more compartment models). The parameters A, α, and β in the modified EMM can be directly compared with two-compartment models described in eqs. [13–16] of Armitage et al. (15). For example, to compare the EMM with the Tofts model described in eq. [13] of Armitage et al., it can be seen that the $A = Dv_eK^{trans}/V_p(K^{trans} - k_{out}v_e)$, $\beta = k_{out}$, and $\alpha + \beta = K^{trans}/v_e$, where D is the dose of administered contrast agent, v_e is the extravascular extracellular space volume fraction, K^{trans} is the transfer constant, V_p is the volume of the plasma, and k_{out} is the rate constant for contrast media elimination. With such relationships the empirical model can be related to a physiologically motivated model.

There are other limitations to this study:

- Sparse sampling may result in fitting errors. In particular, prior work has suggested that high temporal resolution was required to sample the kinetic curve uptake and transition part of uptake and washout accurately (24).
- Preclinical studies suggest that specificity is improved when the tail of the washout curve is sampled for at least 15 min; the curves studied here are truncated at about 6 min (20).
- Using signal intensity rather than contrast concentration may result in errors due to variability of the native T_1 of the tissue. However, in the present application of the EMM we used signal intensity rather than contrast concentration to follow conventional clinical practice and to minimize noise amplification.
- The present model does not account for variations in the arterial input function (AIF) and this omission can introduce variability and systematic error. The EMM is designed to analyze and accurately fit the signal intensity curves or contrast concentration versus time curves, and these are a function of the AIF and the tissue response to the AIF. The effect of AIF can be removed by deconvoluting it from the contrast concentration curves, so that an impulse response function can be obtained. Future work will focus on deriving deconvolution algorithms and developing mathematical models for the impulse response function.
- To characterize the kinetics of the lesion only a small ROI was used, which results in lower SNR. In addition, one small ROI may not be a reliable representation of the entire lesion, especially for heterogeneously enhancing lesions. Although the ROI was placed on the most rapidly enhancing area of the lesion, as is clinical practice, there is no guarantee this is the region of most diagnostic utility. Also, the ROI was chosen manually, resulting in variations in size and placement.
- Although the total number of lesions studied was relatively large, when considering subtypes of benign and malignant lesions (such as fibroadenoma or ILC) only a few cases were found, raising the issue of statistical validity. In particular, the numbers of lesions may be too small to perform reliable comparisons of the subtypes of benign and malignant lesions presented here.
- Recent parallel imaging techniques render the data we have used here slightly outdated, and the EMM will need to be tested with these new methods. We expect that the EMM will succeed with newer data, since the temporal resolution is comparable to that used in the studies described here. However, with the improved spatial resolution of parallel imaging, the ROI selection could likely be refined.

Despite the shortcomings summarized above, these results show that in our patient group, analysis of conventional 3D DCE-MRI data with the EMM provides at least the diagnostic accuracy of qualitative kinetic parameters described in the BI-RADS lexicon, and offers a few key advantages. It can be used to standardize kinetic data between institutions—currently, when radiologists are presented with an outside MRI for evaluation there is no way to relate the kinetic findings of the outside case to experience at the home institution. For example, if MR images at the outside institution are acquired every 90 sec, and at the home institution the dynamic protocol acquires images every 60 sec, the EMM can be used to present the outside kinetic data with 60-sec time resolution. The EMM can be automated and can provide a more objective classification. The EMM provides continuous variables so that thresholds can be set to achieve desired sensitivity and specificity. It also offers an opportunity to relate semiquantitative parameters (such as SER) to more fundamental EMM parameters. More important, this model allows for more flexibility in improving sensitivity and specificity in the future by correcting for AIFs. This model may become valuable as new protocols are being implemented at higher field strength and become more available. With the devel-

opment of parallel imaging techniques it is now possible to acquire images with relatively high spatial resolution while still acquiring 6 or 7 kinetic data points. Thus, optimizing the diagnostic utility of kinetic data will be more and more important, and these preliminary results have demonstrated that the EMM may be useful for analysis of routine clinical data.

ACKNOWLEDGMENT

The authors thank Dr. Yulei Jiang and Ms. Marieke Heisen for assistance with statistical analysis.

REFERENCES

1. Tabar L, Dean PB. Mammography and breast cancer: the new era. Int J Gynaecol Obstet 2003;82:319–326.
2. Abraham DC, Jones RC, Jones SE, Cheek JH, Peters GN, Knox SM, Grant MD, Hampe DW, Savino DA, Harms SE. Evaluation of neoadjuvant chemotherapeutic response of locally advanced breast cancer by magnetic resonance imaging. Cancer 1996;78:91–100.
3. Boetes C, Mus RD, Holland R, Barentsz JO, Strijk SP, Wobbes T, Hendriks JH, Ruys SH. Breast tumors: comparative accuracy of MR imaging relative to mammography and US for demonstrating extent. Radiology 1995;197:743–747.
4. Warren RM, Pointon L, Thompson D, Hoff R, Gilbert FJ, Padhani A, Easton D, Lakhani SR, Leach MO. Reading protocol for dynamic contrast-enhanced MR images of the breast: sensitivity and specificity analysis. Radiology 2005;236:779–788.
5. Heywang-Kobrunner SH, Bick U, Bradley WG Jr, Bone B, Casselman J, Coulthard A, Fischer U, Muller-Schimpfle M, Oellinger H, Patt R, Teubner J, Friedrich M, Newstead G, Holland R, Schauer A, Sickles EA, Tabar L, Waisman J, Wernecke KD. International investigation of breast MRI: results of a multicentre study (11 sites) concerning diagnostic parameters for contrast-enhanced MRI based on 519 histopathologically correlated lesions. Eur Radiol 2001;11:531–546.
6. Orel SG. MR imaging of the breast. Radiol Clin North Am 2000;38:899–913.
7. Kuhl CK, Schild HH, Morakkabati N. Dynamic bilateral contrast-enhanced MR imaging of the breast: trade-off between spatial and temporal resolution. Radiology 2005;236:789–800.
8. Goto M, Ito H, Akazawa K, Kubota T, Kizu O, Yamada K, Nishimura T. Diagnosis of breast tumors by contrast-enhanced MR imaging: comparison between the diagnostic performance of dynamic enhancement patterns and morphologic features. J Magn Reson Imaging 2007;25:104–112.
9. Bazzocchi M, Zuiani C, Panizza P, Del Frate C, Soldano F, Isola M, Sardanelli F, Giuseppetti GM, Simonetti G, Lattanzio V, Del Maschio A. Contrast-enhanced breast MRI in patients with suspicious microcalcifications on mammography: results of a multicenter trial. AJR Am J Roentgenol 2006;186:1723–1732.
10. Szabo BK, Aspelin P, Wiberg MK, Bone B. Dynamic MR imaging of the breast. Analysis of kinetic and morphologic diagnostic criteria. Acta Radiol 2003;44:379–386.
11. Esserman L, Hylton N, George T, Weidner N. Contrast-enhanced magnetic resonance imaging to assess tumor histopathology and angiogenesis in breast carcinoma. Breast J 1999;5:13–21.
12. Kuhl CK, Schild HH. Dynamic image interpretation of MRI of the breast. J Magn Reson Imaging 2000;12:965–974.
13. Kuhl CK, Mielcareck P, Klaschik S, Leutner C, Wardelmann E, Gieseke J, Schild HH. Dynamic breast MR imaging: are signal intensity time course data useful for differential diagnosis of enhancing lesions? Radiology 1999;211:101–110.
14. Cron GO, Kelcz F, Santyr GE. Improvement in breast lesion characterization with dynamic contrast-enhanced MRI using pharmacokinetic modeling and bookend T(1) measurements. Magn Reson Med 2004;51:1066–1070.
15. Armitage P, Behrenbruch C, Brady M, Moore N. Extracting and visualizing physiological parameters using dynamic contrast-enhanced magnetic resonance imaging of the breast. Med Image Anal 2005;9:315–329.
16. Furman-Haran E, Degani H. Parametric analysis of breast MRI. J Comput Assist Tomogr 2002;26:376–386.
17. Furman-Haran E, Schechtman E, Kelcz F, Kirshenbaum K, Degani H. Magnetic resonance imaging reveals functional diversity of the vasculature in benign and malignant breast lesions. Cancer 2005;104:708–718.
18. Tofts PS, Berkowitz B, Schnall MD. Quantitative analysis of dynamic Gd-DTPA enhancement in breast tumors using a permeability model. Magn Reson Med 1995;33:564–568.
19. Heiberg EV, Perman WH, Herrmann VM, Janney CG. Dynamic sequential 3D gadolinium-enhanced MRI of the whole breast. Magn Reson Imaging 1996;14:337–348.
20. Fan X, Medved M, River JN, Zamora M, Corot C, Robert P, Bourrinet P, Lipton M, Culp RM, Karczmar GS. New model for analysis of dynamic contrast-enhanced MRI data distinguishes metastatic from nonmetastatic transplanted rodent prostate tumors. Magn Reson Med 2004;51:487–494.
21. Moate PJ, Dougherty L, Schnall MD, Landis RJ, Boston RC. A modified logistic model to describe gadolinium kinetics in breast tumors. Magn Reson Imaging 2004;22:467–473.
22. Evelhoch JL. Key factors in the acquisition of contrast kinetic data for oncology. J Magn Reson Imaging 1999;10:254–259.
23. Buadu LD, Murakami J, Murayama S, Hashiguchi N, Sakai S, Masuda K, Toyoshima S, Kuroki S, Ohno S. Breast lesions: correlation of contrast medium enhancement patterns on MR images with histopathologic findings and tumor angiogenesis. Radiology 1996;200:639–649.
24. Fan X, Medved M, Karczmar GS, Yang C, Foxley S, Arkani S, Recant W, Zamora MA, Abe H, Newstead GM. Diagnosis of suspicious breast lesions using an empirical mathematical model for dynamic contrast-enhanced MRI. Magn Reson Imaging 2007;25:593–603.
25. Kelcz F, Santyr GE, Cron GO, Mongin SJ. Application of a quantitative model to differentiate benign from malignant breast lesions detected by dynamic, gadolinium-enhanced MRI. J Magn Reson Imaging 1996;6:743–752.
26. Callicott C, Thomas JM, Goode AW. The magnetization transfer characteristics of human breast tissues: an in vitro NMR study. Phys Med Biol 1999;44:1147–1154.
27. Hulka CA, Smith BL, Sgroi DC, Tan L, Edmister WB, Semple JP, Campbell T, Kopans DB, Brady TJ, Weisskoff RM. Benign and malignant breast lesions: differentiation with echo-planar MR imaging. Radiology 1995;197:33–38.
28. Jacobs MA, Barker PB, Bluemke DA, Maranto C, Arnold C, Herskovits EH, Bhujwalla Z. Benign and malignant breast lesions: diagnosis with multiparametric MR imaging. Radiology 2003;229:225–232.
29. Metz CE, Herman BA, Shen JH. Maximum likelihood estimation of receiver operating characteristic (ROC) curves from continuously-distributed data. Stat Med 1998;17:1033–1053.
30. Arpino G, Laucirica R, Elledge RM. Premalignant and in situ breast disease: biology and clinical implications. Ann Intern Med 2005;143:446–457.
31. Kumar AS, Chen DF, Au A, Chen YY, Leung J, Garwood ER, Gibbs J, Hylton N, Esserman LJ. Biologic significance of false-positive magnetic resonance imaging enhancement in the setting of ductal carcinoma in situ. Am J Surg 2006;192:520–524.
32. Jansen S, Newstead G, Abe H, Shimauchi A, Schmidt R, Karczmar GS. Pure ductal carcinoma in situ: kinetics, morphology and comparison with mammographic presentation and nuclear grade. Radiology 2007;245:684–691.

DCEMRI of breast lesions: Is kinetic analysis equally effective for both mass and nonmass-like enhancement?

Sanaz A. Jansen, Xiaobing Fan, Gregory S. Karczmar, Hiroyuki Abe, Robert A. Schmidt, Maryellen Giger, and Gillian M. Newstead[a)]
Department of Radiology, The University of Chicago, 5841 South Maryland Avenue MC2026 Chicago, Illinois 60637

(Received 5 December 2007; revised 24 March 2008; accepted for publication 24 April 2008; published 13 June 2008)

To perform a pilot study investigating whether the sensitivity and specificity of kinetic parameters can be improved by considering mass and nonmass breast lesions separately. The contrast media uptake and washout kinetics in benign and malignant breast lesions were analyzed using an empirical mathematical model (EMM), and model parameters were compared in lesions with mass-like and nonmass-like enhancement characteristics. 34 benign and 78 malignant breast lesions were selected for review. Dynamic MR protocol: 1 pre and 5 postcontrast images acquired in the coronal plane using a 3D T1-weighted SPGR with 68 s timing resolution. An experienced radiologist classified the type of enhancement as mass, nonmass, or focus, according to the BI-RADS® lexicon. The kinetic curve obtained from a radiologist-drawn region within the lesion was analyzed quantitatively using a three parameter EMM. Several kinetic parameters were then derived from the EMM parameters: the initial slope ($\text{Slope}_{\text{ini}}$), curvature at the peak (κ_{peak}), time to peak (T_{peak}), initial area under the curve at 30 s (iAUC_{30}), and the signal enhancement ratio (SER). The BI-RADS classification of the lesions yielded: 70 mass lesions, 38 nonmass, 4 focus. For mass lesions, the contrast uptake rate (α), contrast washout rate (β), iAUC_{30}, SER, $\text{Slope}_{\text{ini}}$, T_{peak} and κ_{peak} differed substantially between benign and malignant lesions, and after correcting for multiple tests of significance SER and T_{peak} demonstrated significance ($p<0.007$). For nonmass lesions, we did not find statistically significant differences in any of the parameters for benign vs. malignant lesions ($p>0.5$). Kinetic parameters could distinguish benign and malignant mass lesions effectively, but were not quite as useful in discriminating benign from malignant nonmass lesions. If the results of this pilot study are validated in a larger trial, we expect that to maximize diagnostic utility, it will be better to classify lesion morphology as mass or nonmass-like enhancement prior to kinetic analysis. © *2008 American Association of Physicists in Medicine.* [DOI: 10.1118/1.2936220]

Key words: nonmass lesions, malignant, DCEMRI, sensitivity, specificity

I. INTRODUCTION

Dynamic contrast enhanced magnetic resonance imaging (DCEMRI) is being used in breast imaging for several purposes, including determining extent of malignant disease and post-treatment evaluation.[1,2] When analyzing lesion presentation on breast DCEMRI, the radiologists assesses the morphology as well as the contrast media uptake and washout—or kinetics—of the lesion following the breast imaging reporting and data system (BI-RADS®) lexicon.

According to the BI-RADS® lexicon, the first step in assessing lesion morphology is to classify the type of enhancement as mass, nonmass, focus (Fig. 1). Then, subsequent descriptors of other lesion features (such as shape, distribution, margins, enhancement pattern) are selected, which differ depending on the type of enhancement. The BI-RADS® lexicon also classifies the initial rise of the kinetic curve, and the delayed phase as persistent, plateau, or washout.

The level of suspicion for malignancy is determined by assessing both the morphologic as well as the kinetic characteristics of the lesion. Invasive cancers often present as heterogeneously enhancing masses with irregular or spiculated margins, and kinetic curves that typically rise rapidly and subsequently wash out over time. Benign lesions, on the other hand, often present as homogeneously enhancing masses with smooth margins and tend to enhance more slowly and persistently take up contrast over time.[3] To move beyond the qualitative BI-RADS® description of kinetics, many prior studies have calculated quantitative parameters from the kinetic curve data. Chen *et al.* used automated and fuzzy *c*-means clustering to extract the most enhancing voxels within a lesion and then calculated empirical parameters, such as maximum enhancement percentage, time to peak enhancement, uptake rate, and washout rate.[4] Others have applied mathematical models to DCEMRI kinetic data, such as the two-compartment model, to extract diagnostically useful parameters.[5–10] Early work by Hayton and Brady combined both breast segmentation and registration with pharmacokinetic modeling to produce color kinetic parameter maps that were shown to be useful for cancerous lesion localization and characterization.[11] However, for low time resolution 3D DCEMRI data, the accuracy of physiological parameters obtained from compartmental models is questionable. In addition these models require an arterial input function (AIF),

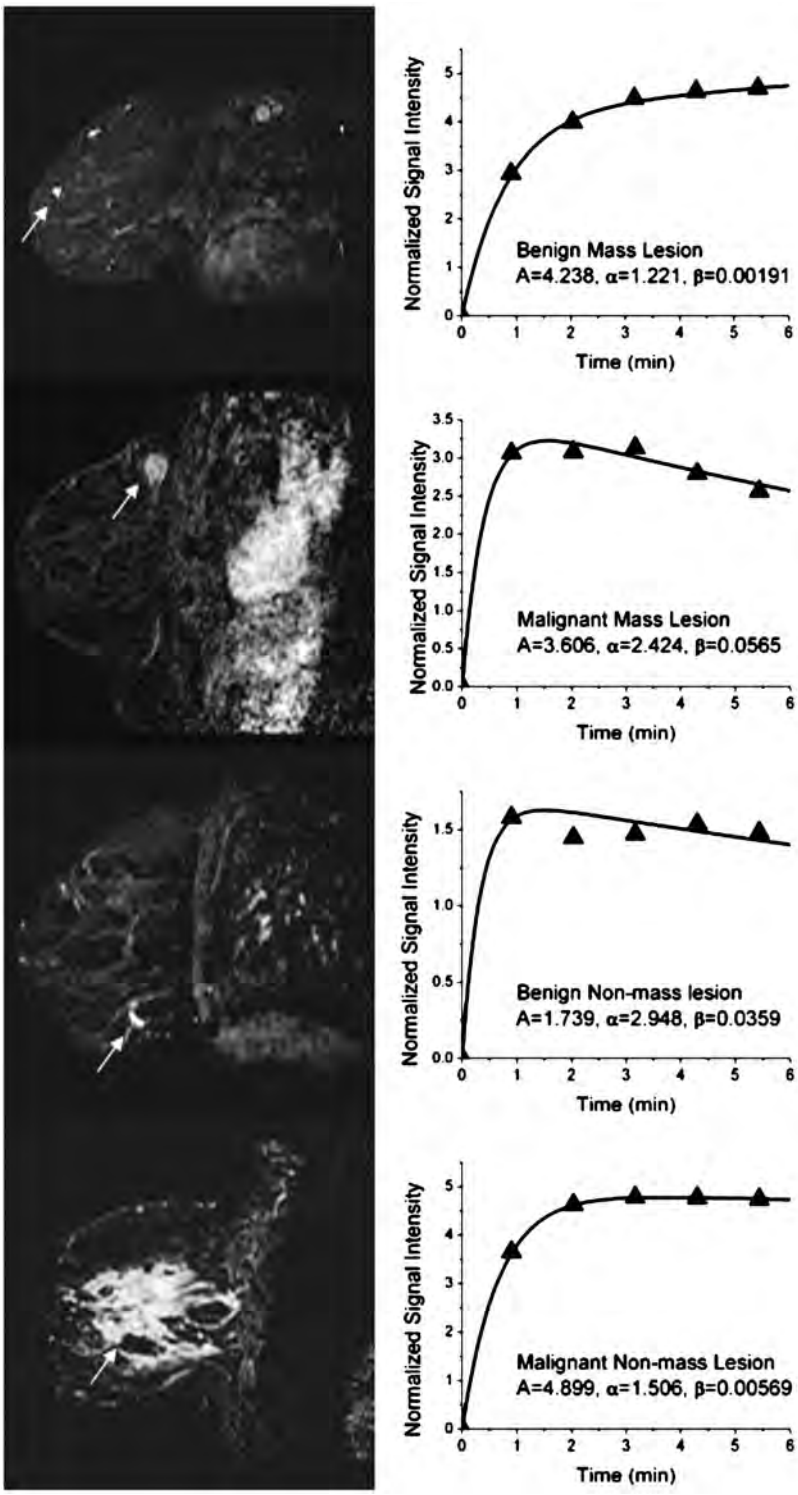

FIG. 1. Examples of four breast lesions with measured and EMM fitted kinetic curves. For each kinetic curve, the measured signal intensity values are indicated with triangles, and the fitted EMM curve with solid lines. From the top to bottom: Benign mass lesion, malignant mass lesion, benign nonmass lesion, and malignant nonmass lesion. The lesions are indicated by a white arrow.

which is difficult to estimate accurately. As an alternative to these approaches, mathematical equations can be used to fit the kinetic curves.[10,12]

The majority of preinvasive ductal carcinoma *in situ* (DCIS) lesions and some invasive cancers present as nonmass-like enhancement in a segmental distribution with a clumped enhancement pattern.[13–17] Benign lesions, such as atypical ductal hyperplasia, can also present with nonmass-like enhancement, as can normal parenchyma. DCIS is considered to be a nonobligate precursor of invasive cancer, and if treated has dramatically higher survival than invasive cancers.[18,19] Yet the sensitivity and specificity of DCEMRI for detection of DCIS needs improvement,[15,16,20–27] particularly given recent American Cancer Society guidelines recommending breast MRI in the screening of women at high risk of developing breast cancer.[28] It is likely that mass-like and nonmass-like enhancement patterns reflect differences in the underlying physiology and vasculature of these lesions,

which may in turn affect the kinetic characteristics. The kinetic parameters that can distinguish benign and malignant mass lesions may not work well with nonmass lesions, and vice versa. However, while there have been several studies on nonmass lesions such as DCIS, the efficacy of kinetic analysis in mass-like vs. nonmass-like enhancement has not been well characterized.[29–33]

We have performed a pilot study to investigate whether kinetic analysis is more diagnostically useful in mass lesions compared with nonmass lesions. In addition to using conventional BI-RADS® descriptors of kinetics, we have also applied a mathematical model to the kinetic data. The limited temporal resolution in conventional 3D bilateral DCEMRI implies that complex mathematical models cannot be directly applied to kinetic curves to obtain a unique solution. In this study, a three parameter empirical mathematical model (EMM) was used to analyze 3D bilateral DCEMRI breast data. Thus, using both qualitative and quantitative means, we evaluated kinetic patterns of enhancement separately in (i) benign vs. malignant mass lesions, and (ii) benign vs. malignant nonmass lesions.

II. METHODS

II.A. Patients

At our institution, it is a routine protocol to obtain breast MR imaging for evaluation of extent of malignant disease, for post-treatment evaluation of the cancer patient, and for high-risk screening. The institutional review board approved our HIPAA compliant retrospective study with waiver of informed consent. Bilateral 3D DCEMRI data from 100 female patients acquired between May 2002 and June 2003 were reviewed for study. The age range of the subjects was 24–81 years (mean age $=56.2\pm13.3$ years). Based on the consensus opinion of two experienced pathologists, there were a total of 112 lesions of which 35 were benign and 77 malignant.

II.B. MRI analysis

MR imaging was performed on a 1.5 T GE Signa scanner (GE Healthcare, Milwaukee, WI) using a dedicated four-channel breast coil (Invivo, Orlando, FL) with the patient in the prone position. One pre and five postcontrast images were acquired in the coronal plane using a 3D T_1-weighted spoiled grass sequence (TR/TE$=$7.7/4.2 ms, flip angle $=30°$, slice thickness$=3$ mm, and in plane resolution $=1.4$ mm), without fat suppression. The first postcontrast acquisition was started 20 s after contrast injection and the remaining images were acquired every 68 s; 20 ml of 0.5 M Gadodiamide (Omniscan; Nycomed-Amersham, Princeton, NJ) was injected intravenously followed by a 20 ml saline flush at the rate of 2.0 ml/s.

One experienced radiologist retrospectively reviewed the images and classified lesion morphology and kinetics. The lesions were assessed according to the BI-RADS® lexicon as mass, nonmass, or focus. To generate the kinetic curve, the radiologist traced a small region of interest (ROI) around what was perceived to be the most enhancing part of the lesion on the first postcontrast image. The plot of signal intensity vs. time for this ROI was assessed by the radiologist according to the BI-RADS® lexicon, which describes the "initial rise" (rapid, medium, slow) and "delayed phase" (persistent, plateau, washout) of the kinetic curve.

II.C. Simplified empirical mathematical model

The kinetic curve obtained above was analyzed quantitatively using a simplified empirical mathematical model (EMM). To implement the model, the average signal intensity as a function of time ($S(t)$) was first calculated in the selected ROI. Next, the relative signal changes after contrast injection were calculated: $\Delta S=(S_n-S_0)/S_0$, where S_0 is the average signal intensity in the precontrast scan, and S_n is the signal intensity at the nth postcontrast time point. Then $\Delta S(t)$ was fit to

$$\Delta S(t) = A\cdot(1-e^{-\alpha t})\cdot e^{-\beta t}, \tag{1}$$

where A is the upper limit of the signal intensity, α (min^{-1}) is the rate of signal increase, and β (min^{-1}) is the rate of the signal decrease during washout. This is a modified version of a more complicated five-parameter empirical mathematical model that has proven to be diagnostically useful.[12]

The 3D bilateral DCEMRI data were processed using software written in IDL (Research Systems, Inc., Boulder, CO). From the primary EMM parameters A, α and β, we derived kinetic parameters that are commonly used in the literature: iAUC$_{30}$, Slope$_{\text{ini}}$, T_{peak}, SER, κ_{peak}[9,34–38] which are described in Table I.

II.D. Data analysis and statistical evaluation

We compared the kinetic characteristics of benign and malignant lesions as evaluated by the BI-RADS® lexicon as well as the EMM. The kinetic characteristics of benign and malignant lesions within mass and nonmass lesions were compared: (i) benign vs. malignant mass lesions, and (ii) benign vs. malignant nonmass lesions. In addition, we also compared the kinetic characteristics of malignant mass vs. malignant nonmass lesions.

To compare the proportion of washout vs. plateau and persistent (or rapid vs. medium and slow) curves between benign and malignant lesions overall, as well as stratified by type of enhancement, we used the Pearson's χ^2 test for significance, with a p value of <0.05 indicating statistical significance.

After fitting the kinetic curve to the EMM the goodness of fit parameter R^2 was calculated for each lesion. Two-tailed unequal variance student's t-tests were performed to evaluate which EMM parameters showed significant differences between the benign and malignant breast lesions overall, as well as the subpopulations of mass and nonmass lesions. The Holm–Bonferroni correction method was applied to test for the multiple tests of significance.[39]

Receiver operating characteristic (ROC) analysis was performed to compare the diagnostic performance of the EMM parameters on mass lesions vs. nonmass lesions. ROCKIT

TABLE I. A list and description of the EMM parameters derived from the primary parameters A, α, and β.

Description	Equation
$iAUC_{30}$: Initial area under the kinetic curve at 30 s[a,b]	$iAUC_\tau = A\cdot[(1-e^{-\beta\tau})/\beta + (e^{-(\alpha+\beta)\tau}-1)/(\alpha+\beta)]$ Here we used $\tau = 30$ s.
$Slope_{ini}(min^{-1})$: Initial slope of the kinetic curve[a,c,d]	$Slope_{ini} \approx A\alpha$
T_{peak} (min): Time to peak enhancement[c]	$T_{peak} = 1/\alpha \log(1+\alpha/\beta)$ Note that when $\beta \leqslant 0$, the curves did not reach the peak within the duration of the experiment. In these cases, we used the last time point as T_{peak}.
κ_{peak}: Curvature at the peak of enhancement T_{peak}[c]	$\kappa_{peak} \approx -A\alpha\beta$
SER: Signal enhancement ratio[e]	$SER = \Delta S_1/\Delta S_L = e^{(t_L-t_1)\beta}\cdot(1-e^{-\alpha t_1})/(1-e^{-\alpha t_L})$ Here, $t_1 = 60$ s and $t_L = 300$ s used in this study. A SER value greater than 1.1 indicates the signal intensity decreases with respect to its value at 60 s; SER less than 0.9 indicates that signal intensity continues to rise; and SER between 0.9 and 1.1 represents a plateau relative to intensity at 60 s.

[a]Reference 34.
[b]Reference 35.
[c]Reference 36.
[d]Reference 37.
[e]Reference 38.

software (ROCKIT 0.9B Beta Version, Charles E. Metz, University of Chicago) was used to generate the ROC curves.

III. RESULTS

III.A. Qualitative (BI-RADS) kinetic findings

Of the 112 lesions, 70 were classified by the expert breast radiologist based on the BI-RADS lexicon as mass lesions, 44 of which were malignant and 26 benign; 38 were classified as nonmass lesions, with 31 malignant and seven benign. Of the remaining four focus lesions, two were benign and two malignant. In the subsequent analyses, focus lesions were excluded. The distribution of the BI-RADS® assessments of initial uptake and delayed phase for all malignant and benign lesions is shown in Table II. Overall, malignant lesions exhibited a substantially higher proportion of curves showing "rapid" initial rise, at 90% (69/77), compared with benign lesions, at 74% (26/35). Malignant and benign lesions also differed in delayed phase distribution with 65% (50/77) and 40% (14/35) classified as "washout" curves, respectively ($p = 0.023$).

The classification of initial rise and delayed phase for mass and nonmass lesions is also shown in Table II. The kinetic curves of 77% (34/44) of mass-like malignant lesions were classified as "washout," compared with 38% (10/26) of mass-like benign lesions ($p = 0.001$). Seventy three percent (19/26) of benign mass lesions showed "rapid" initial rise compared with 93% (41/44) of malignant mass lesions. However, we did not find a significant difference in the distribution of initial rise or delayed phase classification of nonmass malignant and nonmass benign lesions ($p > 0.65$).

III.B. Quantitative (EMM) kinetic findings

The EMM was able to accurately fit the curves, with a goodness of fit parameter R^2 greater than 0.90 for all lesions studied. Some examples of benign and malignant mass and

TABLE II. Distributions of BI-RADS® categories for the qualitative assessment of the initial rise and delayed phased of kinetic curves for benign and malignant lesions, as well as the subtypes of benign and malignant lesions considered here. There were two benign and two malignant lesions classified as focus type enhancement, which do not appear in the table below.

		Benign			Malignant		
		All ($n=35$)	Mass ($n=26$)	Nonmass ($n=7$)	All ($n=77$)	Mass ($n=44$)	Nonmass ($n=31$)
BIRADS® Initial rise	*Rapid*	**26**	19	5	**69**	41	27
	Medium	**8**	6	2	**6**	3	3
	Slow	**1**	1	0	**2**	0	1
BIRADS® Delayed phase	*Washout*	**14**	10	2	**50**	34	16
	Plateau	**15**	12	3	**19**	9	9
	Persistent	**6**	4	2	**8**	1	6

TABLE III. The primary and derived diagnostic parameters calculated from the EMM in malignant and benign lesions. Reported values are mean ± standard deviation of the sample for all cases. The *p* value after Student *t*-test is shown for each parameter, along with the required *p* value for significance according to the Holm–Bonferroni correction for multiple tests of significance. Numbers in bold indicate that there was a statistically significant difference between benign and malignant lesions, according to the Student's *t*-test and after using the Holm–Bonferroni correction for multiple comparisons.

EMM parameter	All Benign ($n=35$)	All Malignant ($n=77$)	*p* values	Required *p* value
A	4.2 ± 2.2	4.1 ± 2.2	$p=0.703$	$p=0.05$
α ($\mathbf{min^{-1}}$)	1.6 ± 1.1	2.1 ± 1.1	$p=0.047$	$p=0.01$
β ($\mathbf{min^{-1}}$)	0.045 ± 0.047	0.059 ± 0.061	$p=0.24$	$p=0.025$
$\mathbf{iAUC_{30}}$	0.55 ± 0.34	0.71 ± 0.54	$p=0.07$	$p=0.013$
$\mathbf{Slope_{ini}}$ ($\mathbf{min^{-1}}$)	6.1 ± 4.6	8.8 ± 8.4	$p=0.04$	$p=0.008$
[a]$\boldsymbol{T_{peak}}$ (**min**)	3.4 ± 1.8	2.7 ± 1.8	$p=0.12$	$p=0.017$
$\boldsymbol{\kappa_{peak}}$	-0.30 ± 0.48	-0.68 ± 1.19	$p=0.02$	$p=0.007$
SER	$\mathbf{0.88 \pm 0.31}$	$\mathbf{1.14 \pm 0.49}$	$\boldsymbol{p=0.001}$	$\boldsymbol{p=0.006}$

[a]For those curves which did not reach a peak within the duration of the experiment, we assumed a time to peak of 5 min.

nonmass lesions, along with the fitted kinetic curves, are shown in Fig. 1. After fitting the kinetic curves, the five derived parameters were calculated using the equations in Table I. The average values of all primary and derived parameters are displayed in Table III. *T*-test comparisons demonstrated a trend that malignant lesions had substantially faster contrast uptake (α) steeper initial slope ($\text{Slope}_{\text{ini}}$), larger enhancement ratio (SER) and sharper curvature (κ_{peak}) than benign lesions. However, after applying the Holm–Bonferroni correction for multiple comparisons,[39] only the parameter SER was significant, probably due to our database size.

All of the primary and derived EMM parameters α, β, T_{peak}, iAUC_{30}, SER, $\text{Slope}_{\text{ini}}$, and κ_{peak} except for A differed substantially between benign and malignant mass lesions (Fig. 2). That is, kinetic curves of malignant mass lesions, exhibited stronger contrast uptake (α, iAUC_{30}, $\text{Slope}_{\text{ini}}$), earlier peak enhancement (T_{peak}), and sharper, stronger washout (SER, κ_{peak}, β) compared with benign mass lesions. After applying the Holm–Bonferroni correction for multiple tests of significance only the parameters SER and T_{peak} were significant, likely due to our database size. However, for nonmass lesions, we found no statistical differences in any of the primary or derived EMM parameters for benign vs. malignant lesions ($p>0.51$ for all, Fig. 2). Considering malignant lesions only, those with mass-like enhancement had substantially larger A, β, iAUC_{30}, and $\text{Slope}_{\text{ini}}$ compared with malignant nonmass lesions, and after the Holm–Bonferroni correction only the parameter A remained significant ($p=0.004$).

ROC analysis was used to evaluate the diagnostic accuracy of the primary and derived EMM parameters. ROC curves were generated for each parameter separately among mass and nonmass lesions. The A_z values in mass lesions ranged from 0.54 (A) to 0.72 (SER), and in nonmass lesions from 0.52 (α) to 0.60 (A). For all parameters except for A, the A_z values were higher in mass lesions, but this was not significant ($p>0.19$), likely due to the small number of benign nonmass lesions considered. The ROC curves for these parameters are shown in Fig. 3.

IV. DISCUSSION

We have found that kinetic parameters have the potential to distinguish benign and malignant *mass* lesions more effectively, but failed to demonstrate usefulness in discriminating benign from malignant *nonmass* lesions. This trend was found both for the qualitative BI-RADS® and quantitative EMM measures of kinetics. Malignant mass lesions exhibited a higher proportion of washout type curves as well as a higher initial uptake (α, iAUC_{30}, $\text{Slope}_{\text{ini}}$) and faster, stronger washout (β, T_{peak}, SER, κ_{peak}) compared with benign mass lesions, although after accounting for multiple tests of significance only the differences in SER and T_{peak} were significant. Conversely, the kinetic characteristics of malignant and benign nonmass lesions appeared not to differ according to either the BI-RADS® lexicon or EMM. These results translated into diagnostic performance: the A_z values derived from ROC curves also demonstrated that the diagnostic performance of all EMM parameters except one (A) was improved in mass lesions. Among malignant lesions, the parameters A, β, iAUC_{30} and $\text{Slope}_{\text{ini}}$ differed between mass and nonmass lesions, and the parameter A was significant after correcting for multiple comparisons.

Kinetic curve shape is related to the perfusion, capillary permeability, and diffusion of contrast media from blood vessels to the extracellular space—these biological properties ultimately explain the differences between mass and nonmass lesions noted above. One important class of malignant lesions that most often displays nonmass-like enhancement is *in situ* lesions, in which neoplastic ductal epithelial cells remain confined to mammary ducts. The growth of vasculature associated with DCIS is not well understood. Guidi *et al.* showed an increase in vessel density around ducts with DCIS, although with variable patterns.[40] Heffelfinger found that the expression of angiogenic growth factors (such as VEGF) increases from hyperplasia to DCIS.[41,42] The physiology of DCIS is distinct from invasive ductal carcinoma (IDC), in which cancer cells have invaded the surrounding stroma with well-defined but infiltrative margins. The vasculature associated with IDC lesions is dense and leaky.[43,44] These physiological differences of DCIS and IDC lesions are likely related to the corresponding differences in MR presentation, in which IDC predominantly presents as a mass lesion on MRI.[17]

Although most DCIS lesions display a distinctive nonmass-like enhancement at MR imaging, they do not exhibit a consistent kinetic pattern. Unlike invasive cancers, the kinetic curves of DCIS lesions can often exhibit persistent signal increase, or signal intensity that plateaus over time.[13,14,16] Because of the variable kinetic pattern of DCIS lesions, some have suggested that kinetic information—specifically, the BI-RADS® qualitative assessment of de-

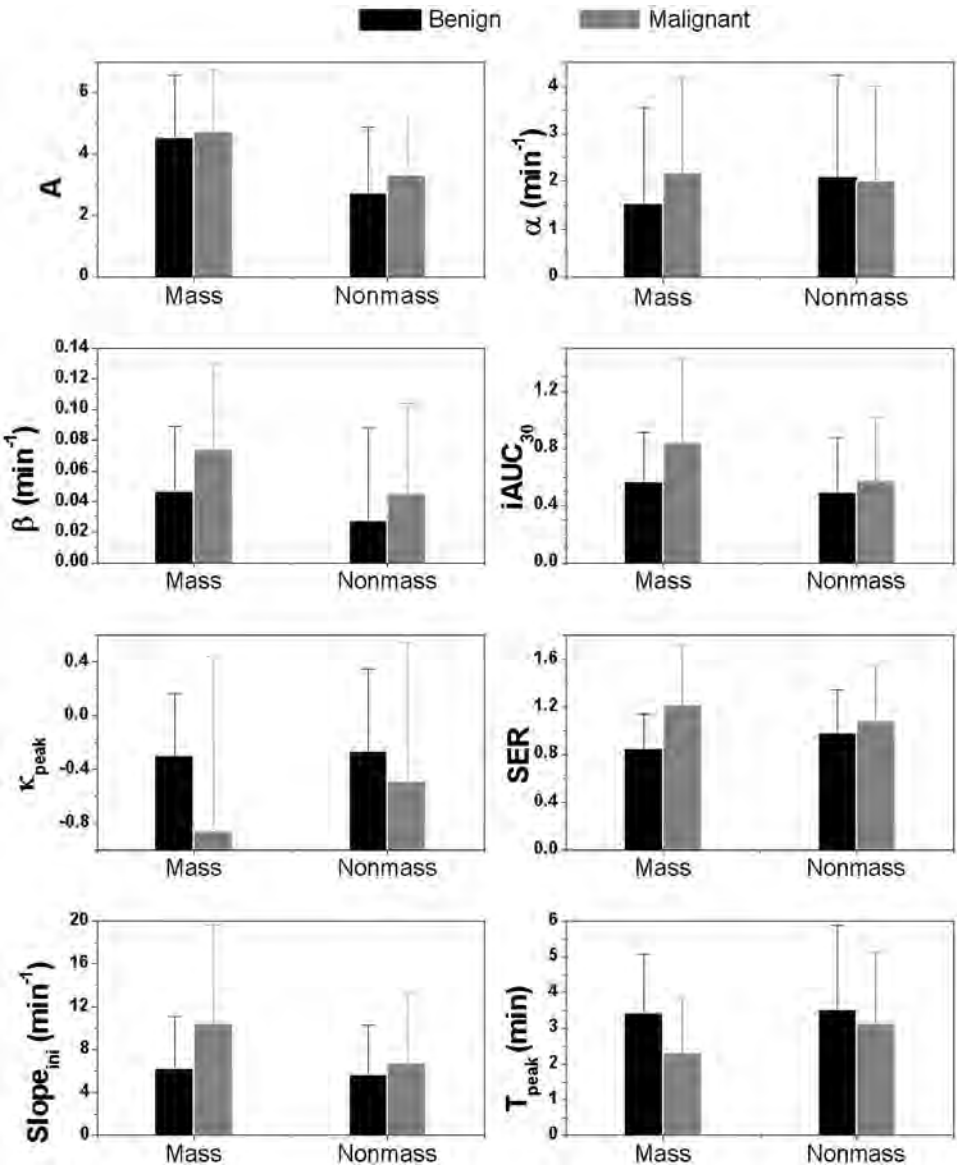

FIG. 2. The average value ± standard deviation for each EMM parameter in benign (white bars) and malignant (gray bars) lesions, stratified by type of enhancement as mass or nonmass. After correcting for multiple tests of significance, the parameters SER and T_{peak} demonstrated significant differences among malignant and benign mass lesions.

layed phase—is not useful in diagnosing DCIS lesions and instead, morphologic analysis should be favored.[45] Our results support this prior work, in that we have found large overlap in the kinetic characteristics of benign and malignant nonmass lesions. However, given that the physiological basis of enhancement is likely different in nonmass vs. mass lesions, it may be that new quantitative kinetic parameters need to be developed that are tailored for nonmass lesions. We found that malignant nonmass lesions exhibited significantly lower contrast uptake compared with malignant mass lesions; this underscores the importance of early imaging to distinguish nonmass lesions from enhancing normal parenchyma which has a similar nonmass morphology. Perhaps other imaging techniques may be important; recent work by Bartella *et al.* suggested that using proton spectroscopy to measure choline peaks yielded high sensitivity and specificity to malignant nonmass lesions.[29]

There are several limitations to this study.

- While the total number of lesions studied was relatively large, there were only seven nonmass-like benign lesions, which may be too small to perform reliable comparisons of the subtypes of benign and malignant lesions presented here. It is important to verify the results of this pilot study in a larger number of patients. In particular, because of the multiple parameters calculated in this study, the Holm–Bonferroni correction reduced the statistical significance of our findings. With larger numbers of lesions, this may no longer be the case.
- 40% of benign lesion kinetic curves were classified as washout, which is higher than many reports. The benign lesions considered were suspicious enough to warrant biopsy. Since most obviously benign lesions exhibit persistent type kinetic curves and would not be sent to biopsy, this may skew the delayed phase distribution in this study away from the persistent curve type. However, in other studies, where only histologically proven benign lesions were considered, comparable values were found.[36]

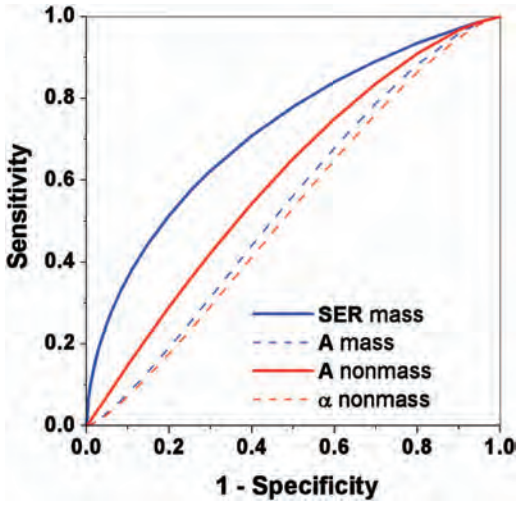

FIG. 3. Fitted binormal ROC curves generated by the ROCKIT software are shown for the EMM parameters with the highest, and lowest, A_z values in mass and nonmass lesions. SER (solid blue line) and A (solid red line) had the highest A_z values in mass and nonmass lesions, respectively. A (dashed blue line) and α (dashed red line) had the lowest A_z values in mass and nonmass lesions, respectively.

- The placement and size of the ROI was determined manually, and only one small ROI was used to characterize the whole lesion. This single ROI may not capture the heterogeneity of kinetic enhancement patterns in the lesion. In addition, partial volume effects may compromise the accuracy of the kinetic curve, especially in lesions with nonmass-like enhancement. It is possible that partial volume effects produce the observed differences between mass and nonmass lesion. Furthermore, in our study the ROI was selected by one single radiologist. It is likely that other radiologists may select slightly different ROIs, which in turn would affect the kinetic curve of the lesion. Future studies should be performed to test the results of this pilot study both with increased numbers of lesions and more observers.
- Although the EMM fit the curves very well, sparse sampling of the kinetic curve may result in more fitting errors in the uptake phase. In addition, preclinical studies suggest that specificity of the EMM is improved when the tail of the washout curve is sampled for at least 15 min; the curves studied here were truncated at approximately 6 min.[9,12]

Despite these shortcomings, as a pilot study our results suggest that current kinetic analysis may not be effective in nonmass lesions, while it may be effective in mass lesions, and that the enhancement kinetics of malignant nonmass and mass lesions are different. If the results of this study are validated in a larger trial, we expect that it may be useful in computer aided detection and diagnosis (CAD) algorithms. By training classifiers on mass and nonmass lesions separately, it may be that (i) detection of nonmass lesions could be improved by choosing accurate thresholds, (ii) the probability of malignancy in mass lesions may be improved, and (iii) new kinetic parameters that are diagnostically effective in cases of nonmass-like enhancement may be discovered. Future work will focus on a larger group of lesions with detailed pathology analysis, to investigate new parameters targeted at nonmass lesions. In addition, pixel by pixel analysis, acquiring high spatial/temporal resolution of MR images, or following the later phase of the kinetic curves for a longer time, could be used to help improve the differentiation of nonmass malignant from nonmass benign lesions.

ACKNOWLEDGMENTS

The authors would like to thank the Segal Foundation, the Biological Sciences Division at the University of Chicago, DOD Grant No. W81XWH-06-1-0329 and NIH Grant No. R21 CA104774-01 A2 and 2 R01 CA078803-05A2 for financial support.

[a]Author to whom correspondence should be addressed; electronic mail: gnewstead@radiology.bsd.uchicago.edu

[1]D. C. Abraham, R. C. Jones, S. E. Jones, J. H. Cheek, G. N. Peters, S. M. Knox, M. D. Grant, D. W. Hampe, D. A. Savino, and S. E. Harms, "Evaluation of neoadjuvant chemotherapeutic response of locally advanced breast cancer by magnetic resonance imaging," Cancer **78**, 91–100 (1996).
[2]C. Boetes, R. D. Mus, R. Holland, J. O. Barentsz, S. P. Strijk, T. Wobbes, J. H. Hendriks, and S. H. Ruys, "Breast tumors: Comparative accuracy of MR imaging relative to mammography and US for demonstrating extent," Radiology **197**, 743–747 (1995).
[3]C. K. Kuhl and H. H. Schild, "Dynamic image interpretation of MRI of the breast," J. Magn. Reson Imaging **12**, 965–974 (2000).
[4]W. Chen, M. L. Giger, U. Bick, and G. M. Newstead, "Automatic identification and classification of characteristic kinetic curves of breast lesions on DCE-MRI," Med. Phys. **33**, 2878–2887 (2006).
[5]G. O. Cron, F. Kelcz, and G. E. Santyr, "Improvement in breast lesion characterization with dynamic contrast-enhanced MRI using pharmacokinetic modeling and bookend T(1) measurements," Magn. Reson. Med. **51**, 1066–1070 (2004).
[6]P. Armitage, C. Behrenbruch, M. Brady, and N. Moore, "Extracting and visualizing physiological parameters using dynamic contrast-enhanced magnetic resonance imaging of the breast," Med. Image Anal. **9**, 315–329 (2005).
[7]E. Furman-Haran, E. Schechtman, F. Kelcz, K. Kirshenbaum, and H. Degani, "Magnetic resonance imaging reveals functional diversity of the vasculature in benign and malignant breast lesions," Cancer **104**, 708–718 (2005).
[8]P. S. Tofts, B. Berkowitz, and M. D. Schnall, "Quantitative analysis of dynamic Gd-DTPA enhancement in breast tumors using a permeability model," Magn. Reson. Med. **33**, 564–568 (1995).
[9]X. Fan, M. Medved, G. S. Karczmar, C. Yang, S. Foxley, S. Arkani, W. Recant, M. A. Zamora, H. Abe, and G. M. Newstead, "Diagnosis of suspicious breast lesions using an empirical mathematical model for dynamic contrast-enhanced MRI," Magn. Reson. Imaging **25**, 593–603 (2007).
[10]E. V. Heiberg, W. H. Perman, V. M. Herrmann, and C. G. Janney, "Dynamic sequential 3D gadolinium-enhanced MRI of the whole breast," Magn. Reson. Imaging **14**, 337–348 (1996).
[11]P. Hayton, M. Brady, L. Tarassenko, and N. Moore, "Analysis of dynamic MR breast images using a model of contrast enhancement," Med. Image Anal. **1**, 207–224 (1997).
[12]X. Fan, M. Medved, J. N. River, M. Zamora, C. Corot, P. Robert, P. Bourrinet, M. Lipton, R. M. Culp, and G. S. Karczmar, "New model for analysis of dynamic contrast-enhanced MRI data distinguishes metastatic from nonmetastatic transplanted rodent prostate tumors," Magn. Reson. Med. **51**, 487–494 (2004).
[13]S. A. Jansen, G. Newstead, H. Abe, A. Shimauchi, R. Schmidt, and G. S. Karczmar, "MR imaging of pure ductal carcinoma in situ: Kinetics, morphology and comparison with mammographic presentation and nuclear grade," Radiology **245**, 684–691 (2007).

[14]H. Neubauer, M. Li, R. Kuehne-Heid, A. Schneider, and W. A. Kaiser, "High grade and non-high grade ductal carcinoma in situ on dynamic MR mammography: Characteristic findings for signal increase and morphological pattern of enhancement," Br. J. Radiol. **76**, 3–12 (2003).
[15]J. H. Menell, E. A. Morris, D. D. Dershaw, A. F. Abramson, E. Brogi, and L. Liberman, "Determination of the presence and extent of pure ductal carcinoma in situ by mammography and magnetic resonance imaging," Breast J. **11**, 382–390 (2005).
[16]M. Van Goethem, K. Schelfout, E. Kersschot, C. Colpaert, J. Weyler, I. Verslegers, I. Biltjes, A. De Schepper, and P. M. Parizel, "Comparison of MRI features of different grades of DCIS and invasive carcinoma of the breast," Jbr-Btr **88**, 225–232 (2005).
[17]C. Kuhl, "The current status of breast MR imaging. Part I. Choice of technique, image interpretation, diagnostic accuracy, and transfer to clinical practice," Radiology **244**, 356–378 (2007).
[18]A. Recht, E. J. Rutgers, I. S. Fentiman, J. M. Kurtz, R. E. Mansel, and J. P. Sloane, "The fourth EORTC DCIS Consensus meeting (Chateau Marquette, Heemskerk, The Netherlands, 23–24 January 1998)—conference report," Eur. J. Cancer **34**, 1664–1669 (1998).
[19]T. Suzuki, M. Toi, S. Saji, K. Horiguchi, T. Aruga, E. Suzuki, S. Horiguchi, N. Funata, K. Karasawa, and N. Kamata, "Early breast cancer," Int. J. Clin. Oncol. **11**, 108–119 (2006).
[20]C. K. Kuhl, S. Schrading, H. B. Bieling, E. Wardelmann, C. C. Leutner, R. Koenig, W. Kuhn, and H. H. Schild, "MRI for diagnosis of pure ductal carcinoma in situ: A prospective observational study," Lancet **370**, 485–492 (2007).
[21]P. Viehweg, D. Lampe, J. Buchmann, and S. H. Heywang-Kobrunner, "In situ and minimally invasive breast cancer: Morphologic and kinetic features on contrast-enhanced MR imaging," Magn. Reson. Mater. Phys., Biol., Med. **11**, 129–137 (2000).
[22]R. Gilles, B. Zafrani, J. M. Guinebretiere, M. Meunier, O. Lucidarme, A. A. Tardivon, F. Rochard, D. Vanel, S. Neuenschwander, and R. Arriagada, "Ductal carcinoma in situ: MR imaging-histopathologic correlation," Radiology **196**, 415–419 (1995).
[23]A. Shiraishi, Y. Kurosaki, T. Maehara, M. Suzuki, and M. Kurosumi, "Extension of ductal carcinoma in situ: Histopathological association with MR imaging and mammography," Magn. Reson. Med. Sci. **2**, 159–163 (2003).
[24]A. P. Schouten van der Velden, C. Boetes, P. Bult, and T. Wobbes, "The value of magnetic resonance imaging in diagnosis and size assessment of in situ and small invasive breast carcinoma," Am. J. Surg. **192**, 172–178 (2006).
[25]S. G. Orel, "MR imaging of the breast," Radiol. Clin. North Am. **38**, 899–913 (2000).
[26]J. M. Lee, J. B. Kaplan, M. P. Murray, M. Mazur-Grbec, T. Tadic, D. Stimac, and L. Liberman, "Underestimation of DCIS at MRI-guided vacuum-assisted breast biopsy," AJR, Am. J. Roentgenol. **189**, 468–474 (2007).
[27]K. J. Macura, R. Ouwerkerk, M. A. Jacobs, and D. A. Bluemke, "Patterns of enhancement on breast MR images: Interpretation and imaging pitfalls," Radiographics **26**, 1719–1734; quiz 1719 (2006).
[28]D. Saslow, C. Boetes, W. Burke, S. Harms, M. O. Leach, C. D. Lehman, E. Morris, E. Pisano, M. Schnall, S. Sener, R. A. Smith, E. Warner, M. Yaffe, K. S. Andrews, and C. A. Russell, "American Cancer Society guidelines for breast screening with MRI as an adjunct to mammography," Ca-Cancer J. Clin. **57**, 75–89 (2007).
[29]L. Bartella, S. B. Thakur, E. A. Morris, D. D. Dershaw, W. Huang, E. Chough, M. C. Cruz, and L. Liberman, "Enhancing nonmass lesions in the breast: Evaluation with proton (1H) MR spectroscopy," Radiology **245**, 80–87 (2007).
[30]L. Bartella, L. Liberman, E. A. Morris, and D. D. Dershaw, "Nonpalpable mammographically occult invasive breast cancers detected by MRI," AJR, Am. J. Roentgenol. **186**, 865–870 (2006).
[31]M. A. van den Bosch, B. L. Daniel, M. N. Mariano, K. N. Nowels, R. L. Birdwell, K. J. Fong, P. S. Desmond, S. Plevritis, L. A. Stables, M. Zakhour, R. J. Herfkens, and D. M. Ikeda, "Magnetic resonance imaging characteristics of fibrocystic change of the breast," Invest. Radiol. **40**, 436–441 (2005).
[32]L. Liberman, E. A. Morris, D. D. Dershaw, A. F. Abramson, and L. K. Tan, "Ductal enhancement on MR imaging of the breast," AJR, Am. J. Roentgenol. **181**, 519–525 (2003).
[33]L. Liberman, E. A. Morris, M. J. Lee, J. B. Kaplan, L. R. LaTrenta, J. H. Menell, A. F. Abramson, S. M. Dashnaw, D. J. Ballon, and D. D. Dershaw, "Breast lesions detected on MR imaging: Features and positive predictive value," AJR, Am. J. Roentgenol. **179**, 171–178 (2002).
[34]P. J. Moate, L. Dougherty, M. D. Schnall, R. J. Landis, and R. C. Boston, "A modified logistic model to describe gadolinium kinetics in breast tumors," Magn. Reson. Imaging **22**, 467–473 (2004).
[35]J. L. Evelhoch, "Key factors in the acquisition of contrast kinetic data for oncology," J. Magn. Reson Imaging **10**, 254–259 (1999).
[36]B. K. Szabo, P. Aspelin, M. K. Wiberg, and B. Bone, "Dynamic MR imaging of the breast. Analysis of kinetic and morphologic diagnostic criteria," Acta Radiol. **44**, 379–386 (2003).
[37]L. D. Buadu, J. Murakami, S. Murayama, N. Hashiguchi, S. Sakai, K. Masuda, S. Toyoshima, S. Kuroki, and S. Ohno, "Breast lesions: Correlation of contrast medium enhancement patterns on MR images with histopathologic findings and tumor angiogenesis," Radiology **200**, 639–649 (1996).
[38]L. Esserman, N. Hylton, T. George, and N. Weidner, "Contrast-enhanced magnetic resonance imaging to assess tumor histopathology and angiogenesis in breast carcinoma," Breast J. **5**, 13–21 (1999).
[39]S. Holm, "A simple sequentially rejective multiple test procedure," Scand. J. Stat. **6**, 65–70 (1979).
[40]A. J. Guidi, L. Fischer, J. R. Harris, and S. J. Schnitt, "Microvessel density and distribution in ductal carcinoma in situ of the breast," J. Natl. Cancer Inst. **86**, 614–619 (1994).
[41]S. C. Heffelfinger, M. A. Miller, R. Yassin, and R. Gear, "Angiogenic growth factors in preinvasive breast disease," Clin. Cancer Res. **5**, 2867–2876 (1999).
[42]S. C. Heffelfinger, R. Yassin, M. A. Miller, and E. Lower, "Vascularity of proliferative breast disease and carcinoma in situ correlates with histological features," Clin. Cancer Res. **2**, 1873–1878 (1996).
[43]A. Rice and C. M. Quinn, "Angiogenesis, thrombospondin, and ductal carcinoma in situ of the breast," J. Clin. Pathol. **55**, 569–574 (2002).
[44]E. Furman-Haran, F. Kelcz, and H. Degani, "Magnetic resonance imaging of breast cancer angiogenesis: A review," J. Eval Clin. Pract. **21**, 47–54 (2002).
[45]S. E. Harms, "The use of breast magnetic resonance imaging in ductal carcinoma in situ," Breast J. **11**, 379–381 (2005).

IOP PUBLISHING PHYSICS IN MEDICINE AND BIOLOGY

Phys. Med. Biol. **53** (2008) 5481–5493 doi:10.1088/0031-9155/53/19/014

Detection of *in situ* mammary cancer in a transgenic mouse model: *in vitro* and *in vivo* MRI studies demonstrate histopathologic correlation

S A Jansen[1], S D Conzen[2], X Fan[1], T Krausz[3], M Zamora[1], S Foxley[1], J River[1], G M Newstead[1] and G S Karczmar[1]

[1] Department of Radiology, The University of Chicago, 5841 S Maryland Avenue, MC 2026, Chicago, IL 60637, USA
[2] Department of Medicine & The Ben May Department for Cancer Research, The University of Chicago, 5841 S Maryland Ave, MC 2115, Chicago, IL 60637, USA
[3] Department of Pathology, The University of Chicago, 5841 S Maryland Avenue, MC 6101, Chicago, IL 60637, USA

E-mail: gskarczm@uchicago.edu

Received 24 January 2008, in final form 9 June 2008
Published 9 September 2008
Online at stacks.iop.org/PMB/53/5481

Abstract

Improving the prevention and detection of preinvasive ductal carcinoma *in situ* (DCIS) is expected to lower both morbidity and mortality from breast cancer. Transgenic mouse models can be used as a 'test bed' to develop new imaging methods and to evaluate the efficacy of candidate preventive therapies. We hypothesized that despite its microscopic size, early murine mammary cancer, including DCIS, might be accurately detected by MRI. C3(1) SV40 TAg female mice ($n = 23$) between 10 and 18 weeks of age were selected for study. Eleven mice were subjected to *in vitro* imaging using a T_2-weighted spin echo sequence and 12 mice were selected for *in vivo* imaging using a T_1-weighted gradient echo, a T_2-weighted spin echo and high spectral and spatial resolution imaging sequences. The imaged glands were carefully dissected, formalin fixed and paraffin embedded, and then H&E stained sections were obtained. The ratio of image-detected versus histologically detected cancers was obtained by reviewing the MR images and H&E sections independently and using histology as the gold standard. MR images were able to detect 12/12 intramammary lymph nodes, 1/1 relatively large (∼5 mm) tumor, 17/18 small (∼1 mm) tumors and 13/16 ducts distended with DCIS greater than 300 μm. Significantly, there were no false positives—i.e., image detection always corresponded to a histologically detectable cancer in this model. These results indicate that MR imaging can reliably detect both preinvasive *in situ* and early invasive mammary cancers in mice with high sensitivity. This technology is an important step toward the more effective

use of non-invasive imaging in pre-clinical studies of breast cancer prevention, detection and treatment.

(Some figures in this article are in colour only in the electronic version)

Introduction

Women diagnosed with breast cancer today have significantly better survival outcomes compared with their counterparts 30 years ago (Jemal *et al* 2004). This is attributed to improvements in treatment as well as improved detection of early stage cancer due to screening mammography (Berry *et al* 2005). Currently, 15–25% of newly diagnosed breast cancers are preinvasive ductal carcinoma *in situ* (DCIS) (Tsikitis and Chung 2006), and with improvements in imaging these percentages are likely to increase. Women diagnosed with DCIS have the best prognosis with long-term survival rates of 97–99% (Morrow *et al* 2002). Half of all newly diagnosed invasive carcinomas are stage I, which is the earliest form of invasive breast cancer and does not involve metastatic spread to the lymph nodes (Li *et al* 2003). Some have suggested that improving the detection of early cancers is essential for further decreasing mortality rates (Duffy *et al* 2003). Thus, to help increase survival rates it is clearly essential to improve detection and effective treatment of early breast cancer.

Dynamic contrast-enhanced MR imaging (DCEMRI) of the breast has been shown to improve the detection of early stage invasive cancers, and has recently been recommended by the American Cancer Society for the screening of women at high risk for developing breast cancer (Saslow *et al* 2007). However, initial reports studying the presentation of DCIS on DCEMRI found poorer sensitivity and specificity compared with x-ray mammography (Gilles *et al* 1995, Menell *et al* 2005, Orel *et al* 1997, Schouten van der Velden *et al* 2006). Although recent work has demonstrated that the sensitivity of DCEMRI for DCIS is increasing (Kuhl *et al* 2007), there is clearly room for improvement in diagnostic accuracy. It is anticipated that studies of the physiological and biological characteristics of early breast cancers will help improve imaging methods and analysis, because these insights will help to guide imaging approaches to find physiologically abnormal tissues seen in cancer.

Due to the urgency of surgery in early human breast cancer, studies of the natural history of such cancers in patients are difficult to perform. Therefore, transgenic and xenografted mouse models of breast cancer are widely used to investigate the biological basis of human breast cancer, to evaluate new therapies and to develop improved imaging methods. The usefulness of these mouse models depends on how closely they resemble human breast cancer. This is one reason why transgenic mouse models are appealing and have led to improvements in detection and treatment of cancers: the tumors arise without additional carcinogens and the early tumors progress through the stages of disease, i.e. from *in situ* to invasive, closely mimicking their human counterpart. If mice are to be used as successful models of human cancer biology, then imaging methods that detect *in situ* tumors are required to accurately assess preventive, diagnostic and therapeutic interventions. To date, however, there have been no reports of *in vivo* imaging of *in situ* or even nonpalpable invasive mammary gland cancers in mice (Abbey *et al* 2004, Artemov *et al* 2003, Bremer *et al* 2005, Galie *et al* 2004, Geninatti Crich *et al* 2006, Hsueh *et al* 2006, Jenkins *et al* 2005, Robinson *et al* 2003, Rodrigues *et al* 2004, 2006, Seemann *et al* 2006, Tian *et al* 2003). In fact, most imaging studies of mouse mammary cancer have focused on large tumors that are extremely advanced. Relative

to DCIS and early invasive cancers, these more advanced cancers are not realistic models of the majority of newly diagnosed breast cancers in women.

In this project, our goal was to determine whether MR imaging of early murine mammary cancer, including *in situ* carcinoma, is feasible. We studied the SV40 Tag transgenic mouse model of breast cancer in which mammary cancer develops at about 16 weeks and progresses through histological stages that are similar to human breast cancer progression. We developed our imaging technique by first detecting microscopic cancers *ex vivo* in excised mammary glands. We then were able to successfully advance to *in vivo* imaging of *in situ* carcinoma in living animals.

Materials and methods

Animals

Twenty-three C3(1) SV40 large T antigen (Tag) transgenic mice were used for MR imaging (Maroulakou *et al* 1994). This mouse model targets expression of large Tag to the female mammary gland via the C3(1) promoter. Female mice develop mammary cancer that resembles human ductal breast carcinoma, including progression through atypical ductal hyperplasia (∼8 weeks), DCIS (∼12 weeks) and IDC (∼16 weeks) (Green *et al* 2000). Eleven of the 23 mice were selected for *in vitro* imaging, and the remaining 12 for *in vivo* imaging. All procedures were carried out in accordance with our institution's Animal Care and Use Committee approval. Animals were anesthetized prior to imaging experiments, and anesthesia was maintained during imaging at 1.5% isoflorane. Body temperature was maintained with a warm air blower. The temperature, heart rate and respiration rate were monitored with data taken every minute and the signal from the respiration sensor was used to obtain gated images.

MRI experiments

Imaging was performed with a Bruker 4.7 tesla magnet equipped with a self-shielded gradient set that delivers maximum gradient strength of 20 Gauss cm^{-1}.

In vitro. A homebuilt 6-leg low-pass half-open birdcage coil (3 cm length $\times$ 2 cm width $\times$ 1 cm height) was built for mammary gland *in vitro* imaging using a multi-slice multiple spin-echo sequence (rapid acquisition with refocused echoes (RARE) (Friedburg *et al* 1987), four RARE partitions, TR/TE: 4000/50 ms, field of view (FOV) = 3.0 $\times$ 1.5 cm, number of excitations (NEX) = 2, slice thickness = 0.75 mm and inplane resolution = 117 μm). Twenty-two excised and fixed inguinal mammary gland specimens were imaged from 11 mice between 8 and 22 weeks of age. Inguinal mammary glands are *l*-shaped with a typical size of 2 cm $\times$ 2 cm and 2–3 mm thick, unless a larger tumor is present. For MR imaging, the glands were laid flat in the coil and three to seven slices were obtained from the top down.

In vivo. Another homebuilt 8-leg low-pass half-open birdcage coil (3 cm length $\times$ 3 cm width $\times$ 2 cm height) that produced high flux density in the mammary gland (Fan *et al* 2006) was used for *in vivo* imaging. Several pulse sequences were evaluated. Initially, two sets of multislice gradient-recalled echo (GRE) images were obtained (TR/TE: 675/7 ms, FOV = 3.0 $\times$ 3.0 cm, matrix size = 256 $\times$ 256, NEX = 2, slices = 21, slice thickness = 0.5 mm, in-plane resolution = 117 μm and flip angle = 30°) across the entire sensitive volume of the coil to map out the whole gland. Based on this initial evaluation,

six to ten slices that contained structures of interest (i.e., candidate cancers) were evaluated further: (i) GRE with fat suppression (same imaging parameters as above), (ii) spin-echo (SE) images (multi-slice RARE, TR/TE: 3000/29 ms, RARE acceleration factor = 4, FOV = 3.0 × 3.0 cm, matrix size = 256 × 256, NEX = 2, slice thickness = 0.5 mm and in-plane resolution = 117), (iii) SE with fat suppression. Finally, in order to improve fat suppression, high spectral and spatial (HiSS) resolution imaging was obtained of a single slice (using echo-planar spectroscopic imaging (EPSI) (Mansfield 1984) with a spectral resolution of ∼6 Hz, FOV = 3.0 × 3.0 cm, matrix size = 256 × 256, number of echoes = 32, NEX = 2, slices = 1, slice thickness = 0.5 mm and in-plane resolution = 117 μm). The HiSS method has been detailed in prior work (Du *et al* 2005); briefly, HiSS acquisitions sample the entire free induction decay in each voxel, and after processing water peak-height images can be displayed—this provides complete fat suppression. With a typical mouse respiration rate of less than 1 s under anesthesia (equivalent to TR ∼900 ms), the time required for each set of gated GRE images was approximately 7.5 min (5.8 min without gating), and for each set of gated SE images approximately 6.5 min (6.4 min without gating). Finally, it took approximately 7.5 min to acquire one slice using HiSS (approximately 6.8 min non-gated), which is considerably less efficient than the GRE acquisition that acquired many more slices in the same amount of time. The total experiment time was approximately 1.5 h.

The inguinal mammary glands on the left side of 12 mice between the ages of 10 and 18 weeks were selected for imaging. To facilitate spatial correlations between MR images and histology (below), a fine polyethylene mesh ∼3.0 cm × 2.0 cm in size with 3.0 mm spacing was embedded in partially deuterated agar and wrapped around each mouse. It also served to eliminate the air–tissue interface near the mammary gland, which is expected to reduce susceptibility artifacts.

Correlation of MRI with histology

Hematoxylin and eosin (H&E) stained sections of the imaged mammary glands were obtained (5 μm thick H&E sections every 50 μm) and evaluated by an experienced breast and mouse mammary gland pathologist (TK). Intramammary lymph nodes, invasive tumors and ducts distended with DCIS with diameters greater than 300 μm were identified and used as the gold standard. For the *in vitro* study, the H&E stained sections were acquired in the same orientation as the MR images and thus the two were easily compared, after being reviewed independently. For the *in vivo* study, the agar grid served as a coordinate system of fiducial markers with which to compare the H&E stained sections of the whole gland with axial MR images, which represent cross-sectional slices through the mammary gland. During imaging, the agar grid was wrapped around the mouse and the grid positions were marked on the skin. After excision and H&E staining, the mammary glands maintained the same orientation relative to these skin markers since they remained attached to the skin throughout. We were thus able to infer the grid coordinates of cancers found on the H&E sections. In addition, the agar grid was MR-visible; the grid coordinates of candidate lesions could therefore be determined directly from the MR images. To determine the sensitivity of MRI: (i) one representative H&E section was selected per mouse and the grid coordinates of cancers were noted by an experienced pathologist, (ii) the MR images were reviewed independently by a separate reader, and grid coordinates of candidate lesions were noted, (iii) using histology as the gold-standard for diagnosis, the locations of cancers found on the H&E section were compared with the location of lesions detected by MRI, and the ratio of MR-detected versus H&E confirmed cancers was calculated.

Image analysis

The signal-to-noise ratio (SNR) of lymph nodes, DCIS and invasive tumors was calculated in the GRE and RARE SE images as follows:

$$\mathrm{SNR} = \frac{\overline{S}}{\sigma_{\mathrm{noise}}},$$

where $\overline{S}$ is the average signal intensity in a region of interest (ROI) drawn around the lesion or lymph node, and σ_{noise} was averaged from the standard deviations of signal intensities measured in a 0.5 cm $\times$ 0.5 cm ROI drawn in the lower left and right corners of the image. In addition, the contrast-to-noise ratio (CNR) of lymph nodes, DCIS and invasive tumors was calculated relative to muscle and normal mammary glandular tissue (MGT) as follows:

$$\mathrm{CNR}_{\mathrm{lesion-muscle}} = \mathrm{SNR}_{\mathrm{lesion}} - \mathrm{SNR}_{\mathrm{muscle}}$$
$$\mathrm{CNR}_{\mathrm{lesion-MGT}} = \mathrm{SNR}_{\mathrm{lesion}} - \mathrm{SNR}_{\mathrm{MGT}}.$$

Lesion morphology. The morphology of the lesions and lymph nodes detected by *in vivo* noncontrast MRI was analyzed using descriptors analogous to those used for clinical contrast-enhanced breast MRI of women. For clinical examinations, the Breast Imaging-Reporting and Data System (BI-RADS) lexicon classifies the type, shape, margins and enhancement pattern of the lesion (ACR 2003). Although contrast was not used in our study, the morphology of the lesions was classified using an approach analogous to a simplified version of the BI-RADS lexicon as follows: type (mass or non-mass), shape/distribution (for mass lesions: round, oval, lobular or irregular; for non-mass lesions: linear, ductal or segmental), margins (for mass lesions only: smooth or irregular) and pattern (for mass lesions: homogeneous or heterogeneous; for nonmass lesions: homogeneous, stippled or clumped).

Results

In vitro MRI

H&E stained sections were obtained from six of the 22 excised mammary gland specimens. Analysis of the histologic slides confirmed that many stages of the development of mammary carcinoma were present in the specimens, including DCIS, small invasive tumors (<3 mm) and large tumors (>3 mm). Figure 1 shows four representative examples of the correlation between RARE SE MR images and histology. After reviewing the MR images and H&E sections separately using the pathologist's report as the gold standard for cancer diagnosis, it can be seen that the MR images matched the H&E stained sections, demonstrating intramammary lymph nodes, DCIS and both large and small invasive tumors. Review of the MR images of all 22 excised specimens demonstrated 6 large tumors (>3 mm), 30 small tumors (<3 mm), 32 DCIS lesions and 22 lymph nodes.

In vivo MRI

An *in vivo* MR image of a normal mammary gland is shown in figures 2(a) and (b), demonstrating that after fat suppression the signal from the background mammary gland decreases. However, careful inspection reveals a diffuse background signal that may be due to normal parenchyma. Figures 2(c) and (d) also demonstrate the procedure used

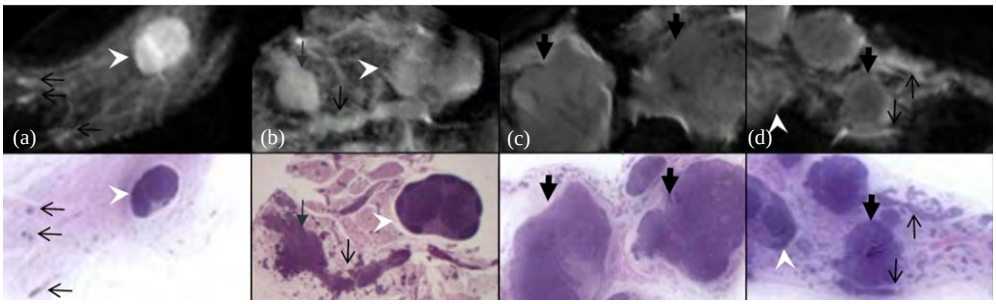

Figure 1. *In vitro* MR images (RARE SE) with corresponding H&E stained sections of the different stages of mammary cancer. For each MR image, the display FOV is 0.8 × 0.48 cm. White arrowheads point to lymph nodes, thin black arrows to DCIS and thick black arrows to invasive tumors. The lymph nodes here are approximately 2–3 mm in size, while invasive tumors range from approximately 2–4 mm in size. The ducts distended with DCIS range from one to a few hundred microns in diameter. In (a) approximately 120 μm ducts with very early DCIS are detected. In (b) the ducts are now distended further with DCIS to a few hundred microns in diameter, and an area of microinvasion—i.e., where the cancer cells have penetrated through the basement membrane—is evident (thin gray arrow). This marks the beginning of the transition from *in situ* to invasive carcinoma. In (c) two relatively large ∼4 mm invasive tumors are shown. In (d) smaller ∼2 mm invasive tumors and DCIS are demonstrated.

in this study to correlate MR images with histology using the agar grid. We found that DCIS and early invasive tumors appeared clearly against a darker background of mammary glandular tissue/fat. DCIS lesions were typically a few millimeters in length and 0.5 mm wide, while invasive tumors were small and round. Two representative examples illustrating the correlation between axial GRE MR images and histology are shown in figure 3. The MR images correlated well with the corresponding H&E stained sections of the mammary glands. H&E stained sections were obtained from the inguinal glands of all of the 12 mice selected for *in vivo* MR imaging. Based on the histologic review of the pathologist, there were 12 lymph nodes, one large (∼5 mm) tumor, 18 small nonpalpable tumors ∼0.5–3 mm in size and 16 ducts distended with DCIS greater than 300 μm in diameter. The sensitivity of GRE imaging was 100% for lymph nodes (12/12); 100% for tumors larger than 5 mm (1/1); 94% for small tumors 0.5–3 mm in size (17/18); and 81% for DCIS (13/16). Significantly, there were no false positives—i.e., an MR finding corresponded to cancer in all glands examined. Three more examples of early murine mammary cancer are shown in figure 4.

The GRE images with fat suppression provided the clearest images of early murine mammary cancer. In comparison, T_2-weighted RARE images with and without fat suppression did not depict the cancers or lymph nodes well, as shown for one case in figure 5. This qualitative observation was validated by calculations of SNR and CNR, as shown in table 1. For GRE images with fat suppression, the average SNR of lymph nodes, tumors and DCIS lesions were comparable to each other and to muscle, but were three to four times higher than normal mammary gland tissue. The average SNR of lymph nodes, tumors and DCIS lesions in RARE SE images with fat suppression were higher than muscle. However, unlike GRE images, RARE SE images of early murine mammary cancers and lymph nodes had comparable SNR to the normal mammary gland tissue. Thus, because of the high background signal of the mammary gland tissue, early cancer was not well-visualized on RARE SE images. In contrast, HiSS water peak-height images provided excellent lesion visualization with complete fat suppression (figure 5).

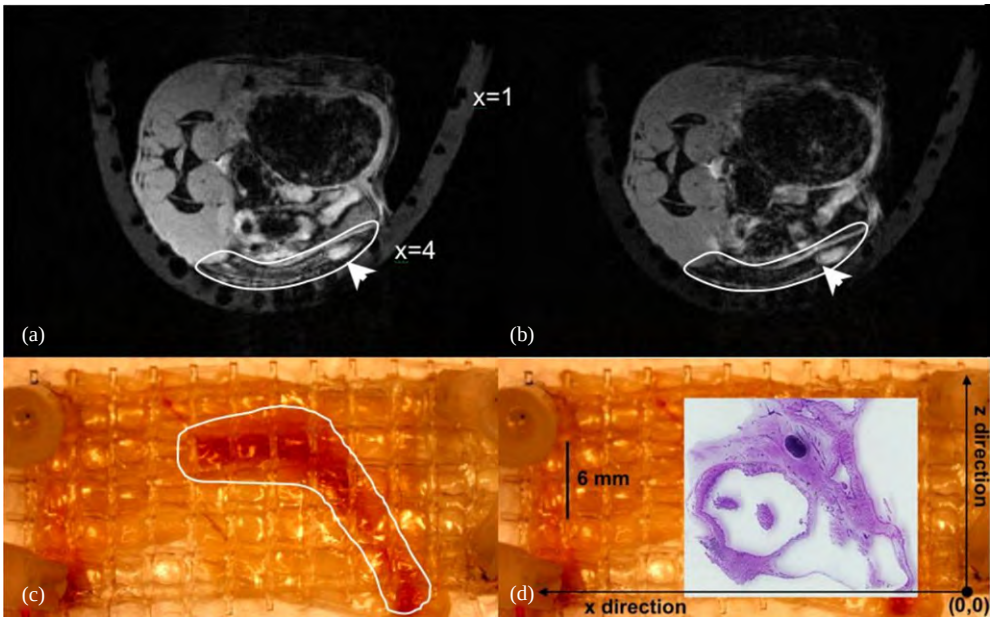

Figure 2. Axial GRE MR image of normal mammary gland (outlined in white) (a) without fat suppression, (b) with fat suppression. The display FOV is 3.0 × 2.0 cm. After fat suppression, signal from the mammary gland decreases. In (c) and (d), we illustrate how histology is compared to the MR image in (a). In (c), the same gland as imaged in (a) is excised (outlined in white) and the grid is visible on top, (d) the H&E section is superimposed and the grid coordinate system is noted, with z indicating the direction of the main magnetic field. The MR image in (a) represents one axial slice through the mammary gland along the z direction (in this case, $\sim z = 4$). The x dimension of the agar grid was wrapped around the mouse during imaging, and the coordinates $x = 1$ and $x = 4$ are labeled. After examining the H&E section in (d), a lymph node is identified at position $\sim$ ($z = 4$, $x = 4$–5). After examining all axial slices through the mammary gland, a structure is identified in (a) at position ($z = 4$, $x = 4$–5). Thus, by relating these positions it is evident that the GRE MR image successfully detected the lymph node (white arrowheads).

Table 1. (a) The average signal-to-noise ratio (SNR) of muscle, normal mammary gland tissue (MGT), lymph nodes, tumors and DCIS lesions for gradient echo (GRE) images with fat suppression (FS) and RARE spin-echo (SE) images with fat suppression. (b) The average contrast-to-noise ratio (CNR) of tumors, DCIS and lymph nodes relative to muscle and normal mammary glandular tissue. Numbers are mean ± standard deviation.

(a) Average SNR Pulse sequence	Muscle	MGT	Tumor	DCIS	Lymph node	
GRE with FS	33.9 ± 6.0	10.3 ± 4.2	34.3 ± 12.2	30.0 ± 8.7	40.3 ± 7.4	
RARE SE with FS	26.5 ± 3.0	39.0 ± 5.5	50.0 ± 5.4	38.9±8.6	44.4 ± 7.5	
(b) Average CNR Pulse sequence	Tumor–muscle	DCIS–muscle	Lymph node–muscle	Tumor–MGT	DCIS-MGT	Lymph node–MGT
GRE with FS	3.78 ± 6.1	−3.6 ± 8.9	6.8 ± 5.6	21.3 ± 8.3	20.6 ± 7.6	29.9 ± 6.2
RARE SE with FS	21.7 ± 5.2	13.2 ± 7.3	18.0 ± 5.9	7.08 ± 3.4	2.46 ± 5.2	5.4 ± 6.8

Lesion morphology. The morphology of tumors, DCIS and lymph nodes was assessed on GRE images with fat suppression. These images were acquired on a subset of slices and

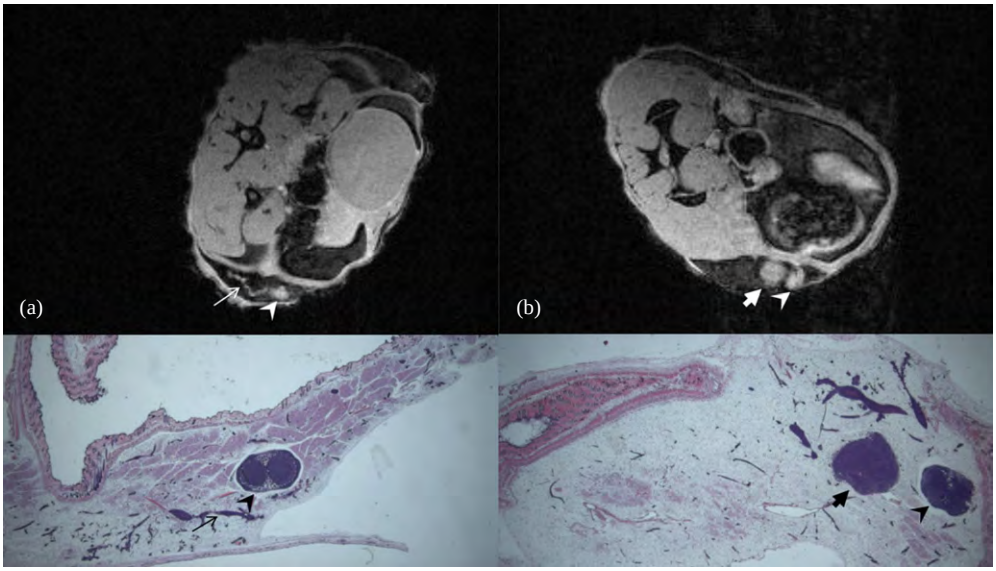

Figure 3. *In vivo* axial MR images (GRE with fat suppression) and corresponding H&E stained sections. The MR images and H&E stained sections represent different orientations. During imaging, the mammary glands are attached to the skin of the mouse, and are therefore wrapped around the body of the mouse. For excision, the glands are peeled back from the body of the mouse and laid flat, so that coronal H&E stained sections can be obtained. Each axial MR image represents one cross-sectional slice through the mammary gland. We used an agar grid (a polyethylene mesh embedded in partially deuterated agar, see figures 2(c) and (d)) to register the axial MR images with the H&E stained sections. (a) Lymph node (arrowhead) and DCIS (thin arrow). (b) Lymph node (arrowhead) and small tumor (thick arrow). For each MR image, the display FOV is 3.0 × 2.0 cm.

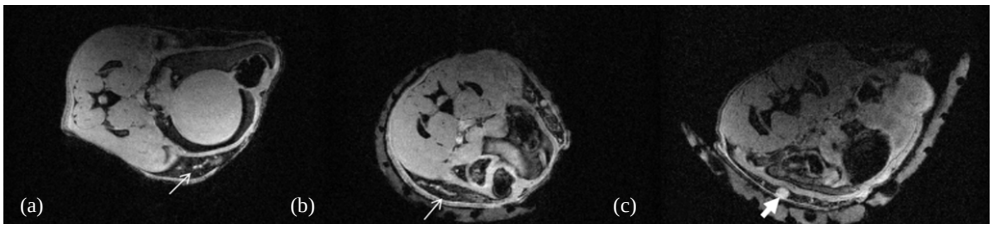

Figure 4. Examples of GRE images with fat suppression of: (a) DCIS (thin arrow), (b) DCIS (thin arrow) and (c) small tumor (thick arrow). The display FOV is 3.0 × 2.0 cm. In (b) and (c), the agar grid is visible wrapped around the mouse.

contained a total of 11 lymph nodes, 9 invasive tumors and 12 DCIS lesions. Nine of 9 invasive tumors were mass lesions, with a round (6/9) or irregular (3/9) shape, with smooth (6/9) or irregular (3/9) margins, and with a homogeneous (7/9) pattern. As with invasive tumors, 11/11 of lymph nodes were mass lesions, but the predominant shape was lobular (8/11) with smooth (10/11) margins, and a homogeneous (11/11) pattern. Eleven of 12 DCIS were nonmass lesions, with a linear (7/12) or ductal (4/12) shape, and a stippled (4/12), clumped (3/12) or homogeneous (5/12) pattern. Overall, the patterns show a similar distribution to human tumor morphologies.

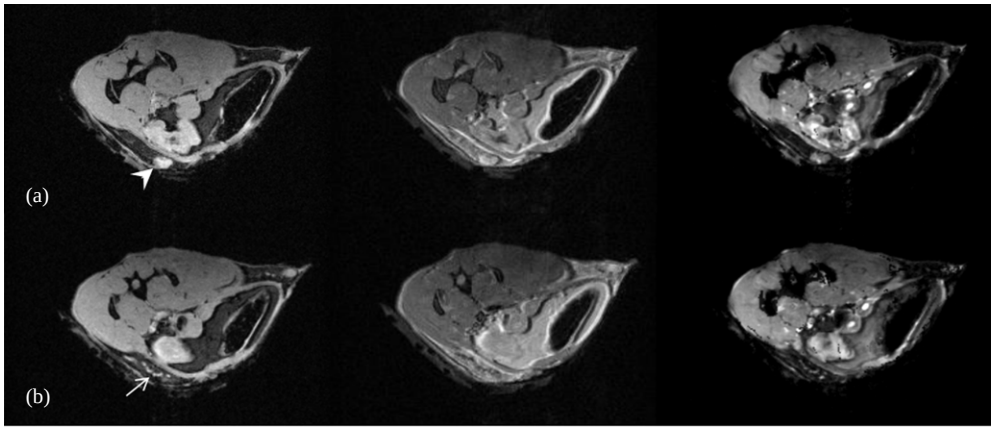

Figure 5. Demonstration of the same axial slice of (a) lymph node (arrowhead) and (b) DCIS (thin arrow), for three different imaging acquisitions, from left to right: GRE with fat suppression, RARE SE with fat suppression and high spectral and spatial imaging (HiSS), which yields water peak height images (shown). The display FOV is 3.0 × 2.0 cm. The GRE with fat suppression produced clearer images of the cancer and lymph node compared with SE. The HiSS images show the lymph node and DCIS along with excellent fat suppression.

Discussion

In this study, we show that MR imaging techniques can be successfully applied to non-palpable, microscopic invasive and *in situ* murine mammary cancers. The importance of this accomplishment lies in the fact that (i) modeling early cancers in transgenic animals heretofore required sacrifice of the animals to assess the impact of potential therapies, and (ii) these tumors are realistic models of the most frequently detected human cancers, i.e., those early tumors that are small. We found that MRI can reliably detect the microscopic stages of both *in situ* and invasive murine mammary cancers with high sensitivity. We also found that all image-detected lesions were determined to be cancer upon pathological diagnosis. To our knowledge, this is the first report of *in vivo* MR imaging of microscopic murine mammary cancer (Arkani *et al* 2007). Abbey *et al* used PET to image DCIS and early murine mammary cancer; however, the correlation with histology was made *ex vivo* (Abbey *et al* 2004). In addition, MR imaging offers superior spatial resolution compared with PET for lesion localization and characterization. We next plan to combine the excellent anatomic detail of *in vivo* MRI with molecular imaging modalities, such as PET and optical imaging.

Our study was performed primarily to determine whether or not MR imaging of early murine mammary cancer was feasible. Since there have been no previous reports of MR imaging of murine DCIS or early invasive cancers, optimal methods for MRI of murine DCIS had not yet been developed. Therefore, we evaluated several pulse sequences and found that gradient echo (GE) images with modest T_1- weighting (although variable due to respiratory gating) and fat suppression produced the clearest *in vivo* images of mammary glands and cancer compared with T_2-weighted spin-echo (SE) images. To image murine mammary cancer, suppression of signal from the mammary fat pad is important, which was achieved effectively in the GE and HiSS images. The pulse sequences and parameters used in this initial study probably do not provide the best possible images of murine mammary glands. It will now be important to perform quantitative measurements of the T_1, T_2, T_2^* and proton density

of early murine mammary cancer compared with normal tissue in order to further optimize imaging methods.

The mechanisms that produce the definitive contrast that we observed between murine mammary cancers and surrounding fibroglandular tissue and fat are not clear. Mammary glands are composed of fatty tissue, stroma and ductal/lobular structures that are lined by epithelial cells. Our results from T_1-weighted gradient-echo and HiSS images suggest that early murine mammary cancers are conspicuous because they have both a shorter T_1 and a longer T_2^* compared to normal glandular tissue and stroma. The larger size/proton density of DCIS and small tumors compared to normal glandular tissue may also make these lesions visible. Another possibility is that fat suppression is very effective in the present experiments because of the small field of view and the large chemical shift difference between water and fat.

Interestingly, we noted that the morphology of early murine mammary cancers on MRI is similar to the MR presentation of early human breast cancer. For example, DCIS lesions were nonmass lesions and appeared in a ductal or linear shape (Esserman *et al* 2006, Jansen *et al* 2007), while small invasive cancers appeared as round masses with smooth margins. In clinical DCEMRI of the human breast, contrast is administered to visualize the lesion. However, in the present study we used noncontrast-enhanced imaging techniques to detect early cancer, which represents a significant difference compared with clinical MRI of the human breast. This disparity may have several causes, including: (i) differences in the composition and/or distribution of glandular tissue, stroma and fat within the murine versus human mammary gland, (ii) the larger size of the murine mammary cancer relative to the whole gland when compared to human cancers, (iii) MR relaxation parameters that are significantly different in murine versus human cancers and/or normal glandular tissue or (iv) imaging at high field may yield novel contrast characteristics. Further work is needed to understand the differences between the current results in mice and those obtained in routine clinical practice. This will include precise measurements of relaxation times and proton density differences between DCIS, invasive tumors, lymph nodes and normal parenchyma in the mouse mammary glands at high field; we anticipate this will help us to determine the mechanisms underlying lesion conspicuity in our murine model. Our results also suggest the possibility of using non-contrast-enhanced techniques to image human cancers, a goal which is currently the subject of ongoing research (Du *et al* 2002, Medved *et al* 2006, Santyr 1994).

The results of the present study suggest that in the future MR imaging can be used to assess the effectiveness of therapies for cancers of all stages—*in situ*, early invasive and advanced. In addition, using the MR imaging techniques we have shown here, new contrast agents and imaging techniques that target DCIS and early invasive cancers can be developed, optimized and evaluated. DCIS is generally considered to be a precursor of invasive cancer (Recht *et al* 1998). However, because its progression cannot be routinely observed in women, the natural history of DCIS is not well understood. Evidence from studies where DCIS was initially misdiagnosed as a benign disease suggests that 14–53% of DCIS may progress to become invasive cancer (Erbas *et al* 2006). Autopsy studies have shown that DCIS is found in 5–14% of women, implying that there is a large pool of undetected DCIS in the general population (Erbas *et al* 2006). Although it is a preinvasive disease, due to the uncertainty of the natural history of individual lesions, DCIS is currently managed with obligate surgical excision (Duffy *et al* 2005). The techniques we report here provide a first step toward the use of noninvasive imaging to investigate the progression of DCIS in an animal model, and may allow us to study the characteristics of those tumors that become invasive cancers compared to those that do not. This information can be used to improve clinical management of early breast cancers.

In summary, the present study was designed to develop MR approaches to detecting early murine mammary cancer *in vivo*. We selected a transgenic mouse model with nearly 100% penetrance of mammary cancer. A logical extension of the work discussed here will be to test our MRI detection methods of early cancers in other mouse strains that develop mammary cancer with a much lower percentage penetrance. We also plan to acquire and analyze the DCEMRI kinetic parameters of early murine mammary cancer for comparison with noncontrast-enhanced images, and are investigating the mechanism of contrast enhancement in DCIS using x-ray fluorescence microscopy to measure the distribution of Gd-DTPA (an MR contrast agent) in murine DCIS lesions. It will also be important to image thoracic mammary glands in addition to the inguinal glands reported here. However, these experiments provide proof of principle that microscopic mammary tumors can indeed be detected and followed in a mouse model of breast cancer. This is an important step toward the more effective use of non-invasive imaging in pre-clinical studies of early breast cancer.

Acknowledgments

We would like to thank the Segal Foundation, the Florsheim Foundation, the Biological Sciences Division at the University of Chicago, the University of Chicago Cancer Center, DOD Award W81XWH-06-1-0329 and NIH grants R21 CA104774-01A2, 1 R01 EB003108-04 and R21/R33 CA100996 for financial support. We would also like to thank Erica Markiewicz, Diana Pang, Brad Williams and So-young Kim for help with acquiring and imaging the mice.

References

Abbey C K, Borowsky A D, McGoldrick E T, Gregg J P, Maglione J E, Cardiff R D and Cherry S R 2004 *In vivo* positron-emission tomography imaging of progression and transformation in a mouse model of mammary neoplasia *Proc. Natl Acad. Sci. USA* **101** 11438–43

ACR 2003 'American College of Radiology (ACR) Breast Imaging Reporting and Data System Atlas (BI-RADS)' (Reston, VA: ACR)

American Cancer Society. Breast Cancer Facts & Figures 2005–2006 Atlanta, GA: American Cancer Society, Inc.) Online at http://www.cancer.org/downloads/STT/CAFF2005BrFacspdf2005.pdf. (Accessed March 2007)

Arkani S, Conzen S, Krausz T, Newstead G and Karczmar G S 2007 MRI of ductal carcinoma *in situ* and other early mammary cancers in transgenic mice *Proc. Joint Annu. Meeting ISMRM_ESMRMB (Berlin, Germany)*

Artemov D, Mori N, Ravi R and Bhujwalla Z M 2003 Magnetic resonance molecular imaging of the HER-2/neu receptor *Cancer Res.* **63** 2723–7

Berry D A *et al* 2005 Effect of screening and adjuvant therapy on mortality from breast cancer *N. Engl. J. Med.* **353** 1784–92

Bremer C, Ntziachristos V, Weitkamp B, Theilmeier G, Heindel W and Weissleder R 2005 Optical imaging of spontaneous breast tumors using protease sensing 'smart' optical probes *Invest. Radiol.* **40** 321–7

Du W, Du Y P, Bick U, Fan X, MacEneaney P M, Zamora M A, Medved M and Karczmar G S 2002 Breast MR imaging with high spectral and spatial resolutions: preliminary experience *Radiology* **224** 577–85

Du W, Fan X, Foxley S, Zamora M, River J N, Culp R M and Karczmar G S 2005 Comparison of high-resolution echo-planar spectroscopic imaging with conventional MR imaging of prostate tumors in mice *NMR Biomed.* **18** 285–92

Duffy S W, Agbaje O, Tabar L, Vitak B, Bjurstam N, Bjorneld L, Myles J P and Warwick J 2005 Overdiagnosis and overtreatment of breast cancer: estimates of overdiagnosis from two trials of mammographic screening for breast cancer *Breast Cancer Res.* **7** 258–65

Duffy S W, Tabar L, Vitak B, Day N E, Smith R A, Chen H H and Yen M F 2003 The relative contributions of screen-detected *in situ* and invasive breast carcinomas in reducing mortality from the disease *Eur. J. Cancer* **39** 1755–60

Erbas B, Provenzano E, Armes J and Gertig D 2006 The natural history of ductal carcinoma *in situ* of the breast: a review *Breast Cancer Res. Treat.* **97** 135–44

Esserman L J *et al* 2006 Magnetic resonance imaging captures the biology of ductal carcinoma *in situ J. Clin. Oncol.* **24** 4603–10

Fan X, Markiewicz E J, Zamora M, Karczmar G S and Roman B B 2006 Comparison and evaluation of mouse cardiac MRI acquired with open birdcage, single loop surface and volume birdcage coils *Phys. Med. Biol.* **51** N451–9

Friedburg H, Henning J and Schumacher M 1987 RARE-MR myelography in routine clinical practice. Experience with 175 cases *Rofo* **146** 584–90

Galie M, D'Onofrio M, Calderan L, Nicolato E, Amici A, Crescimanno C, Marzola P and Sbarbati A 2004 *In vivo* mapping of spontaneous mammary tumors in transgenic mice using MRI and ultrasonography *J. Magn. Reson. Imaging* **19** 570–9

Geninatti Crich S *et al* 2006 *In vitro* and *in vivo* magnetic resonance detection of tumor cells by targeting glutamine transporters with Gd-based probes *J. Med. Chem.* **49** 4926–36

Gilles R *et al* 1995 Ductal carcinoma *in situ*: MR imaging—histopathologic correlation *Radiology* **196** 415–9

Green J E *et al* 2000 The C3(1)/SV40 T-antigen transgenic mouse model of mammary cancer: ductal epithelial cell targeting with multistage progression to carcinoma *Oncogene* **19** 1020–7

Hsueh W A, Kesner A L, Gangloff A, Pegram M D, Beryt M, Czernin J, Phelps M E and Silverman D H 2006 Predicting chemotherapy response to Paclitaxel with 18F-Fluoropaclitaxel and PET *J. Nucl. Med.* **47** 1995–1999

Jansen S A, Newstead G M, Abe H, Shimauchi A, Schmidt R A and Karczmar G S 2007 Pure ductal carcinoma *in situ*: kinetic and morphologic MR characteristics compared with mammographic appearance and nuclear grade *Radiology* **245** 684–91

Jemal A *et al* 2004 Annual report to the nation on the status of cancer, 1975–2001, with a special feature regarding survival *Cancer* **101** 3–27

Jenkins D E, Hornig Y S, Oei Y, Dusich J and Purchio T 2005 Bioluminescent human breast cancer cell lines that permit rapid and sensitive *in vivo* detection of mammary tumors and multiple metastases in immune deficient mice *Breast Cancer Res.* **7** R444–54

Kuhl C K, Schrading S, Bieling H B, Wardelmann E, Leutner C C, Koenig R, Kuhn W and Schild H H 2007 MRI for diagnosis of pure ductal carcinoma *in situ*: a prospective observational study *Lancet* **370** 485–92

Li C I, Malone K E and Daling J R 2003 Differences in breast cancer stage, treatment, and survival by race and ethnicity *Arch. Intern. Med.* **163** 49–56

Mansfield P 1984 Spatial mapping of the chemical shift in NMR *Magn. Reson. Med.* **1** 370–86

Maroulakou I G, Anver M, Garrett L and Green J E 1994 Prostate and mammary adenocarcinoma in transgenic mice carrying a rat C3(1) simian virus 40 large tumor antigen fusion gene *Proc. Natl Acad. Sci. USA* **91** 11236–40

Medved M, Newstead G M, Abe H, Zamora M A, Olopade O I and Karczmar G S 2006 High spectral and spatial resolution MRI of breast lesions: preliminary clinical experience *AJR Am. J. Roentgenol.* **186** 30–7

Menell J H, Morris E A, Dershaw D D, Abramson A F, Brogi E and Liberman L 2005 Determination of the presence and extent of pure ductal carcinoma *in situ* by mammography and magnetic resonance imaging *Breast J.* **11** 382–90

Morrow M *et al* 2002 Standard for the management of ductal carcinoma *in situ* of the breast (DCIS) *CA Cancer J. Clin.* **52** 256–76

Orel S G, Mendonca M H, Reynolds C, Schnall M D, Solin L J and Sullivan D C 1997 MR imaging of ductal carcinoma *in situ Radiology* **202** 413–20

Recht A, Rutgers E J, Fentiman I S, Kurtz J M, Mansel R E and Sloane J P 1998 The fourth EORTC DCIS Consensus meeting (Chateau Marquette, Heemskerk, The Netherlands, 23–24 Jan. 1998)—conference report *Eur. J. Cancer* **34** 1664–9

Robinson S P, Rijken P F, Howe F A, McSheehy P M, van der Sanden B P, Heerschap A, Stubbs M, van der Kogel A J and Griffiths J R 2003 Tumor vascular architecture and function evaluated by non-invasive susceptibility MRI methods and immunohistochemistry *J. Magn. Reson. Imaging* **17** 445–54

Rodrigues L M, Stubbs M, Robinson S P, Newell B, Mansi J and Griffiths J R 2004 The C-neu mammary carcinoma in oncomice; characterization and monitoring response to treatment with herceptin by magnetic resonance methods *MAGMA* **17** 260–70

Rodriguez O *et al* 2006 Contrast-enhanced *in vivo* imaging of breast and prostate cancer cells by MRI *Cell Cycle* **5** 113–9

Santyr G E 1994 MR imaging of the breast. Imaging and tissue characterization without intravenous contrast *Magn. Reson. Imaging Clin. N. Am.* **2** 673–90

Saslow D *et al* 2007 American Cancer Society guidelines for breast screening with MRI as an adjunct to mammography *CA Cancer J. Clin.* **57** 75–89

Schouten van der Velden A P, Boetes C, Bult P and Wobbes T 2006 The value of magnetic resonance imaging in diagnosis and size assessment of *in situ* and small invasive breast carcinoma *Am. J. Surg.* **192** 172–8

Seemann M D, Beck R and Ziegler S 2006 *In vivo* tumor imaging in mice using a state-of-the-art clinical PET/CT in comparison with a small animal PET and a small animal CT *Technol. Cancer Res. Treat.* **5** 537–42

Tian X, Aruva M R, Rao P S, Qin W, Read P, Sauter E R, Thakur M L and Wickstrom E 2003 Imaging oncogene expression *Ann. N Y Acad. Sci.* **1002** 165–88

Tsikitis V L and Chung M A 2006 Biology of ductal carcinoma *in situ* classification based on biologic potential *Am. J. Clin. Oncol.* **29** 305–10

Kinetic curves of malignant lesions are not consistent across MR systems: The need for improved standardization of breast DCEMRI acquisitions.

Sanaz A. Jansen PhD, Akiko Shimauchi MD, Lindsay Zak BSc, Xiaobing Fan PhD, Abbie M. Wood BSc, Gregory S. Karczmar PhD and Gillian M. Newstead MD*.

Institution Address:
University of Chicago
Department of Radiology
5841 S. Maryland Ave, MC 2026
Chicago, IL 60637

**Corresponding Author*
Gillian M. Newstead
Professor of Radiology
University of Chicago
Department of Radiology
5841 S. Maryland Ave
MC 2026
Chicago, IL 60637

Phone: 773-702-2781
Fax: (773) 702-2940
Email: gnewstead@radiology.bsd.uchicago.edu

Submitted as an Original Research article to: American Journal of Roentgenology
Word Count: 3434

Acknowledgements

We would like to thank the Segal Foundation and DOD Award W81XWH-06-1-0329 for financial support.

ABSTRACT

Objective: To compare the MR kinetic curve data of malignant lesions acquired by three different MR systems.

Subject and Methods: 601 patients with 682 breast lesions (185 benign, 497 malignant) were selected for an IRB approved review. The malignant lesions were classified as ductal carcinoma in situ (DCIS), invasive ductal carcinoma (IDC) and „other'. Dynamic MR protocol: 1 pre and 3-7 post-contrast images, acquired using one of three imaging protocol and systems (IPS): IPS1, IPS2 and IPS3. Analysis of kinetic curve shape was made by an experienced radiologist according to the BI-RADS lexicon. Several quantitative kinetic parameters were calculated, and the kinetic parameters of malignant lesions were compared between the three systems.

Results: 304 malignant lesions (185 IDC, 62 DCIS) were imaged on IPS1, 107 lesions (72 IDC, 21 DCIS) on IPS2, and 86 on IPS3 (64 IDC, 17 DCIS). Compared to both IPS1 and IPS2, IDC lesions acquired on IPS3 demonstrated significantly lower initial enhancement, longer time to peak enhancement and slower washout rate ($p < 0.0004$). Only 46% of IDC lesions imaged with IPS3 exhibited "washout" type curves, compared to 75% and 74% of those imaged with IPS2 and IPS1, respectively. Diagnostic accuracy of kinetic analysis was lower for IPS3, but not significantly.

Conclusions: The kinetic curve data of malignant lesions acquired by one system exhibited significantly lower initial contrast uptake and different curve shape compared with the other two. Differences in k-space sampling, T1 weighting or magnetization transfer effects may be possible explanations.

INTRODUCTION

Dynamic contrast enhanced MR imaging (DCEMRI) of the breast is being used increasingly for a variety of clinical purposes, including post-treatment evaluation, evaluating extent of malignant disease and for screening of high-risk women[1-3]. The advantage of DCEMRI is its high sensitivity, particularly for early invasive tumors. This is an important benefit since detecting breast cancer at an earlier stage could have a strong impact on improving outcomes[4]. Unfortunately, the specificity of DCEMRI has been reported to be variable [2]. In addition, there is concern that the diagnostic accuracy of DCEMRI for the earliest stage of breast cancer, ductal carcinoma *in situ* (DCIS), may not be high [5]. More recent studies have suggested that on both these counts, DCEMRI performs comparably to or better than x-ray mammography [6, 7]. However, these perceived or actual drawbacks, combined with the increased cost of DCEMRI, have limited the widespread use of MR imaging in the management of breast cancer patients at this time [8, 9].

Lesions are characterized on DCEMRI by both their morphology and contrast uptake and washout kinetics. The ability of DCEMRI to detect cancers is governed mostly by whether the lesion exhibits sufficient contrast enhancement to be discerned from normal tissue. The specificity of DCEMRI lies in how accurately the morphologic or kinetic descriptors can identify malignant lesions. In an effort to improve the specificity of DCEMRI, the kinetic and morphologic characteristics of malignant and benign lesions have been extensively studied [10-16]. In addition, recent multicenter trials have evaluated the diagnostic efficacy of kinetic and morphologic parameters and determined features most useful for interpretation of breast

DCEMRI[17, 18]. Such studies have helped to form general principles with regards to the interpretation of kinetic data in DCEMRI that are designed to help improve specificity:

General principle 1. Malignant lesions tend to show rapid uptake and washout, while benign lesions show slower uptake and persistent contrast uptake over time [19, 20], and

General principle 2. The kinetic characteristics of DCIS are variable, overlapping considerably with benign lesions, and demonstrating slower contrast uptake and washout compared with invasive ductal carcinomas (IDC) [5, 21-25].

Standardization of breast MR image acquisition is not widespread at this time. That is, there are no universally applied quality assurance procedures to ensure that as newer systems are utilized clinically, the measured kinetic curves continue satisfy these two principles. There are several manufacturers of MR systems, with different k-space sampling methods, pulse sequences and coils that continue to be modified and improved over time. Furthermore, dynamic imaging protocols differ across institutions as to timing resolution, use of fat suppression, plane of acquisition, use of parallel imaging and imaging protocols. Yet radiologists and imaging physicists should expect that the two principles outlined above would be applicable in all clinical acquisitions, so that similar interpretation criteria can be applied and similar diagnostic accuracy can be achieved, even as newer technology (such as parallel imaging, newer k-space sampling techniques and commercial computer aided detection (CAD) systems) is implemented. At our institution, we are in a unique position to address these concerns; here, breast MR imaging has been performed on three different MR systems and we also maintain a database of all MRI detected lesions imaged on these systems. The purpose of this study was to validate the above

two principles on different MR systems, and determine whether, absent standardization procedures, malignant lesions present similarly on all three systems.

METHODS

Patients

At our institution, DCEMRI is obtained for several reasons including pre-operative staging, post-chemotherapy evaluation, and screening of high-risk women. We prospectively maintain a HIPAA compliant database that includes the MR morphology, kinetic curve data and subsequent pathology (when available) for all lesions detected in women who were enrolled with an IRB approved waiver of consent or informed consent process. A retrospective review of this database yielded 682 consecutive lesions with pathology findings (based on biopsy or final pathology reports) in 601 patients that were eligible for study. These images were acquired May 2002-April 2007, and the average patient age was 56 ±13.5 years. After review of pathology reports, 497 lesions were determined to be malignant and 185 benign.

MR imaging protocols

DCEMRI has been performed at our institution using three different systems outlined in Table 1. From May 2002-August 2005, patients were imaged using imaging protocol and system 1 (IPS1). From September 2005-April 2007, this was replaced by two new protocol/systems that were used concurrently (denoted IPS2 and IPS3). Although these two new systems were from different manufacturers (GE and Philips), collaborative efforts between breast radiologists and MR physicists were undertaken to ensure that similar parameters and techniques be used for both so that comparable images would be obtained. For all patients, the first post-contrast images were acquired 20 seconds after intravenous injection of 20cc of 0.5M Gadodiamide (Omniscan; Nycomed-Amersham, Princeton, NJ) followed by a 20 ml saline flush at the rate of 2.0 ml /sec.

Kinetic Analysis

Signal intensity vs. time—or kinetic—curves for each lesion were retrospectively generated in two ways. For lesions acquired with IPS1, kinetic curves were generated by an experienced radiologist using institutional software. Specifically, the radiologist viewed all slices containing the lesion and manually traced a region of interest (ROI) around what they perceived to be the most enhancing area of the lesion on a single slice. The average size of manually drawn ROIs was 7.4 pixels. For lesions acquired with IPS2 and IPS3, the kinetic curves were extracted from a commercially available computer aided detection (CAD) system (CADstream research version 5.0 (Confirma, CA)). In addition to assigning color maps to lesions, this software generates a volumetric ROI encompassing the lesion and selects the most suspicious curve (that is, the one with the most rapid uptake and washout) in a 3x3 pixel ROI within the volume. This representative curve and its corresponding ROI was then examined by the same radiologist, and manually modified if necessary. In the case that the lesion was not recognized by the CAD software, the radiologist manually selected an ROI on what was perceived to be the most enhancing area of the lesion. Although the temporal resolution of the scans on each system differed somewhat (Table 1), the last time point was at similar times for all protocols, and was used to determine the delayed phase. Having generated the kinetic curve, the radiologist classified the initial rise of the curve according to the BI-RADS lexicon as „rapid', „medium' or „slow', and the delayed phase as „persistent', „plateau' or „washout'. This was based on a purely qualitative assessment of curve shape, and was made blinded to lesion pathology. In addition, several quantitative parameters were calculated for each curve: the initial enhancement percentage ($\mathbf{E_1}$), the peak enhancement percentage ($\mathbf{E_{peak}}$), the time to peak enhancement ($\mathbf{T_{peak}}$)

and the signal enhancement ratio (**SER),** a measure of washout. Further details on these parameters can be found in the Appendix.

Statistical Analysis

Our aim was to evaluate the two principles presented in the introduction. Because three different MR systems were used, we performed this evaluation separately in each. To do so, each lesion was classified as having been imaged with IPS1, IPS2 or IPS3. In addition, the pathology of each malignant lesion was assigned to be IDC, DCIS or „other' based on review of pathology reports.

We first began with studying the kinetic curves of malignant and benign lesions that were imaged by the same protocol/system. The qualitative BI-RADS descriptors of initial rise and delayed phase were compared between benign and malignant lesions, using the χ^2-test for significance, with $p < 0.05$ indicating significance. The Student's *t*-test was used to test for differences in the quantitative parameters $\mathbf{E_1}$, $\mathbf{E_{peak}}$, **SER** and $\mathbf{T_{peak}}$ between benign and malignant lesions, with a p value < 0.05 indicating significance and using the Holm-Bonferroni correction for multiple comparisons. In addition, the *t*-test was also used to compare values of $\mathbf{E_1}$, $\mathbf{E_{peak}}$, **SER** and $\mathbf{T_{peak}}$ between DCIS vs. IDC and DCIS vs. benign lesions.

We next turned to evaluating whether the assessment of contrast kinetics was affected by which protocol/system was used. The qualitative descriptors of malignant and benign lesions imaged with IPS1, IPS2 and IPS3 were compared using the χ^2-test, while the quantitative parameters were compared using the Students *t*-test. The diagnostic accuracy of kinetic

parameters was evaluated separately for each protocol. For the qualitative BI RADS descriptors, the sensitivity and specificity of „rapid', „washout' and „washout/plateau' were calculated. Receiver operating characteristic (ROC) analysis was performed to evaluate the diagnostic performance of the quantitative kinetic parameters. ROCKIT software (ROCKIT 0.9B Beta Version, Charles E. Metz, University of Chicago[26]) was used to generate the ROC curves and to compare area under the curve (A_z) values using the area test.

RESULTS

Overall, the majority of lesions—137 benign and 304 malignant—were imaged with IPS1. Of the remaining benign lesions, 21 and 27 were imaged with IPS2 and IPS3, respectively; of the remaining malignant lesions, 107 and 86 were imaged with IPS2 and IPS3, respectively. The majority of malignant lesions were classified as IDC (Table 2). DCIS lesions comprised approximately 20% of malignant lesions imaged on IPS1, IPS2 and IPS3. Final pathology (i.e., lumpectomy or mastectomy) reports were available for 81/100 DCIS lesions, while 19/100 were classified as DCIS based on biopsy alone. After review of final pathology reports, 66% (66/100) of DCIS lesions were determined to be pure DCIS, 5% (5/100) were DCIS with microinvasion, and 10% (10/100) of DCIS lesions were geographically separated from an ipsilateral invasive cancer. The remaining group of „other' malignant lesions were comprised of : 31 invasive lobular carcinoma, 26 carcinoma (unspecified), 3 invasive tubular carcinoma, 7 Pagets disease of the nipple, 2 invasive papillary carcinoma, 3 inflammatory carcinoma, 3 mucinous carcinoma and 1 colloid carcinoma. Examples of malignant IDC lesions acquired with IPS1, IPS2 and IPS3, as well as their corresponding kinetic curves, are shown in Figure 1.

BI-RADS Assessment of Curve Shape

Kinetic curves of malignant lesions imaged with IPS1 exhibited a higher proportion of curves with „rapid' initial rise, at 89%, compared to 55% of benign lesions ($p < 0.0001$, Table 2). Malignant lesions imaged with IPS2 and IPS3, on the other hand, exhibited comparable proportions of „rapid' curves compared to their benign counterparts. For all three protocols, a higher proportion of malignant lesions demonstrated „washout' curves compared with benign

lesions (p <0.004, Table 2). Comparable proportions of DCIS lesions imaged with IPS1 and IPS3 exhibited „washout', „plateau' and „persistent' curve shapes, whereas the majority of DCIS imaged with IPS2 were classified as „washout' or „plateau' (Table 2).

Although malignant and benign lesions imaged on each protocol exhibited differences in their delayed phase characteristics, the actual frequencies of BI-RADS descriptors—e.g., the proportion of curves classified as „rapid' or „washout'—varied between protocols. For example, malignant lesions imaged with IPS3 exhibited a slightly lower proportion of curves classified as „rapid' initial rise, at 81%, compared to malignant lesions acquired with IPS1 and IPS2 (Table 2). Notably, the assessment of delayed phase revealed a marked difference: 69% and 66% of malignant lesions acquired with IPS2 and IPS1 were classified as „washout', respectively, compared to only 44% of those acquired with IPS3 (Figure 5.2, $p < 0.0008$). This was re-demonstrated for IDC lesions separately: only 47% of IDC lesions imaged with IPS3 were classified as „washout' compared to 75% and 74% of IDC lesions imaged with IPS2 and IPS1, respectively.

Quantitative Kinetic Parameters

The qualitative observations noted above were further confirmed upon quantitative analysis. Benign lesions imaged with IPS1 exhibited a lower $\mathbf{E_1}$, **SER** and a longer $\mathbf{T_{peak}}$ compared with malignant lesions acquired with the same protocol (Table 3, $p < 10^{-6}$). $\mathbf{E_{peak}}$ was also lower in benign lesions, but this was not significant. Benign lesions acquired with IPS2 and IPS3 also exhibited similar trends compared to their malignant counterparts. After the Holm-

Bonferroni correction for multiple comparisons, $\mathbf{E_1}$ and $\mathbf{E_{peak}}$ were significant for IPS2 lesions (p<0.004). No parameters were found to be statistically significant in IPS3 lesions.

We next examined the kinetic parameters of DCIS compared with other lesions. We found that DCIS lesions acquired with IPS1 exhibited lower $\mathbf{E_1}$, $\mathbf{E_{peak}}$, **SER** and longer $\mathbf{T_{peak}}$ compared to IDC lesions acquired with the same protocol (Table 3, $p < 0.0008$). On the other hand, DCIS and benign lesions exhibited considerable overlap in all parameters; there was a trend for DCIS to have lower $\mathbf{E_1}$ and $\mathbf{E_{peak}}$, and higher **SER** compared with benign lesions, but these were not significant after the Holm-Bonferroni correction. This latter finding persisted for IPS2 and IPS3: DCIS and benign lesions did not demonstrate significant differences. However, unlike lesions acquired with IPS1, we did not find a significant difference in the kinetics parameters of DCIS and IDC lesions acquired with IPS2 or IPS3.

Having analyzed the kinetic characteristics of benign and malignant lesions within each imaging protocol, the kinetic parameters were then compared between protocols. Earlier we noted that according to the qualitative BI-RADS classification of curve shape, malignant lesions imaged with IPS3 exhibited fewer „rapid' and „washout' curve types. This finding was further amplified upon quantitative analysis. Malignant lesions imaged with IPS3 exhibited significantly lower $\mathbf{E_1}$ ($p< 10^{-5}$), $\mathbf{E_{peak}}$ (p=0.004), **SER** ($p <10^{-22}$) and longer $\mathbf{T_{peak}}$ (p =0.003) than those imaged with IPS1. Compared to malignant lesions imaged with IPS2, malignant IPS3 lesions also exhibited a lower $\mathbf{E_1}$, $\mathbf{E_{peak}}$, **SER** and $\mathbf{T_{peak}}$, and after the Holm-Bonferroni correction $\mathbf{E_1}$ and $\mathbf{E_{peak}}$ remained significant ($p < 0.001$, Table 5.3). Malignant lesions acquired

with IPS2 also demonstrated a lower **SER** compared to those acquired with IPS1 (p =0.002), but otherwise we found no significant difference in the kinetic parameters between IPS1 and IPS2.

Diagnostic Accuracy of Kinetic Parameters Using Different Imaging Protocols

The discrepancies found in the kinetic characteristics of malignant lesions between the three protocols studied led us to investigate the effect on the diagnostic accuracy of kinetic analysis. Considering the descriptors „washout' and „plateau' to be indicative of malignancy, their sensitivity in IPS1, IPS2 and IPS3 was 88% (95% confidence interval (CI) 83%-91%), 93% (CI 85%-97%) and 85% (CI 75%-91%), respectively. The specificity was 41% (CI 33%-50%) in IPS1, 45% (CI 28%-64%) in IPS2 and 37% (CI 20%-58%) in IPS3. In other words, the diagnostic accuracy of the BI RADS descriptors typically used to identify malignant lesions was reduced in IPS3, although not significantly.

Similarly, ROC analysis of the diagnostic accuracy of the parameters $\mathbf{E_1}$, $\mathbf{E_{peak}}$, **SER** and $\mathbf{T_{peak}}$ yielded A_z values showing a trend for compromised diagnostic performance in IPS3 (Figure 3). There was a trend for **SER** to be less useful diagnostically on IPS3 vs. IPS1, while the diagnostic performance of $\mathbf{E_{peak}}$ was improved on IPS2 compared to the others. However, these differences were not statistically significant. The highest A_z values for each of IPS3, IPS2 and IPS1 were 0.64 ($\mathbf{T_{peak}}$), 0.68 ($\mathbf{E_1}$) and 0.73 (**SER**), respectively.

DISCUSSION

We set out to evaluate whether kinetic curve data acquired on each of three different MR imaging protocol/systems (denoted IPS1, IPS2 and IPS3) satisfied two principles pertaining to the interpretation of DCEMRI kinetic data. The first principle, related to the general curve shape of malignant lesions (rapid uptake and washout) compared to benign lesions (persistent uptake), met with uneven success. We found that in the largest database of lesions imaged with the older IPS1, both of these observations held true: a majority of malignant lesions were classified as „washout', while „persistent' was the most likely descriptor of benign lesions. Most malignant lesions imaged with IPS2 were also classified as „washout', but only 19% of benign lesions were classified as „persistent'. More significantly, using IPS3 *less* than half of malignant lesion kinetic curves were classified as „washout'. Although these differences are certainly important to recognize and address, the effect on diagnostic accuracy of kinetic parameters was not drastic: there was a trend for compromised sensitivity and specificity with IPS3, but it was not statistically significant. In addition, IPS1 had considerably greater number of lesions than the other two groups, which may affect the results presented here.

The second principle we investigated pertained to the kinetic characteristics of DCIS, which have been reported to be variable, to overlap with benign lesions and to exhibit marked differences in uptake and washout compared to IDC. We found that the kinetic variability of DCIS was validated in the larger IPS1 database, in which DCIS demonstrated 44% „washout', 22% „plateau' and 34% „persistent' curve types—in other words, all curve types were found. Similarly, DCIS lesions imaged with IPS3 demonstrated 29% „washout', 30% „plateau' and 41%

„persistent' curve types. However, for IPS2 imaged lesions there was less variability, with 62% (13/21) DCIS classified as „washout', 33% as „plateau' and only 5% (1/21) as „persistent'. We found that the quantitative kinetic parameters of benign and DCIS lesions exhibited overlap in all three protocol/systems. However, only those DCIS and IDC lesions imaged with IPS1 demonstrated statistically significant differences from one another.

Overall, we have found that the typical kinetic presentation of malignant lesions is not consistent across different MR systems, which represents a potential clinical problem. For example, in the follow-up MRI assessment of women undergoing pre-operative neoadjuvant chemotherapy, our results imply that it is important to perform repeat imaging using the same system, lest differences due to system choice be mistaken for tumor response. It is important to note that every effort was taken to try to reproduce similar MR acquisition protocols on these different systems, particularly for IPS2 and IPS3 which were used concurrently—both were acquired with fat saturation, similar dynamic timing, parallel imaging and similar T_1 weighting. We emphasize that we are not suggesting that MR systems from one manufacturer are preferable to another. Neither are we challenging the principles outlined in the introduction. Rather, our results underscore the importance of developing improved standardization procedures[20, 27], so that all women undergoing breast DCEMRI can be imaged adequately ensuring malignant lesions will enhance sufficiently and exhibit similar curve shapes. We are currently working on designing experimental phantoms for this purpose.

The differences in average kinetic parameters between the three protocol/systems may be attributable to numerous factors. One may be that kinetic curves were not generated in the same way for every lesion. Images from lesions imaged with IPS1 were displayed and analyzed using homemade software, while images from IPS2 and IPS3 were analyzed using a commercially available CAD system. It should be noted, however, that this significant limitation is applicable only to comparisons of IPS1 with IPS2 or IPS3. It cannot explain the differences noted between IPS3 and IPS2 malignant lesions, since DCEMRI data was processed and analyzed in the same way for both. Specifically, the markedly lower $\mathbf{E_1}$ and **SER**, and the smaller fraction of „washout' type curves in IPS3 malignant lesions—less than half—is likely not attributable to using a CAD system to analyze kinetic data. The lower initial enhancement percentage and differences in overall curve shape may be due to other effects, such as fat suppression, parallel imaging, post-acquisition processing and k-space sampling techniques. It could be that using contrast concentration rather than signal intensity may help to eliminate inter-system variability. We are currently exploring these and other potential factors by imaging the same lesion with different systems and imaging protocols.

There are several limitations to this study. One that was already mentioned is that curve selection was not performed in a uniform manner for all lesions. Another shortcoming is that the benign lesions in this study were histologically proven benign cases i.e., they were suspicious enough to warrant biopsy. It could be that with increased experience over time, the radiologists' evaluation of borderline benign cases improved, and hence the benign lesions included in IPS2 and IPS3 are even more suspicious that those included in IPS1, resulting in a biased lesion

population. Also, the reliability of the kinetic parameters $\mathbf{E_{peak}}$ and $\mathbf{T_{peak}}$ may be compromised by the several different timing acquisitions used, and by the coarse sampling of kinetic data. On the other hand, the parameters $\mathbf{E_1}$ and **SER** are not as adversely affected by these two concerns since they depend on signal intensities measured at the initial and last time points, which are at similar times for all protocols. Finally, we have not evaluated morphology in this study; in order to assess the full diagnostic accuracy of DCEMRI, morphologic descriptors need to be included.

In summary, this study has demonstrated that in one large database of consisting of kinetic data from 441 malignant and benign lesions acquired on an older system, the general principles regarding lesion kinetics presented in the Introduction hold. Unfortunately, they are not consistently applicable for lesions acquired with other systems: the kinetic curves of malignant lesions acquired with one newer system exhibited lower initial uptake and fewer „washout' type curves compared with the two others. The markedly lower initial enhancement percentage for lesions acquired with our Philips system, regardless of whether malignant or benign, is important to note and address. This study underscores the importance of standardization of DCEMRI acquisition protocols, so that as newer technology is implemented (i) malignant lesions are sufficiently conspicuous, and (ii) similar interpretation guidelines can be consistently applied across all systems and protocols. Such standardization will be important if breast DCEMRI is to be used routinely in patient management.

APPENDIX

The *percent enhancement* measures the uptake of contrast in the lesion relative to the pre-contrast signal level[13],

$$E_1 = 100 \times \frac{S_1 - S_0}{S_0}$$

$$E_{peak} = 100 \times \frac{S_{peak} - S_0}{S_0},$$

where E_1 is the initial percent enhancement, E_{peak} is the peak percent enhancement, S_1 is the signal in the ROI at the first post contrast point, S_{peak} is the peak signal intensity and S_0 is the pre-contrast signal intensity in the ROI.

The *time to peak enhancement* (T_{peak}) is the time in seconds between the injection of contrast and the peak of the signal intensity vs. time curve.

The parameter used to quantify washout is the *signal enhancement ratio*, which is a measure of the relative signal decrease from the first post contrast time point to the final post contrast point[28, 29],

$$SER = \frac{S_1 - S_0}{S_{last} - S_0}.$$

Here, *SER* is the signal enhancement ratio and S_{last} is the signal intensity in the ROI at the last post contrast point. We can use the *SER* parameter to quantify the washout in the curve by choosing threshold values. A *SER* value of less than 0.9 means that the final signal intensity

increases relative to the first post-contrast point (persistent increase); a *SER* value between 0.9 and 1.1 indicates the final signal intensity is comparable to the first post-contrast point (plateau); a *SER* greater than 1.1 indicates that the final signal intensity decreases relative to the first post-contrast point (washout).

The *SER* measures washout relative to the first post contrast point, whereas the BI-RADS® assessment of delayed phase can involve any part of the kinetic curve. *SER* values > 1.1 correspond to washout relative to the first post contrast time point. Therefore, any curves with *SER* >1.1 that are classified as „plateau' or „persistent' are inconsistent. *SER* values between 0.9 and 1.1 correspond to a plateau relative to the first post contrast time point. Therefore, any curves with 0.9 < *SER* < 1.1 that are classified as „persistent' are inconsistent. Note that these curves could be classified as „washout'—the curve may peak at the second post contrast point, for example, and washout from then on, but still plateau relative to the first post contrast time point. *SER* values < 0.9 correspond to a persistent increase relative to the first post contrast time point. Note that these curves could be classified as „plateau' or „washout' as well, depending on the curve data at other time points.

FIGURE CAPTIONS

Fig. 1—Examples of IDC lesions (white arrow) acquired with IPS1 (top), IPS2 (middle) and IPS3 (bottom). Adjacent to each MR image is the corresponding kinetic curve with quantitative kinetic parameters noted.

Fig. 2—The BI-RADS descriptors of initial rise (left) and delayed phase (right) for malignant lesions acquired with IPS1, IPS2 or IPS3.

Fig. 3—Area under the curve (A_z) values for the four kinetic parameters used in this study, E_1, E_{peak}, SER and T_{peak}. For each parameter, three A_z values are presented for IPS1, IPS2 and IPS3. Error bars indicate 95% confidence interval.

Table 1: Summary of the three different MR systems and protocols used at our institution.

	Imaging protocol and system 1 (IPS1)	**Imaging protocol and system 2 (IPS2)**	**Imaging protocol and system 3 (IPS3)**
Dates Used	May 2002-Sept 2005	Sept 2005-April 2007	Sept 2005-April 2007
Magnet	1.5T GE Genesis Signa	1.5T GE Signa Excite	1.5T Philips Achieva
Number of Coil channels	4	8	7
Acquisition plane	Coronal	Axial	Axial
Pulse sequence	3D SPGR	3D FGRE	3D FFE
TR/TE (ms)	7.7/4.2	4.3/2.0	7.9/3.9
Flip angle (degree)	30	10	10
Slice thickness (mm)	3.00	2.00	2.00
In plane resolution (mm)	1.4	0.82	0.94
Temporal resolution (s)	68	58	55
# of post-contrast	3 or 5*	4 or 6	4 or 6**
Fat suppression (y/n)	n	y	y
Parallel imaging (y/n)	n	y	y

* The first post-contrast acquisition was started 20 seconds after contrast injection and the first two post-contrast images were acquired every 68 seconds. For the five point dynamic protocol, the remaining three images were acquired with 68 second resolution. For the three point dynamic protocol, the first two post-contrast acquisitions were followed by acquisition of high spatial resolution sagittal images for 128 seconds, and returning to a final dynamic, 68 second, acquisition.

** For both IPS2 (or IPS3), the first post-contrast acquisition was again started 20 seconds after contrast injection and the first three post-contrast images were acquired every 58 (or 55) seconds. For the six point dynamic protocol, the remaining three images were acquired with 58 (or 55) second resolution. For the four point dynamic protocol, the first two post-contrast acquisitions were followed by acquisition of high spatial resolution sagittal images and returning to a final dynamic acquisition.

Table 2: The BI-RADS descriptors of initial rise and delayed phase for benign and malignant lesions acquired with the three protocols, as well as data from two subtypes of malignant lesions, DCIS and IDC. The *p* values comparing proportions of washout vs. plateau and persistent in benign and malignant lesions are also indicated.

			Initial Rise			***Delayed Phase***			
	Type of lesions	**No. cases**	***Rapid***	***Medium***	***Slow***	***Washout***	***Plateau***	***Persistent***	***p* value**
IPS1	**Benign**	**137**	**75(55%)**	**25(18%)**	**37(27%)**	**42(31%)**	**39(28%)**	**56(41%)**	***p* <0.0001**
	All Malignant	**304**	**270(89%)**	**22(7%)**	**12(4%)**	**202(66%)**	**64(21%)**	**38(13%)**	
	DCIS	62	43	12	7	27	14	21	
	IDC	185	177	4	4	137	36	12	
	Other	57	50	6	1	38	14	5	
IPS2	**Benign**	**21**	**18(86%)**	**3(14%)**	**0(0%)**	**6(29%)**	**11(52%)**	**4(19%)**	***p* =0.001**
	All Malignant	**107**	**98(92%)**	**7(7%)**	**2(2%)**	**74(69%)**	**25(23%)**	**8(7%)**	
	DCIS	21	16	5	0	13	7	1	
	IDC	72	70	2	0	54	14	4	
	Other	14	12	0	2	7	4	3	
IPS3	**Benign**	**27**	**20(74%)**	**3(11%)**	**4(15%)**	**3(11%)**	**14(52%)**	**10(37%)**	***p*=0.004**
	All Malignant	**86**	**70(81%)**	**13(15%)**	**3(3%)**	**38(44%)**	**35(41%)**	**13(15%)**	
	DCIS	17	11	3	3	5	5	7	
	IDC	64	55	9	0	30	29	5	
	Other	5	4	1	0	3	1	1	

Table 3: The quantitative kinetic parameters of benign and malignant lesions acquired with the three protocols. This table also includes data from two subtypes of malignant lesions, DCIS and IDC.

	Type of lesions	No. cases	E1 (%)	Epeak (%)	T_{peak} (sec)	SER
IPS1	**Benign**	**137**	**204±158**	**302±192**	**233±107**	**0.76±0.36**
	All Malignant	**304**	**286±158**	**330±155**	**165±105**	**1.07±0.48**
	DCIS	62	194±138	252±147	222±108	0.89±0.44
	IDC	185	313±151	352±149	144±98	1.15±0.50
IPS2	**Benign**	**21**	**163±78**	**221±82**	**198±102**	**0.81±0.23**
	All Malignant	**107**	**245±214**	**301±213**	**178±126**	**0.94±0.32**
	DCIS	21	219±189	269±197	209±201	0.97±0.31
	IDC	72	264±236	319±232	160±96	0.97±0.33
IPS3	**Benign**	**27**	**61±38**	**149±56**	**251±110**	**0.45±0.28**
	All Malignant	**86**	**122±281**	**213±356**	**211±100**	**0.57±0.33**
	DCIS	17	119±204	187±192	241±125	0.62±0.45
	IDC	64	125±309	223±401	203±91	0.56±0.26

REFERENCES

1. Newstead GM. MR imaging in the management of patients with breast cancer. *Semin Ultrasound CT MR* **2006**;27:320-332
2. DeMartini W, Lehman C. A review of current evidence-based clinical applications for breast magnetic resonance imaging. *Top Magn Reson Imaging* **2008**;19:143-150
3. Saslow D, Boetes C, Burke W, et al. American Cancer Society guidelines for breast screening with MRI as an adjunct to mammography. *CA Cancer J Clin* **2007**;57:75-89
4. Duffy SW, Tabar L, Vitak B, et al. The relative contributions of screen-detected in situ and invasive breast carcinomas in reducing mortality from the disease. *Eur J Cancer* **2003**;39:1755-1760
5. Harms SE. The use of breast magnetic resonance imaging in ductal carcinoma in situ. *Breast J* **2005**;11:379-381
6. Kuhl CK. Concepts for differential diagnosis in breast MR imaging. *Magn Reson Imaging Clin N Am* **2006**;14:305-328, v
7. Kuhl CK, Schrading S, Bieling HB, et al. MRI for diagnosis of pure ductal carcinoma in situ: a prospective observational study. *Lancet* **2007**;370:485-492
8. Houssami N, Ciatto S, Macaskill P, et al. Accuracy and surgical impact of magnetic resonance imaging in breast cancer staging: systematic review and meta-analysis in detection of multifocal and multicentric cancer. *J Clin Oncol* **2008**;26:3248-3258
9. Morrow M. Magnetic resonance imaging in the breast cancer patient: curb your enthusiasm. *J Clin Oncol* **2008**;26:352-353
10. Veltman J, Mann R, Kok T, et al. Breast tumor characteristics of BRCA1 and BRCA2 gene mutation carriers on MRI. *Eur Radiol* **2008**;18:931-938
11. Chen W, Giger ML, Lan L, Bick U. Computerized interpretation of breast MRI: investigation of enhancement-variance dynamics. *Med Phys* **2004**;31:1076-1082
12. Orel SG. MR imaging of the breast. *Radiol Clin North Am* **2000**;38:899-913
13. Szabo BK, Aspelin P, Wiberg MK, Bone B. Dynamic MR imaging of the breast. Analysis of kinetic and morphologic diagnostic criteria. *Acta Radiol* **2003**;44:379-386
14. Kaiser WA, Zeitler E. MR imaging of the breast: fast imaging sequences with and without Gd-DTPA. Preliminary observations. *Radiology* **1989**;170:681-686
15. Kaiser WA. [Magnetic resonance tomography of the breast. The results of 253 examinations]. *Dtsch Med Wochenschr* **1989**;114:1351-1357
16. Heywang SH, Wolf A, Pruss E, Hilbertz T, Eiermann W, Permanetter W. MR imaging of the breast with Gd-DTPA: use and limitations. *Radiology* **1989**;171:95-103
17. Schnall MD, Blume J, Bluemke DA, et al. Diagnostic architectural and dynamic features at breast MR imaging: multicenter study. *Radiology* **2006**;238:42-53
18. Heywang-Kobrunner SH, Bick U, Bradley WG, Jr., et al. International investigation of breast MRI: results of a multicentre study (11 sites) concerning diagnostic parameters for contrast-enhanced MRI based on 519 histopathologically correlated lesions. *Eur Radiol* **2001**;11:531-546

19. Kuhl CK, Mielcareck P, Klaschik S, et al. Dynamic breast MR imaging: are signal intensity time course data useful for differential diagnosis of enhancing lesions? *Radiology* **1999**;211:101-110
20. Kuhl CK, Schild HH. Dynamic image interpretation of MRI of the breast. *J Magn Reson Imaging* **2000**;12:965-974
21. Jansen SA, Newstead GM, Abe H, Shimauchi A, Schmidt RA, Karczmar GS. Pure ductal carcinoma in situ: kinetic and morphologic MR characteristics compared with mammographic appearance and nuclear grade. *Radiology* **2007**;245:684-691
22. Jansen SA, Fan X, Karczmar G, et al. DCEMRI of breast lesions: In kinetic analysis equally effective for both mass and nonmass-like enhancement? *Medical Physics* **2008**;35:3102-3109
23. Furman-Haran E, Schechtman E, Kelcz F, Kirshenbaum K, Degani H. Magnetic resonance imaging reveals functional diversity of the vasculature in benign and malignant breast lesions. *Cancer* **2005**;104:708-718
24. Viehweg P, Lampe D, Buchmann J, Heywang-Kobrunner SH. In situ and minimally invasive breast cancer: morphologic and kinetic features on contrast-enhanced MR imaging. *Magma* **2000**;11:129-137
25. Van Goethem M, Schelfout K, Kersschot E, et al. Comparison of MRI features of different grades of DCIS and invasive carcinoma of the breast. *Jbr-Btr* **2005**;88:225-232
26. Metz CE, Herman BA, Shen JH. Maximum likelihood estimation of receiver operating characteristic (ROC) curves from continuously-distributed data. *Stat Med* **1998**;17:1033-1053
27. Kuhl C. The current status of breast MR imaging. Part I. Choice of technique, image interpretation, diagnostic accuracy, and transfer to clinical practice. *Radiology* **2007**;244:356-378
28. Li KL, Partridge SC, Joe BN, et al. Invasive breast cancer: predicting disease recurrence by using high-spatial-resolution signal enhancement ratio imaging. *Radiology* **2008**;248:79-87
29. Esserman L, Hylton N, George T, Weidner N. Contrast-Enhanced Magnetic Resonance Imaging to Assess Tumor Histopathology and Angiogenesis in Breast Carcinoma. *Breast J* **1999**;5:13-21

Figure 1(.tiff, .jpg)

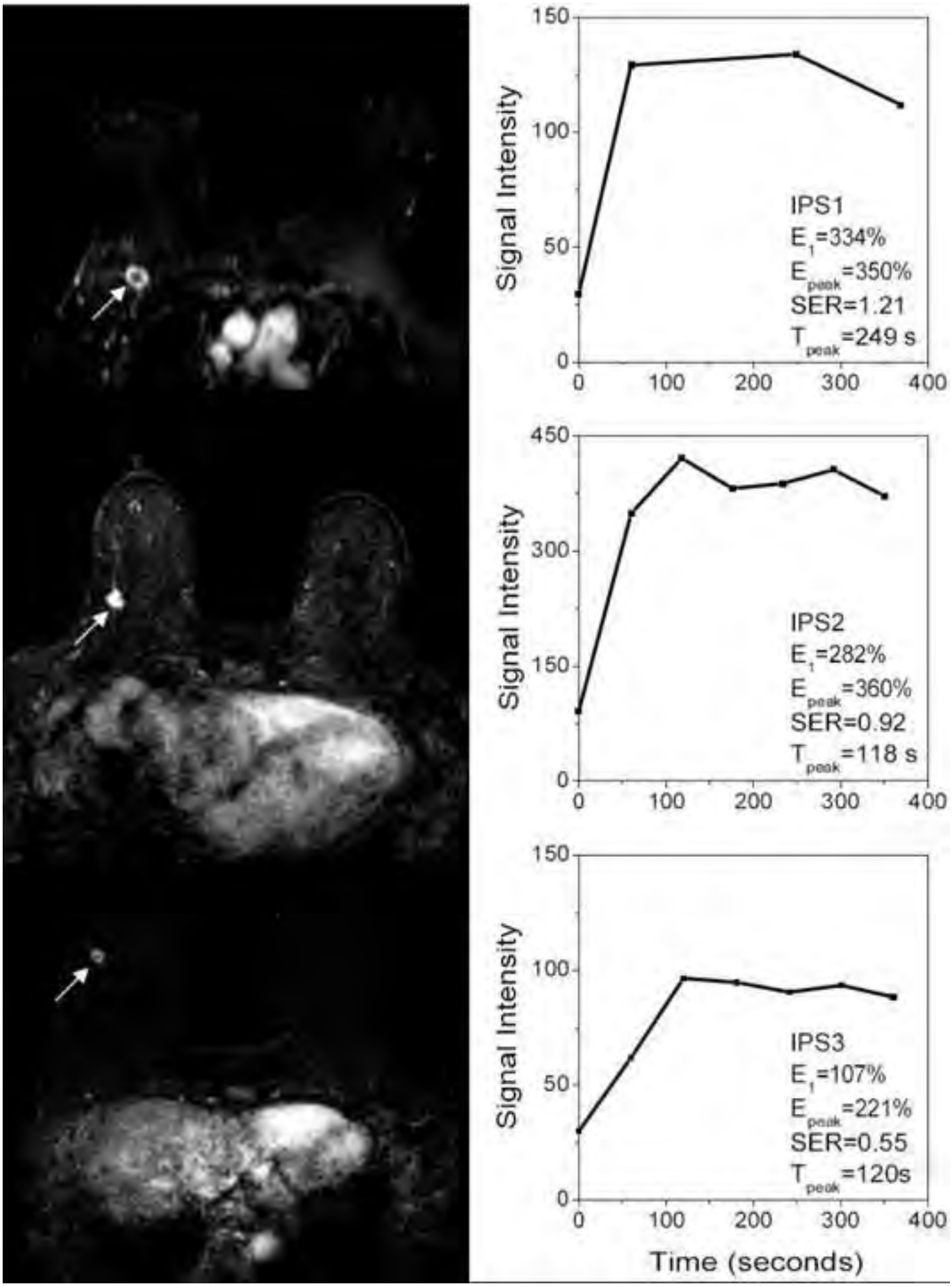

Figure 2(.tiff, .jpg)

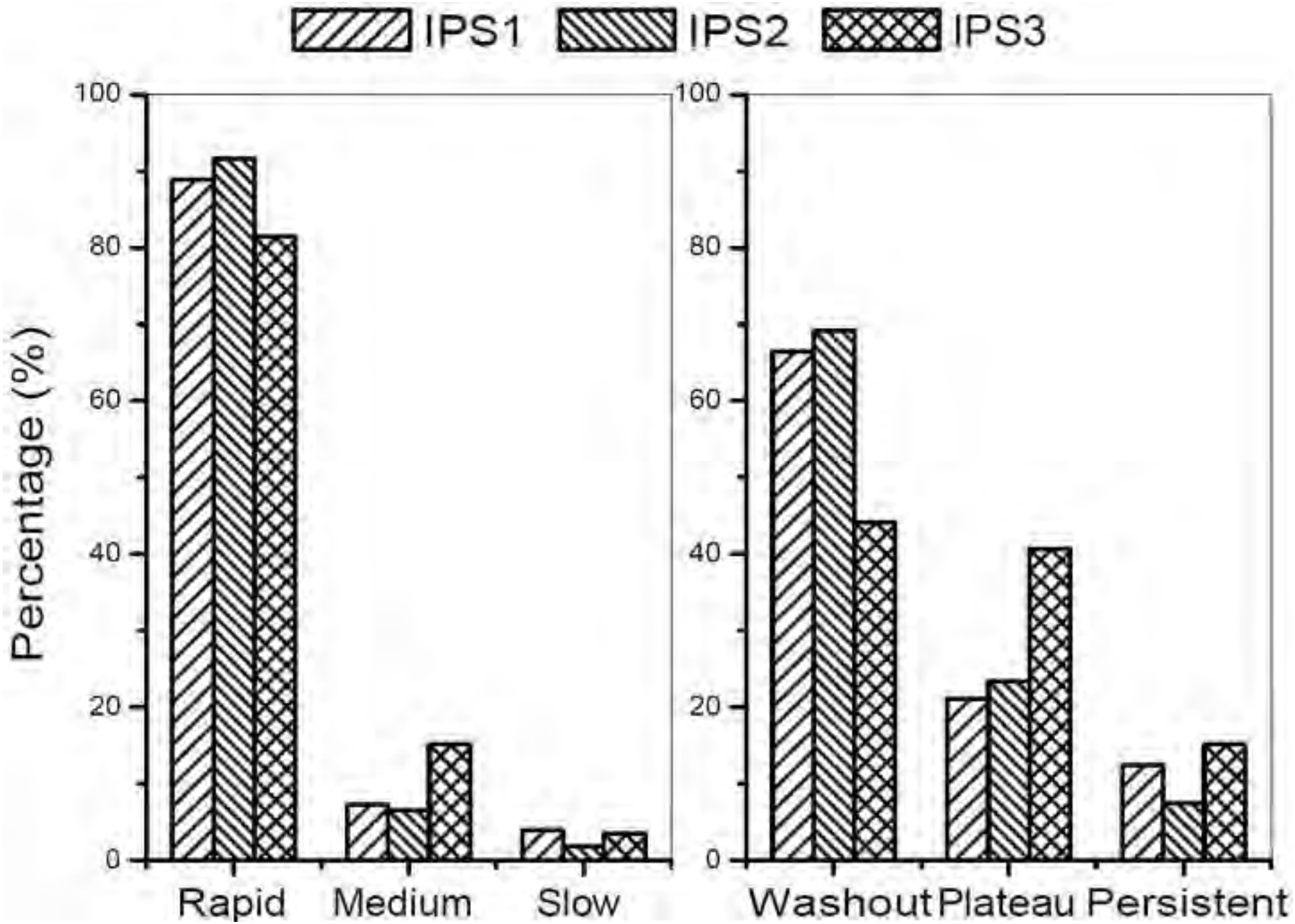

Figure 3(.tiff, .jpg)

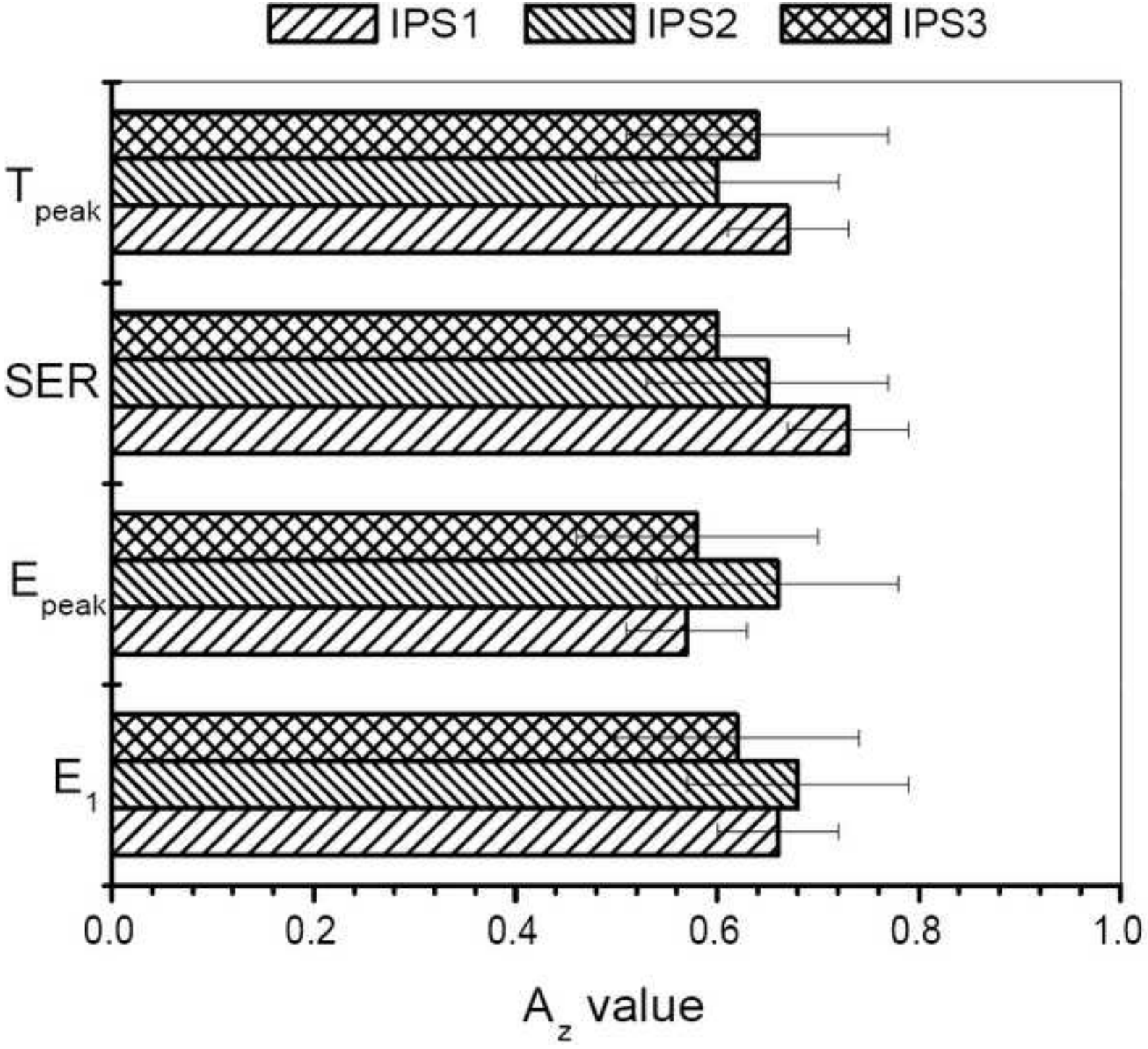

X-ray fluorescence microscopy and DCEMRI of murine ductal carcinoma *in situ* reveals gadolinium uptake within neoplastic mammary ducts

Original Research

Advances in Knowledge:

1. THIS STUDY REPRESENTS THE FIRST FUNCTIONAL CHARACTERIZATION OF MURINE DCIS VI
WE HAVE DEMONSTRATED THAT DESPITE ITS SMALL SIZE, MURINE DCIS CAN BE RELIABLY IM
MRI. POST-IMAGING TISSUE HARVESTING FOLLOWED BY HISTOLOGY CONFIRMED THE PRESE

2. ELEMENTAL MAPPING OF THE SAMPLES BY X-RAY FLUORESCENCE MICROSCOPY AS WELL
DCEMRI OF MURINE DCIS BOTH INDEPENDENTLY DEMONSTRATE GADOLINIUM UPTAKE ALON
DUCTS WITH DCIS. PRESENCE OF GADOLINIUM IN THE DUCT LUMEN OF DCIS PROVIDES AN IM
INSIGHT INTO THE REASON FOR CONTRAST ENHANCEMENT OF DCIS LESIONS ON CLINICAL DC
BREAST. PERHAPS THE BASEMENT MEMBRANES OF NEOPLASTIC MAMMARY DUCTS ARE LEA
DIFFUSION OF GADOLINIUM INSIDE. THIS DISCOVERY OPENS UP NEW POSSIBILITIES FOR PRE
STUDIES OF EARLY BREAST CANCER.

3. TWO MAIN FINDINGS OF THIS STUDY ARE THE HIGH EXTRA-VASCULAR EXTRACELLULAR S
DCIS AND THE FACT THAT GADOLINIUM IS PRESENT IN HIGH CONCENTRATIONS INSIDE MAMM
THESE FINDINGS HELP TO EXPLAIN THE PRESENTATION OF DCIS ON CLINICAL DCEMRI EXAMS
LIKE ENHANCEMENT, IN A DUCTAL/SEGMENTAL DISTRIBUTION, AND KINETIC CURVES THAT
OR ‘PLATEAU’ IN SHAPE.

Implications for Patient Care:

1. UNDERSTANDING THE UPTAKE OF GADOLINIUM IN MAMMARY DUCTS MAY LEAD TO IMPROV
IMAGING METHODS, MATHEMATICAL MODELING OF KINETIC DATA AND INTERPRETATION OF
EXAMPLE, OUR RESULTS INDICATE THAT THE TWO-COMPARTMENT PHARMACOKINETIC MOD
VS. EXTRAVASCULAR EXTRACELLULAR SPACE MAY NOT BE VALID FOR MODELING THE KINE
CONTRAST EXCHANGE WITH MAMMARY DUCTS REPRESENTS A THIRD COMPARTMENT.

2. LEAKINESS OF THE DUCT BASEMENT MEMBRANE MAY PROVE TO BE A MARKER FOR DCIS L
LIKELY TO BECOME INVASIVE, WHICH COULD LEAD TO IMPROVEMENTS IN THE CLINICAL MA
DCIS.

ABSTRACT

Purpose: ALTHOUGH DYNAMIC CONTRAST ENHANCED MR IMAGING (DCEMRI) CAN DETECT DU
CARCINOMA *in situ* (DCIS) BREAST CANCERS AFTER INJECTION OF A GADOLINIUM (GD) CHELA
UNDERLYING PHYSIOLOGICAL BASIS OF GD UPTAKE IS NOT CLEAR. OUR PURPOSE WAS TO C
WITH X-RAY FLUORESCENCE MICROSCOPY (XFM) OF MAMMARY GLAND TISSUE SAMPLES FR
TAG TRANSGENIC MICE TO IDENTIFY THE SPATIAL DISTRIBUTION OF GD FOLLOWING IV INJE

Materials and Methods: C3(1) SV40 TAG TRANSGENIC MICE (N=23) WERE STUDIED WITH IACUC
COMPLIANCE. DCEMRI WAS OBTAINED ON 12 MICE AFTER INJECTION OF GD-DTPA, AND GD
CONCENTRATION VS. TIME CURVES WERE FIT TO A TWO-COMPARTMENT PHARMACOKINETIC
PARAMETERS K^{TRANS}, V_E). ELEVEN MICE WERE INJECTED WITH GD-DTPA, SACRIFICED AFTER 2 MINUT
FROZEN SECTIONS CONTAINING DUCTS DISTENDED WITH MURINE DCIS WERE PREPARED FOR
ELEMENTAL CONCENTRATIONS OF GD WERE DETERMINED IN AND AROUND THE DUCTS WITH
SECTIONS OF MAMMARY TISSUES WERE OBTAINED FOLLOWING DCEMRI OR XFM.

Results: DUCTS CONTAINING DCIS WERE UNAMBIGUOUSLY IDENTIFIED IN MR IMAGES. DCEM
DEMONSTRATED CONTRAST UPTAKE ALONG THE LENGTH OF DUCTS WITH DCIS, WITH AVERA
K_{TRANS}=0.21±0.14(MIN^{-1}) AND V_E=0.40±0.16. INTERESTINGLY, XFM DEMONSTRATED GD UPTAKE *inside*
DUCTS WITH DCIS, WITH AN AVERAGE CONCENTRATION OF 0.475±0.380MM, WHICH WAS COM
THE *in vivo* DCEMRI VALUE OF 0.031MM.

Conclusion: OURRESULTS PROVIDE A NEW INSIGHT INTO THE PHYSIOLOGICAL BASIS OF CONTR ENHANCEMENT OF DCIS LESIONS ON DCEMRI: GD PENETRATES AND COLLECTS INSIDE NEOPL UNDERSTANDING THE UPTAKE OF GD IN MAMMARY DUCTS MAY LEAD TO IMPROVEMENTS IN METHODS, MATHEMATICAL MODELING OF KINETIC DATA AND INTERPRETATION OF DCEMRI.

INTRODUCTION

DYNAMIC CONTRAST ENHANCED MAGNETIC RESONANCE IMAGING (DCEMRI) HAS DEMO EQUAL OR SUPERIOR SENSITIVITY AND SPECIFICITY AT DETECTING EARLY INVASIVE CANCER RAY MAMMOGRAPHY (1). HOWEVER, THIS HAS NOT BEEN CONSISTENTLY DEMONSTRATED FO CARCINOMA *in situ* (DCIS), A NON-OBLIGATE PRECURSOR TO INVASIVE BREAST CANCER, IN WH CELLS ARE STILL CONFINED BY THE BASEMENT MEMBRANE OF MAMMARY DUCTS. BECAUSE EARLIEST STAGE OF BREAST CANCER WITH THE BEST PROGNOSIS, IT IS LIKELY THAT FURTHE DETECTING BREAST CANCERS AT A PREINVASIVE STAGE MAY IMPROVE PATIENT OUTCOMES. HAVE FOUND DECREASED DIAGNOSTIC ACCURACY OF DCEMRI FOR DCIS(2, 3), WHILE OTHERS COMPARABLE OR EVEN HIGHER PERFORMANCE COMPARED WITH X-RAY MAMMOGRAPHY (4, SENSITIVITY OF DCEMRI FOR DCIS MAY BE COMPROMISED IF THE LESION EITHER DOES NOT E SUFFICIENT CONTRAST UPTAKE OR IF IT IS OBSCURED BY STRONGLY ENHANCING PARENCHY WHEN DCIS IS DETECTED BY DCEMRI, IT CAN BE MISIDENTIFIED DUE TO (I) MORPHOLOGY: TH CHARACTERISTIC NONMASS-LIKE ENHANCEMENT OF DCIS COULD BE MISTAKEN FOR ENHANC PARENCHYMA, AND (II) KINETICS: DCIS OFTEN EXHIBITS ‘PLATEAU’ OR ‘PERSISTENT’ KINETIC WHICH ARE NOT TYPICAL OF MALIGNANT LESIONS (8). THUS, THERE IS A CLINICAL NEED TO I DIAGNOSTIC ACCURACY OF DCEMRI FOR DCIS (9).

A BETTER UNDERSTANDING OF THE MECHANISM OF CONTRAST ENHANCEMENT OF DCI HELPFUL FOR IMPROVING QUANTITATIVE ANALYSIS OF DCEMRI DATA, AND THUS FOR INCRE SENSITIVITY AND SPECIFICITY. INVASIVE TUMORS DEMONSTRATE UPTAKE OF THE GADOLIN USED AS MR CONTRAST AGENTS DUE TO THEIR DENSE AND LEAKY NEOVASCULATURE. CONT

KINETICS ARE OFTEN MODELED AS CONTRAST EXCHANGE BETWEEN TWO PHYSIOLOGIC COM
VASCULAR AND EXTRA-CELLULAR EXTRA-VASCULAR SPACE WITHIN THE TUMOR (10). HOWE
ARE NOT ALWAYS ASSOCIATED WITH DENSE VASCULATURE ESPECIALLY AT THEIR EARLY ST
MECHANISM OF DISTRIBUTION OF GD IS NOT WELL UNDERSTOOD. IN PARTICULAR, IT IS UNK
PENETRATES THE BASEMENT MEMBRANE TO ENTER MAMMARY DUCTS DISTENDED WITH DC

UNFORTUNATELY, IT IS DIFFICULT TO PERFORM DIRECT AND DETAILED MEASUREMEN
CONCENTRATIONS IN DCIS LESIONS IN WOMEN. THUS, THE PURPOSE OF THIS RESEARCH WAS
TRANSGENIC MOUSE MODEL OF BREAST CANCER (C3(1) SV40 TAG TRANSGENIC MICE) WITH A
THAT IS SIMILAR TO THAT OF HUMAN DISEASE TO INVESTIGATE THE DISTRIBUTION OF GD IN
SPECIFICALLY, OUR STUDY INVOLVED (I) PERFORMING *in vivo* DCEMRI OF MURINE DCIS AND (I
X-RAY FLUORESCENCE MICROSCOPY (XFM) TO VISUALIZE THE SPATIAL DISTRIBUTION OF GD
WITH SPATIAL RESOLUTION OF A FEW MICRONS.

MATERIALS AND METHODS

Animals

THE C3(1) SV40 LARGE T ANTIGEN (TAG) MOUSE MODEL WAS USED IN THIS STUDY. FEM
MICE DEVELOP SPONTANEOUS, ORTHOTOPIC MAMMARY CANCER THAT RESEMBLES HUMAN
INCLUDING PROGRESSION THROUGH ATYPICAL DUCTAL HYPERPLASIA (~8 WEEKS), DCIS (~12
INVASIVE DUCTAL CARCINOMA (IDC) (~16 WEEKS)(11). A TOTAL OF 23 SV40 TAG MICE WERE S
FOR THIS STUDY: (I) 12 FOR *in vivo* MR IMAGING, AND (II) 11 FOR X-RAY FLUORESCENCE MICRO
(XFM). ALL PROCEDURES WERE CARRIED OUT IN ACCORDANCE WITH OUR INSTITUTION'S AN
USE COMMITTEE APPROVAL.

MRI Experiments

IMAGING WAS PERFORMED WITH A BRUKER 4.7 TESLA MAGNET EQUIPPED WITH A SELF
GRADIENT SET THAT DELIVERS MAXIMUM GRADIENT STRENGTH OF 20 GAUSS/CM. A HOMEBU
PASS HALF-OPEN BIRDCAGE COIL (3.0 CM INNER DIAMETER, 2.0 CM HEIGHT) (12) WAS USED FOR *in*
vivo IMAGING. MULTI-SLICE AXIAL GRADIENT ECHO (GRE) IMAGES (TR/TE= 675/3.7 MS, FOV=3.0 ×
CM, NEX=2, SLICE THICKNESS=0.5MM, #SLICES=42, IN-PLANE RESOLUTION=117 MICRONS AND
ANGLE=30°) WITH FAT SUPPRESSION WERE ACQUIRED TO LOCALIZE LESIONS, AS PRIOR WORK
DEMONSTRATED THAT EARLY MURINE MAMMARY CANCERS CAN BE RELIABLY DETECTED IN
IMAGES (13). SUBSEQUENTLY, DCEMRI OF THREE SLICES AROUND THE LESION WERE OBTAIN
30/3.5 MS, SLICE THICKNESS = 1.0 MM, IN-PLANE RESOLUTION = 256 MICRONS, FLIP ANGLE=20°)
BASELINE IMAGES (N= 5) WERE ACQUIRED BEFORE CONTRAST INJECTION AND 128 IMAGES WE

POST-CONTRAST INJECTION SO THAT CONTRAST UPTAKE AND WASHOUT WAS FOLLOWED FO
MINUTES.

ANIMALS WERE ANESTHETIZED PRIOR TO IMAGING EXPERIMENTS, AND ANESTHESIA W
DURING IMAGING AT 1.5% ISOFLORANE. THE TEMPERATURE, HEART RATE AND RESPIRATION
MONITORED AND THE RESPIRATION RATE WAS USED TO OBTAIN GATED IMAGES. A 24G ANGI
IMPLANTED INTO THE TAIL VEIN FOR THE INJECTION OF 0.2CC OF 0.0184M GADODIAMIDE (OM
NYCOMED-AMERCHAM, PRINCETON NJ).

Histologic Evaluation

HEMATOXYLIN AND EOSIN (H&E) STAINED SECTIONS OF THE IMAGED MAMMARY GLAN
OBTAINED (5-MICRON THICK H&E SECTIONS EVERY 50 MICRONS) AND EVALUATED BY A BREA
MAMMARY GLAND PATHOLOGIST WITH OVER 20 YEARS OF EXPERIENCE. INTRAMAMMARY L
INVASIVE TUMORS AND DUCTS DISTENDED WITH DCIS WITH DIAMETERS GREATER THAN 300
IDENTIFIED AND USED AS THE GOLD STANDARD. MR IMAGES WERE CORRELATED WITH H&E
AN AGAR GRID AS DETAILED IN PRIOR WORK (13) IN ORDER TO IDENTIFY DCIS, INVASIVE TUM
NODES AND AREAS OF NORMAL MAMMARY GLAND (NMG) ON THE IMAGES.

DCEMRI Analysis

ALL DATA ANALYSIS WAS PERFORMED USING SOFTWARE WRITTEN IN IDL (RESEARCH S
BOULDER, CO). A SIMPLE TWO-COMPARTMENT MODEL (TCM) OF BLOOD PLASMA VS. EXTRAV
EXTRACELLULAR SPACE (EES), WAS USED TO DESCRIBE THE DISTRIBUTION OF GADODIAMIDE

INJECTION. SPECIFICALLY, THE MODEL PREDICTS THE CHANGE IN CONTRAST AGENT CONCENTRATIO
AS FOLLOWS:

$$\frac{dC(t)}{dt} = K^{trans} \cdot (C_p(t) - C(t)/v_e), \quad [1]$$

WHERE K^{TRANS} (MIN^{-1}) IS THE VOLUME TRANSFER CONSTANT BETWEEN BLOOD PLASMA AND EES, V
VOLUME OF EES PER UNIT VOLUME OF TISSUE AND $C_p(t)$ IS THE CONTRAST CONCENTRATION IN BLOOD PLA
(CALCULATED USING A 'REFERENCE TISSUE APPROACH'(14). C(T) CURVES WERE GENERATED
ROI'S: DCIS, INVASIVE TUMORS, LYMPH NODES, MUSCLE AND NORMAL MAMMARY GLAND (N
DETERMINE HOW WELL THE TCM FIT THE ROI CONCENTRATION CURVES, THE GOODNESS OF F
WAS USED, WITH $R^2 > 0.7$ INDICATING A GOOD FIT. FURTHER DETAILS ON THIS MODEL AND ANALY
FOUND IN THE APPENDIX. IN ADDITION, THE AVERAGE CONTRAST CONCENTRATION AT 2 MIN
CALCULATED FOR DCIS LESIONS FOR COMPARISON WITH X-RAY FLUORESCENCE MICROSCOP

X-ray fluorescence microscopy (XFM)

TEN MICE BETWEEN 12-14 WEEKS OF AGE WERE INJECTED WITH 0.2CC OF 0.0184 M
GADODIAMIDE AND SACRIFICED 2 MINUTES AFTER INJECTION. INGUINAL MAMMARY GLAND
IMMEDIATELY EXCISED, PLACED IN PLASTIC MOLDS WITH OCT COMPOUND EMBEDDING MED
INC. DIAGNOSTIC DIVISION, ELKHART, IN) AND FROZEN IN LIQUID NITROGEN. IN ADDITION, C
INJECTED WITH 0.2CC OF SALINE TO SERVE AS A CONTROL. FROZEN SECTIONS (7 MICRONS TH
OF MAMMARY GLANDS WITH DCIS, LYMPH NODES OR TUMORS WERE MOUNTED ON SILICON
WINDOWS (AREA, 3.0 X 3.0 MM; THICKNESS, 200 NM, SILSON, BLISWORTH, U.K.). ADJACENT H&
SECTIONS WERE ACQUIRED TO AID IN LESION IDENTIFICATION. SPECIMENS WERE IMAGED W
X-RAY MICROPROBE AT BEAMLINE 2-ID-E AT THE ADVANCED PHOTON SOURCE (ARGONNE, IL

WERE RASTER-SCANNED BY 10 KEV INCIDENT X-RAYS IN STEPS OF 3.0 -5.0 µM, AND FLUORESC
SPECTRA
WERE COLLECTED FOR 1- TO 2-SEC DWELL TIMES.

Elemental Concentrations from XFM

IMAGE PROCESSING AND ELEMENTAL CONCENTRATION ANALYSIS WAS PERFORMED W
SOFTWARE(15). THE FLUORESCENCE SPECTRA WERE CONVERTED FROM COUNTS TO A TWO-D
CONCENTRATION IN MICROGRAMS PER SQUARE CENTIMETER BY FITTING AGAINST THE SPEC
THIN-FILM STANDARDS NBS-1832 AND NBS-1833 (NATIONAL BUREAU OF STANDARDS, GAITHE
MD). TWO-DIMENSIONAL CONCENTRATIONS WERE CONVERTED TO THREE-DIMENSIONAL CO
MILLIMOLAR (MM) BY USING THE THICKNESS OF EACH SECTION (7 MICRONS) AND THE MOLE
GD (157.3 G/MOL). ELEMENTAL CONCENTRATION MAPS WERE DERIVED FOR SEVERAL ELEME
THEIR K OR L CHARACTERISTIC X-RAY FLUORESCENCE. IN THIS STUDY, WE SHOW PHOSPHORU
AND GD DATA. PHOSPHORUS CONCENTRATION MAPS ARE OFTEN USED TO LOCATE CELL NUC
ALONG WITH ADJACENT H&E SECTIONS TO DETERMINE CELLULARITY AND LOCATE MAMMA
NODES AND TUMORS. IRON CONCENTRATION MAPS CAN SERVE AS POTENTIAL INDICATORS O
BLOOD CELLS/VESSELS. WE USED THE PHOSPHOROUS CONCENTRATION MAPS TO DRAW ROI'
CONCENTRATION OF GD WAS QUANTIFIED: (I) DUCTS WITH DCIS, (II) LYMPH NODES, AND (III)
TUMORS.

RESULTS

DCEMRI of Murine DCIS

WE FOUND THAT DCIS LESIONS AND EARLY INVASIVE TUMORS APPEARED IN NONCONT
IMAGES CLEARLY AGAINST A DARKER BACKGROUND OF MAMMARY GLANDULAR TISSUE/FA
STAINED SECTIONS WERE OBTAINED FROM THE INGUINAL GLANDS OF ALL 12 MICE SELECTE
IMAGING. BASED ON HISTOLOGIC REVIEW, THERE WERE 11 LYMPH NODES, 1 LARGE (~5MM) T
SMALL NON-PALPABLE TUMORS ~0.5-3 MM IN SIZE, AND 15 DUCTS DISTENDED WITH DCIS GRE
300 MICRONS IN DIAMETER, WHICH WERE CLEARLY VISUALIZED AND ACCURATELY SEGMEN
SURROUNDING TISSUE FOR ACCURATE MEASUREMENTS OF CONTRAST MEDIA KINETICS.

DCEMRI DATA WAS ANALYZED ON 9 DUCTS WITH DCIS, 3 TUMORS, 11 LYMPH NODES, 12
MUSCLES AND 10 NORMAL MAMMARY GLAND AREAS (FIGURE 1). INTERESTINGLY, DCIS LESI
CONTRAST UPTAKE ALONG THE DUCT. SIGNAL INTENSITIES WERE CONVERTED TO GADODIA
WHICH IS EQUIVALENT TO GD CONCENTRATION. THE AVERAGE GD CONCENTRATION MEASU
IN DCIS LESIONS AT 2 MINUTES WAS 0.13 MM. THE TCM MODEL FIT MOST OF THE C(T) CURVES
WELL, BUT WAS A POOR MODEL FIT ($r^2 < 0.2$) FOR 3/9 DCIS AND 2/11 LYMPH NODES (FIGURE 2). DCIS
LESIONS ADEQUATELY FIT BY THE TCM EXHIBITED A WIDE RANGE OF KINETIC CURVE SHAPE
CORRESPONDING K^{TRANS} AND v_E VALUES. THE TCM WAS PARTICULARLY COMPROMISED IN THE NORMA
MAMMARY GLAND: ONLY 4/10 CURVES WERE FIT WELL. THIS IS LIKELY DUE TO THE POOR CO
MANY NORMAL MAMMARY GLAND AREAS.

FOR THOSE CURVES THAT WERE ADEQUATELY FIT BY THE TCM, THE VALUES OF K^{TRANS} AND v_E WERE COMPARED. THERE WAS CONSIDERABLE OVERLAP IN THE VALUES OF K^{TRANS} AND v_E IN DCIS LESIONS, INVASIVE TUMORS AND LYMPH NODES (TABLE 1). THERE WAS A TREND FOR DCIS LESIONS TO K^{TRANS} COMPARED WITH LYMPH NODES AND TUMORS. TCM PARAMETERS FOR BACK MUSCLE C $K^{TRANS} = 0.11$ MIN^{-1} AND $v_E = 0.20$, WHILE NORMAL MAMMARY GLAND AREAS DEMONSTRATED CONS LOWER K^{TRANS} AND v_E VALUES COMPARED TO DCIS, LYMPH NODES AND TUMORS (TABLE 1). INTERES THE v_E VALUES WERE QUITE HIGH IN DCIS AND TUMORS.

XFM of Gadolinium

THE RESULTS FROM DCEMRI OF MURINE DCIS SUGGESTED CONTRAST UPTAKE ALONG I DISTENDED WITH DCIS. IN ORDER TO EXAMINE THIS IN MORE DETAIL, WE TURNED TO XFM TO SPATIAL DISTRIBUTION OF GD IN MOUSE MAMMARY GLANDS WITH DCIS WITH MICRON RESO ELEMENTAL CONCENTRATION MAPS OF GD, FE, P AND OTHER ELEMENTS WERE OBTAINED FO MAMMARY GLANDS CONTAINING: DUCTS DISTENDED WITH DCIS (N=26), LYMPH NODES (N=2) (N=1). FOR MICE THAT HAD BEEN INJECTED WITH GADODIAMIDE, GD WAS DETECTED IN THE OUTSIDE OF NEOPLASTIC DUCTS, WHICH IN GENERAL MAY BE COMPRISED OF FAT, STROMA, N BLOOD VESSELS. INTERESTINGLY, XFM ALSO REVEALED GD UPTAKE IN TUMORS, LYMPH NOD DUCTS DISTENDED WITH DCIS. THE AVERAGE CONCENTRATION OF GD INSIDE DUCTS BY XFM 0.380 MM (TABLE 2). GD UPTAKE WITHIN DUCTS WAS DEMONSTRATED BOTH FOR LARGER DU TO A FEW HUNDRED MICRONS (FIGURE 3A AND 3B), AS WELL AS SMALLER DUCTS WITH DCIS A 100 MICRONS IN SIZE (FIGURE 3C). ON THE OTHER HAND, FE WAS NOT STRONGLY PRESENT WI MAMMARY DUCTS, SUGGESTING THAT NO RED BLOOD CELLS ACCUMULATED INSIDE THE DU

THAT GD DIFFUSES FROM BLOOD VESSELS INTO DUCTS WITH DCIS. LYMPH NODES AND A TU
EXHIBITED COMPARABLE CONCENTRATIONS OF GD AS IN DCIS.

CLOSER EXAMINATION OF THE VARIATION OF GD CONCENTRATION WITHIN DUCTS REV
HETEROGENEOUS DISTRIBUTION. THIS IS ILLUSTRATED WELL IN ONE SAMPLE WHERE A DUC
DCIS TO 300 MICRONS HAD BEEN SECTIONED LONGITUDINALLY (FIGURE 4A AND 4B). GD CON
WAS HIGHEST AROUND THE CANCER CELLS NEAR THE DUCT/STROMA INTERFACE, THEN DEC
CELLS FURTHER INTO THE DUCT, BUT COLLECTED ONCE AGAIN IN THE LUMEN. A POSSIBLE E
COULD BE THAT GD DIFFUSES INTO THE DUCT FROM THE SURROUNDING STROMA, THEN COL
IN THE LARGER UNOBSTRUCTED VOLUME OF THE DUCT LUMEN.

DISCUSSION

Using a transgenic mouse model of breast cancer to investigate contrast enhancement of DCIS on clinical DCEMRI of the breast, we have shown via two independent routes—DCEMRI and XFM—that after injection with Gadodiamide there is evidence for Gd uptake inside ducts distended with murine DCIS. FURTHERMORE, THESE TWO COMPLEMENTARY METHODS YIELDED SIMILAR VALUES FOR THE CONCENTRATION OF GD INS DUCTS AT 2 MINUTES: 0.475 MM FROM XFM, AND 0.30 MM FROM DCEMRI. IN THE DCEMRI DAT CANCER CONTAINING DUCTS WERE FAIRLY EFFECTIVELY ISOLATED FROM SURROUNDING TIS HAVE BEEN SOME PARTIAL VOLUME EFFECTS DUE TO SLICE THICKNESS. HOWEVER, THE XFM THAT GD PENETRATES *inside* DUCTS WITH DCIS. THIS IS A NEW INSIGHT INTO THE PHYSIOLOGIC BASI CONTRAST ENHANCEMENT OF THESE LESIONS.

SEVERAL OTHER GROUPS HAVE INVESTIGATED THE DISTRIBUTION OF GADOLINIUM IN OTHEN USING X-RAY FLUORESCENCE SPECTROSCOPY. GILBERT ET AL FOUND GD UPTAKE IN GI AFTER EXPOSURE TO GD-DTPA BOTH *in vitro* AND *in vivo*, FOR THE PURPOSES OF NEUTRON CAPT (16, 17). THE UPTAKE OF GD BY TISSUES IS OF PARTICULAR RECENT INTEREST GIVEN CONCER DISSOCIATED GD BY THE KIDNEY CAN RESULT IN NEPHROGENIC SYSTEMIC FIBROSIS (18). IT W OUR STUDY WHETHER THE GD DETECTED BY XFM IN TISSUE REMAINED CHELATED (AS GD-DT DISSOCIATED FROM THE CHELATE. FUTURE WORK USING X-RAY ABSORPTION SPECTROSCOP PERFORMED TO INVESTIGATE THE CHELATION-STATE OF THE GD DETECTED INSIDE DUCTS. I

SINGLE CANCER CELLS SHOULD BE PERFORMED TO DETERMINE WHETHER GD HAS PENETRATED I
BEEN DONE ELSEWHERE IN THE CONTEXT OF FOLLOWING TARGETED NANOPARTICLES (19, 20

OUR STUDY REPRESENTS THE FIRST FUNCTIONAL CHARACTERIZATION OF MURINE DCI
WHICH HAS AN ADVANTAGE COMPARED TO ITS HUMAN COUNTERPART: DUCTS WITH DCIS CA
VISUALIZED WITHOUT CONTRAST INJECTION, AND THUS AN ROI CAN BE PLACED DIRECTLY O
DUCT TO MORE ACCURATELY MEASURE ITS KINETIC PARAMETERS, MINIMIZING THE PARTIAL
COMPLICATES HUMAN KINETIC DATA. WE FOUND THAT K_{ep} OF DCIS WAS RELATIVELY HIGH COMPARED TO OTH
REPORTS OF RODENT TUMORS, WHICH ARE USUALLY LARGE AND AT AN ADVANCED STAGE (21, 22). THE
OBSERVATION OF GD PENETRATION AND ACCUMULATION IN THE LUMEN OF NEOPLASTIC MAM
CONSISTENT WITH A HIGH K_{ep}. HOWEVER, IT ALSO IMPLIES THAT THE TWO-COMPARTMENT MODEL,
WIDELY USED TO MODEL CONTRAST KINETICS IN CANCERS (23), MAY NOT BE VALID FOR DCIS
EXCHANGE INTO MAMMARY DUCTS REPRESENTS A THIRD COMPARTMENT. THUS, FOR ACCU
MODELING THE PATH THAT GD TAKES FROM BLOOD VESSELS TO MAMMARY DUCTS NEEDS E
LIKELY EXPLANATION OF THE MECHANISM UNDERLYING OUR FINDINGS IS THAT GD DIFFUSE
INTO THE EXTRA-DUCTAL SPACE, REACHES LEAKY DUCT BASEMENT MEMBRANES AND COLL
LUMEN. THE VARIABLE KINETIC CURVE SHAPES OF DCIS FOUND IN THIS STUDY (FIGURE 2) CA
INSIGHTS INTO THE HETEROGENEOUS PHYSIOLOGY OF DCIS AND SURROUNDING TISSUE; THE
VESSELS TO THE DUCTS, THE PERMEABILITY OF THE BASEMENT MEMBRANES AND THE VOLU
AVAILABLE FOR GD ACCUMULATION, ARE PHYSIOLOGIC FACTORS THAT CAN DIRECTLY IMPA
ENHANCEMENT KINETIC CURVES OF THESE LESIONS.

WE CAN TRANSLATE THE MURINE RESULTS TO WOMEN IF WE ASSUME CERTAIN PHYSIC
SIMILARITIES BETWEEN MAMMARY GLANDS ACROSS SPECIES, IN PARTICULAR THAT THE PER
MAMMARY DUCT BASEMENT MEMBRANES TO GADOLINIUM IS SIMILAR IN BOTH SPECIES. TH
NEEDS FURTHER EXPLORATION—IT MAY BE DUE TO PROTEASE SECRETION BY CANCER CELL
TO BE A MARKER FOR DCIS LESIONS THAT ARE LIKELY TO BECOME INVASIVE, PERHAPS LEAD
IMPROVEMENTS IN THE CLINICAL MANAGEMENT OF DCIS. THE AVERAGE CONCENTRATION C
MEASURED IN OUR STUDY WAS HIGH ENOUGH TO BE A SIGNIFICANT SOURCE OF MEASURED M
CLINICAL DCEMRI. THIS MAY IN PART EXPLAIN THE TYPICAL MORPHOLOGY OF DCIS LESIONS
DCEMRI: NONMASS LIKE ENHANCEMENT, IN A SEGMENTAL/LINEAR/DUCTAL DISTRIBUTION (4
ADDITION, THE HIGHER K^{trans} VALUES, AND THE LIKELY LONGER TIMESCALE OF GD EXCHANGE INTO AN
DUCTS MAY EXPLAIN THE PERSISTENT AND PLATEAU CURVE TYPES OFTEN FOUND FOR DCIS(

THERE ARE SEVERAL LIMITATIONS TO THIS STUDY. FIRST, BECAUSE OF THE SMALL LES
CURVES WERE SUBJECT TO NOISE AND MOTION ARTIFACTS, POTENTIALLY COMPROMISING TI
SECOND, ALTHOUGH SAMPLES WERE PREPARED FOR XFM ACCORDING TO ACCEPTED METHOD
LOW-MOLECULAR WEIGHT INJECTED AGENTS, DIFFUSION OF GADOLINIUM IN THE SAMPLE W
WORTH NOTING, HOWEVER, THAT AIR-DRYING AND FREEZE-DRYING OF TISSUE SECTIONS FO
IDENTICAL GD DISTRIBUTION PATTERNS (DATA NOT SHOWN). THEREFORE, WHILE SOME GD "
SAMPLES MAY BE EXPECTED DUE TO SAMPLE PREPARATION, IT IS LIKELY NOT VISIBLE AT TH
IN THESE STUDIES (μM-STEP SCANS). FINALLY, PATHOLOGIC EVALUATION OF THE ENTIRE SPECI
NOT PERFORMED TO DETERMINE WHETHER THE DUCTS IMAGED WERE PURE DCIS, OR WHETH
IN OTHER SECTIONS WAS PRESENT WHICH COULD BE THE ENTRY POINT OF THE GD. HOWEVE

DUCTS WITH DCIS, IN WHICH MICROINVASION WAS NOT LIKELY, ALSO EXHIBITED CONTRAST

3C AND DATA NOT SHOWN).

Practical Applications: UNDERSTANDING THE UPTAKE OF GD BY MAMMARY DUCTS MAY HELP T

IMPROVE THE SENSITIVITY AND SPECIFICITY OF DCEMRI BY IMPROVED INTERPRETATION AN

EXISTING DATA, AND IN DESIGNING NEW ACQUISITION TECHNIQUES TARGETED FOR DCIS. FO

CLINICAL DCEMRI DATA FROM PATIENTS HAS RELATIVELY COARSE SPATIAL RESOLUTION, A

VOXELS MAY CONTAIN DCIS AND BLOOD VESSELS. ONE COULD DECOMPOSE C(T) FOR DCIS V

FAST COMPONENT (REPRESENTING BLOOD VESSELS) AND A SLOW COMPONENT (REPRESENTING

GD IN DUCTS).

WE HAVE PRESENTED A GENERAL APPROACH TO USE MOUSE MODELS OF BREAST CANCE

UNDERSTAND DCIS IN WOMEN. PRIOR WORK HAS DEMONSTRATED THAT MRI PROVIDES EXCE

MORPHOLOGIC EVALUATION OF EARLY MURINE MAMMARY CANCERS (13). WE HAVE NOW U

TO PERFORM THE FIRST FUNCTIONAL CHARACTERIZATION OF THE CONTRAST KINETICS OF M

ALONG WITH XFM, HAVE DEMONSTRATED CONTRAST UPTAKE INSIDE AND ALONG NEOPLAST

DUCTS. IN FUTURE WORK, WE PLAN TO USE SERIAL MR IMAGING TO CHARACTERIZE BOTH TH

AND FUNCTIONAL CHANGES THAT OCCUR DURING THE DEVELOPMENT AND PROGRESSION OF

CARCINOMA.

APPENDIX: Two compartment modeling of contrast media kinetics.

Calculating Contrast Concentration: SIGNAL INTENSITY S(T) VS. TIME CURVES WERE GENERATED F
SEVERAL REGIONS OF INTEREST (ROI): DCIS, INVASIVE TUMOR, INTRAMAMMARY LYMPH NOD
MUSCLE AND NMG. BY ASSUMING THAT SIGNAL INTENSITY IS A LINEAR FUNCTION OF T
THESE VALUES CAN BE CONVERTED TO CONCENTRATION C(T) AS A FUNCTION OF TIME, USING

$$C(t) = \frac{1}{R_1 \cdot T_{1(muscle)}} \frac{S(t) - S(0)}{S_{muscle}(0)} \qquad [2]$$

HERE, R_1=4.3 $MM^{-1}S^{-1}$ IS THE LONGITUDINAL RELAXIVITY OF THE GADOLINIUM CHELATE, $T_{1(MUSCLE)}$ IS 1.285 SECONDS
AT 4.7 T AND $S_{MUSCLE}(0)$ IS THE SIGNAL INTENSITY IN AN ROI DRAWN IN THE BACK MUSCLE BEFORE
INJECTION. THE SELECTED ROI'S WERE MUCH SMALLER THAN THE COIL AND THE B1 FIELD W
BE UNIFORM OVER THE SELECTED AREAS, BASED ON PRIOR PHANTOM EXPERIMENTS. ALL DA
NORMALIZED TO THE INJECTED DOSE, TO ALLOW FOR MORE ACCURATE COMPARISONS BETW

Calculating Arterial Input Function: TO CALCULATE $C_P(T)$, THE CONTRAST CONCENTRATION IN $C_{MUSCLE}(T)$
NORMAL MUSCLE WAS FIRST CALCULATED AND FIT TO AN EMPIRICAL MATHEMATICAL MOD
USING PUBLISHED VALUES FOR GADODIAMIDE K^{TRANS} IN MUSCLE ($0.11\ MIN^{-1}$) AND 0.2, V_E
RESPECTIVELY (14)), EQUATION [1] WAS USED TO OBTAIN THE INPUT FUNCTION.

Data Analysis: USING SOFTWARE WRITTEN IN IDL (RESEARCH SYSTEMS, INC., BOULDER, CO).C(T
FOR DCIS, INVASIVE TUMORS, LYMPH NODES, MUSCLE AND NMG WERE FIT TO EQUATION [1] U
GOLDEN SECTION SEARCH IN TWO DIMENSIONS, AND THE PARAMETERS (K^{TRANS}, V_E) WERE OF BEST FIT (K

DETERMINED. TO DETERMINE HOW WELL THE TCM FIT THE ROI CONCENTRATION CURVES, THE R^2 ERROR

WAS USED

$$R^2 = 1.0 - \frac{SS_{error}}{SS_{total}}, \qquad [3]$$

WHERE SS_{ERROR} IS THE SUM OF THE SQUARES OF THE DISTANCES OF THE EXPERIMENTAL POINTS FROM THE

FIT CURVE DETERMINED, AND SS_{TOTAL} IS THE SUM OF THE SQUARE OF THE DISTANCES OF THE EXPERIMENTAL

POINTS FROM A HORIZONTAL LINE THROUGH THE MEAN OF ALL THE DATA POINTS. WHEN R^2 EQUALS 0.0 THE BEST-FIT

CURVE FITS THE DATA NO BETTER THAN A HORIZONTAL LINE GOING THROUGH THE MEAN OF ALL THE DATA POINTS. WHEN R^2

EQUALS 1.0 ALL EXPERIMENTAL DATA POINTS LIE EXACTLY ON THE BEST-FIT CURVE. IF R^2 IS LESS THAN 0.7 THE TCM WAS

CONSIDERED TO NOT ADEQUATELY FIT THE CONCENTRATION CURVES.

REFERENCES

1. SASLOW D, BOETES C, BURKE W, ET AL. AMERICAN CANCER SOCIETY GUIDELINES FOR
SCREENING WITH MRI AS AN ADJUNCT TO MAMMOGRAPHY. CA CANCER J CLIN 2007; 57
2. GILLES R, MEUNIER M, LUCIDARME O, ET AL. CLUSTERED BREAST MICROCALCIFICATIO
BY DYNAMIC CONTRAST-ENHANCED SUBTRACTION MRI. J COMPUT ASSIST TOMOGR 19
3. WESTERHOF JP, FISCHER U, MORITZ JD, OESTMANN JW. MR IMAGING OF MAMMOGRAPH
DETECTED CLUSTERED MICROCALCIFICATIONS: IS THERE ANY VALUE? RADIOLOGY 19
4. ESSERMAN LJ, KUMAR AS, HERRERA AF, ET AL. MAGNETIC RESONANCE IMAGING CAPTU
BIOLOGY OF DUCTAL CARCINOMA IN SITU. J CLIN ONCOL 2006; 24:4603-4610.
5. KUHL CK, SCHRADING S, BIELING HB, ET AL. MRI FOR DIAGNOSIS OF PURE DUCTAL CAR
SITU: A PROSPECTIVE OBSERVATIONAL STUDY. LANCET 2007; 370:485-492.
6. KUHL CK, BIELING HB, GIESEKE J, ET AL. HEALTHY PREMENOPAUSAL BREAST PARENCH
DYNAMIC CONTRAST-ENHANCED MR IMAGING OF THE BREAST: NORMAL CONTRAST M
ENHANCEMENT AND CYCLICAL-PHASE DEPENDENCY. RADIOLOGY 1997; 203:137-144.
7. WEINREB JC, NEWSTEAD G. MR IMAGING OF THE BREAST. RADIOLOGY 1995; 196:593-610.
8. JANSEN SA, NEWSTEAD GM, ABE H, SHIMAUCHI A, SCHMIDT RA, KARCZMAR GS. PURE D
CARCINOMA IN SITU: KINETIC AND MORPHOLOGIC MR CHARACTERISTICS COMPARED V
MAMMOGRAPHIC APPEARANCE AND NUCLEAR GRADE. RADIOLOGY 2007; 245:684-691.
9. HARMS SE. THE USE OF BREAST MAGNETIC RESONANCE IMAGING IN DUCTAL CARCINO
BREAST J 2005; 11:379-381.
10. ARMITAGE P, BEHRENBRUCH C, BRADY M, MOORE N. EXTRACTING AND VISUALIZING
PHYSIOLOGICAL PARAMETERS USING DYNAMIC CONTRAST-ENHANCED MAGNETIC RES
OF THE BREAST. MED IMAGE ANAL 2005; 9:315-329.
11. GREEN JE, SHIBATA MA, YOSHIDOME K, ET AL. THE C3(1)/SV40 T-ANTIGEN TRANSGENIC
MODEL OF MAMMARY CANCER: DUCTAL EPITHELIAL CELL TARGETING WITH MULTIST
CARCINOMA. ONCOGENE 2000; 19:1020-1027.
12. FAN X, MARKIEWICZ EJ, ZAMORA M, KARCZMAR GS, ROMAN BB. COMPARISON AND
EVALUATION OF MOUSE CARDIAC MRI ACQUIRED WITH OPEN BIRDCAGE, SINGLE LOOP
VOLUME BIRDCAGE COILS. PHYS MED BIOL 2006; 51:N451-459.
13. JANSEN SA, CONZEN SD, FAN X, ET AL. DETECTION OF IN SITU MAMMARY CANCER IN A
MOUSE MODEL: IN VITRO AND IN VIVO MRI STUDIES DEMONSTRATE HISTOPATHOLOGI
PHYS MED BIOL 2008; 53:5481-5493.
14. KOVAR DA, LEWIS M, KARCZMAR GS. A NEW METHOD FOR IMAGING PERFUSION AND C
EXTRACTION FRACTION: INPUT FUNCTIONS DERIVED FROM REFERENCE TISSUES. J MA
IMAGING 1998; 8:1126-1134.
15. VOGT S. MAPS: A SET OF SOFTWARE TOOLS FOR ANALYSIS AND VISUALIZATION OF 3D X
FLUORESCENCE DATA SETS. J PHYS IV 2003; 104:635-638.
16. DE STASIO G, CASALBORE P, PALLINI R, ET AL. GADOLINIUM IN HUMAN GLIOBLASTOMA
GADOLINIUM NEUTRON CAPTURE THERAPY. CANCER RES 2001; 61:4272-4277.

17. DE STASIO G RD, CASALBORE P, DANIELS MJ, ERHARDT RJ, FRAZER BH, EW
HJ, WIESE LM, RIC
KL, SONDEREGGER BR, GILBERT B, SCHAUB S, CANNARA RJ, CRAWFORD JF, GILLES MK,
TYLISZCZAK T, FOWLER JF, LAROCCA LM, HOWARD SP, MERCANTI D, MEHTA MP, PALLI
ARE GADOLINIUM CONTRAST AGENTS SUITABLE FOR GADOLINIUM NEUTRON CAPUTRE
RES 2005; 27:387-398.
18. SIEBER MA, LENGSFELD P, FRENZEL T, ET AL. PRECLINICAL INVESTIGATION TO COMPAR
GADOLINIUM-BASED CONTRAST AGENTS REGARDING THEIR PROPENSITY TO RELEASE
AND TO TRIGGER NEPHROGENIC SYSTEMIC FIBROSIS-LIKE LESIONS. EUR RADIOL 2008.
19. PAUNESKU T, KE T, DHARMAKUMAR R, ET AL. GADOLINIUM-CONJUGATED TIO2-DNA
OLIGONUCLEOTIDE NANOCONJUGATES SHOW PROLONGED INTRACELLULAR RETENTIC
WEIGHTED CONTRAST ENHANCEMENT IN MAGNETIC RESONANCE IMAGES. NANOMEDIC
4:201-207.
20. ENDRES PJ, PAUNESKU T, VOGT S, MEADE TJ, WOLOSCHAK GE. DNA-TIO2 NANOCONJUGA
LABELED WITH MAGNETIC RESONANCE CONTRAST AGENTS. J AM CHEM SOC 2007; 129:1
15761.
21. WEIDENSTEINER C, RAUSCH M, MCSHEEHY PM, ALLEGRINI PR. QUANTITATIVE DYNAMI
CONTRAST-ENHANCED MRI IN TUMOR-BEARING RATS AND MICE WITH INVERSION REC
AND TWO CONTRAST AGENTS AT 4.7 T. J MAGN RESON IMAGING 2006; 24:646-656.
22. YANKEELOV TE, DEBUSK LM, BILLHEIMER DD, ET AL. REPEATABILITY OF A REFERENCE
MODEL FOR ANALYSIS OF MURINE DCE-MRI DATA AT 7T. J MAGN RESON IMAGING 2006;
24:1140-1147.
23. FURMAN-HARAN E, SCHECHTMAN E, KELCZ F, KIRSHENBAUM K, DEGANI H. MAGNETIC
RESONANCE IMAGING REVEALS FUNCTIONAL DIVERSITY OF THE VASCULATURE IN BEN
BREAST LESIONS. CANCER 2005; 104:708-718.
24. NEUBAUER H, LI M, KUEHNE-HEID R, SCHNEIDER A, KAISER WA. HIGH GRADE AND NON-
GRADE DUCTAL CARCINOMA IN SITU ON DYNAMIC MR MAMMOGRAPHY: CHARACTERIS
SIGNAL INCREASE AND MORPHOLOGICAL PATTERN OF ENHANCEMENT. BR J RADIOL 20
25. MENELL JH, MORRIS EA, DERSHAW DD, ABRAMSON AF, BROGI E, LIBERMAN L.
DETERMINATION OF THE PRESENCE AND EXTENT OF PURE DUCTAL CARCINOMA IN SITU
MAMMOGRAPHY AND MAGNETIC RESONANCE IMAGING. BREAST J 2005; 11:382-390.
26. VAN GOETHEM M, SCHELFOUT K, KERSSCHOT E, ET AL. COMPARISON OF MRI FEATURES
DIFFERENT GRADES OF DCIS AND INVASIVE CARCINOMA OF THE BREAST. JBR-BTR 2005
27. OREL SG, MENDONCA MH, REYNOLDS C, SCHNALL MD, SOLIN LJ, SULLIVAN DC. MR IMA
OF DUCTAL CARCINOMA IN SITU. RADIOLOGY 1997; 202:413-420.
28. GROVES AM, WARREN RM, GODWARD S, RAJAN PS. CHARACTERIZATION OF PURE HIGH-
DCIS ON MAGNETIC RESONANCE IMAGING USING THE EVOLVING BREAST MR LEXICON
CAN IT BE DIFFERENTIATED FROM PURE INVASIVE DISEASE? MAGN RESON IMAGING 20
738.
29. FAN X, MEDVED M, RIVER JN, ET AL. NEW MODEL FOR ANALYSIS OF DYNAMIC CONTRA
MRI DATA DISTINGUISHES METASTATIC FROM NONMETASTATIC TRANSPLANTED RODE
TUMORS. MAGN RESON MED 2004; 51:487-494.

Table 1: VALUES OF K^{TRANS} AND V_E IN VARIOUS ROI'S. DATA SHOWN ARE AVERAGE ± STANDARD DEV AND ARE CALCULATED ONLY FOR THOSE CURVES THAT WERE FIT WELL BY THE TCM ($R^2 > 0.7$)

Region of Interest	No. cases	Average ROI volume (mm^3)	No. cases fit well	$K^{trans}(min^{-1})$	v_e
DCIS	9	0.10 ± 0.06	6	0.21±0.14	0.40±0.16
Tumor	3	0.26 ± 0.19	3	0.36±0.05	0.62±0.18
Lymph node	11	0.11 ± 0.03	9	0.38±0.23	0.51±0.17
Back Muscle	12	0.84 ± 0.25	12	0.11±0.014	0.21±0.034
Normal Mammary Gland	10	0.25 ± 0.11	4	0.084±0.037	0.21±0.16

Table 2: CONCENTRATION OF GADOLINIUM IN VARIOUS REGIONS OF INTEREST. THE AVERAGE CONCENTRATION OF GD INSIDE DUCTS BY XFM WAS 0.486 MM IN COMPARISON, FOR THOSE MICE THAT HAD BEEN INJECTED WITH ONLY SALINE AS A CONTROL, THE AVERAGE CONCENTRATION WITH DCIS WAS 0.010.004 MM, APPROXIMATELY 50 TIMES LOWER THAN FOR THOSE MICE INJECTED WITH GADODIAMIDE. THIS SEEMINGLY HIGH CONCENTRATION OF BACKGROUND GD IS LIKELY CONSIDERABLE OVERLAP OF THE GD L PEAK WITH THE FE K PEAK. IT SHOULD THUS BE THOUGHT MEASUREMENT ERROR, WHICH WHEN SUBTRACTED FROM THE MEASURED VALUES REDUCES THE AVERAGE CONCENTRATION OF GD IN DUCTS FROM 0.486 MM TO 0.475 MM.

Region of Interest	No. cases	Measured Gd concentration (mM)	Gd concentration adjusted for background (mM)
Inside ducts with DCIS (mice injected with saline as control)	4	0.011±0.004	_
Inside ducts with DCIS (mice injected with Gadodiamide)	22	0.486±0.380	0.475±0.380
Intramammary lymph node	2	0.376	0.365
Tumor	1	0.226	0.215

CAPTIONS FOR ILLUSTRATIONS

Figure 1: *Left.* AXIAL GRADIENT ECHO IMAGES WITH FAT SUPPRESSION REPRESENTING CROSS-
SLICES THROUGH THE MAMMARY GLANDS OF THREE MICE, DEMONSTRATING A) NORMAL MA
(DARKER AREA OUTLINED IN WHITE), B) INTRAMAMMARY LYMPH NODE (ARROWHEAD), B) DC
AND C) TUMOR (THICK ARROW). THE DISPLAY FOR THE LYMPH NODE, DCIS AND TUMOR
APPEAR CLEARLY AGAINST A DARKER BACKGROUND OF THE NORMAL MAMMARY GLAND. *R*
CURVES C(T) AND TWO COMPARTMENT MODEL (TCM) FITS FOR ROI'S A) NORMAL MAMMARY
LYMPH NODE, C) DCIS AND D) TUMOR ARE SHOWN IN BLACK. IN EACH OF A)-D), THE GREY CU
REPRESENTS THE CONCENTRATION CURVE IN AN ROI DRAWN ON THE BACK MUSCLE, FOR CO
PLOTS ARE SCALED FROM -0.1 MM – 0.6 MM.

Figure 2: EXAMPLES OF CONCENTRATION CURVES (POINTS) AND CORRESPONDING TWO-COMP
(TCM) FITS (SOLID LINES) FROM THREE DCIS LESIONS. IN THE BLACK AND RED CURVES, THE C
CURVES WERE FIT WELL BY THE TCM. HOWEVER, THE CONCENTRATION CURVE IN BLUE WAS
FIT BY THE TCM, POSSIBLY DUE TO THE HIGH NOISE LEVEL.

Figure 3: EXAMPLES OF XFM OF THE CROSS SECTION OF DUCTS WITH DCIS, INDICATED IN THE
SECTIONS ON THE LEFT. FOR A)-C) THE CONCENTRATION MAPS FROM LEFT TO RIGHT ARE OF
IRON (FE) AND GADOLINIUM (GD). ON THE RAINBOW SCALE, BLUE INDICATES LOWER, GREEN
HIGHEST CONCENTRATIONS. FOR EACH ELEMENT, THE IMAGES ARE ALL WINDOWED SIMILAR
$\mu G/CM^2$; FE, 0-0.7 $\mu G/CM^2$; GD, 0-0.1 $\mu G/CM^2$ (WHICH IS EQUIVALENT TO 0.91 MM PER PIXEL). IN ALL,
GD UPTAKE IS DEMONSTRATED WITHIN THE DUCT. IN THE FE MAP OF B) WHITE ARROWS POIN

THAN WIDE STRUCTURE WITH HIGHER FE CONCENTRATIONS THAT COULD BE A BLOOD VESSE
B) ALSO DEMONSTRATES HIGHER CONCENTRATIONS IN THIS REGION, WHICH COULD IMPLY GI
BLOOD VESSELS, ALTHOUGH DUE TO THE OVERLAP OF THE GD-L AND FE- K FLUORESCENCE P
DIFFICULT TO CONCLUDE DEFINITIVELY.

Figure 4: XFM CONCENTRATION MAPS DEMONSTRATING THE HETEROGENEITY OF GD DISTRIB
WITH DCIS. THE LIGHT MICROGRAPH IN A) DEMONSTRATES A DUCT WITH DCIS SECTIONED LO
OUTLINED IN YELLOW ON THE LEFT. ON THE RIGHT, THREE PORTIONS OF THE SAME DUCT AR
WHICH SUBSEQUENT ELEMENTAL CONCENTRATION MAPS ARE DISPLAYED IN B)-D). THE CON
FROM LEFT TO RIGHT ARE OF PHOSPHORUS (P), IRON (FE) AND GADOLINIUM (GD). FOR EACH E
IMAGES ARE ALL WINDOWED SIMILARLY WITH P, 0-50.7 $\mu G/CM^2$; GD, 0-0.1 $\mu G/CM^2$ (WHICH IS
EQUIVALENT TO 0.91 MM PER PIXEL). IN B) GD UPTAKE IS DEMONSTRATED WITHIN THE DUCT;
OF THE DUCT CONTAINS DENSELY PACKED CANCER CELLS, AND THE LUMEN IS NOT VISIBLE.
ZOOMED INTO A SEGMENT OF THE DUCT, AND FIND THAT GD CONCENTRATION IS HIGHER NE
MEMBRANE (GREEN ARROW) THAN CLOSER TO THE CENTER OF THE DUCT (BLUE ARROW). FU
DUCT, A PORTION OF THE DUCT LUMEN IS VISIBLE IN D) DEMONSTRATING INCREASED GD CO
LUMEN.

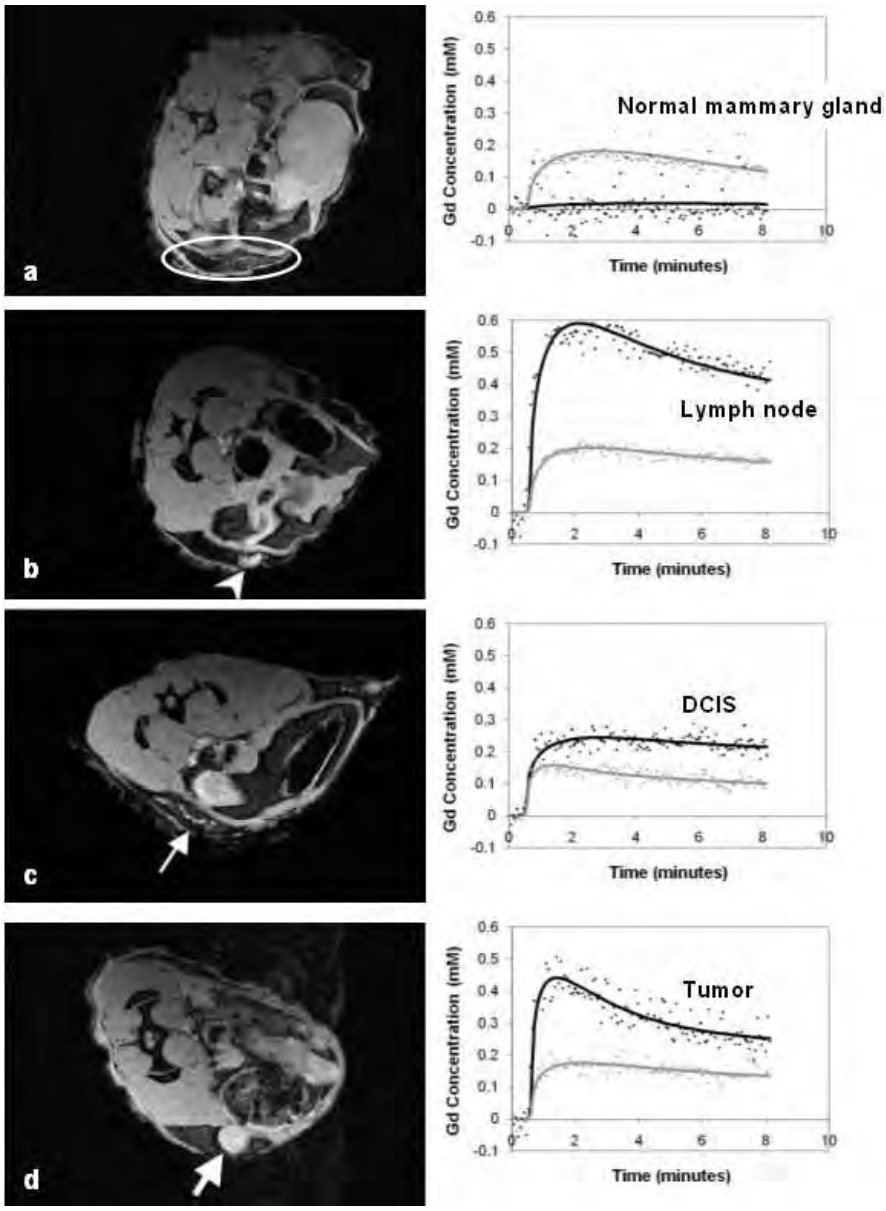

Left. Axial gradient echo images with fat suppression representing cross-sectional slices through the mammary glands of three mice, demonstrating a) normal mammary gland (darker area outlined in white), b) intramammary lymph node (arrowhead), b) DCIS (thin arrow), and c) tumor (thick arrow). The display FOV is 3.0 × 2.0 cm. The lymph node, DCIS and tumor appear clearly against a darker background of the normal mammary gland. Right. Concentration curves C(t) and two compartment model (TCM) fits for ROI's a) normal mammary gland, b) lymph node, c) DCIS and d) tumor are shown in black. In each of a)-d), the grey curve represents the concentration curve in an ROI drawn on the back muscle, for comparison. All plots are scaled from -0.1 mM □ 0.6 mM.
48x66mm (300 x 300 DPI)

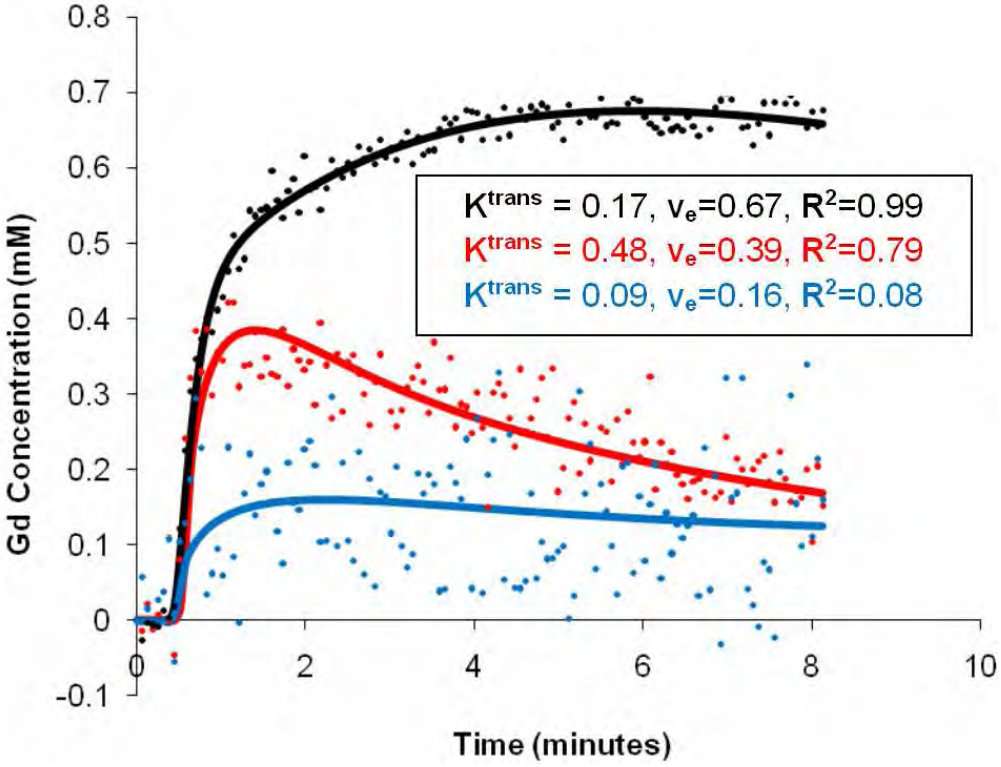

Examples of concentration curves (points) and corresponding two-compartment model (TCM) fits (solid lines) from three DCIS lesions. In the black and red curves, the concentration curves were fit well by the TCM. However, the concentration curve in blue was not adequately fit by the TCM, possibly due to the high noise level.
80x61mm (300 x 300 DPI)

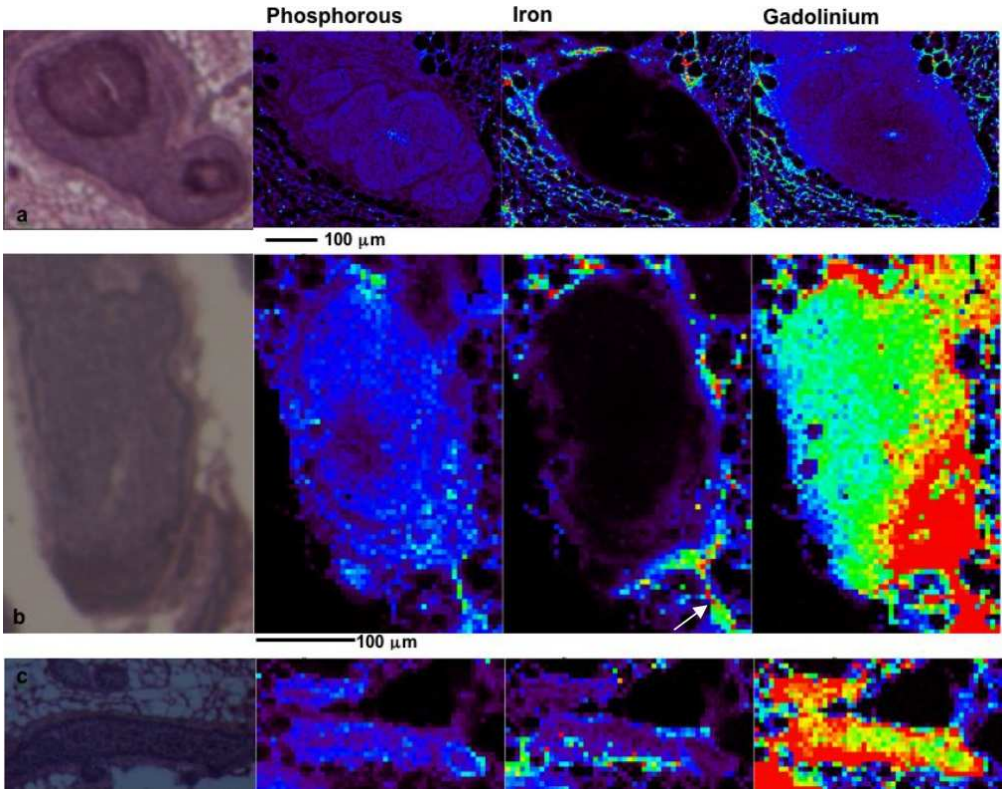

Examples of XFM of the cross section of ducts with DCIS, indicated in the H&E sections on the left. For a)-c) the concentration maps from left to right are of phosphorus (P), iron (Fe) and gadolinium (Gd). On the rainbow scale, blue indicates lower, green higher and red highest concentrations. For each element, the images are all windowed similarly: P, 0-15 μg/cm2; Fe, 0-0.7 μg/cm2; Gd, 0-0.1 μg/cm2 (which is equivalent to 0.91 mM per pixel). In all, Gd uptake is demonstrated within the duct. In the Fe map of b) white arrows point to a longer than wide structure with higher Fe concentrations that could be a blood vessel. The Gd map in b) also demonstrates higher concentrations in this region, which could imply Gd presence in blood vessels, although due to the overlap of the Gd-L and Fe- K fluorescence peaks this is difficult to conclude definitively.
85x66mm (300 x 300 DPI)

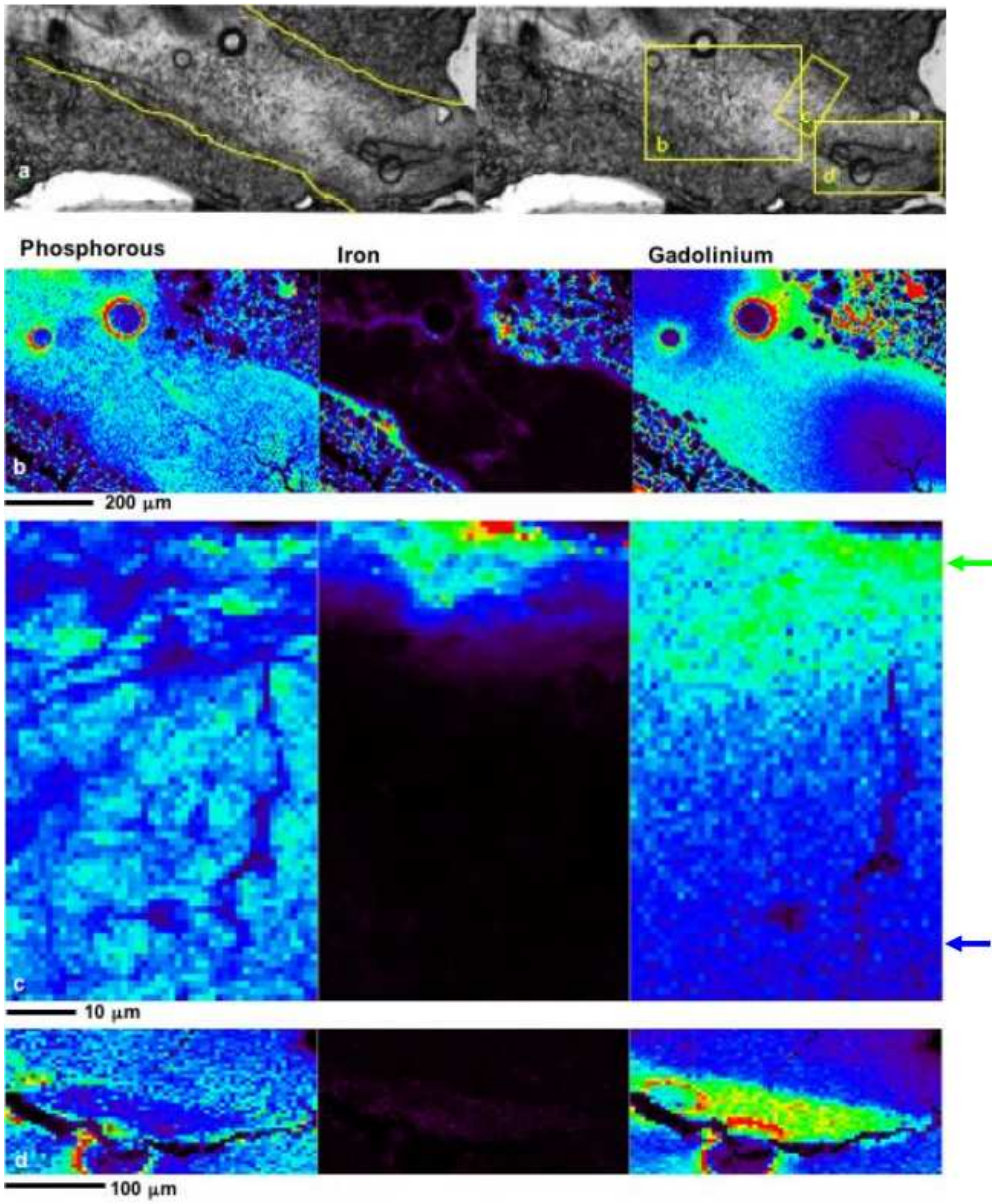

XFM concentration maps demonstrating the heterogeneity of Gd distribution in a duct with DCIS. The light micrograph in a) demonstrates a duct with DCIS sectioned longitudinally, outlined in yellow on the left. On the right, three portions of the same duct are outlined for which subsequent elemental concentration maps are displayed in b)-d). The concentration maps from left to right are of phosphorus (P), iron (Fe) and gadolinium (Gd). For each element, the images are all windowed similarly: P, 0-15 μg/cm2; Fe, 0-0.7 μg/cm2; Gd, 0-0.1 μg/cm2 (which is equivalent to 0.91 mM per pixel). In b) Gd uptake is demonstrated within the duct; this portion of the duct contains densely packed cancer cells, and the lumen is not visible. In c) we have zoomed into a segment of the duct, and find that Gd concentration is higher near the basement membrane (green arrow) than closer to the center of the duct (blue arrow). Further down the duct, a portion of the duct lumen is visible in d) demonstrating increased Gd concentration in the lumen.
54x66mm (300 x 300 DPI)

Kinetic and pathologic characteristics of 457 breast lesions detected at MR imaging as focus, mass or nonmass-like enhancement.

Sanaz A. Jansen PhD, Akiko Shimauchi MD, Lindsay Zak BSc,
Xiaobing Fan PhD, Gregory S. Karczmar PhD
and Gillian M. Newstead MD.*

Address for all authors:

Department of Radiology
The University of Chicago
5841 S. Maryland Ave MC2026
Chicago, IL 60637

Submitted as an Original Research Article to American Journal of Roentgenology
Word count: 2916

*Corresponding Author:

Professor Gillian Newstead, M.D.
Department of Radiology
University of Chicago
5841 S. Maryland Ave, MC 2026
Chicago, IL 60637

Phone: (773) 702-2781
Fax: (773) 834-9047
Email: gnewstead@radiology.bsd.uchicago.edu

ACKNOWLEDGMENTS

We would like to thank the Segal Foundation and the Department of Defense Predoctoral Award WX81XWH-06-1-0329 for financial support.

ABSTRACT

Objective: To compare the pathologic and kinetic characteristics of lesions with focus, mass and nonmass-like enhancement.

Subjects and Methods: 457 MR detected breast lesions in 401 patients were selected for an IRB approved review. Dynamic MR protocol: 1 pre and 3 or 5 post-contrast images acquired in the coronal plane. An experienced radiologist classified the type of enhancement according to the BI-RADS lexicon (mass, non-mass or focus) and generated a kinetic curve by tracing a region of interest around the most enhancing part of the lesion. Several quantitative parameters were derived from the curve including the initial enhancement percentage ($\mathbf{E_1}$), time to peak enhancement ($\mathbf{T_{peak}}$) and signal enhancement ratio (**SER**, a measure of signal washout). These parameters were compared between malignant and benign lesions within each morphologic type.

Results: 300 lesions were classified as mass (213 malignant and 87 benign), 140 as nonmass (106 malignant and 34 benign) and 27 as focus (6 malignant and 21 benign). Most common pathology of malignant/benign lesions: for mass, invasive ductal carcinoma/fibroadenoma; for nonmass, ductal carcinoma in situ (DCIS)/fibrocystic change(FCC); for focus, DCIS/FCC. Benign mass lesions exhibited significantly lower $\mathbf{E_1}$, longer $\mathbf{T_{peak}}$ and lower **SER** compared with malignant mass lesions ($p < 0.0007$). Benign nonmass lesions, on the other hand, exhibited only a lower **SER** compared to malignant nonmass lesions (p=0.01). Diagnostic performance was improved in mass lesions compared to nonmass and focus lesions.

Conclusions: Kinetic parameters capturing the initial uptake, peak and washout phase of the curve could distinguish benign and malignant mass lesions, but parameters related only to washout were useful in discriminating nonmass-like benign from malignant lesions. Our results suggest that kinetic analysis is more diagnostically useful for mass-like enhancement.

INTRODUCTION

The high sensitivity of dynamic contrast enhanced magnetic resonance imaging (DCEMRI) for the detection of invasive breast cancer has expanded its clinical role to now include high risk screening, pre-operative staging, and post-treatment followup [1, 2]. Several prior reports have shown that DCEMRI provides excellent depiction of lesion morphology and, compared to other imaging modalities, most accurately determines pathologic disease extent [3-5]. In addition, qualitative and quantitative measures of contrast media uptake and washout—or kinetic—time course curves have been correlated with prognostic and predictive biomarkers, such as estrogen receptor expression, microvessel density, proliferative index and nuclear grade [6, 7]. Thus, DCEMRI of the breast allows for simultaneous characterization of both lesion morphology and biology, via analysis of kinetic curves.

Classification of morphology according to the BIRADS lexicon begins with categorizing the 'type' of enhancement as focus, mass or nonmass-like, while kinetic curves are classified as exhibiting 'washout', 'plateau' or 'persistent' shape (Figure 1)[8]. Mass lesions are the most common finding: benign mass lesions are often round or oval in shape, with smooth margins, and exhibit 'persistent' type curves, while malignant mass lesions are often irregularly shaped, with irregular or spiculated margins and display 'washout' type curves [9, 10]. Nonmass-like enhancement is less common, although it is the predominant morphology of preinvasive ductal carcinoma *in situ* (DCIS) which exhibits variable kinetic curve shapes [11-13]. While several reports have documented the morphologic and kinetic characteristics of benign and malignant lesions, relatively few have studied the relationship between lesion morphology and kinetics.

Indeed, it could be that focus, mass and nonmass enhancement patterns reflect fundamental differences in the underlying physiology and vasculature of these lesions, which may in turn affect their kinetic curve characteristics. More specifically, it is possible that the kinetic parameters and criteria that work best to distinguish benign and malignant mass lesions may not work well with focus or non-mass lesions, and vice versa. In a recent pilot study based on a relatively small number of patients [14], we used an empirical mathematical model to analyze kinetic curves in nonmass vs. mass lesions. We found that nonmass lesions exhibited significantly lower contrast uptake and slower washout compared to mass lesions. Furthermore, sensitivity and specificity of kinetic analysis was reduced in nonmass lesions compared to mass lesions. Our goal in this study was to test whether these preliminary results are valid in a larger number of patients. Instead of using a mathematical equation to model the kinetic curve data, we applied qualitative and quantitative analysis methods that are more closely aligned with how radiologists routinely classify kinetic curves. In addition, focus lesions are included in the present study, which were excluded previously, as well as a more detailed analysis of the pathology findings of these three types of enhancement.

METHODS

Patients

At our institution, we maintain a HIPAA compliant research database in which patient image data is collected under an IRB approved informed consent process or waiver of consent. For each patient presenting for DCEMRI of the breast, the database stores the radiologist-determined MR findings. In addition, the corresponding pathologic diagnosis for each MR detected lesion is recorded (when available) based on consensus opinion of two pathologists. The most common indications for breast DCEMRI are pre-operative staging of newly diagnosed cancers, post-operative and treatment follow-up, and screening of women at high-risk for developing breast cancer. A retrospective review of patients imaged May 2002-August 2005 yielded 457 lesions with pathologic findings in 401 women. The average patient age was 54.5 ±13.6 years. After review of pathology reports, 137 lesions were determined to be benign and 320 malignant. The malignant lesions were further classified as invasive ductal carcinoma (IDC), ductal carcinoma *in situ* (DCIS), invasive lobular carcinoma (ILC) or 'other' based on review of final pathology reports. Similarly, the benign lesions were classified as fibroadenoma, papilloma, fibrocystic change (FCC), breast tissue, or 'other'.

MR imaging protocol and analysis

MR imaging was performed on a 1.5T GE Signa scanner (GE Healthcare, Milwaukee, WI) using a dedicated 4 channel breast coil (Invivo, Orlando, FL) with the patient in the prone position. Two protocols were used. In the first, one pre and five post-contrast images were acquired in the coronal plane using a 3D T_1-weighted spoiled grass sequence (TR/TE = 7.7/4.2 msec, flip angle = 30˚, slice thickness = 3 mm, and in plane resolution = 1.4 mm), without fat

suppression, with 68 second timing. In the second dynamic protocol there were three post-contrast acquisitions. The first two post-contrast acquisitions were obtained as before, followed by acquisition of high spatial resolution sagittal images for 128 seconds, and returning to a final dynamic, 68 second, acquisition. In both protocols, the first post-contrast acquisition was started 20 seconds after contrast. 20cc of 0.5M Gadodiamide (Omniscan; Nycomed-Amersham, Princeton, NJ) was injected intravenously followed by a 20 ml saline flush at the rate of 2.0 ml /sec.

One experienced radiologist retrospectively reviewed the images and classified lesion morphology and kinetics. The type of enhancement was assessed according to the BI-RADS lexicon as mass, nonmass or focus. To generate the kinetic curve, the radiologist used an institutional workstation to trace a small region of interest (ROI) around what was perceived to be the most enhancing part of the lesion on the first post-contrast image. The plot of signal intensity vs. time for this ROI was assessed by the radiologist according to the BI-RADS lexicon, which describes the initial rise ('rapid', 'medium', 'slow') and delayed phase ('persistent', 'plateau', 'washout') of the kinetic curve.

In addition to this qualitative assessment of kinetics, several quantitative parameters were calculated. The initial and peak enhancement percentages ($\mathbf{E_1}$ and $\mathbf{E_{peak}}$) quantify the contrast uptake of the curve[9],

$$E_1 = 100 \times \frac{S_1 - S_0}{S_0}, \quad E_{peak} = 100 \times \frac{S_{peak} - S_0}{S_0}$$

where S_0 in the precontrast signal intensity, and S_1 is the first post contrast signal intensity, and S_{peak} is the peak signal intensity. The signal enhancement ratio (**SER)** has been used in prior studies to quantify the degree of washout of the curve [15],

$$SER = \frac{S_1 - S_0}{S_{last} - S_0},$$

where S_{last} is the signal intensity at the last post contrast time point. A larger **SER** implies greater washout relative to the first post contrast point. Higher **SER** has been correlated with increased vascularity and malignancy in other reports [15-17]. Finally, the time to peak enhancement ($\mathbf{T_{peak}}$) was calculated in seconds[9].

Statistical Analysis

To compare the proportion of 'washout' vs. 'plateau' and 'persistent' (or 'rapid' vs. 'medium' and 'slow') curves we used the Pearson's χ^2 – test, with a *p* value of < 0.05 indicating statistical significance. Two-tailed unequal variance Student's *t*-tests were performed to evaluate which quantitative kinetic parameters showed significant differences between the focus, mass and nonmass lesions, as well as subpopulations of benign and malignant, with a *p* value < 0.05 indicating statistical significance. The Holm-Bonferroni correction method was applied to test for significance of multiple comparisons[18].

The sensitivity and specificity of BI-RADS kinetic descriptors were calculated separately in focus, mass and nonmass lesions. In addition, receiver operating characteristic (ROC) analysis was performed to compare the diagnostic performance of the kinetic parameters on focus vs. mass vs. nonmass lesions. ROCKIT software (ROCKIT 0.9B Beta Version, Charles E. Metz, University of Chicago) was used to generate the ROC curves and to compare area under the curve (A_z) values using the area test.

RESULTS

Pathology of Focus, Mass and Nonmass Lesions

Overall, **300** lesions were classified as exhibiting mass-like enhancement, with 70.3% (211/300) malignant and 29.7% (89/300) benign; **130** were classified as nonmass lesions, with 80% (104/130) malignant and 20% (26/130) benign; **27** were classified as focus, with 18.5% (5/27) malignant and 81.5% (22/27) benign. Examples of malignant and benign focus, mass, and nonmass lesions are shown in Figure 1, with corresponding kinetic curves. The pathology findings of benign and malignant lesions in each type of enhancement are given in Table 1. Malignant and benign mass lesions were predominantly IDC and fibroadenomas/FCC, respectively. Half of malignant nonmass lesions were DCIS, while FCC and papillomas comprised the majority of benign nonmass lesions. The predominant pathology of focus lesions was FCC and breast tissue; only one was classified as IDC.

BI-RADS Kinetic Classification of Focus, Mass, Nonmass Lesions

The initial rise and delayed phase BI-RADS classification of kinetic curve shape for morphology types overall, as well as benign and malignant subpopulations, are shown in Figure 2. Overall, mass lesions exhibited a higher proportion of curves classified as ‘rapid’ initial uptake and ‘washout’ delayed phase compared with nonmass lesions (p <0.02). Only a minority of focus lesion kinetic curves were classified as ‘rapid’ and ‘washout’.

Malignant mass lesions demonstrated a significantly higher proportion of curves classified as having ‘rapid’ initial rise at 91%, compared to benign mass lesions at 57% (p=0.001). In addition, 72% of malignant mass lesions exhibited ‘washout’ type curves,

compared to only 35% of benign mass lesions ($p < 0.0001$). Malignant and benign nonmass lesions did not exhibit significant differences in initial rise characteristics, however they differed in delayed phase: 56% of malignant nonmass lesions were classified as 'washout', compared to only 12% of nonmass benign lesions (p=0.003). Focus lesions exhibited predominantly 'persistent' curve shapes, and none of the malignant focus lesions exhibited 'washout'.

Quantitative Kinetic Parameters of Focus, Mass and Nonmass Lesions

The average values of the quantitative kinetic parameters are displayed in Table 2. Analogous to what was found above in the qualitative curve assessment, mass lesions exhibited significantly higher $\mathbf{E_1}$ ($p<10^{-5}$), $\mathbf{E_{peak}}$ ($p<10^{-7}$), **SER** (p=0.015) and shorter $\mathbf{T_{peak}}$ (p=0.0054) compared with nonmass lesions. Malignant mass lesions exhibited higher $\mathbf{E_1}$**, SER** and shorter $\mathbf{T_{peak}}$ compared with benign mass lesions whereas nonmass malignant lesions exhibited only significantly higher **SER** i.e., stronger washout, compared with nonmass benign lesions.

Diagnostic Accuracy of Kinetic Parameters in Focus, Mass and Nonmass Lesions

For both the qualitative and quantitative descriptors of contrast media kinetics, diagnostic accuracy was improved in mass lesions. The sensitivity and specificity of the BIRADS descriptors are displayed in Table 3. Considering 'rapid' to be indicative of malignancy, sensitivity was reduced in nonmass and focus lesions compared to mass lesions, while specificity remained similar for both mass and nonmass lesions, and increased in focus lesions. For descriptors of delayed phase, sensitivity was again compromised in nonmass and focus lesions, but specificity was improved slightly**.** However, the 95% confidence intervals were quite large and demonstrated considerable overlap among types of enhancement.

To evaluate diagnostic performance of the quantitative kinetic parameters, ROC analysis yielded A_z values for each kinetic parameter evaluated separately in focus, mass and nonmass lesions (Figure 3). The A_z values were higher in mass lesions for all parameters except $\mathbf{E_{peak}}$. This illustrates that considering mass lesions separately from focus and nonmass lesions could improve diagnostic performance of kinetic analysis. Differences in A_z values of mass vs. nonmass lesions were not statistically significant. The ROC curves of **SER—**generated by assuming that a higher **SER** i.e., stronger washout is indicative of malignancy**—**in focus, mass and nonmass lesions are displayed in Figure 4. From these ROC curves, at a sensitivity of ~ 80% the specificity of **SER** is 55% in mass lesions, and only 35% and 15% in nonmass and focus lesions, respectively. In fact, for focus lesions it seems that *smaller* **SER** is more indicative of malignancy.

DISCUSSION

We set out to determine whether observations regarding kinetic analysis in mass and nonmass from a previous pilot study [14] were valid in a large database of malignant and benign lesions.

(i) *Pilot study result*: Malignant mass lesions exhibit faster contrast uptake, shorter time to peak enhancement, and stronger washout compared to benign mass lesions; malignant and benign nonmass lesions do not exhibit significant kinetic differences. *Current study result*: We find similar results, with high statistical significance. The only new observation here is that here we found that malignant nonmass lesions exhibited a significantly higher **SER** compared to benign nonmass lesions.

(ii) *Pilot study result*: That kinetic parameters differed most strongly among benign and malignant *mass* lesions, translated into diagnostic performance: diagnostic accuracy (i.e., ability to distinguish benign from malignant lesions) of kinetic parameters related to initial contrast uptake and washout is improved in mass lesions compared to nonmass lesions, but not for parameters quantifying the peak magnitude of contrast uptake. *Current study result*: We again find similar results; A_z values were improved in mass lesions compared to nonmass lesions, except for E_{peak}. As in the prior study, however, these differences were not statistically significant.

In the current study, we also extended our analysis to include foci. The majority (81.5%) of foci were found to be benign, and almost one-third of these represented normal breast tissue on subsequent biopsy, reiterating the importance of better understanding the presentation of normal breast parenchyma to avoid unnecessary biopsies. The high proportion of benign foci

found here is concordant with other studies [19] and suggests that perhaps short-term follow-up would be more appropriate for these lesions. While benign and malignant foci did not exhibit statistically significant differences in kinetic parameters, there was a trend for benign foci to exhibit traditionally *malignant* kinetic features i.e., higher contrast uptake, stronger washout, and a higher proportion of curves classified as 'washout'. This affected diagnostic performance: the A_z values of foci were not only lower than mass and nonmass lesions, they were *less* than 0.5.

Our results underscore the importance of improving the accuracy of DCEMRI for identifying malignant nonmass and especially foci. Several prior reports have noted that the increased false-positive rates of DCEMRI for these types of lesions, particularly for foci of enhancement, is a drawback limiting the widespread use of breast DCMERI [20, 21]. Others have pointed out the considerable overlap of kinetic patterns of DCIS with benign lesions compromises its reliable identification [12, 22-24]. For nonmass lesions, several potential avenues can be explored to improve the accuracy of DCEMRI. For example, using an automated algorithm to select a representative kinetic curve, or applying measures of kinetic heterogeneity may be useful [25]. Some have suggested using spectroscopic techniques may increase specificity for nonmass lesions [26]. It is likely that incorporating other morphologic descriptors, such as distribution or internal enhancement pattern, will also improve specificity. For foci, however, the path to increased accuracy is not clear, as these lesions are by definition too small to be characterized morphologically or to exhibit kinetic heterogeneity. Perhaps imaging at higher resolution will be necessary to improve reliable identification of malignant focus lesions.

Given the stark morphologic and kinetic differences found among focus, mass and nonmass lesions, it is likely that these types of enhancement reflect fundamental differences in

lesion physiology. Understanding the physiologic basis for contrast media kinetics may aid in the development of improved mathematical modeling and interpretation of kinetic data that can ultimately improve sensitivity and specificity of kinetic analysis, particularly for nonmass and focus lesions. For example, it was recently suggested that a significant reason for contrast uptake of DCIS—which comprised half the nonmass lesions in our study— may be that gadolinium penetrates through leaky basement membranes of neoplastic ducts and collects in the lumen[27]. This observation could help to explain the nonmass-like enhancement pattern of DCIS, the persistent and plateau curve type often noted for these lesions, and to improve modeling of contrast kinetics in some nonmass lesions.

There are several limitations to this study. First, the benign lesions in our study exhibit a relatively high proportion of 'washout' and 'plateau' curve types, which compromised the specificity of these descriptors. This may be due to the fact that we only included those benign lesions that were suspicious enough to warrant biopsy and pathologic evaluation; the "persistent" curve shape has long been associated with benign disease [10] and perhaps more obviously benign lesions would not be sent for biopsy. Second, the kinetic curves of nonmass lesions and enhancing foci are vulnerable to partial volume effects, as small ROI's encompassing the lesion may also capture some of the surrounding normal tissue. It is possible that the observed differences noted here between mass vs. nonmass or focus enhancement are due to partial volume effects. Third, the use of two dynamic imaging protocols and also of sparse temporal sampling may affect the reliability of the quantitative kinetic parameters used. In particular, the parameters $\mathbf{E_{peak}}$ and $\mathbf{T_{peak}}$ would be most compromised, while **SER** and $\mathbf{E_1}$ will be less adversely affected as they depend on the first and last time points which are at similar times for both protocols. Fourth, kinetic analysis was performed only on one curve selected manually by

one radiologist. It is likely that another radiologist may have selected a different curve, resulting in different kinetic parameters. Finally, the data included was using an older system which did not employ parallel imaging or high spatial resolution commonly used in newer state-of-the-art systems. Validation of our findings should be performed on other imaging systems.

To summarize, we have found that kinetic parameters are different in focus vs. mass vs. nonmass lesions. This observation may be useful for CAD systems, suggesting that if kinetic classifiers are trained separately in lesions based on type of enhancement diagnostic accuracy can be improved. We have also found that the efficacy of kinetic analysis is improved in mass lesions compared to nonmass and focus lesions. Although the significance of our findings needs to be strengthened, perhaps by using a computer algorithm to automatically select kinetic curve [28] or by considering kinetic heterogeneity, it does suggest a new guideline for the interpretation of DCEMRI. Kinetic analysis should be performed after lesions have been classified as exhibiting mass, nonmass or focus type enhancement; in mass lesions, kinetic analysis of contrast uptake and washout is of increased diagnostic value.

REFERENCES

1. Newstead GM. MR imaging in the management of patients with breast cancer. *Semin Ultrasound CT MR* **2006**;27:320-332
2. Saslow D, Boetes C, Burke W, et al. American Cancer Society guidelines for breast screening with MRI as an adjunct to mammography. *CA Cancer J Clin* **2007**;57:75-89
3. Beatty JD, Porter BA. Contrast-enhanced breast magnetic resonance imaging: the surgical perspective. *Am J Surg* **2007**;193:600-605; discussion 605
4. Esserman LJ, Kumar AS, Herrera AF, et al. Magnetic resonance imaging captures the biology of ductal carcinoma in situ. *J Clin Oncol* **2006**;24:4603-4610
5. Kuhl C, Kuhn W, Braun M, Schild H. Pre-operative staging of breast cancer with breast MRI: one step forward, two steps back? *Breast* **2007**;16 Suppl 2:S34-44
6. Teifke A, Behr O, Schmidt M, et al. Dynamic MR imaging of breast lesions: correlation with microvessel distribution pattern and histologic characteristics of prognosis. *Radiology* **2006**;239:351-360
7. Szabo BK, Aspelin P, Kristoffersen Wiberg M, Tot T, Bone B. Invasive breast cancer: correlation of dynamic MR features with prognostic factors. *Eur Radiol* **2003**;13:2425-2435
8. ACR. *American College of Radiology (ACR) Breast Imaging Reporting and Data System Atlas (BI-RADS)*. Reston, VA., **2003**
9. Szabo BK, Aspelin P, Wiberg MK, Bone B. Dynamic MR imaging of the breast. Analysis of kinetic and morphologic diagnostic criteria. *Acta Radiol* **2003**;44:379-386

10. Kuhl CK, Mielcareck P, Klaschik S, et al. Dynamic breast MR imaging: are signal intensity time course data useful for differential diagnosis of enhancing lesions? *Radiology* **1999**;211:101-110

11. Groves AM, Warren RM, Godward S, Rajan PS. Characterization of pure high-grade DCIS on magnetic resonance imaging using the evolving breast MR lexicon terminology: can it be differentiated from pure invasive disease? *Magn Reson Imaging* **2005**;23:733-738

12. Jansen SA, Newstead GM, Abe H, Shimauchi A, Schmidt RA, Karczmar GS. Pure ductal carcinoma in situ: kinetic and morphologic MR characteristics compared with mammographic appearance and nuclear grade. *Radiology* **2007**;245:684-691

13. Viehweg P, Lampe D, Buchmann J, Heywang-Kobrunner SH. In situ and minimally invasive breast cancer: morphologic and kinetic features on contrast-enhanced MR imaging. *Magma* **2000**;11:129-137

14. Jansen SA, Fan X, Karczmar G, et al. DCEMRI of breast lesions: In kinetic analysis equally effective for both mass and nonmass-like enhancement? *Medical Physics* **2008**;35:3102-3109

15. Esserman L, Hylton N, George T, Weidner N. Contrast-Enhanced Magnetic Resonance Imaging to Assess Tumor Histopathology and Angiogenesis in Breast Carcinoma. *Breast J* **1999**;5:13-21

16. Li KL, Partridge SC, Joe BN, et al. Invasive breast cancer: predicting disease recurrence by using high-spatial-resolution signal enhancement ratio imaging. *Radiology* **2008**;248:79-87

17. Li KL, Henry RG, Wilmes LJ, et al. Kinetic assessment of breast tumors using high spatial resolution signal enhancement ratio (SER) imaging. *Magn Reson Med* **2007**;58:572-581

18. Holm S. A simple sequentially rejective multiple test procedure. *Scandinavian J Statist* **1979**;6:65-70

19. Langer SA, Horst KC, Ikeda DM, Daniel BL, Kong CS, Dirbas FM. Pathologic correlates of false positive breast magnetic resonance imaging findings: which lesions warrant biopsy? *Am J Surg* **2005**;190:633-640

20. Kuhl CK, Braun M. [Magnetic resonance imaging in preoperative staging for breast cancer: pros and contras]. *Radiologe* **2008**;48:358-366

21. Lehman CD, Isaacs C, Schnall MD, et al. Cancer yield of mammography, MR, and US in high-risk women: prospective multi-institution breast cancer screening study. *Radiology* **2007**;244:381-388

22. Harms SE. The use of breast magnetic resonance imaging in ductal carcinoma in situ. *Breast J* **2005**;11:379-381

23. Neubauer H, Li M, Kuehne-Heid R, Schneider A, Kaiser WA. High grade and non-high grade ductal carcinoma in situ on dynamic MR mammography: characteristic findings for signal increase and morphological pattern of enhancement. *Br J Radiol* **2003**;76:3-12

24. Van Goethem M, Schelfout K, Kersschot E, et al. Comparison of MRI features of different grades of DCIS and invasive carcinoma of the breast. *Jbr-Btr* **2005**;88:225-232

25. Williams TC, DeMartini WB, Partridge SC, Peacock S, Lehman CD. Breast MR imaging: computer-aided evaluation program for discriminating benign from malignant lesions. *Radiology* **2007**;244:94-103

26. Bartella L, Thakur SB, Morris EA, et al. Enhancing nonmass lesions in the breast: evaluation with proton (1H) MR spectroscopy. *Radiology* **2007**;245:80-87

27. Jansen SA, Paunesku T, Woloschak G, et al. Why does ductal carcinoma in situ enhance on dynamic contrast enhanced MRI of the breast? Using x-ray fluorescence and MRI to track the spatial distribution of Gd-DTPA in murine DCIS. In: *International Society for Magnetic Resonance in Medicine*. Toronto, Canada., **2008**

28. Chen W, Giger ML, Bick U, Newstead GM. Automatic identification and classification of characteristic kinetic curves of breast lesions on DCE-MRI. *Med Phys* **2006**;33:2878-2887

TABLES

Table 1: Pathology classification of focus, mass and nonmass lesions. The overall numbers of benign and malignant lesions are noted, as well as the pathological subtypes.

Type of lesions	**Overall (n=457)**	**Mass (n=300)**	**Nonmass (n=130)**	**Focus (n=27)**
All Benign	**137**	**89**	**26**	**22**
Fibroadenoma	27	23	3	1
Papilloma	17	12	4	1
FCC	42	22	10	10
Breast tissue	26	18	1	7
Other	25	14	8	3
All Malignant	**320**	**211**	**104**	**5**
DCIS	68	12	52	4
IDC	192	160	31	1
ILC	26	17	9	0
Other	34	22	12	0

Table 2: Quantitative kinetic parameters of focus, mass and nonmass lesions stratified by pathology as benign or malignant. The *p* values of *t*-test comparisons of benign and malignant lesions within each type of enhancement pattern for each parameter are also shown.

Type of lesions	**No. cases**	**E_1 (%)**	**E_{peak} (%)**	**T_{peak} (sec)**	**SER**
All Mass	**300**	**281±160**	**348±170**	**165±104**	**1.02±0.50**
Malignant	211	307±154	352±157	139±91	1.13±0.51
Benign	89	221±160	336±198	227±106	0.75±0.36
p-value		$< 10^{-4}$	--	$< 10^{-8}$	$< 10^{-9}$
All Nonmass	**130**	**207±134**	**258±141**	**204±109**	**0.91±0.37**
Malignant	104	214±135	263±141	194±105	0.95±0.38
Benign	26	179±128	242±148	242±114	0.77±0.29
p-value		--	--	--	0.01
All Focus	**27**	**152±159**	**228±180**	**255±99**	**0.745±0.40**
Malignant	5	97±39	193±150	310±35	0.60±0.20
Benign	22	164±174	237±189	243±105	0.78±0.43
p-value		--	--	--	--

Table 3. Diagnostic performance (sensitivity and specificity) of qualitative BIRADS descriptors of kinetic curves in mass, nonmass and focus lesions. Numbers in parentheses represent 95% confidence intervals.

	BIRADS Descriptor		
	Initial Rise: Rapid	**Delayed Phase: Washout**	**Delayed Phase: Washout or Plateau**
Sensitivity			
Mass	91% (86% to 94%)	72% (65% to 78%)	92% (87% to 95%)
Nonmass	77% (68% to 85%)	56% (46% to 65%)	76% (66% to 84%)
Focus	40% (7% to 83%)	0% (0% to 54%)	40% (7% to 83%)
Specificity			
Mass	43% (32% to 54%)	65% (54% to 75%)	36% (26% to 47%)
Nonmass	42% (24% to 63%)	89% (69% to 97%)	46% (27% to 66%)
Focus	59% (37% to 79%)	64% (41% to 82%)	55% (33% to75%)

FIGURE LEGENDS

Fig. 1—T_1 weighted axial post-contrast subtraction images demonstrating: a) mass-like enhancement in a 47 year old woman representing IDC, b) nonmass-like enhancement in a 54 year old woman representing DCIS, and c) focus enhancement in a 61 year old woman representing DCIS. Representative kinetic curves of malignant and benign lesions of each enhancement type are shown on the left.

Fig. 2—BIRADS qualitative descriptors of initial rise (bottom) and delayed phase (top), in focus, mass and nonmass lesions overall, as well as benign and malignant subtypes.

Fig. 3—Diagnostic performance of the quantitative kinetic parameters $\mathbf{E_1}$, $\mathbf{E_{peak}}$, **SER** and $\mathbf{T_{peak}}$. Area under the curve (A_z) values, calculated from generated ROC curves, are displayed. For each kinetic parameter, three A_z values are presented for focus, mass and nonmass lesions. Error bars indicate 95% confidence interval.

Fig. 4—ROC curves of the parameter **SER** in focus lesions (blue line), mass lesions (black line), and nonmass lesions (red line). This plot demonstrates improved diagnostic performance of **SER** in mass compared with nonmass and focus lesions.

Fig.1—T_1weighted axial post-contrast subtraction images demonstrating: a) mass-like enhancement in a 47 year old woman representing IDC, b) nonmass-like enhancement in a 54 year old woman representing DCIS, and c) focus enhancement in a 61 year old woman representing DCIS. Representative kinetic curves of malignant (dark grey) and benign (light grey) lesions of each enhancement type are shown on the left.

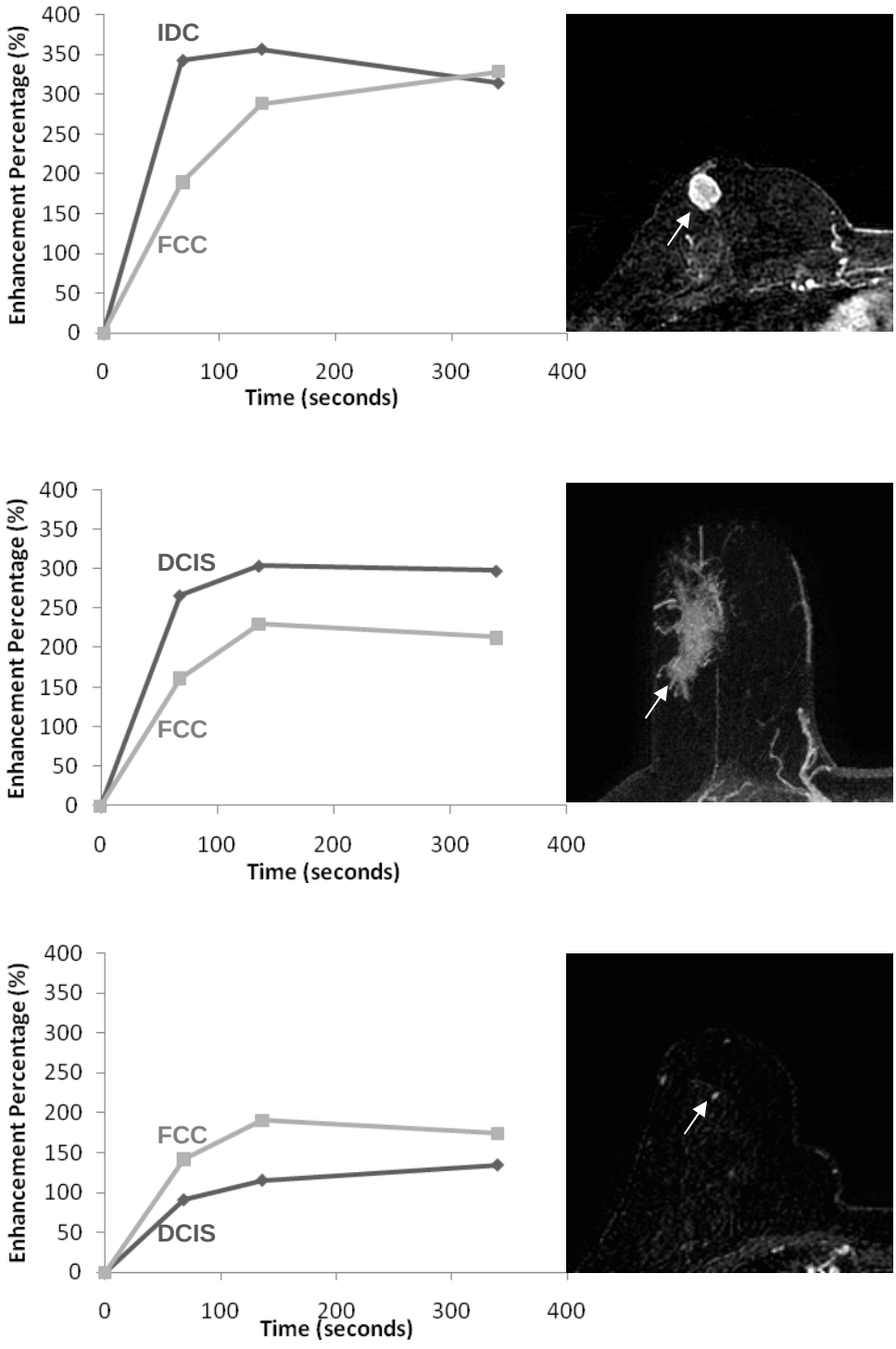

Fig.2—BIRADS qualitative descriptors of initial rise (bottom) and delayed phase (top), in focus, mass and nonmass lesions overall, as well as benign and malignant subtypes.

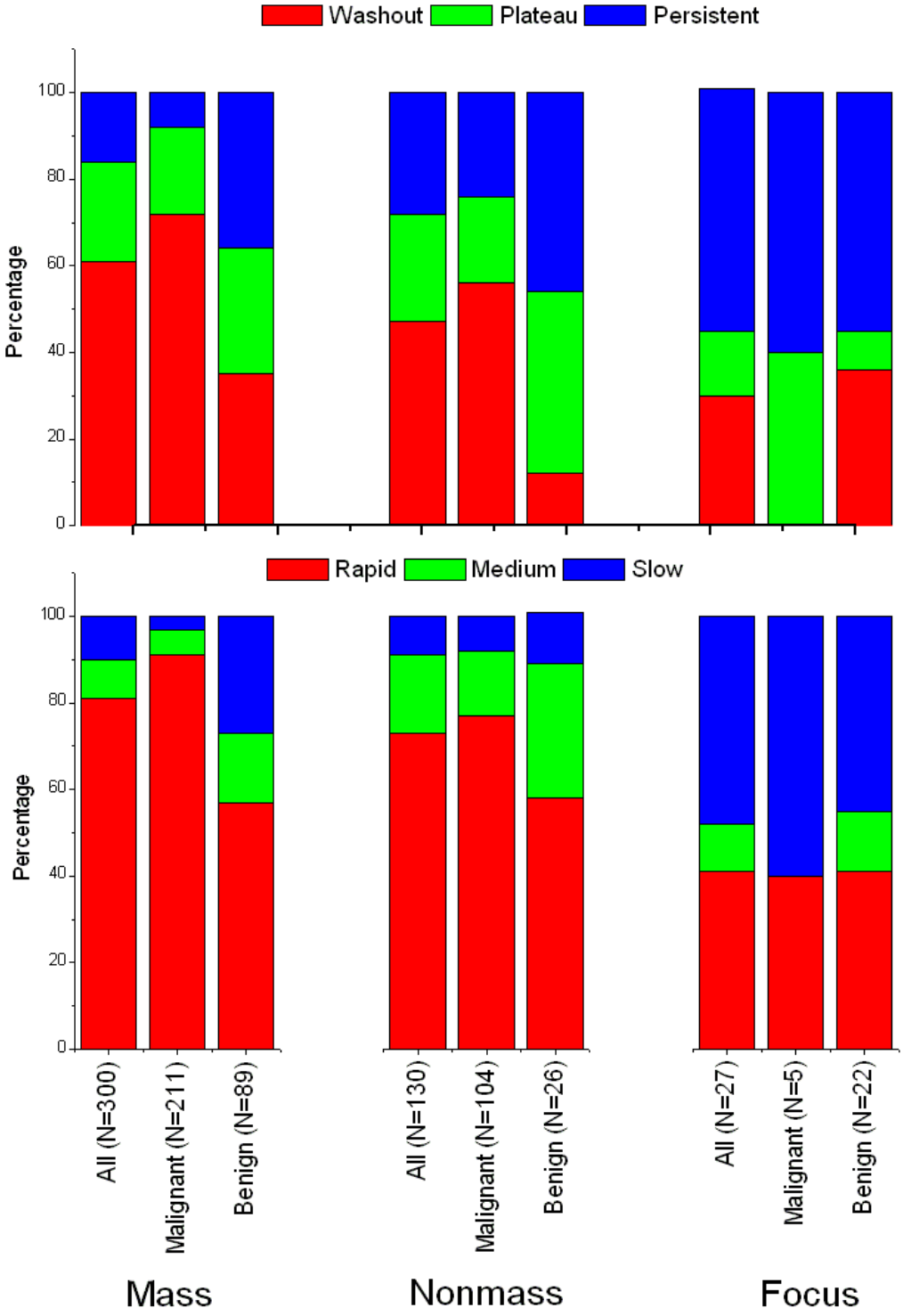

Fig. 3—Diagnostic performance of the quantitative kinetic parameters **E_1**, **E_{peak}**, **SER** and **T_{peak}**. Area under the curve (A_z) values, calculated from generated ROC curves, are displayed. For each kinetic parameter, three A_z values are presented for focus, mass and nonmass lesions. Error bars indicate 95% confidence interval.

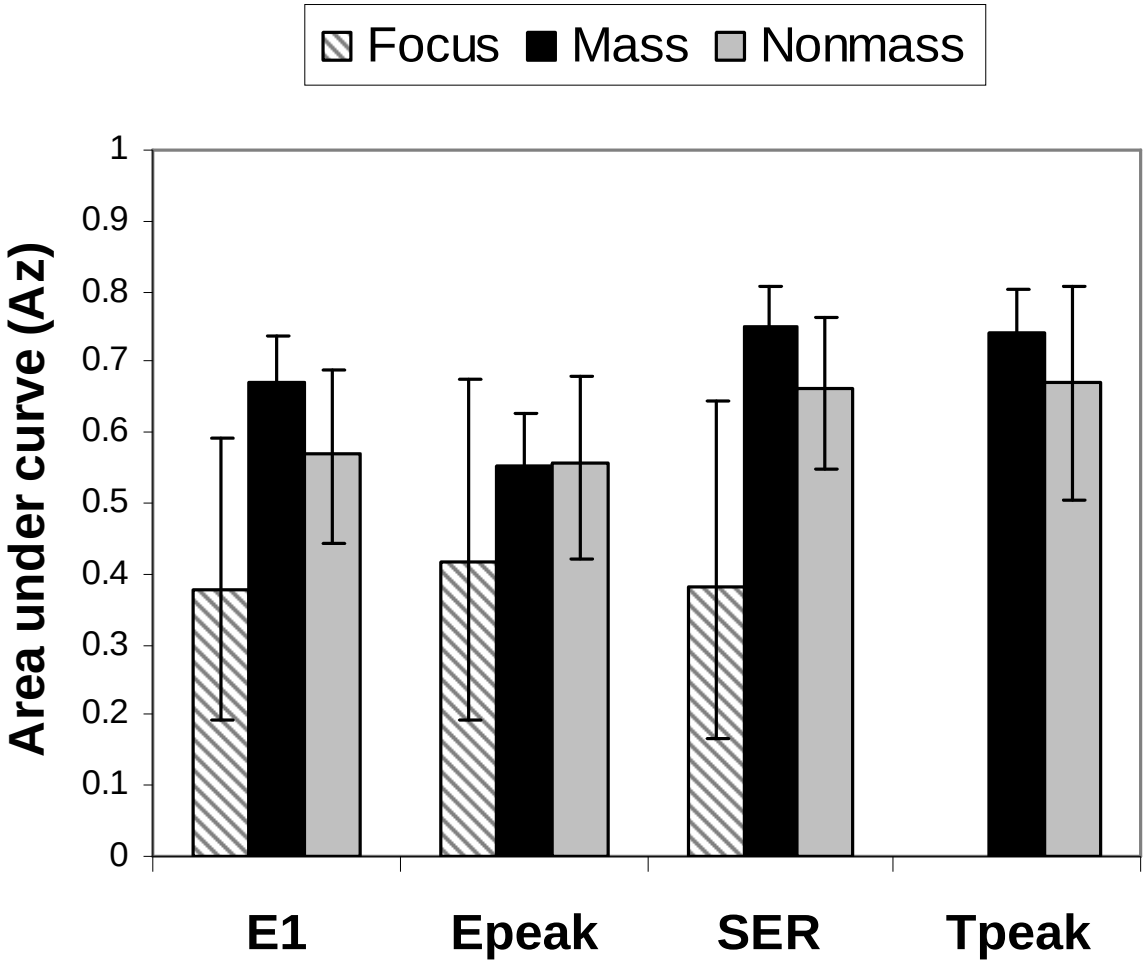

Fig. 4—ROC curves of the parameter **SER** in focus lesions (blue line), mass lesions (black line), and nonmass lesions (red line). This plot demonstrates improved diagnostic performance of **SER** in mass compared with nonmass and focus lesions.

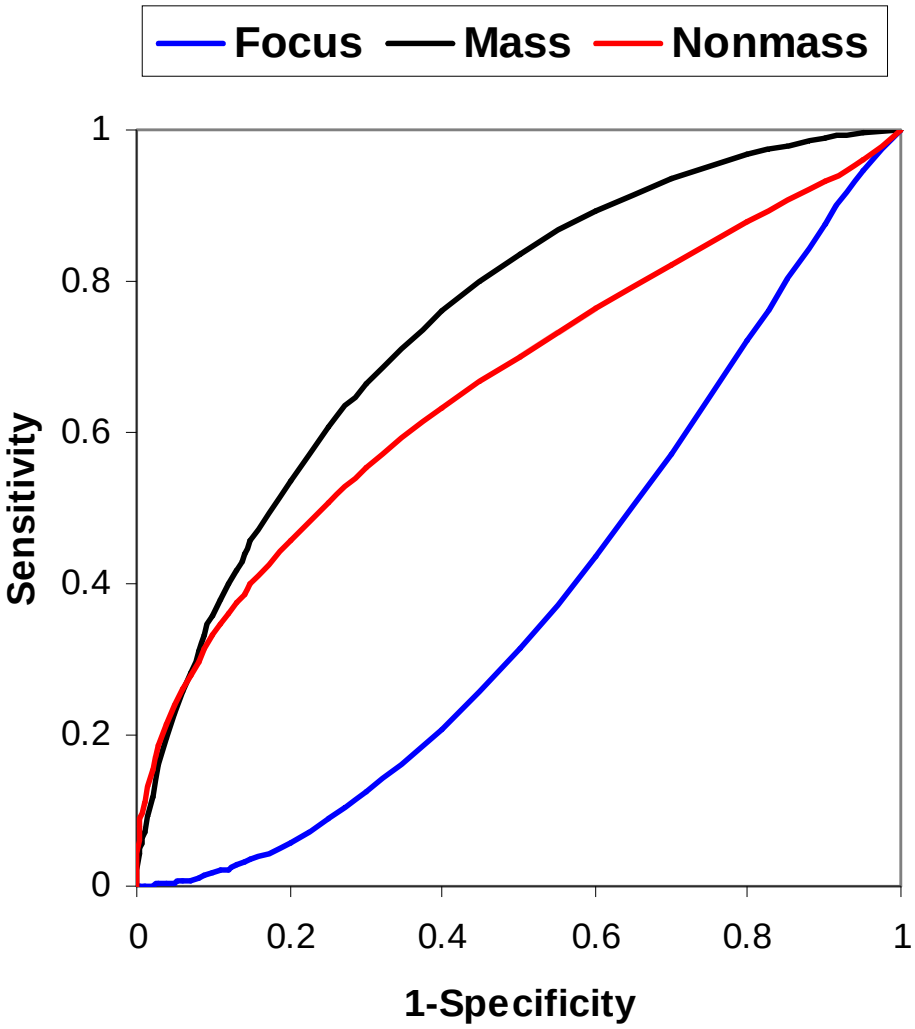

Magnetic resonance imaging reveals the progression, regression and indolence of *in situ* mammary carcinoma in transgenic mice

Sanaz A. Jansen[1] PhD, Suzanne D. Conzen[2] MD, Xiaobing Fan[1] PhD, Erica Markiewicz[1] Bsc, Gillian M. Newstead[1] MD and Gregory S. Karczmar[1*] PhD.

University of Chicago
Departments of [1]Radiology, [2]Hematology/Oncology
5841 S. Maryland Ave, [1]MC2026, [2]MC2115
Chicago, IL 60637

Submitted to Breast Cancer Research as an Original Research Article
Word count: 3918 (Introduction to Conclusion)

Email addresses:

Sanaz A. Jansen	sajansen@uchicago.edu
Suzanne Conzen	sconzen@medicine.bsd.uchicago.edu
Xiaobing Fan	xfan@uchicago.edu
Erica Markiewicz	ejmark@uchicago.edu
Gillian Newstead	gnewstead@radiology.bsd.uchicago.edu
Gregory Karczmar	gskarczm@uchicago.edu

***Corresponding Author**
Gregory S. Karczmar
Professor of Radiology
University of Chicago
Department of Radiology
5841 S. Maryland Ave
MC 2026
Chicago, IL 60637

Phone: 773-702-0214
Fax: 773-834-9047
Email: gskarczm@uchicago.edu

ABSTRACT

Introduction: Because of the small size of *in situ* mammary cancers in mouse models, high-resolution imaging techniques are required to effectively observe how lesions develop, grow and progress over time. Our purpose was to use magnetic resonance imaging (MRI) to track *in vivo* the transition of *in situ* to invasive cancer in transgenic mice.

Methods: MR images of 12 SV40 Tag mice, which develop mammary intraepithelial neoplasia (MIN) that is similar to human ductal carcinoma *in situ* (DCIS) including progression to invasive tumors, were serially obtained every 2- 3 weeks. MIN lesions were identified and followed as they grew, and several lesion features were measured including volume, growth rate and morphology. For those MIN lesions that progressed to invasive cancer the progression time was measured.

Results: Overall, 21 MIN lesions were initially detected at an average at an average initial volume of 0.3±0.2 mm^3 with an average growth rate of -0.15 ±0.66 $week^{-1}$. Even though these mice are genetically predisposed to develop invasive carcinoma, these lesions took vastly different progression paths: (i) 9 lesions progressed to invasive tumors with an average progression time of 4.6 ± 1.9 weeks (ii) 2 lesions regressed, i.e., were not detected on future images, and (iii) 5 were stable for over 8 weeks, and were demonstrated by a statistical model to represent indolent disease.

Conclusions: To our knowledge, the results reported here are the first direct measurements of the timescales and characteristics of progression from *in situ* to invasive carcinoma and provide direct evidence that DCIS may be a non-obligate precursor lesion. In addition, this is the first step towards developing methods for image acquisition and analysis that can predict which *in situ* cancers will become invasive and which would not.

INTRODUCTION

The processes that characterize and trigger progression of preinvasive ductal carcinoma *in situ* (DCIS) to invasive breast cancer remain elusive. DCIS is a heterogeneous disease, in which neoplastic cancer cells are still confined by the basement membrane of ducts. Progression to invasive ductal carcinoma (IDC) is thought to occur by first degradation of the basement membrane, microinvasion of cancer cells into the surrounding stroma and growth of a solid tumor. The use of screening mammography has increased rates of detection of DCIS [1], which has in turn expanded knowledge about the biology of these earliest stage breast cancers. However, clinical imaging provides only a snapshot of tumor biology. Basic characteristics of DCIS development over time (i.e., growth rates and changes in morphology), and progression to IDC are still largely unknown[2].

Fundamental questions regarding the natural history of DCIS have remained unanswered largely because they are difficult to study in women. Due to obligate surgical excision of most newly diagnosed cancers, subsequent lesion progression cannot be followed. A few studies have examined outcome in a small number of women whose DCIS was initially misdiagnosed as benign disease, i.e., treated by biopsy alone [3, 4]. In one such study, 6 of 13 DCIS progressed to invasive breast cancer in an average of 9 years. In another, 11 of 28 women with misdiagnosed low-grade DCIS developed invasive carcincoma in the same quadrant, the majority within 15 years. These studies and others [5] have prompted some to suggest that DCIS may be over-diagnosed and over-treated [6-8] as not all will progress to invasive cancer. If this is the case, it is clinically important to identify predictive markers that can distinguish those

DCIS that will remain indolent from those that will progress to life-threatening disease. Some studies suggest that a higher nuclear grade is related to an aggressive phenotype, as these lesions are more likely to recur as invasive tumors [9]. While human studies provide important insights into the natural history of DCIS, they usually suffer from having small patient numbers, having a biased lesion population (i.e., only those DCIS that were initially misdiagnosed), performing interventions that could alter disease state and progression (i.e., biopsy or lumpectomy), and focusing on outcome rather than detailed measurements of lesion morphology or biology. It is difficult to fully understand DCIS development or the key steps involved in progression of *in situ* disease without detailed empirical data directly following DCIS as it develops and progresses over time.

Transgenic mouse models of cancer provide an experimental framework with which to begin to understand the natural history of DCIS. Because of the small size of *in situ* mammary cancers in mouse models, high-resolution imaging techniques are required to effectively observe how lesions develop, grow and progress over time. Recently, our laboratory has reported high-resolution *in vivo* magnetic resonance (MR) images of pre-invasive ductal carcinoma *in situ* (DCIS) in a mouse model of human breast cancer [10]. In the current study, we used these new techniques to follow *in situ* mammary cancer over time using magnetic resonance imaging (MRI). Specifically, the timescales and characteristics of the development and progression of *in situ* to invasive carcinoma were evaluated, and predictive markers of progression were explored.

MATERIALS AND METHODS

Animals

All procedures were carried out in accordance with our institution's Animal Care and Use Committee approval. The C3(1) SV40 large T antigen mouse model of breast cancer was used in this research. In this model, expression of large T antigen is targeted to the mammary gland in females via the C3 promoter. Female mice develop mammary cancer that resembles human ductal carcinoma, including progression through atypical ductal hyperplasia (~8 weeks), mammary intraepithelial neoplasia (MIN) [11] which is similar to human DCIS (~12 weeks), and invasive tumors (~16 weeks)[12]. A total of 12 mice were selected for serial MR imaging. Four of 12 mice were selected for serial imaging every two weeks from ages 10-20 weeks. Eight of 12 were selected for serial imaging every three weeks from 12-21 weeks.

MRI Experiments

The inguinal mammary glands on the left side of each mouse were selected for repeat *in vivo* imaging performed with a Bruker 9.4 Tesla magnet. Axial gradient recalled echo (GRE) images with fat suppression (TR/TE: 675/7 ms, FOV=3.0 × 3.0 cm, matrix size = 256 × 256, NEX=2, #slices=42, slice thickness=0.5mm, in-plane resolution=117 microns and flip angle=30°) across the entire sensitive volume of an open birdcage surface coil were obtained, so that images of the complete inguinal glands were obtained [10, 13]. To facilitate spatial correlations between serial MR images, a fine polyethylene mesh ~ 3.0 cm x 2.0 cm in size with 3.0 mm spacing was embedded in partially deuterated agar and wrapped around each mouse. This grid produced a pattern on MRI that was used for registration of serial MRI images so that lesions could be located and followed over time [10]. Animals were anesthetized prior to imaging experiments,

and anesthesia was maintained during imaging at 1.5% isoflorane. The temperature, heart rate and respiration rate were monitored with data taken every minute, and the respiration rate was used to obtain gated images.

Lesion identification

In a prior study, we found that MR images acquired with a GRE pulse sequence demonstrated high sensitivity for MIN and early invasive tumors (Figure 1) [10]. C3(1) SV40 Tag mice were imaged at various stages of cancer development and sacrificed afterwards to perform detailed correlations with histology using an agar grid. Several lesion features were evaluated, including morphology based on a simplified version of the Breast Imaging Reporting and Data System (BI-RADS) lexicon [14] as follows: *type* (mass or nonmass), *shape/distribution* (for mass lesions: round, oval, lobular or irregular; for nonmass lesions: linear, ductal or segmental), *margins* (for mass lesions only: smooth or irregular) and *pattern* (for mass lesions: homogeneous or heterogeneous; for nonmass lesions: homogeneous, stippled or clumped). We found that the *type* descriptors 'mass' and 'nonmass' were highly specific to invasive tumors and MIN, respectively. The results from this prior study provided the basis for the present work by demonstrating that (i) all MR findings in the gland correspond to cancer i.e., there are no false positives, (ii) MIN, early invasive tumors and lymph nodes can be confidently identified based on morphology, and (iii) an agar grid can be used to localize and follow lesions over time.

Analysis of lesion features and development

All image analysis was performed using software written in IDL (Research Systems, Inc., Boulder, CO). The images of mouse mammary glands were analyzed in a manner analogous to

methods used when evaluating human breast images. In women, cancers are often assigned a location by dividing the breast in quadrants relative to the nipple: upper-outer, upper-inner, lower-outer and lower-inner. Cancers within a quadrant are usually grouped as one, and the worst pathology determines the overall diagnosis—in other words, an invasive cancer with nearby extensive DCIS is considered an invasive tumor. For the mice, we proceeded with a similar analysis (Figure 2). The inguinal mammary glands were divided into three regions, this time using the intramammary lymph node as a reference point. Regions were examined to identify all ducts with MIN and invasive tumors, using the morphologic classification of lesion *type* (as defined above). Lesions within each region were grouped together (if necessary) and the following features were then evaluated: age at initial lesion detection (weeks), volume (mm^3), further morphologic classification (as above, shape/distribution, margins and pattern) and distance from the intramammary lymph node (mm).

Using the agar grid and lesion location relative to the intramammary lymph node, lesion development was followed over time. This could only be assessed in cases where the lesion had been imaged at least twice. Growth rate was calculated according to

$$V(t) = V_0 e^{\alpha t} \quad , \qquad [1]$$

where V is lesion volume (mm^3), t is the time in weeks, and α is the growth rate ($week^{-1}$). This was calculated separately for MIN (α_{MIN}) and invasive tumors (α_{tumor}). Changes in morphology as lesions developed were also examined, separately for *in situ* and invasive tumors.

Analysis of MIN progression into invasive cancer

Each MIN was followed over time to determine whether invasive cancer developed in that region in the future. Specifically, if *any* invasive tumor developed in the same region on subsequent

images, the lesion was classified as having progressed and the progression time T_{prog} (in weeks) was calculated: T_{prog} = Age at initial detection of invasive tumor – Age at initial detection of MIN. The average progression time μ_{prog} and the standard deviation of progression times σ_{prog} was then calculated. If an invasive tumor was not found in subsequent images, the latency time T_{lat} (in weeks) was determined: T_{lat} = Age at final imaging session - Age at initial detection of MIN. To determine whether some latent lesions truly represented non-progressing or "indolent" disease, a threshold T_0 was found so that MIN lesions with $T_{lat} > T_0$ could be considered a biologically distinct class of "indolent" lesions. Details of the statistical method used are in the Appendix. In addition, the prior images of all invasive tumors were evaluated to determine how many were preceded by MIN.

Analysis of predictive markers for progression

We next investigated whether certain lesion features were predictors of *in situ* cancer progression i.e., whether they could distinguish progressing from indolent MIN. We tested if having a larger distance from the lymph node, larger volume, earlier age at initial detection and a larger growth rate (α_{MIN}) were predictors of whether that MIN lesion would progress in the future to an invasive tumor. The average value of each of these parameters was calculated separately in progressing and indolent MIN, and compared using the Student's *t*-test. Receiver operating curve (ROC) analysis (ROCKIT 0.9B Beta Version, Charles E. Metz, University of Chicago) was performed to determine the diagnostic accuracy for each parameter in the task of distinguishing progressing from indolent MIN. For each parameter, ROC analysis yielded area under the curve (A_z) values that quantified diagnostic accuracy. To evaluate the efficacy of the

morphologic descriptors at identifying progressing MIN, the positive predictive value (PPV) and negative predictive value (NPV) of each morphology descriptor was also evaluated.

RESULTS

Lesion features and development

Overall, 2 of 12 mice did not develop any cancerous lesion in the imaged inguinal glands. In the remaining 10 mice, a total of 21 MIN lesions developed. In 8 of these mice a total of 14 invasive tumors developed (not always preceded by MIN in the same region). The lesion features at initial detection are summarized in Table 1. Most MIN lesions developed in the mid (10/21) or lower (9/21) gland regions, at an average age of 12.7 ± 2.6 weeks and an average initial volume of 0.34± 0.22 mm^3. MIN typically presented in a ductal or segmental shape and a homogenous pattern. Invasive tumors also developed predominantly in the mid (8/14) or lower (5/14) gland region. Tumors appeared at an average age of 16.3±3.2 weeks at an initial volume at the time of detection of 17.2± 41.6 mm^3. The latter value was skewed due to two tumors that presented initially at a very large volume (>120 mm^3); excluding these two tumors reduced the average initial tumor volume to 1.96± 2.01 mm^3. The typical invasive tumor morphology at initial detection was a round shape with smooth margins and a homogeneous pattern.

The subsequent development of MIN was studied in those 15/21 lesions that were imaged as MIN at least twice. Interestingly, the average growth rate was slightly negative α_{MIN}=-0.15 ±0.66 $week^{-1}$. Several lesions exhibited close to zero growth (Figure 3); two in particular exhibited considerably negative growth because upon subsequent imaging they were no longer detected (Figure 4a). This could be evidence of *in situ* cancer disappearance; at the least, it indicates the lesion has substantially reduced in size i.e., regressed. Some of the MIN lesions also exhibited morphological changes as they developed. 2/15 mice exhibited a change in lesion

shape from ductal to segmental. More significantly, 8/15 showed changes in lesion pattern from homogeneous to clumped or stippled.

Early invasive tumors exhibited less variability compared to MIN as they grew over time. For the 8/14 invasive tumors that were imaged at least twice, the average growth rate was 0.53 ± 0.38 week $^{-1}$, significantly higher than that of MIN. Although the growth rates of invasive tumors varied considerably (Figure 3), none of the tumors reduced in size over time. Furthermore, tumors maintained similar morphologic characteristics as they developed. Only 2/8 tumors changed morphology over time: one transitioned from a round to lobular shape, and the other from a round mass with smooth margins to an irregular mass with irregular margins. This suggests that the growth patterns of early invasive tumors are more stable than MIN lesions.

Progression of MIN into early invasive cancers

Nine of 21 MIN lesions progressed into invasive cancers with an average progression time of T_{prog}=4.6 $\pm$1.9 weeks (Figure 4b). Of these, 5 MIN lesions progressed to invasive cancer in 2-3 weeks, 3 within 6-7 weeks, and 1 in 8-10 weeks. Eleven of 21 MIN were found to have not progressed to invasive tumors with an average latency time of T_{lat}=5.8$\pm$3.8 weeks (Figure 4c). Of these, 4 did not progress for at least 2-3 weeks, 2 for at least 6-7 weeks and 5 were stable for at least 8-10 weeks ($T_{lat} \geq 8$ weeks). One of 21 MIN developed at the last imaging time point (21 weeks of age) and thus subsequent development was unknown. Nine of 14 invasive tumors were preceded by MIN that was detected by MRI; MIN was not detected in the prior images of four tumors, and one tumor was detected at the first imaging session (age 12 weeks) and thus prior history was unknown.

Using the statistical method outlined in the Appendix, and with N_{prog}=9, μ_{prog}=4.56 and σ_{prog}=1.9 weeks, we found that there is a less than 0.5% probability that lesions with T_{lat} greater than or equal to 8 weeks could be from the same population as progressing MIN. In other words, according to our methods, MIN lesions with T_{lat} ≥8 weeks represented indolent disease that is biologically different from the MIN lesions that progress.

Predictive markers for progression

There was a trend for indolent MIN lesions to develop earlier than progressing lesions, to be closer to the lymph node and to have a lower growth rate compared with progressing MIN (Table 2). However, these differences were not statistically significant. The positive and negative predictive values of the morphology descriptors ranged from 0.25 to 0.70, with very large confidence intervals due to the small number of lesions included in this study.

DISCUSSION

We have used serial MR imaging to study how *in situ* lesions grow to become invasive cancers. Key timescales of cancer initiation and progression in C3(1) SV40 Tag mice that can only be derived from repeated non-invasive imaging were measured: progression times, latency times, and growth rates of MIN and early invasive tumors. Significantly, we found that even in these mice that are genetically predisposed to develop invasive carcinoma, a substantial proportion of *in situ* cancers did *not* progress to invasive tumors. To our knowledge, these results provide the first detailed, high-resolution measurements of early mammary cancer natural history in mice.

Abbey et al have used PET imaging to follow malignant transformation of pre-neoplastic lesions similar to DCIS in a transplantable tissue model of breast cancer[15, 16]. Our work differs from theirs in several ways. To begin with, the mouse models are different. Abbey et al performed tissue transplantation into a cleared mammary fat pad, rather than utilizing a transgenic model. Furthermore, unlike SV40 Tag mice, *in situ* cancers grew extensively in their model covering over 60% of the mammary gland before the appearance of focal tumors. Secondly, there are inherent limitations of PET compared to MR imaging. PET imaging is an excellent modality for evaluating treatment response, as has been done by Namba et al on early mammary cancers [17]. However, the coarse spatial resolution of PET compared to MRI renders it unsuitable for detailed morphological studies of disease initiation and progression and correlations with histology. For example, the image voxel size in Abbey et al was approximately 5mm^3, compared to our voxel size of 0.0068 mm^3—three orders of magnitude smaller. This compromised spatial resolution limited the size of PET-detected *in situ* lesions to 10-50 mm^3,

compared to our average value of 0.34 mm^3. Similarly, invasive tumors in Abbey et al were over 50 mm^3, compared to our average value (excluding two outliers) of 1.96 mm^3. With these differences noted, our finding that the growth rates of invasive cancers were higher than that of *in situ* cancers is concordant with the work of Abbey et al.

The C3(1) SV40 Tag mouse model is being used increasingly in a wide variety of studies, ranging from evaluating effects of interventional and preventative therapies [18-31], to understanding molecular and genetic alterations occurring at various stages of disease progression [32-37]. Our results contribute new observations regarding this mouse model of breast cancer:

- MIN lesions grow slowly on average, and can both progress to invasive tumors or remain indolent, as has been suggested to be true for DCIS in women [2-4]. This implies that at least a second transformational event beyond expression of Tag is required for cancer progression in this model [34]. We have also found evidence for *in situ* cancer regression, which if validated in larger numbers with detailed pathology correlation, would be direct demonstration of spontaneous breast cancer regression [38-40]. The heterogeneity of progression paths demonstrates that the C3(1) SV40 mouse model may be good candidate for assessing the effect of therapies that delay progression of DCIS.
- Early invasive tumors show less variability in morphology as they grow compared with MIN. Although there was a wide variability of growth rates of early invasive cancers, overall they grew much faster than *in situ* cancers, and none decreased in size or regressed.

- Increased lesion volume was not a predictor of future progression, but there was a trend for increased growth rate to be related to the eventual development of invasive carcinoma. Unfortunately, in this pilot study the number of cases was too small to draw conclusions with statistical significance. If this observation was validated in a larger study, it would imply that it is how quickly DCIS is growing, not the lesion size, that is related to whether or not it will progress.

It will be important to assess similar characteristics in other mouse models of human breast cancer. If some features can be found that persist across mouse models, they may ultimately demonstrate applicability to human disease.

Given that the natural history of breast cancer is still an open question, there are many theories of the mechanisms governing the growth and progression of early breast cancers in women. The 'angiogenic switch' is thought to be a crucial step during breast tumorigenesis, and has been hypothesized to occur at or before the *in situ* stage[41]. Franks et al have used non-linear mathematical models to predict that invasion will occur at the middle of ducts distended DCIS due to increased mechanical pressure [42-44]. Tabar et al posit that true *in situ* lesions in fact originate in lobules, and that a separate more aggressive disease representing a duct-forming invasive carcinoma is being wrongly included with other *in situ* cancers [45, 46]. Due to an absence of empirical data of the detailed morphological, and other changes that occur during progression of i*n situ* cancers, such theories may be difficult to evaluate. Our work and extensions thereof, for example using dynamic contrast enhanced MRI to probe changes in

vasculature, can provide detailed and direct measurements of tumorigenesis on which these mathematical and physiological models of disease initiation and progression can be evaluated.

There are several limitations to this study. First, lesion morphology was assessed using 2D axial slices rather than a 3D rendering of the inguinal glands. This could compromise the assessment of lesion morphology, particularly of MIN located in the lower gland area. Second, there may have been some errors in lesion identification. Although the descriptors of 'nonmass' and 'mass' are highly specific to MIN and invasive tumors, respectively, the 'mass' descriptor is not perfectly correlated, implying that some MIN lesions may have been misidentified as invasive tumors. More generally, in this study it may have been difficult to distinguish focal MIN from invasive cancer, or to pinpoint the exact point of transition from MIN to invasion due to the 2-3 week sampling interval. A larger sensitivity/specificity study will be required to better correlate a wider variety of image-based features with histology, in order to minimize this confusion. Third, the numbers of lesions studied was rather small, limiting the statistical significance of our findings. To address this, both an increased number of mice should be imaged as well as an increased number of mammary glands (rather than only the inguinal glands on one side). In this way, cancer development can be assessed in the whole mouse, and data can be analyzed to determine whether lesions in the same animal can be considered as independent. Fourth, in this study we did not consistently perform end-point histologic evaluation of imaged mammary glands. Fifth, changes in the parenchyma that preceded the development of MIN could not be easily observed because of the poor signal-to-noise ratio of the normal tissue. Recent improvements in imaging methods have provided greatly enhanced images of normal

parenchyma, opening up the possibility of studying changes in the normal mammary glandular tissue that are precursors to cancer development.

Finally, the new framework we have presented for analyzing early carcinogenesis in mice may need improvement. For example, the number of MIN lesions that progressed to invasive tumors may have been over-estimated. Our criterion was only that an invasive tumor appeared in the same region on subsequent imaging; however this tumor may have been independent of the MIN detected previously. The transition from MIN to invasive tumors was rarely observed directly. In addition, cancer growth rates could only be calculated for lesions imaged at least twice, i.e., 15/21 MIN and 8/14 invasive tumors. The remaining lesions were excluded from any analysis of growth rates, which may have introduced a bias. These two limitations could be addressed by conducting serial imaging at higher frequency (i.e., every few days) so that each MIN lesion can be definitively linked with its subsequent invasive phase, and so that growth rates can be measured for all. Lastly, the statistical model we used to identify indolent lesions could likely be improved or modified.

In prior work, we introduced the MR imaging methods for imaging early murine mammary cancer, and subsequently reported on how those techniques could be used to better interpret clinical MR imaging of the breast [47]. Here, we have established a new role for MR imaging in preclinical studies of the natural history of early breast cancer. In future work, we plan to perform more detailed studies of carcinogenesis, by imaging more frequently and at higher resolution. Other MR imaging techniques, such as DCEMRI, diffusion weighted imaging and high spectral-spatial resolution imaging, could be used to probe the changes in vasculature

and cellularity that occur during progression. In addition, molecular imaging and gene/protein expression studies could be used in conjunction with MRI to interrogate the molecular mechanisms involved in cancer initiation and progression.

CONCLUSIONS

We have used longitudinal noninvasive imaging to gain new insights into the natural history of early mammary cancer in the C3(1) SV40 Tag mouse model of human breast cancer. We found that some *in situ* mammary cancers did not progress to invasive cancers, and investigated potential predictive markers of progression. This study represents a first step towards detailed studies of functional and morphological characteristics of mammary tumorigenesis, and developing methods for image acquisition and analysis that can predict which *in situ* cancers will become invasive and which would not. Such investigations would have an important impact on clinical management of patients with DCIS.

APPENDIX: Statistical method for identifying indolent MIN.

We consider two groups of MIN: (i) lesions in which progression to invasive cancer was observed, with average time to progression $T_{prog} = \mu_{prog} \pm \sigma_{prog}$, and (ii) lesions in which progression to invasive cancer was *not* observed, with a range of latency times T_{lat}. Our goal is to determine which lesions in the second group, if any, truly represent non-progressing or indolent disease. We begin first with the population of MIN lesions in which progression to invasive cancer was observed. We assume the progression time T_{prog} for each lesion is normally distributed $N(\mu_{\mathbf{prog}}, \sigma_{\mathbf{prog}})$, and denote N_{prog} as the number of lesions in the progressing group. We next consider a subset of the latent MIN lesions with latency times T_{lat} longer than a threshold T_0, and denote N_0 the number of lesions with $T_{lat} > T_0$. The probability that after randomly drawing $n = N_{prog} + N_0$ lesions from $N(\mu_{\mathbf{prog}}, \sigma_{\mathbf{prog}})$, we have selected at most N_{prog} lesions with $T_{prog} < T_0$ can be found using cumulative form of the binomial distribution, given by the following density function:

$$P(k) = \binom{n}{k} p^k (1-p)^{n-k}, \qquad [3]$$

where p is the probability that one progressing lesion can have $T_{prog} < T_0$ (can be calculated using the cumulative distribution function of the normal distribution) and $k = N_{prog}$. Thus, for each T_0 we obtain a probability that lesion with $T_{lat} > T_0$ are part of the progressing group.

LIST OF ABBREVIATIONS

DCIS	Ductal carcinoma in situ
MIN	Mammary intraepithelial neoplasia
SV40 Tag	Simian virus 40 large T antigen
MR	Magnetic resonance
MRI	Magnetic resonance imaging
GRE	Gradient recalled echo
TR	Repetition time
TE	Echo time
FOV	Field of view
NEX	Number of excitation
BIRADS	Breast imaging a reporting data system
ROC	Receiver operating curve
PET	Positron emission tomography
ROI	Region of interest

COMPETING INTERESTS

SJ has no competing interests.

SC has no competing interests.

XF has no competing interests.

EJ has no competing interests.

GN has no competing interests.

GK has no competing interests.

AUTHOR'S CONTRIBUTIONS

SJ conceived of the study and experiment design, conducted the imaging experiments, performed the data analysis and drafted the manuscript. SC participated in conception and design of the study and provided transgenic mice for imaging. XF helped to draft the manuscript and perform data analysis. EJ is the veterinary technician that participated in all imaging experiments. GM helped conceive and design the study. GK conceived of the study and experiment design, and participated in its coordination and helped to draft the manuscript. All authors read and approved the final manuscript.

ACKNOWLEDGEMENTS

We would like to thank the Segal Foundation, the Florsheim Foundation, DOD predoctoral award W81XWH-06-1-0329, NIH grants P50 CA125183-01 (SPORE) and R33 CA100996-02 for financial support. In addition, we thank Brad Williams for help in obtaining the animals used in these experiments, and Lorenzo Pesce for useful discussions regarding statistical modeling.

REFERENCES

1. Ernster VL, Barclay J, Kerlikowske K, Grady D, Henderson C: **Incidence of and treatment for ductal carcinoma in situ of the breast**. *Jama* 1996, **275**(12):913-918.
2. Thomson JZ, Evans AJ, Pinder SE, Burrell HC, Wilson AR, Ellis IO: **Growth pattern of ductal carcinoma in situ (DCIS): a retrospective analysis based on mammographic findings**. *Br J Cancer* 2001, **85**(2):225-227.
3. Sanders ME, Schuyler PA, Dupont WD, Page DL: **The natural history of low-grade ductal carcinoma in situ of the breast in women treated by biopsy only revealed over 30 years of long-term follow-up**. *Cancer* 2005, **103**(12):2481-2484.
4. Collins LC, Tamimi RM, Baer HJ, Connolly JL, Colditz GA, Schnitt SJ: **Outcome of patients with ductal carcinoma in situ untreated after diagnostic biopsy: results from the Nurses' Health Study**. *Cancer* 2005, **103**(9):1778-1784.
5. Erbas B, Provenzano E, Armes J, Gertig D: **The natural history of ductal carcinoma in situ of the breast: a review**. *Breast Cancer Res Treat* 2006, **97**(2):135-144.
6. Duffy SW, Agbaje O, Tabar L, Vitak B, Bjurstam N, Bjorneld L, Myles JP, Warwick J: **Overdiagnosis and overtreatment of breast cancer: estimates of overdiagnosis from two trials of mammographic screening for breast cancer**. *Breast Cancer Res* 2005, **7**(6):258-265.
7. Duffy SW, Tabar L, Vitak B, Day NE, Smith RA, Chen HH, Yen MF: **The relative contributions of screen-detected in situ and invasive breast carcinomas in reducing mortality from the disease**. *Eur J Cancer* 2003, **39**(12):1755-1760.
8. Yen MF, Tabar L, Vitak B, Smith RA, Chen HH, Duffy SW: **Quantifying the potential problem of overdiagnosis of ductal carcinoma in situ in breast cancer screening**. *Eur J Cancer* 2003, **39**(12):1746-1754.
9. Kerlikowske K, Molinaro A, Cha I, Ljung BM, Ernster VL, Stewart K, Chew K, Moore DH, 2nd, Waldman F: **Characteristics associated with recurrence among women with ductal carcinoma in situ treated by lumpectomy**. *J Natl Cancer Inst* 2003, **95**(22):1692-1702.
10. Jansen SA, Conzen SD, Fan X, Krausz T, Zamora M, Foxley S, River J, Newstead GM, Karczmar GS: **Detection of in situ mammary cancer in a transgenic mouse model: in vitro and in vivo MRI studies demonstrate histopathologic correlation**. *Phys Med Biol* 2008, **53**(19):5481-5493.
11. Cardiff RD, Anver MR, Gusterson BA, Hennighausen L, Jensen RA, Merino MJ, Rehm S, Russo J, Tavassoli FA, Wakefield LM *et al*: **The mammary pathology of genetically engineered mice: the consensus report and recommendations from the Annapolis meeting**. *Oncogene* 2000, **19**(8):968-988.
12. Maroulakou IG, Anver M, Garrett L, Green JE: **Prostate and mammary adenocarcinoma in transgenic mice carrying a rat C3(1) simian virus 40 large tumor antigen fusion gene**. *Proc Natl Acad Sci U S A* 1994, **91**(23):11236-11240.
13. Fan X, Markiewicz EJ, Zamora M, Karczmar GS, Roman BB: **Comparison and evaluation of mouse cardiac MRI acquired with open birdcage, single loop surface and volume birdcage coils**. *Phys Med Biol* 2006, **51**(24):N451-459.

14. ACR: **American College of Radiology (ACR) Breast Imaging Reporting and Data System Atlas (BI-RADS)**. Reston, VA.; 2003.
15. Abbey CK, Borowsky AD, Gregg JP, Cardiff RD, Cherry SR: **Preclinical imaging of mammary intraepithelial neoplasia with positron emission tomography**. *J Mammary Gland Biol Neoplasia* 2006, **11**(2):137-149.
16. Abbey CK, Borowsky AD, McGoldrick ET, Gregg JP, Maglione JE, Cardiff RD, Cherry SR: **In vivo positron-emission tomography imaging of progression and transformation in a mouse model of mammary neoplasia**. *Proc Natl Acad Sci U S A* 2004, **101**(31):11438-11443.
17. Namba R, Young LJ, Abbey CK, Kim L, Damonte P, Borowsky AD, Qi J, Tepper CG, MacLeod CL, Cardiff RD *et al*: **Rapamycin inhibits growth of premalignant and malignant mammary lesions in a mouse model of ductal carcinoma in situ**. *Clin Cancer Res* 2006, **12**(8):2613-2621.
18. Verschoyle RD, Brown K, Steward WP, Gescher AJ: **Consumption of silibinin, a flavonolignan from milk thistle, and mammary cancer development in the C3(1) SV40 T,t antigen transgenic multiple mammary adenocarcinoma (TAg) mouse**. *Cancer Chemother Pharmacol* 2008, **62**(2):369-372.
19. Leong H, Mathur PS, Greene GL: **Inhibition of mammary tumorigenesis in the C3(1)/SV40 mouse model by green tea**. *Breast Cancer Res Treat* 2008, **107**(3):359-369.
20. Kaur S, Greaves P, Cooke DN, Edwards R, Steward WP, Gescher AJ, Marczylo TH: **Breast cancer prevention by green tea catechins and black tea theaflavins in the C3(1) SV40 T,t antigen transgenic mouse model is accompanied by increased apoptosis and a decrease in oxidative DNA adducts**. *J Agric Food Chem* 2007, **55**(9):3378-3385.
21. Liu R, Varghese S, Rabkin SD: **Oncolytic herpes simplex virus vector therapy of breast cancer in C3(1)/SV40 T-antigen transgenic mice**. *Cancer Res* 2005, **65**(4):1532-1540.
22. Wild R, Yokoyama Y, Dings RP, Ramakrishnan S: **VEGF-DT385 toxin conjugate inhibits mammary adenocarcinoma development in a transgenic mouse model of spontaneous tumorigenesis**. *Breast Cancer Res Treat* 2004, **85**(2):161-171.
23. Wu Y, Cui K, Miyoshi K, Hennighausen L, Green JE, Setser J, LeRoith D, Yakar S: **Reduced circulating insulin-like growth factor I levels delay the onset of chemically and genetically induced mammary tumors**. *Cancer Res* 2003, **63**(15):4384-4388.
24. Kavanaugh C, Green JE: **The use of genetically altered mice for breast cancer prevention studies**. *J Nutr* 2003, **133**(7 Suppl):2404S-2409S.
25. Shibata MA, Kavanaugh C, Shibata E, Abe H, Nguyen P, Otsuki Y, Trepel JB, Green JE: **Comparative effects of lovastatin on mammary and prostate oncogenesis in transgenic mouse models**. *Carcinogenesis* 2003, **24**(3):453-459.
26. Calvo A, Yokoyama Y, Smith LE, Ali I, Shih SC, Feldman AL, Libutti SK, Sundaram R, Green JE: **Inhibition of the mammary carcinoma angiogenic switch in C3(1)/SV40 transgenic mice by a mutated form of human endostatin**. *Int J Cancer* 2002, **101**(3):224-234.
27. Calvo A, Feldman AL, Libutti SK, Green JE: **Adenovirus-mediated endostatin delivery results in inhibition of mammary gland tumor growth in C3(1)/SV40 T-antigen transgenic mice**. *Cancer Res* 2002, **62**(14):3934-3938.

28. Wu K, Kim HT, Rodriquez JL, Hilsenbeck SG, Mohsin SK, Xu XC, Lamph WW, Kuhn JG, Green JE, Brown PH: **Suppression of mammary tumorigenesis in transgenic mice by the RXR-selective retinoid, LGD1069**. *Cancer Epidemiol Biomarkers Prev* 2002, **11**(5):467-474.
29. Green JE, Shibata MA, Shibata E, Moon RC, Anver MR, Kelloff G, Lubet R: **2-difluoromethylornithine and dehydroepiandrosterone inhibit mammary tumor progression but not mammary or prostate tumor initiation in C3(1)/SV40 T/t-antigen transgenic mice**. *Cancer Res* 2001, **61**(20):7449-7455.
30. Shibata MA, Yoshidome K, Shibata E, Jorcyk CL, Green JE: **Suppression of mammary carcinoma growth in vitro and in vivo by inducible expression of the Cdk inhibitor p21**. *Cancer Gene Ther* 2001, **8**(1):23-35.
31. Wu K, Kim HT, Rodriquez JL, Munoz-Medellin D, Mohsin SK, Hilsenbeck SG, Lamph WW, Gottardis MM, Shirley MA, Kuhn JG *et al*: **9-cis-Retinoic acid suppresses mammary tumorigenesis in C3(1)-simian virus 40 T antigen-transgenic mice**. *Clin Cancer Res* 2000, **6**(9):3696-3704.
32. Holzer RG, MacDougall C, Cortright G, Atwood K, Green JE, Jorcyk CL: **Development and characterization of a progressive series of mammary adenocarcinoma cell lines derived from the C3(1)/SV40 Large T-antigen transgenic mouse model**. *Breast Cancer Res Treat* 2003, **77**(1):65-76.
33. Yoshidome K, Shibata MA, Couldrey C, Korach KS, Green JE: **Estrogen promotes mammary tumor development in C3(1)/SV40 large T-antigen transgenic mice: paradoxical loss of estrogen receptoralpha expression during tumor progression**. *Cancer Res* 2000, **60**(24):6901-6910.
34. Green JE, Shibata MA, Yoshidome K, Liu ML, Jorcyk C, Anver MR, Wigginton J, Wiltrout R, Shibata E, Kaczmarczyk S *et al*: **The C3(1)/SV40 T-antigen transgenic mouse model of mammary cancer: ductal epithelial cell targeting with multistage progression to carcinoma**. *Oncogene* 2000, **19**(8):1020-1027.
35. Liu ML, Von Lintig FC, Liyanage M, Shibata MA, Jorcyk CL, Ried T, Boss GR, Green JE: **Amplification of Ki-ras and elevation of MAP kinase activity during mammary tumor progression in C3(1)/SV40 Tag transgenic mice**. *Oncogene* 1998, **17**(18):2403-2411.
36. Yoshidome K, Shibata MA, Maroulakou IG, Liu ML, Jorcyk CL, Gold LG, Welch VN, Green JE: **Genetic alterations in the development of mammary and prostate cancer in the C3(1)/Tag transgenic mouse model**. *Int J Oncol* 1998, **12**(2):449-453.
37. Shibata MA, Maroulakou IG, Jorcyk CL, Gold LG, Ward JM, Green JE: **p53-independent apoptosis during mammary tumor progression in C3(1)/SV40 large T antigen transgenic mice: suppression of apoptosis during the transition from preneoplasia to carcinoma**. *Cancer Res* 1996, **56**(13):2998-3003.
38. Zahl PH, Maehlen J, Welch HG: **The natural history of invasive breast cancers detected by screening mammography**. *Arch Intern Med* 2008, **168**(21):2311-2316.
39. Krutchik AN, Buzdar AU, Blumenschein GR, Lukeman JM: **Spontaneous regression of breast carcinoma**. *Arch Intern Med* 1978, **138**(11):1734-1735.
40. Dussan C, Zubor P, Fernandez M, Yabar A, Szunyogh N, Visnovsky J: **Spontaneous regression of a breast carcinoma: a case report**. *Gynecol Obstet Invest* 2008, **65**(3):206-211.

41. Rice A, Quinn CM: **Angiogenesis, thrombospondin, and ductal carcinoma in situ of the breast**. *J Clin Pathol* 2002, **55**(8):569-574.
42. Franks SJ, Byrne HM, Underwood JC, Lewis CE: **Biological inferences from a mathematical model of comedo ductal carcinoma in situ of the breast**. *J Theor Biol* 2005, **232**(4):523-543.
43. Franks SJ, Byrne HM, Mudhar HS, Underwood JC, Lewis CE: **Mathematical modelling of comedo ductal carcinoma in situ of the breast**. *Math Med Biol* 2003, **20**(3):277-308.
44. Franks SJ, Byrne HM, King JR, Underwood JC, Lewis CE: **Modelling the early growth of ductal carcinoma in situ of the breast**. *J Math Biol* 2003, **47**(5):424-452.
45. Tabar L, Tony Chen HH, Amy Yen MF, Tot T, Tung TH, Chen LS, Chiu YH, Duffy SW, Smith RA: **Mammographic tumor features can predict long-term outcomes reliably in women with 1-14-mm invasive breast carcinoma**. *Cancer* 2004, **101**(8):1745-1759.
46. Tabar L, Chen HH, Duffy SW, Yen MF, Chiang CF, Dean PB, Smith RA: **A novel method for prediction of long-term outcome of women with T1a, T1b, and 10-14 mm invasive breast cancers: a prospective study**. *Lancet* 2000, **355**(9202):429-433.
47. Jansen SA, Paunesku T, Fan X, Woloschak GE, Vogt S, Conzen SD, Newstead GM, Karczmar GS: **Why Do Ductal Carcinoma in Situ Lesions Enhance on Dynamic Contrast Enhanced MRI of the Breast? Using X-Ray Fluorescence and MRI to Track the Spatial Distribution of Gd-DTPA in Murine DCIS.** In *Proceedings of the 16th Annual Meeting of the Internal Society for Magnentic Resonance in Medicine: 3-9 May 2008; Toronto.*

FIGURE LEGENDS

Figure 1: *In vivo* axial GRE MR images and corresponding H&E stained sections from a prior study [10]. The MR images and H&E stained sections represent different orientations, as each MR image represents only one cross-sectional slice through the mammary gland while the histologic sections show the entire gland. During imaging, the mammary glands are attached to the skin of the mouse, and are therefore wrapped around the body of the mouse. For excision, the glands are peeled back from the body of the mouse and laid flat, so that coronal H&E stained sections can be obtained. We used an agar grid (a polyethylene mesh embedded in partially deuterated agar) to register the axial MR images with the H&E stained sections. (a) Normal mammary gland, with intramammary lymph node, (b) lymph node and MIN, (c) lymph node and small tumor. For each MR image, the display FOV is approximately 2.0 × 2.0 cm, and in-plane resolution is 117 microns.

Figure 2: Flowchart demonstrating method for analyzing inguinal mammary glands for early murine mammary cancer.

Figure 3: Scatter plot of growth rates and lesion volume at initial detection of MIN and invasive tumors. Note that this plot displays only those lesions in which a growth rate could be calculated i.e., that were imaged at least twice as MIN or invasive tumor.

Figure 4: Examples of MIN progression in three different mice. In A) is an example of possible MIN regression. MIN is visible at 12 weeks of age (left) beside lymph node, but cannot be found six weeks later anywhere near the lymph node. Here, only one slice is shown demonstrating absence of a lesion near the lymph node (right). In B) MIN is first detected early on at 10 weeks of age, and in this axial MR image appears in cross section. The duct grew more distended at 12 and 14 weeks, and by 16 weeks had become an invasive tumor. The tumor then continued to grow and by 20 weeks was quite large. Interestingly, at 20 weeks it appeared that new MIN had developed close to the tumor. In C) MIN has developed at 10 weeks and does not progress to invasive cancer. FOV for all images is 3.0×2.0 cm, and in-plane resolution is 117 microns.

TABLES AND CAPTIONS

Table 1: The features at initial detection of MIN and early invasive cancers.

Feature at initial detection		MIN (n=21)	Invasive cancers (n=14)
Region	Upper gland	2 (9%)	1 (7%)
	Mid gland	10 (48%)	8 (57%)
	Lower gland	9 (43%)	5 (36%)
Distance from lymph node (mm)		3.5 ± 1.8	6.6 ± 7.6
Age (weeks)		12.7 ± 2.6	16.3 ± 3.2
Volume (mm^3)		0.34± 0.22	17.2 ± 41.6*
Morphology			
Type	Nonmass	21 (100%)	0 (0%)
	Mass	0 (0%)	14 (100%)
Distribution (Nonmass)	Ductal	11 (52%)	--
	Segmental	9 (43%)	--
	Linear	1 (5%)	--
Pattern (Nonmass)	Clumped	2 (10%)	--
	Homogeneous	14 (67%)	--
	Stippled	5 (23%)	--
Shape (Mass)	Irregular	--	3 (21%)
	Round	--	9 (64%)
	Lobular	--	2 (14%)
Margins (Mass)	Smooth	--	10 (71%)
	Irregular	--	4 (29%)
Pattern (Mass)	Heterogeneous	--	4 (29%)
	Homogeneous	--	10 (71%)

*If we exclude two tumors that initially presented at over 100 mm^3, the average was 1.96 ± 2.01 mm^3.

Table 2: Values of lesion features in progressing vs. indolent MIN. Student t-test comparisons yielded *p* values shown below. For the A_z values, numbers in parentheses represent 95% confidence intervals.

Feature	Progressing MIN (n=9)	Indolent MIN (n=5)	*p* value	A_z
Age at first detection (weeks)	12.3±2.3	10.6±0.9	0.07	0.83(0.51-0.97)
Maximum volume (mm^3)	0.55±0.66	0.67±0.87	0.81	0.48 (0.19-0.78)
Growth rate ($week^{-1}$)**	0.21±0.29	-0.66±0.952	0.11	0.83 (0.45-0.98)
Distance from lymph node (mm)	4.2±2.2	2.7±1.6	0.18	0.75(0.43-0.94)

** Growth rate could only be measured for those lesions that were imaged as MIN at least twice.

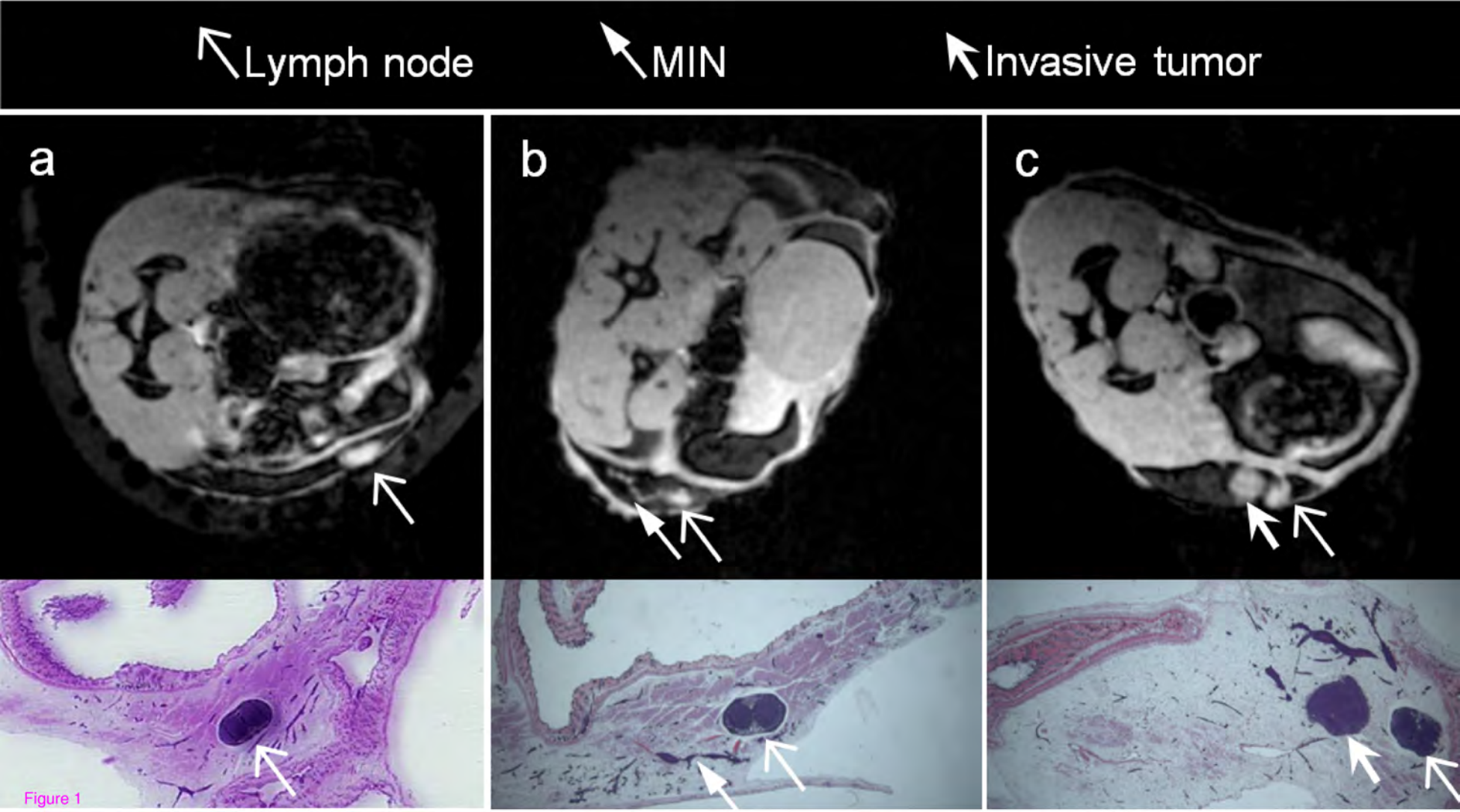

Figure 1

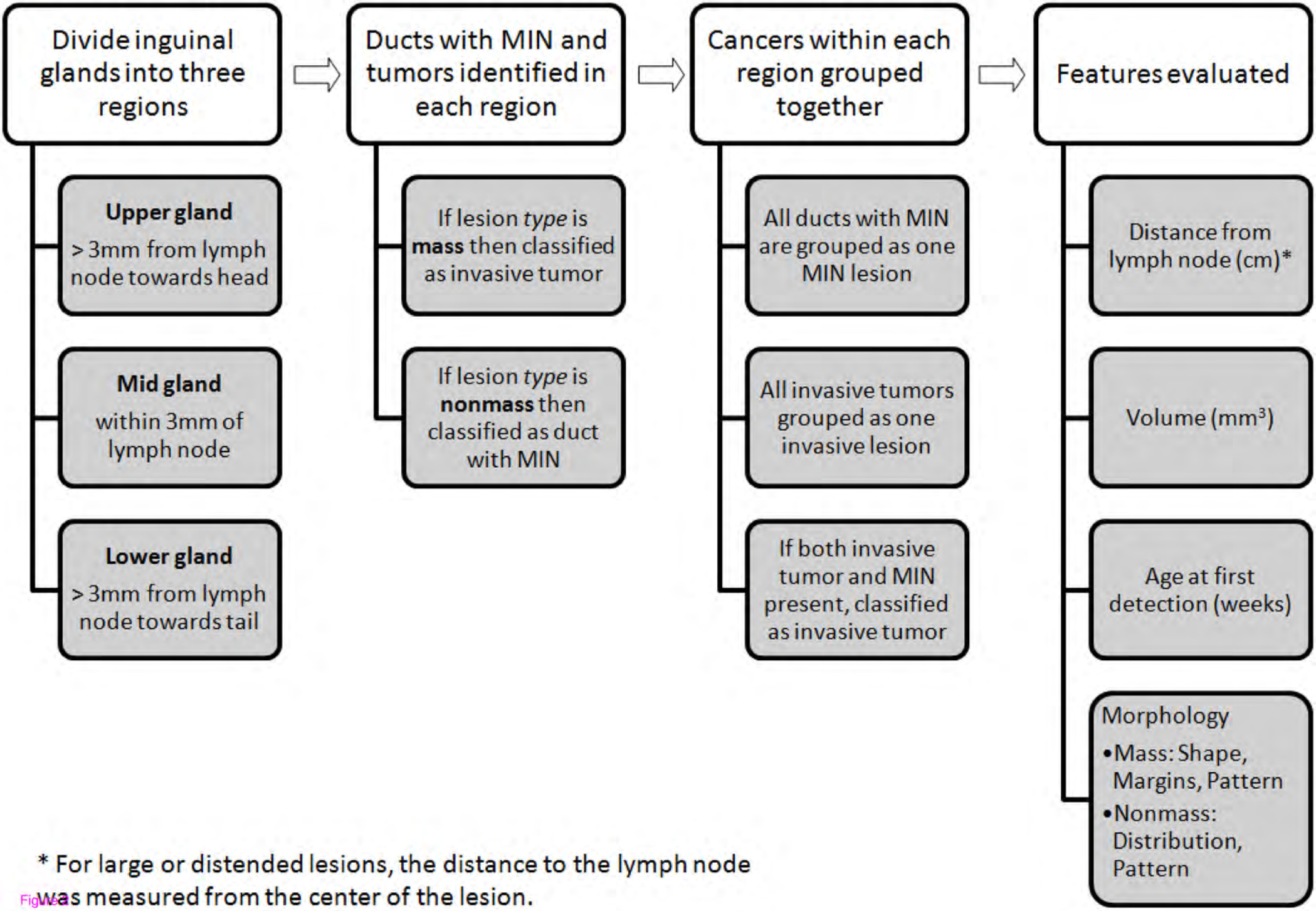
Divide inguinal glands into three regions
Upper gland
> 3mm from lymph node towards head
Mid gland
within 3mm of lymph node
Lower gland
> 3mm from lymph node towards tail
Ducts with MIN and tumors identified in each region
If lesion type is mass then classified as invasive tumor
If lesion type is nonmass then classified as duct with MIN
Cancers within each region grouped together
All ducts with MIN are grouped as one MIN lesion
All invasive tumors grouped as one invasive lesion
If both invasive tumor and MIN present, classified as invasive tumor
Features evaluated
Distance from lymph node (cm)*
Volume (mm3)
Age at first detection (weeks)
Morphology
•Mass: Shape, Margins, Pattern
•Nonmass: Distribution, Pattern
* For large or distended lesions, the distance to the lymph node was measured from the center of the lesion.

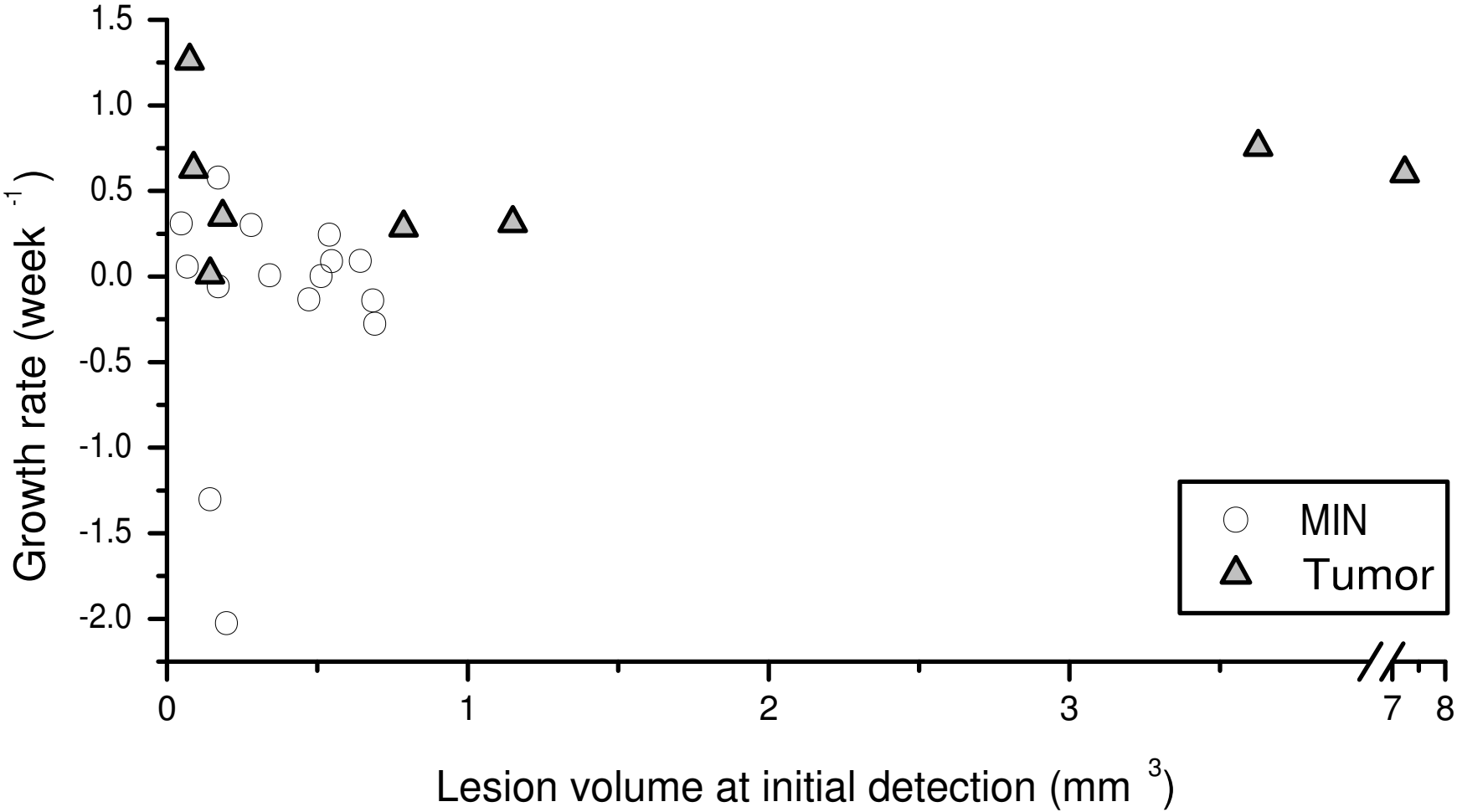
1.5
1.0
0.5
0.0
-0.5
-1.0
-1.5
-2.0
Growth rate (week -1)
0
1
2
3
7
8
Lesion volume at initial detection (mm 3)
MIN
Tumor

Figure 3

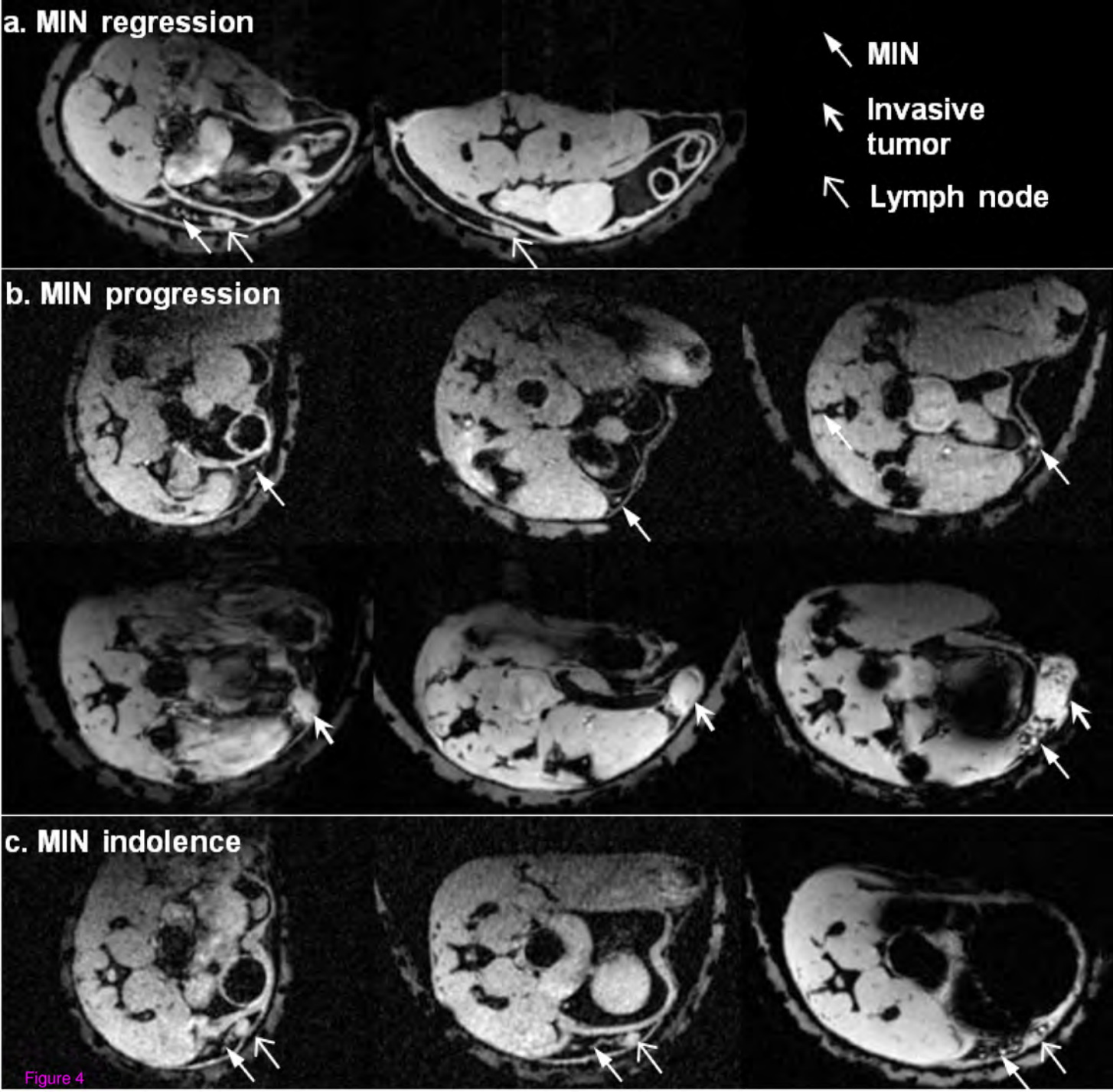
a. MIN regression
MIN
Invasive tumor
Lymph node
b. MIN progression
c. MIN indolence

Figure 4

Relating dose of contrast media administered to uptake and washout of malignant lesions on DCEMRI of the breast.

Sanaz A. Jansen PhD, Xiaobing Fan PhD, Cheng Yang PhD,
Akiko Shimauchi MD, Gregory Karczmar PhD and Gillian M. Newstead* MD.

University of Chicago, Department of Radiology

Submitted as an Original Investigation to Academic Radiology
Word Count: 2370
Short running head: Relating contrast dose to kinetics of malignant lesions

*Corresponding Author
Gillian M. Newstead
Professor of Radiology
University of Chicago
Department of Radiology
5841 S. Maryland Ave
MC 2026
Chicago, IL 60637

Phone: 773-702-2781
Fax: 773-702-0214
Email: gnewstead@radiology.bsd.uchicago.edu

Grant Support: We would like to thank the Segal Foundation and DOD Award W81XWH-06-1-0329 for financial support.

ABSTRACT

Rationale and Objectives: To quantify the relationship between dose of contrast administered and contrast kinetics of malignant breast lesions.

Materials and Methods: 108 patients with 120 malignant lesions were selected for an IRB approved review. Dynamic MR protocol: 1 pre and 3 or 5 post-contrast (at a fixed volume of 20 ml of 0.5M Gadodiamide) images. Patients were stratified into groups based on dose of contrast administered, after calculation of body weight (kg): Dose Group 1 < 0.122 mmol/kg; Dose Group 2 0.123-0.155 mmol/kg; Dose Group 3 >0.155 mmol/kg. Analysis of kinetic curve shape was made according to the BI-RADS lexicon. Several quantitative parameters were calculated including initial and peak enhancement percentage (E_1 and E_{peak}). Linear regression was used to model the variation of kinetic parameters with dose.

Results: There was no difference found in the qualitative BIRADS descriptors of curve shape between the three dose groups. There was a trend for E_1 and E_{peak} to increase from Dose Group 1 to Dose Group 3 in malignant lesions overall, as well as in IDC lesions separately. Each decrement/increment of 0.05 mmol/kg in dose yielded a decrease/increase of 78% and 97% in E_1 for *in situ* and invasive cancers, respectively.

Conclusion: Contrast should be administered at fixed dose to achieve comparable levels of lesion uptake in women of different weight. Our results suggest that reducing the contrast administered to 0.05 mmol.kg, as has been suggested for patients at risk of developing nephrogenic systemic fibrosis, could impair the reliable detection of early cancers.

Keywords: breast MRI, contrast dose, kinetics, breast cancer.

INTRODUCTION

Dynamic contrast enhanced magnetic resonance imaging (DCEMRI) of the breast allows for excellent visualization of lesion morphology and cancerous disease extent(1-3). Due to its high sensitivity for malignant disease, DCEMRI is being used increasingly for staging of the newly diagnosed breast cancer patient, for high-risk screening and for follow-up of patients undergoing therapeutic interventions (4-6). Lesions are visualized after intravenous injection of contrast media, usually a gadolininum chelate, which accumulates in and around malignant tumors due to their dense and leaky neovasculature. Analysis of the timecourse of contrast media uptake and washout (i.e., the kinetic curve) is important for lesion evaluation, as malignant tumors tend to exhibit a 'washout' curve shape, while benign lesions often show 'persistent' contrast uptake over time(7).

The injection of contrast media is a crucial component of breast DCEMRI acquisitions, as it is required for both lesion visualization and characterization. Yet despite years of breast MR imaging and clinical investigations, contrast media is typically used "off-label" for breast DCEMRI. Ideally, it should be expected that (i) sufficient quantity of contrast is injected for reliable detection of all malignancies, (ii) an excessive quantity should be avoided to prevent toxicity, such as development of nephrogenic systemic fibrosis in patients with compromised kidney function (8), and (iii) it is administered in such a way to minimize inter-patient variability, ensuring that similar interpretation criteria can be consistently applied in the evaluation and characterization of lesions. The American College of Radiology (ACR) practice guidelines recommend that contrast be administered at a *fixed dose* of 0.1 mmol/kg via a bolus

injection, followed by at least a 10 ml saline flush (9). By injecting a fixed dose, heavier women receive a larger volume (in ml) of contrast media compared to normal weight women. This is to be distinguished from injecting a *fixed volume* of contrast, so that regardless of weight, all women will receive the same volume of contrast media. This was utilized more commonly in the past, and continues to be employed in some institutions.

The concern with administering a fixed volume of contrast, rather than a fixed dose, is that women of different weights will receive variable doses of contrast, which may in turn result in a variable presentation of lesion kinetic curves. While this is certainly likely to be the case, few reports have quantified this effect. At our institution, for a short while contrast had been injected at a fixed volume rather than a fixed dose. The purpose of this study was to quantify the effect of contrast media dose on the kinetic presentation of malignant lesions.

MATERIALS AND METHODS

Patients

Breast DCEMRI is most often obtained at our institution for pre-operative staging of the newly diagnosed breast cancer patient, post-chemotherapy evaluation and screening of high-risk women. A HIPAA compliant retrospective review of breast MR examinations yielded 108 consecutive patients that were eligible for study under an IRB approved waiver of consent: those with patient history forms available, with MR detected malignant lesions, and with a fixed volume (20 ml) of contrast injected. These images were acquired March 2003-February 2005, and the average patient age was 56.1 ±14.4 years. After review of final pathology reports, the malignant lesions were classified as invasive ductal carcinoma (IDC), ductal carcinoma *in situ* (DCIS) or 'other'.

MR Imaging Protocol and Analysis

MR imaging was performed on a 1.5T GE Signa scanner (GE Healthcare, Milwaukee, WI) using a dedicated 4 channel breast coil (Invivo, Orlando, FL) with the patient in the prone position. Images were acquired in the coronal plane using a 3D T_1-weighted spoiled grass sequence (TR/TE = 7.7/4.2 ms, slice thickness = 3 mm, and in plane resolution = 1.4 mm, flip angle = 30˚), without fat suppression. Two protocols were used, with either 3 or 5 post contrast acquisitions. For both protocols, imaging commenced 20 seconds after contrast injection, and the first, second and last post contrast images were acquired at similar sampling intervals: 68, 136 and 324 second post-contrast, respectively. 20 ml of 0.5mmol/ml Gadodiamide (Omniscan; Nycomed-Amersham, Princeton, NJ) was injected intravenously followed by a 20 ml saline flush

at the rate of 2.0 ml /sec. Thus, the amount in moles of Gadodiamide injected regardless of weight for every patient was 20ml × 0.5 mmol/ml = 10 mmol.

Determination of Dose Groups

Patient history forms completed by patients at the time of MR examination were retrospectively reviewed to determine patient weight in pounds. This weight was then converted into kilograms (kg) so that the injected dose of contrast could be calculated as:

$$\text{Injected dose} = (\text{Injected moles of contrast})/ (\text{Patient weight in kg})$$

$$= 10 \text{ mmol}/(\text{Patient weight in kg})$$

The patients were then divided into three groups based on their administered dose: Dose Group 1, less than 0.122 mmol/kg; Dose Group 2, 0.125-0.155 mmol/kg; and Dose Group 3, greater than 0.155 mmol/kg.

Kinetic Analysis

Qualitative assessment of curve shape. One experienced radiologist retrospectively reviewed the images and classified lesion morphology and kinetics. To generate the kinetic curve, the radiologist used institutional software to trace a small region of interest (ROI) around what was perceived to be the most enhancing part of the lesion on the first post-contrast image. The plot of signal intensity vs. time for this ROI was assessed by the radiologist according to the BI-RADS lexicon, which describes the initial rise (‘rapid’, ‘medium’, ‘slow’) and delayed phase (‘persistent’, ‘plateau’, ‘washout’) of the kinetic curve.

Quantitative parameters. In addition to this qualitative assessment of kinetics, several quantitative parameters were calculated. The initial and peak enhancement percentages (E_1 and E_{peak}) quantify the contrast uptake of the curve(10),

$$E_1 = 100 \times \frac{S_1 - S_0}{S_0}, \quad E_{peak} = 100 \times \frac{S_{peak} - S_0}{S_0}$$

where S_0 in the precontrast signal intensity, and S_1 is the first post contrast signal intensity, and S_{peak} is the peak signal intensity. The signal enhancement ratio (SER) has been used in prior studies to quantify the degree of washout of the curve (11),

$$SER = \frac{S_1 - S_0}{S_{last} - S_0},$$

where S_{last} is the signal intensity at the last post contrast time point. A larger SER implies greater washout relative to the first post contrast point. Higher SER has been correlated with increased vascularity and malignancy in other reports (11-13). Finally, the time to peak enhancement (T_{peak}) was calculated in seconds(10).

Normalizing parameters to fixed dose. To estimate the values of E_1 and E_{peak} had a fixed dose of 0.1 mmol/kg been consistently injected, these parameters were normalized using the normalization factor:

Normalization factor (*NF*) = Injected dose/ (0.1 mmol/kg)

= (10 mmol/Patient weight in kg)/ (0.1 mmol/kg)

=100/(Patient weight in kg)

Thus, for each lesion the following normalized kinetic parameters were also calculated:

$$E_1^{norm} = \frac{E_1}{NF}, \qquad E_{peak}^{norm} = \frac{E_{peak}}{NF}.$$

Statistical Analysis

To compare the proportion of 'washout' vs. 'plateau' and 'persistent' (or 'rapid' vs. 'medium' and 'slow') curves the Pearson's χ^2 – test was used, with a p value of < 0.05 indicating statistical significance. Two-tailed unequal variance Student's *t*-tests were performed to evaluate which quantitative kinetic parameters showed significant differences between the three dose groups with a p value < 0.05 indicating statistical significance. The Holm-Bonferroni correction method was applied to test for significance of multiple comparisons(14). Linear regression was implemented to quantify the relationship of the quantitative parameters E_1, E_{peak}, T_{peak} and SER vs. dose for all lesions using Origin 6.0 software. The line-of-best-fit was used also to estimate the parameter values at an injected dose of 0.1 mmol/kg.

RESULTS

Description of Dose Groups

After review of image and pathology data from all 108 patients, a total of 120 MR detected malignant lesions were included. Of these, 60 were classified as IDC, 39 as DCIS, and 21 as 'other'. The majority of patients were classified in Dose Group 2, having received a contrast dose of between 0.125 and 0.155 mmol/kg (Table 1). 11 patients received a dose less than 0.1 mmol/kg, and the highest dose administered was 0.201 mmol/kg.

Kinetic Analysis

The qualitative BI-RADS descriptors did not vary considerably between the dose groups (p >0.13 for initial rise and p> 0.76 for delayed phase in malignant lesions). For all groups, the majority of lesions were classified as having "rapid" initial rise and "washout" curve shape (Figure 1).

The parameters SER and T_{peak} were not found to be significantly different among the three dose groups (p > 0.08 for malignant lesions overall, Table 2). For DCIS lesions, the SER of Dose Group 1 was higher than that of Dose Group 2 (p=0.02, but not significant after the Holm Bonferroni correction), however this trend was not observed in IDC lesions. There was a trend for E_1 and E_{peak} to increase from lower to higher injected dose in malignant lesions overall, as well as in IDC lesions separately (Table 2). However, these differences were not statistically significant (p>0.048). After normalizing the parameters E_1 and E_{peak} to estimate their values had a fixed dose of 0.1 mmol/kg been administered, this trend was no longer apparent (Figure 2). In other words, the values of E_1^{norm} and E_{peak}^{norm} were comparable among the three dose groups, particularly for IDC lesions.

Linear regression also demonstrated that an increased injected dose yielded an increased E_1 and E_{peak} (Figure 3). Interestingly, DCIS and IDC lesions both demonstrated a similar slope of the line-of-best-fit for the parameters E_1 and $E_{peak.}$ Based on the slope of the fitted line, an increase (or decrease) in dose of 0.05 mmol/kg resulted in an increase (or decrease) of 97% in E_1 and 56% in E_{peak} for IDC lesions, and 78% in E_1 and 82% in E_{peak} for DCIS. In addition, using the line of best fit, the value of E_1 at 0.1 mmol/kg for DCIS was approximately 160%, and for IDC was approximately 353%. However, the 95% confidence bands for all fits were relatively large, thus limiting the accuracy of these approximations. The parameter SER did not vary by dose for IDC lesions. However, for DCIS lesions SER increased slightly with decreasing dose, which is once again related to the higher average SER observed in Dose Group 1.

DISCUSSION

We set out to quantitatively analyze the association of contrast kinetics in malignant lesions with dose of contrast administered. Our results suggest that varying the dose of administered contrast affects the initial uptake and peak enhancement of the kinetic curve when measured quantitatively: those injected with a lower dose exhibit a lower E_1 and E_{peak}, although this difference was not statistically significant. On the other hand, we found no difference in quantitative or qualitative measures of overall kinetic curve shape, suggesting that diagnostic interpretation criteria are not affected when variable doses are administered. After normalizing the parameters E_1 and E_{peak} to approximate their values had contrast been consistently injected at 0.1 mmol/kg, comparable levels of contrast uptake were exhibited across dose groups. This implies that contrast should be administered at fixed dose rather than fixed volume to reduce inter-patient variability of contrast kinetics, which is certainly in concordance with conventional wisdom and guidelines (9). However, studies analyzing the effect of patient weight on contrast kinetics even when a fixed dose is administered should be performed to ensure that similar contrast kinetics are indeed achieved. For example, compromised cardiac output in obese women may be complicating factor.

If injecting contrast media at a fixed dose is preferable, what should this dose be? While the ACR practice guidelines recommend 0.1 mmol/kg, large trials evaluating the efficacy MR screening for women at high risk of developing breast cancer, as well as those studying optimal diagnostic criteria, have used both 0.1 mmol/kg (15-18) and 0.2 mmol/kg (19, 20). While dose-response studies of other contrast agents such as gadobenate dimeglumine have been

performed(21, 22), there have been relatively few papers comparing lesion enhancement with dose of contrast administered. Hewyang-Kolbrunner et al found that injecting contrast at a higher dose of 0.16 mmol/kg increased lesion percent enhancement and conspicuity compared to injecting at 0.1 mmol/kg(23). Based on historical review, it appears that the recommendation of 0.1 mmol/kg stems from the FDA approved dosage for DCEMRI of CNS or body (intrathoracic, intra-abdomincal, pelvic and retroperitoneal) in the early 1990's (24-27). Thus, further investigations of the appropriate magnitude for administered dose of Gd-DTPA for breast MR imaging are likely warranted.

Due to recent concerns regarding dose of administered contrast for patients at risk of developing nephorgenic systemic fibrosis (NSF), the ACR recommends that contrast be administered at half-dose in these patients(9). Our results quantifying the relationship between dose and enhancement percentages caution that injecting at a half dose of 0.05 mmol/kg could potentially drop the typical E_1 of IDC and DCIS lesions to 256% and 83%, respectively (Figure 3). Although our application of linear modeling and extrapolation is certainly limited, it suggests that injecting at half-dose may compromise the reliable detection of the earliest stage of breast cancer. Additional study is needed in order to fully evaluate this effect.

There are several limitations to this retrospective study. Patient weight was determined by reviewing manually completed patient history forms, which may have not been accurately filled. In addition, this study would have been ideally been performed in the same patient, i.e., injecting one patient with different doses to determine the dose response of each lesion separately, rather than calculating a population average of kinetic parameters over all lesions. There were

limitations of the kinetic curve evaluation as well. Two imaging protocols with different timing resolution had been used. This affects the accuracy of the parameters E_{peak} and T_{peak}, however because the first and last post contrast images were acquired at similar times for both protocols E_1 and SER are not adversely affected. Furthermore, the kinetic curve was generated manually by one radiologist; it is likely that other radiologists may have selected different kinetic curves and parameters. Finally, the relationship between enhancement percentage and dose of contrast administered is a nonlinear function of pulse sequence parameters and contrast media concentration(28). We used linear regression here as only a first approximation of the overall behavior.

To summarize, we have quantified the relationship between dose of contrast administered and resulting kinetic curve parameters. In doing so, our results suggest that while under-dosing patients at risk for NSF may be necessary, it may also compromise the reliable detection of DCIS and moderately enhancing invasive cancers. We have confirmed that contrast should be administered at fixed dose, although future work should be done to determine what that dose should be.

REFERENCES

1. Boetes C, Mus RD, Holland R, et al. Breast tumors: comparative accuracy of MR imaging relative to mammography and US for demonstrating extent. Radiology 1995; 197:743-747.
2. Schouten van der Velden AP, Boetes C, Bult P, Wobbes T. The value of magnetic resonance imaging in diagnosis and size assessment of in situ and small invasive breast carcinoma. Am J Surg 2006; 192:172-178.
3. Liberman L. Breast MR imaging in assessing extent of disease. Magn Reson Imaging Clin N Am 2006; 14:339-349, vi.
4. Newstead GM. MR imaging in the management of patients with breast cancer. Semin Ultrasound CT MR 2006; 27:320-332.
5. Saslow D, Boetes C, Burke W, et al. American Cancer Society guidelines for breast screening with MRI as an adjunct to mammography. CA Cancer J Clin 2007; 57:75-89.
6. Hylton N. MR imaging for assessment of breast cancer response to neoadjuvant chemotherapy. Magn Reson Imaging Clin N Am 2006; 14:383-389, vii.
7. Kuhl CK, Mielcareck P, Klaschik S, et al. Dynamic breast MR imaging: are signal intensity time course data useful for differential diagnosis of enhancing lesions? Radiology 1999; 211:101-110.
8. Abraham JL, Thakral C. Tissue distribution and kinetics of gadolinium and nephrogenic systemic fibrosis. Eur J Radiol 2008; 66:200-207.
9. Kanal E, Barkovich AJ, Bell C, et al. ACR guidance document for safe MR practices: 2007. AJR Am J Roentgenol 2007; 188:1447-1474.
10. Szabo BK, Aspelin P, Wiberg MK, Bone B. Dynamic MR imaging of the breast. Analysis of kinetic and morphologic diagnostic criteria. Acta Radiol 2003; 44:379-386.
11. Esserman L, Hylton N, George T, Weidner N. Contrast-Enhanced Magnetic Resonance Imaging to Assess Tumor Histopathology and Angiogenesis in Breast Carcinoma. Breast J 1999; 5:13-21.
12. Li KL, Partridge SC, Joe BN, et al. Invasive breast cancer: predicting disease recurrence by using high-spatial-resolution signal enhancement ratio imaging. Radiology 2008; 248:79-87.
13. Li KL, Henry RG, Wilmes LJ, et al. Kinetic assessment of breast tumors using high spatial resolution signal enhancement ratio (SER) imaging. Magn Reson Med 2007; 58:572-581.
14. Holm S. A simple sequentially rejective multiple test procedure. Scandinavian J Statist 1979; 6:65-70.
15. Schnall MD, Blume J, Bluemke DA, et al. Diagnostic architectural and dynamic features at breast MR imaging: multicenter study. Radiology 2006; 238:42-53.
16. Kuhl CK, Schrading S, Leutner CC, et al. Mammography, breast ultrasound, and magnetic resonance imaging for surveillance of women at high familial risk for breast cancer. J Clin Oncol 2005; 23:8469-8476.
17. Warner E, Plewes DB, Hill KA, et al. Surveillance of BRCA1 and BRCA2 mutation carriers with magnetic resonance imaging, ultrasound, mammography, and clinical breast examination. Jama 2004; 292:1317-1325.

18. Sardanelli F, Podo F, D'Agnolo G, et al. Multicenter comparative multimodality surveillance of women at genetic-familial high risk for breast cancer (HIBCRIT study): interim results. Radiology 2007; 242:698-715.
19. Heywang-Kobrunner SH, Bick U, Bradley WG, Jr., et al. International investigation of breast MRI: results of a multicentre study (11 sites) concerning diagnostic parameters for contrast-enhanced MRI based on 519 histopathologically correlated lesions. Eur Radiol 2001; 11:531-546.
20. Leach MO, Boggis CR, Dixon AK, et al. Screening with magnetic resonance imaging and mammography of a UK population at high familial risk of breast cancer: a prospective multicentre cohort study (MARIBS). Lancet 2005; 365:1769-1778.
21. Knopp MV, Bourne MW, Sardanelli F, et al. Gadobenate dimeglumine-enhanced MRI of the breast: analysis of dose response and comparison with gadopentetate dimeglumine. AJR Am J Roentgenol 2003; 181:663-676.
22. Pediconi F, Catalano C, Occhiato R, et al. Breast lesion detection and characterization at contrast-enhanced MR mammography: gadobenate dimeglumine versus gadopentetate dimeglumine. Radiology 2005; 237:45-56.
23. Heywang-Kobrunner SH, Haustein J, Pohl C, et al. Contrast-enhanced MR imaging of the breast: comparison of two different doses of gadopentetate dimeglumine. Radiology 1994; 191:639-646.
24. FDA. Prohance, Available at:. http://www.fda.gov/cder/foi/label/2007/020131s023,021489s001lbl.pdf; Accessed February 25, 2009.
25. FDA. Magnevist, Available at:. http://www.fda.gov/cder/foi/label/2007/019596s043,021037s018lbl.pdf; Accessed February 25, 2009.
26. FDA. Omniscan, Available at:. http://www.fda.gov/cder/foi/label/2007/020123s034lbl.pdf; Accessed February 25, 2009.
27. FDA. Multihance, Available at:. http://www.fda.gov/cder/foi/label/2007/021357s003,021358s003lbl.pdf; Accessed February 25, 2009.
28. Armitage P, Behrenbruch C, Brady M, Moore N. Extracting and visualizing physiological parameters using dynamic contrast-enhanced magnetic resonance imaging of the breast. Med Image Anal 2005; 9:315-329.

FIGURE CAPTIONS

Figure 1: The distribution of BI-RADS qualitative descriptors of initial rise (left) and delayed phase (right) for each dose group, where Dose Group 1 had been injected with the least dose and Dose Group 3 with the highest. The top two plots are for all malignant lesions, and the bottom two for IDC lesions specifically.

Figure 2: The average values of E_1, E_1^{norm}, $E_{peak}$and E_{peak}^{norm} for each dose group, in IDC and DCIS lesions seperatley.

Figure 3: Scatter plot of kinetic parameters as a function of dose for DCIS and IDC lesions separately. The measured kinetic parameter values are displayed with open circles. The line-of –best-fit is shown in black, while thin gray lines represent 95% confidence bands of each fit.

Table 1: Patients in this study were classified into three groups based on quantity of administered dose.

	Dose Group 1	**Dose Group 2**	**Dose Group 3**
Dose range (mmol/kg)	0.071-0.122	0.123-0.155	0.156-0.201
Average dose (mmol/kg)	0.105±0.015	0.139±0.008	0.175±0.0141
Number of patients	31	53	24
Average patient age (years)	53.6±13.1	55.8±14.1	56.0±16.7
Average patient weight (pounds)	215±36	159±9	127±10
Number malignant lesions	34	58	28
Number of IDC lesions	16	30	14
Number of DCIS lesions	15	15	9

Table 2: Quantitative kinetic parameters E_1, E_{peak}, T_{peak} and SER for malignant, IDC and DCIS lesions in each dose group.

	Type of lesion	No. cases	E_1 (%)	E_{peak} (%)	T_{peak} (sec)	SER
Dose Group 1	All Malignant	34	254±146	298±167	215±97	1.09±0.43
	DCIS	15	184±122	216±134	225±103	1.09±0.46
	IDC	16	301±139	363±169	202±89	1.05±0.36
Dose Group 2	All Malignant	58	284±167	344±166	233±110	0.97±0.37
	DCIS	15	204±106	319±181	318±107	0.74±0.30
	IDC	30	341±179	375±172	183±82	1.09±0.32
Dose Group 3	All Malignant	28	348±205	381±197	202±95	1.06±0.31
	DCIS	9	238±173	275±154	245±113	0.85±0.24
	IDC	14	439±212	467±212	166±71	1.22±0.30

Figure 1

Click here to download high resolution image

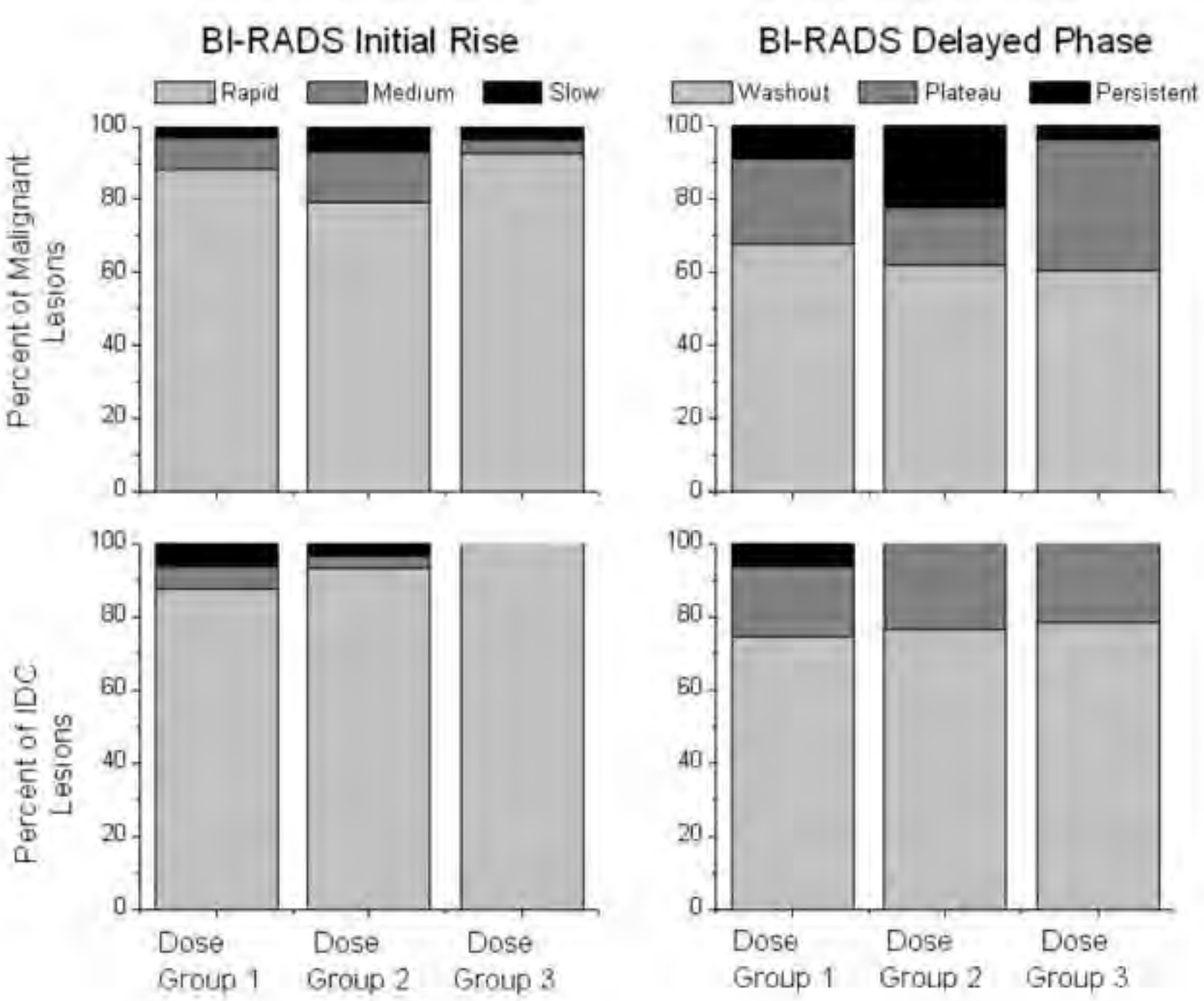

Figure 2

Click here to download high resolution image

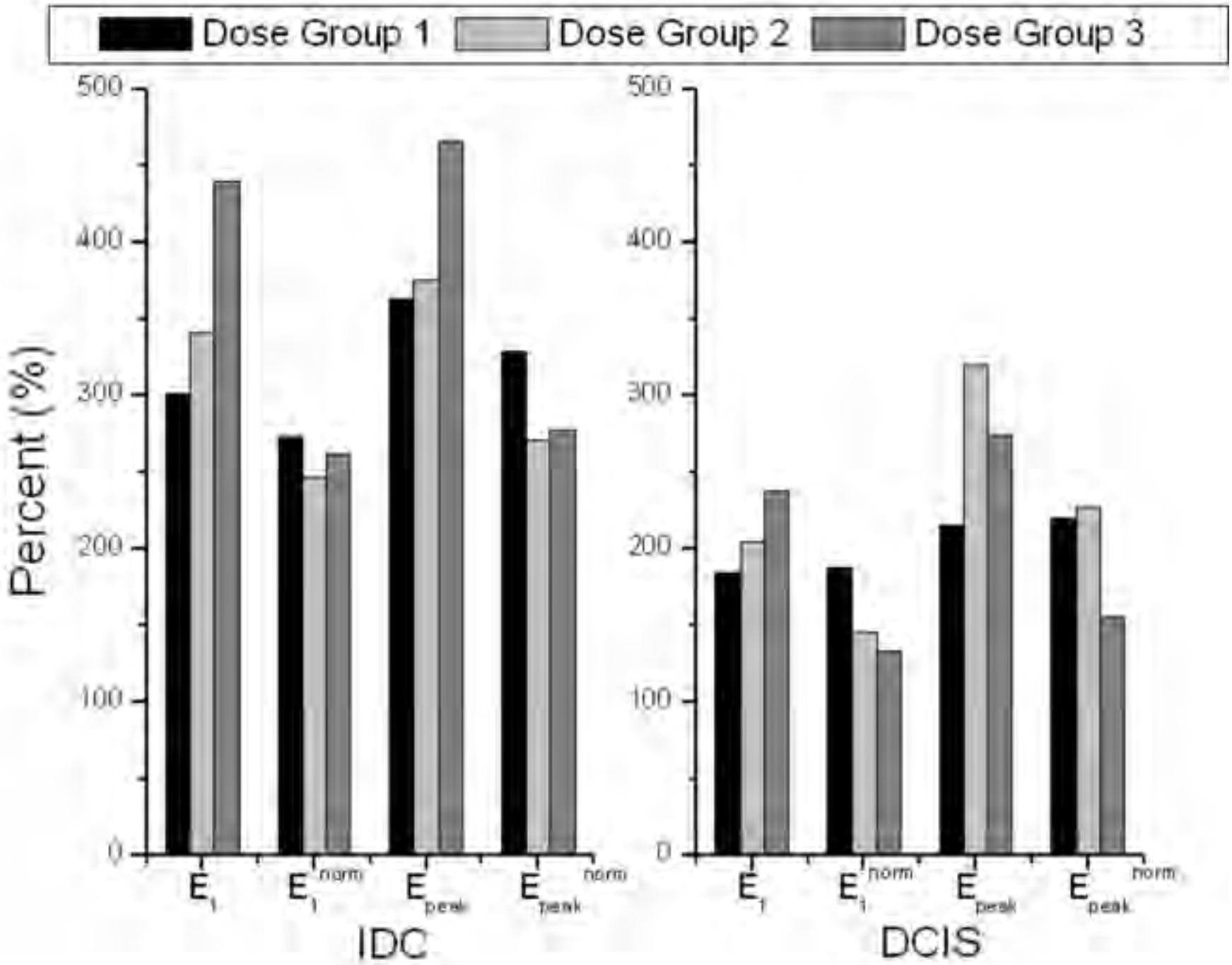

Figure 3

Click here to download high resolution image

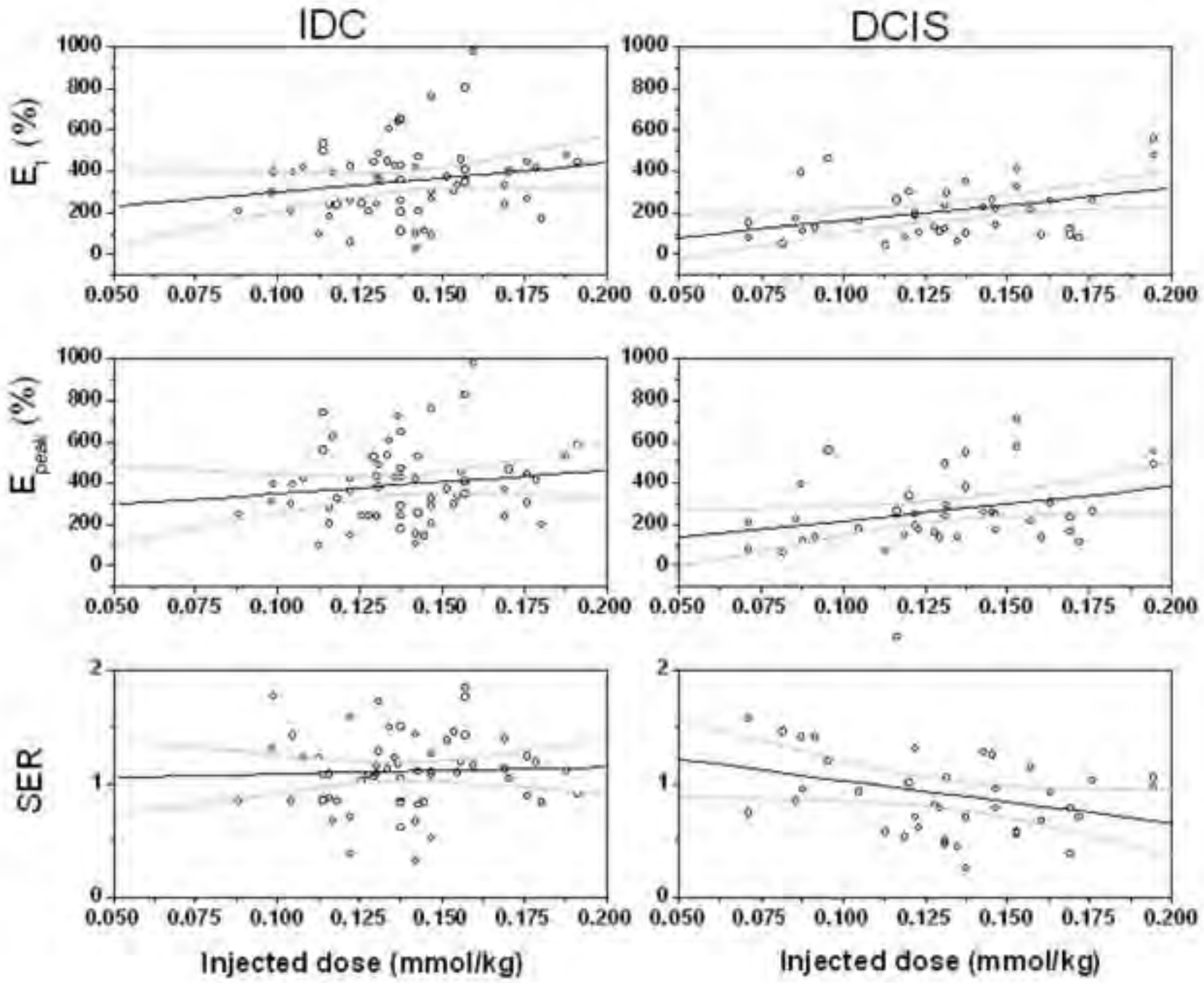

6757

Short T2* components in the normal murine mammary gland and pre-invasive carcinoma may aid in detection of early breast cancer.

S. A. Jansen[1], X. Fan[2], E. Markiewicz[2], G. Newstead[2], and G. Karczmar[1]
[1]University of Chicago, Chicago, IL, United States, [2]University of Chicago

Introduction: Ductal carcinoma *in situ* (DCIS) is the earliest stage of breast cancer, where cancer cells are still confined by mammary ducts. While dynamic contrast enhanced MR imaging (DCEMRI) of the breast has demonstrated excellent sensitivity for early invasive breast cancers, improvements in the diagnostic accuracy of DCEMRI for DCIS is highly desirable. Relaxometry of pure DCIS is important to improve diagnosis of these lesions; however this is difficult to perform in women due to the challenge of isolating and identifying ducts with DCIS. Recently, we have reported for the first time that noncontrast MR imaging techniques can reliably detect early mammary cancer in mice, including single ducts with DCIS. Here, we use transgenic mouse models to perform relaxometry of murine DCIS and normal tissue.

Methods: Female C3(1) SV40 Tag transgenic mice (n=8) were used under IACUC compliance. MR imaging was performed on a 9.4T Bruker magnet. Initially, gradient echo images were acquired for lesion localization (1). Three slices containing normal tissue, DCIS, tumors and lymph nodes were then selected for measurements of T_1 (RARE with variable TR, 4 RARE partitions, TE=12.3 ms, FOV = 3.0×3.0, NEX=2, slice thickness= 1.00 mm, in plane resolution=234 microns), T_2 (spin SE with variable TE, TR/min TE=4000/14.1 ms, FOV=3.0×3.0 cm, NEX=1, slice thickness=1.00, in plane resolution 234 microns) and T_2* (MGE, variable TE, TR/min TE: 400/1.5ms, FOV=3.0×3.0 cm, NEX=1, slice thickness=1.00, in place resolution 234 microns). Signal intensity vs. time curves were generated for several regions of interest: ducts with DCIS, early invasive tumors, normal mammary tissue, and lymph nodes. To calculate T_2 and T_2*, the curves were fit to $S(t) = A_1 \exp(-t / A_2)$ and to test for biexponential decay $S(t) = A_1 \exp(-t / A_2) + A_3 \exp(-t / A_4)$; to calculate T_1 curves were fit to: $S(t) = A_1(1 - \exp(-t / A_2))$.

Results: The average relaxation parameters are displayed in Table 1 for DCIS, normal tissue, tumors and lymph nodes. Normal mammary tissue and DCIS displayed biexponential T_2 and T_2*decay (Figure 1), with short T_2* components: below 3.0 ms for DCIS and 1.0 ms for normal tissue, on average. In comparison, lymph nodes and early invasive tumors exhibited monoexponential decay, with longer T_2 and T_2* decay times. DCIS lesions were better appreciated on shorter TE images, at TE=1.5ms compared to TE=5.0 ms, in terms of morphology, size and signal-to-noise ratio.

ROI	T_1(ms)	T_2 (ms)	T_2* (ms)
DCIS (n=5)	649	36.7	2.4/11.7
Normal tissue (n=8)	1140	90.7	0.7/9.9
Tumor (n=5)	1331	36.5	12.1
Lymph node (n=8)	1480	41.3	11.7

Table 1: Average values of T_1, T_2 and T_2* in various regions of interest. For DCIS and normal tissue, the T_2* decay was bi-exponential, and both low and high T2* components are indicated.

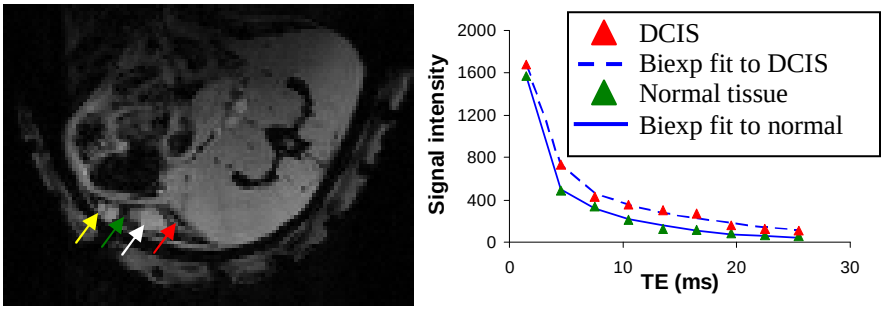

Figure 1: *Left*. Axial GE image demonstrating lymph node (white arrow), small tumor (yellow arrow), duct with DCIS (red arrow) and normal tissue (dark area, green arrow). *Right*. T_2* decay curves of normal tissue and demonstrating bi exponential decay and short T_2* components.

Discussion: These results represent the first direct measurements of the tissue relaxation parameters of early mammary cancer, including DCIS. We found that normal tissue and the earliest stage of breast cancer, DCIS, exhibited biexponential T_2 and T_2* decay, and short T_2* components. Furthermore, the lengthening of T_2* and the loss of biexponential decay accompanied tumorigogensis, and may be a predictive marker identifying when DCIS will progress. Due to the short T_2* components, shorter TE images allow for improved visualization of early cancer and normal tissue. Although further studies are needed in larger numbers of mice, these results do imply that imaging at shorter TE may allow for improved imaging of DCIS and improved characterization of normal breast parenchyma in women, even at lower field.

References: 1.Jansen SA, Conzen SD, Fan X, et al. Detection of in situ mammary cancer in a transgenic mouse model: in vitro and in vivo MRI studies demonstrate histopathologic correlation. Phys Med Biol 2008; 53:5481-5493.

Acknowledgements: We would like to thank the Segal Foundation and Florsheim Foundation for financial support.

2971

Magnetic resonance imaging reveals the progression, regression and indolence of *in situ* carcinoma in transgenic mice.

S. A. Jansen[1], S. Conzen[2], X. Fan[3], E. Markiewicz[3], G. Newstead[3], and G. Karczmar[1]

[1]University of Chicago, Chicago, IL, United States, [2]Medicine, University of Chicago, [3]University of Chicago

Introduction: The processes that trigger progression of preinvasive ductal carcinoma *in situ* (DCIS) to invasive breast cancer remain elusive[1]. Transgenic mouse models of cancer provide an experimental framework with which to begin to determine the key events in progression of breast cancer from DCIS to invasive disease. Because of the small size of *in situ* mammary cancers in mouse models, high-resolution imaging techniques are required to effectively observe how lesions develop, grow and progress over time. Heretofore, due to the challenge of detecting sub millimeter disease, there have been no imaging studies that could observe the trajectory of *in situ* to invasive cancer in mice. Here, we demonstrate that despite its sub-mm size, murine DCIS can be reliably detected by magnetic resonance imaging (MRI), which we use to track *in vivo* the transition of *in situ* to invasive cancer in transgenic mice.

Methods: A total of 24 C3(1) SV40 Tag mice, which develop mammary cancer similar to DCIS including progression to invasive tumors, were used. 12 mice were serially imaged with MRI every 2-3 weeks (FLASH TR/TE: 400/5.5, FOV = 3.0 x 3.0 cm, NEX =2, slice thickness=0.5mm, in-plane resolution =117 microns and flip angle=30)[2]. Another 12 mice were used for dynamic contrast enhanced MR imaging studies (FLASH TR/TE = 30/3.5 ms, slice thickness = 1.0 mm, in-plane resolution = 256 microns, flip angle=20°). The development and progression of DCIS lesions and early invasive tumors was followed, and several lesion features were measured, such as volume, growth rate, morphology, as well as the time to progression of DCIS to small invasive tumor. In addition, two-compartment physiologic model parameters K_{trans} and v_e (related to blood flow, capillary permeability and surface area, and extra-vascular extra-cellular space) were extracted.

Results: Overall, 31 DCIS and 18 invasive tumors were studied. Small invasive tumors demonstrated increased K_{trans} (0.36 ± 0.05 min^{-1}) compared with DCIS (0.21 ± 0.14 min^{-1}). Serial images of 16 DCIS lesions were obtained; these lesions developed at an average initial volume of 0.3 ± 0.2 mm^3 with an average growth rate of -0.15 ± 0.66 week^{-1} (Figure 1). Surprisingly, even in mice that are genetically predisposed to develop invasive carcinoma, these lesions took vastly different progression paths: (i) 9 lesions progressed to invasive tumors with an average progression time of 4.56 ± 1.9 weeks (ii) 5 were stable for over 8 weeks, and were identified by a statistical model to represent indolent disease, and (iii) 2 lesions *regressed*, i.e., the lesion was not detected on future images (Figure 2). Interestingly, larger DCIS volume was *not* a predictor of future progression to invasive tumors, but there was a trend for DCIS growth rate to be related to eventual development of invasiveness.

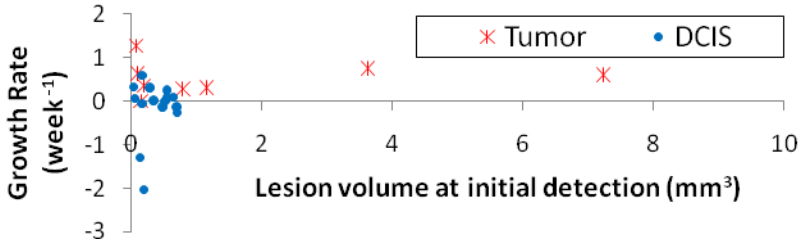

Figure 1: Scatter plot of growth rates and lesion volume at initial detection of DCIS and invasive tumors. Most DCIS lesions had growth rates near 0, and two demonstrated regression resulting in substantially negative growth rates. In contrast, all tumors exhibited positive growth rates. The initial volume of early cancers we have detected here is smaller than in any prior report.

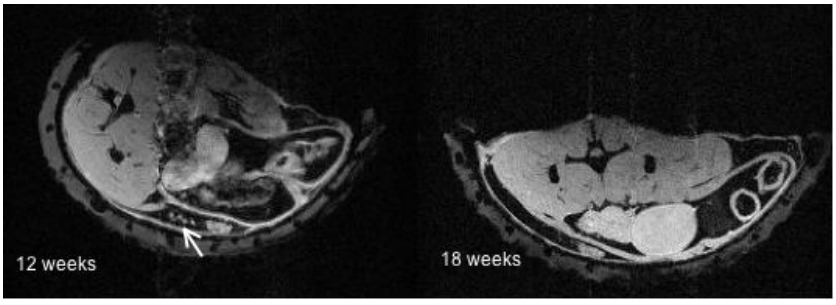

Figure 2: Example of DCIS regression. DCIS is visible at 12 weeks of age (left) beside lymph node (white arrow), but cannot be found six weeks later anywhere near the lymph node, on MR images or on histological specimens. Here, only one slice is shown demonstrating absence of a lesion near the lymph node (right). FOV is 3.0×2.0 cm, and in-plane resolution is 117 microns.

Conclusions: The results reported here are the first direct measurements of the timescales and characteristics of progression from *in situ* to invasive mammary carcinoma in mice, and provide direct evidence that DCIS may be a *non-obligate* precursor lesion. Small invasive cancers exhibited both increased vascularity and growth rates compared to preinvasive DCIS, suggesting that landmark events in disease progression, such as increased angiogenesis and disregulation of cellular growth, occur during the transition from *in situ* to invasive disease. We have presented a new foundation for using non-invasive real-time imaging in pre-clinical studies of *early* mammary cancer progression, in particular for testing the efficacy of preventative and interventional therapies for halting *in situ* disease progression.

References: 1. Erbas B, Provenzano E, Armes J, Gertig D. The natural history of ductal carcinoma in situ of the breast: a review. Breast Cancer Res Treat 2006; 97:135-144. 2. Jansen SA, Conzen SD, Fan X, et al. Detection of in situ mammary cancer in a transgenic mouse model: in vitro and in vivo MRI studies demonstrate histopathologic correlation. Phys Med Biol 2008; 53:5481-5493.

Acknowledgements: We would like to thank the Segal Foundation and the Florsheim Foundation for financial support.

2967

Kinetic curves of malignant lesions are not consistent across MR systems: The need for improved standardization of breast DCEMRI acquisitions.

S. A. Jansen[1], A. Shimauchi[2], L. Zak[2], X. Fan[2], A. Wood[2], G. Karczmar[2], and G. Newstead[2]
[1]University of Chicago, Chicago, IL, United States, [2]University of Chicago

Introduction: Standardization of breast MR image acquisition is not widespread at this time[1]. There are several manufacturers of MR systems, with different k-space sampling methods and coils. Furthermore, dynamic imaging protocols differ across institutions as to timing resolution, use of fat suppression, and pulse sequences. Unlike x-ray mammography, there are no universally applied quality assurance procedures to ensure comparable imaging performance among these different systems and protocols. At our institution, dynamic contrast enhanced MRI (DCEMRI) breast examinations have been performed on three different MR systems. The purpose was to compare the MR kinetic curve data of malignant lesions acquired by these systems.

Methods: 601 patients with 682 breast lesions (185 benign, 497 malignant) were selected for an IRB approved review. The malignant lesions were classified as ductal carcinoma in situ (DCIS), invasive ductal carcinoma (IDC) and 'other'. Dynamic MR protocol: 1 pre and 3-7 post-contrast T_1 weighted images, acquired using one of three imaging protocol and systems (IPS): IPS1 (1.5T GE Genesis Signa, 3D SPGR, TR/TE: 7.7/4.2ms, flip angle:30, resolution: 3.00mm thick, 1.4 mm in plane, temp res:68 sec), IPS2 (1.5T GE Signa Excite, 3D FGRE, TR/TE: 4.3/2.0ms, flip angle:10, resolution: 2.00mm thick, 0.82 mm in plane, temp res: 58 sec) and IPS3(1.5T Philips Achieva, 3D FFE, TR/TE: 7.9/3.9ms, flip angle:10, resolution: 2.00mm thick, 0.94 mm in plane, temp res: 55 sec). Analysis of kinetic curve shape was made by an experienced radiologist according to the BI-RADS lexicon. Several quantitative kinetic parameters were calculated, including the initial enhancement percentage (**E_1**), the peak enhancement percentage (**E_{peak}**), the time to peak enhancement (**T_{peak}**) and the signal enhancement ratio (**SER**, a measure of washout). The kinetic parameters of malignant lesions were compared between the three systems.

Results: 304 malignant lesions (185 IDC, 62 DCIS) were imaged on IPS1, 107 lesions (72 IDC, 21 DCIS) on IPS2, and 86 on IPS3 (64 IDC, 17 DCIS). Compared to both IPS1 and IPS2, IDC lesions (as well as malignant lesions overall) acquired on IPS3 demonstrated significantly lower initial enhancement, longer time to peak enhancement and slower washout rate (Table 1, $p < 0.0004$). Only 46% of IDC lesions imaged with IPS3 exhibited "washout" type curves, compared to 75% and 74% of those imaged with IPS2 and IPS1, respectively. The sensitivity and specificity kinetic analysis was lower for IPS3, but not significantly (Figure 1).

	Type of lesions	No. cases	E1(%)	Epeak(%)	T_{peak} (sec)	SER
IPS1	**All Malignant**	**304**	**286±158**	**330±155**	**165±105**	**1.07±0.48**
	IDC	185	313±151	352±149	144±98	1.15±0.50
IPS2	**All Malignant**	**107**	**245±214**	**301±213**	**178±126**	**0.94±0.32**
	IDC	72	264±236	319±232	160±96	0.97±0.33
IPS3	**All Malignant**	**86**	**122±281**	**213±356**	**211±100**	**0.57±0.33**
	IDC	64	125±309	223±401	203±91	0.56±0.26

Table 1: Average values of kinetic parameters E_1, E_{peak}, SER and T_{peak} in malignant lesions acquired with IPS1, IPS2 and IPS3. Compared to both IPS1 and IPS2, IDC lesions (as well as malignant lesions overall) acquired on IPS3 demonstrated significantly lower initial enhancement, longer time to peak enhancement and slower washout rate

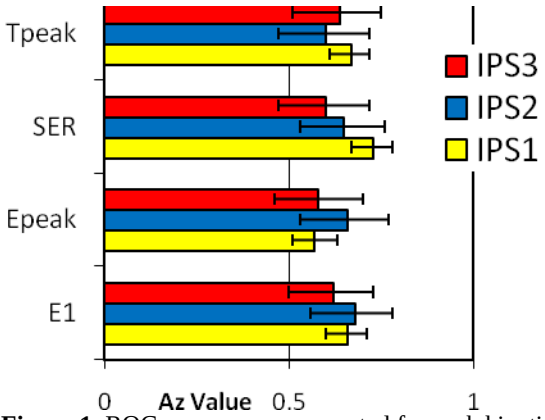

Figure 1: ROC curves were generated for each kinetic parameter E_1, E_{peak}, SER and T_{peak} for distinguishing benign from malignant lesions imaged on the IPS1, IPS2, or IPS3 systems. Area under the curve (A_z) values for the ROC curves are shown above, demonstrating decreased diagnostic performance for IPS3 imaged lesions.

Discussion: The kinetic curve data of malignant lesions acquired by one system exhibited significantly lower initial contrast uptake and different curve shape compared with the other two. These discrepancies in malignant lesion presentation adversely impacted the sensitivity and specificity of kinetic analysis. Differences in k-space sampling, T1 weighting or magnetization transfer effects may be possible explanations. This study underscores the importance of standardization of DCEMRI acquisition protocols, so that (i) malignant lesions are sufficiently conspicuous, and (ii) similar interpretation guidelines can be applied across all systems and protocols. Such standardization will be important if breast DCEMRI is to be used routinely in patient management.

References: 1. Kuhl C. The current status of breast MR imaging. Part I. Choice of technique, image interpretation, diagnostic accuracy, and transfer to clinical practice. Radiology 2007; 244:356-378.

Acknowledgements: We would like to thank the Segal foundation for financial support.

Acquisition of breast magnetic resonance images using different systems: How is the assessment of contrast media uptake and washout in malignant lesions affected?

Purpose: Dynamic contrast enhanced magnetic resonance imaging (DCEMRI) has demonstrated superior sensitivity for detecting earlier cancers compared with x-ray mammography, and is being used increasingly for high-risk screening, diagnostic imaging and to evaluate extent of malignant disease. When assessing lesion malignancy both the morphology and contrast uptake and washout—or kinetics—of the lesion are important. At our institution DCEMRI breast examinations have been performed on three different MR systems. The purpose of this study was to compare the MR kinetic curve data of malignant lesions acquired by these systems.

Methods: 445 patients with 485 malignant lesions were selected for an IRB approved review. The lesions were classified as ductal carcinoma in situ (DCIS), invasive ductal carcinoma (IDC) and 'other'. Dynamic MR protocol: 1 pre and 3-7 post-contrast images, acquired on a system using a non fat-suppressed dynamic sequence (NFS) and 2 newer systems by different manufacturers using fat suppressed dynamic sequences (FS1 and FS2). Kinetic curve data was processed and displayed on a CADstream workstation. Analysis of kinetic curve shape was made by an experienced radiologist according to the BI-RADS lexicon. Several quantitative kinetic parameters were calculated, both directly from the curve data and after fitting to an empirical mathematical model (EMM). The kinetic parameters of malignant lesions were compared between the three systems.

Results: 299 malignant lesions (185 IDC, 57 DCIS) were imaged on NFS, 104 lesions (69 IDC, 21 DCIS) on FS1, and 82 on FS2 (61 IDC, 17 DCIS). Compared to both systems NFS and FS1, IDC lesions acquired on FS2 demonstrated significantly lower initial enhancement, longer time to peak enhancement and slower washout rate ($p < 0.0004$). 80% of IDC lesions acquired on FS1 were classified as 'washout', compared with only 46% of IDC lesions on FS2. On both FS1 and FS2, we did not find a difference in the kinetic parameters of IDC vs. DCIS lesions. However, IDC lesions imaged on NFS exhibited significantly higher contrast uptake, shorter time to peak and stronger washout compared to DCIS lesions ($p < 0.0001$).

Conclusions: The kinetic curve data of malignant lesions acquired by one system exhibited significantly lower initial contrast uptake and different curve shape compared with the other two. In addition, on both newer systems, the kinetic parameters of DCIS were comparable with IDC, which is contrary to what was found on the older system. Differences in k-space sampling, T1 weighting or magnetization transfer effects may be possible explanations. The results of this study underscore the importance of developing standardized acquisition and analysis methods, to ensure that across all available systems (i) malignant lesions are sufficiently conspicuous and thus reliably detected and (ii) interpretation of kinetic data is consistent across systems.

In vivo magnetic resonance imaging to probe the development and progression of murine ductal carcinoma *in situ*

Sanaz A. Jansen[1] PhD, Suzanne D. Conzen[2] MD, Xiaobing Fan[1] PhD, Gillian M. Newstead[1] MD, Erica Markiewicz[1] BSc, Gregory S. Karczmar[1] PhD.
Department of [1]Radiology, [2]Hematology/Oncology, University of Chicago, Chicago IL 60637

Introduction

Transgenic mouse models of cancer provide an experimental framework with which to begin to determine the key events in progression of breast cancer from DCIS to invasive disease. Because of the small size of *in situ* mammary cancers in mouse models, high-resolution imaging techniques are required to effectively observe how lesions develop, grow and progress over time. Heretofore, due to the challenge of detecting sub millimeter disease, there have been no imaging studies that could observe the trajectory of *in situ* to invasive cancer in mice. Here, we demonstrate that despite its sub-mm size, murine DCIS can be reliably detected by magnetic resonance imaging (MRI), which we use to track *in vivo* the transition of *in situ* to invasive cancer in transgenic mice.

Materials and methods

Mice: A total of 24 C3(1) SV40 large T antigen mice were used: 12 for a sensitivity study, 12 for serial MR imaging every 2-3 weeks starting at 10 weeks of age. In this model, female mice develop spontaneous, orthotopic mammary cancer that resembles human ductal carcinoma, including progression through atypical ductal hyperplasia, DCIS and invasive ductal carcinoma (IDC).

MR imaging: Multi-slice axial gradient echo (GRE) images with fat suppression were acquired to localize lesions and follow their progression.

Mouse laying in MR imaging coil. Wrapped around the body of the mouse is an agar grid used for registration of images.

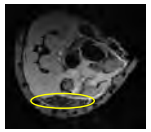

This MR image represents one axial slice through the mouse. The mammary gland is the dark region circles in yellow. This is a normal gland.

Results

MRI can detect murine DCIS. Twelve mice were imaged, then sacrificed and glands excised for sectioning and H&E staining. After correlation with histology, we determined that MRI was able to detect 13/16 ducts distended with DCIS. An example is shown in Figure 1.

What is the natural history of DCIS in SV40 Tag mice? Twelve other mice were imaged serially every 2-3 weeks with MRI. A total of 21 DCIS lesions developed, and the future progression paths of 16 of these lesions were studied with MRI, yielding three outcomes:

Figure 1: On the right is an example of *in vivo* axial MR image (FLASH GE with fat suppression) and corresponding H&E stained section showing DCIS. Each axial MR image represents one cross-sectional slice through the mammary gland. We used an agar grid (a polyethylene mesh embedded in partially deuterated agar) to register the axial MR images with the H&E stained sections. A lymph node (green arrow) and DCIS (yellow arrow) are clearly visible. For the MR image, the display field of view is 3.0 × 2.0 cm.

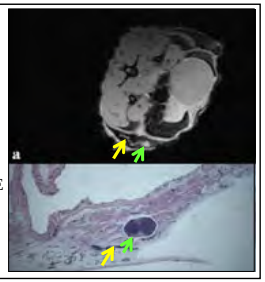

1. DCIS *progression* to invasive carcinoma: 9/16 DCIS lesions progressed to invasive carcinoma. Below is an example: DCIS (yellow arrow) develops at 10 weeks, and in this axial MR image appears in cross section (tiny white dot). By 16 weeks the DCIS lesions has transformed into invasive cancer (thick arrow). At 20 weeks the tumor has grown larger, and *new* DCIS has developed around the tumor.

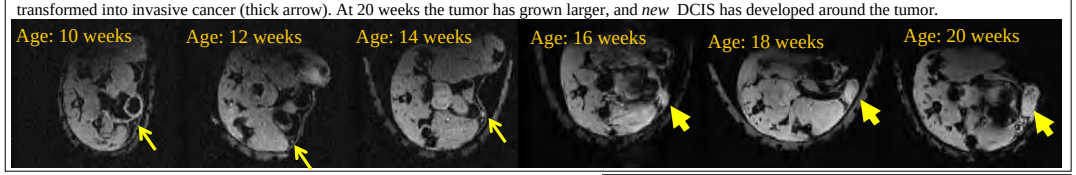

2. DCIS *indolence*: 5/16 DCIS lesions did not progress to invasive carcinoma. Below is an example. DCIS (yellow arrow) has developed at 10 weeks and does not progress to invasive cancer.

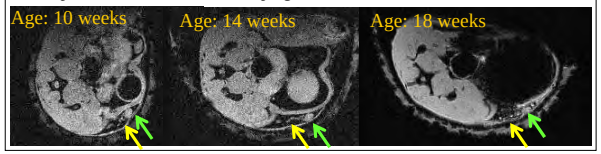

3. DCIS *regression*: 2/16 DCIS lesions regressed. Below is an example. DCIS (yellow arrow) is visible at 12 weeks of age (left) beside lymph node (green arrow), but cannot be found six weeks later anywhere near the lymph node. Here, only one slice is shown demonstrating absence of a lesion near the lymph node (right).

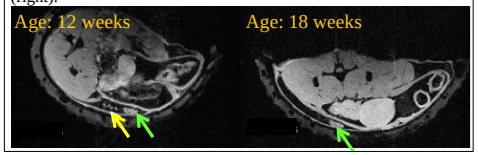

Conclusions

To our knowledge, the results reported here are the first *direct* measurements of the timescales and characteristics of progression from *in situ* to invasive carcinoma. Our results also contribute some new interesting observations regarding SV40 Tag mice:

- Surprisingly, even in these in transgenic mice that are strongly pre-disposed to develop cancer, some DCIS lesions did *not* progress to invasive cancer. This suggests that at least a second transformational event is required for cancer progression, beyond expression of Tag.
- Lesion volume was not a predictor of future progression, but there was a trend for growth rate to be related to future progression.

The methods and data here provide a foundation for using MRI in pre-clinical studies of early cancer progression, prevention and targeted treatment.

Literature cited

1. Jansen SA, Conzen S, Fan X, et al. Detection of in situ mammary cancer in a transgenic mouse model: in vitro and in vivo MRI studies demonstrate histopathologic correlation. Phys Med Biol 2008; 53:5481-93.
2. Green J E, Shibata M A, Yoshidome K, Liu M L, Jorcyk C, Anver M R, Wigginton J, Wiltrout R, Shibata E, Kaczmarczyk S, Wang W, Liu Z Y, Calvo A and Couldrey C 2000 The C3(1)/SV40 T-antigen transgenic mouse model of mammary cancer: ductal epithelial cell targeting with multistage progression to carcinoma *Oncogene* **19** 1020-7

Acknowledgments

We would like to thank the Segal Foundation , the Florsheim Foundation, the University of Chicago Cancer Research Center and the Department of Defense for financial support.

For further information

Please contact sajansen@uchicago.edu. More information on this and other projects can be found at *mris.uchicago.edu.*

Why does ductal carcinoma *in situ* enhance on dynamic contrast enhanced MR imaging of the breast?

SA Jansen, T Paunesku, GE Woloschak, S Vogt, SD Conzen, EJ Markiewicz, GM Newstead, and GS Karczmar

Purpose: The mechanism for contrast enhancement of ductal carcinoma in situ (DCIS) breast lesions—which represent neoplastic cells that are still confined within the mammary ducts—on dynamic contrast enhancement MR imaging (DCEMRI) is not well understood, and is often modeled as a 2 compartment physiologic model. The purpose of this study was tox-ray fluorescence microscopy (XFM) of transgenic mouse models of breast cancer to identify the spatial distribution of Gd following IV injection in mouse mammary glands with DCIS.

Methods: Fourteen C3(1) Sv40 Tag female transgenic mice, which develop mammary cancer similar to DCIS, were selected for XFM following institutional approval. Mice were injected with 0.1 mM/kg Gd-DTPA, sacrificed after 2 minutes, and mammary glands were excised. Frozen sections containing lymph nodes, ducts distended with DCIS, and nearby blood vessels were prepared for XFM at the 2-ID XOR CAT at the Advanced Photon Source at Argonne National Laboratory. Elemental concentrations of Gd, and lighter elements between phosphorus (P) and zinc (Zn) in the periodic table were determined in regions of interest in the ducts, lymph nodes and blood vessels.

Results: XFM verified that Gd-DTPA was present in lymph nodes, blood vessels, small tumors, as well as in portions of mammary ducts distended with DCIS. The average concentration of Gd in the ducts distended with DCIS was 0.045 $\mu g/cm^2$, and in blood vessels was 0.063 $\mu g/cm^2$. As expected, Fe was also found in blood vessels, but not in ducts distended with DCIS.

Conclusion: Our results provide an important new insight into the mechanism of contrast enhancement of DCIS lesions on DCEMRI: Gd-DTPA can leave blood vessels to enter ducts distended with DCIS. These ducts may have leaky basement membranes allowing gadolinium to diffuse inside. This observation suggests that two compartment pharmacokinetic models may be invalid for DCIS lesions, as they ignore exchange of contrast with the mammary duct distended with DCIS (representing a 3^{rd} compartment).

Clinical significance: Understanding the uptake of Gd in mammary ducts may lead to improvements in imaging methods, mathematical modeling of kinetic data and interpretation of DCEMRI.

CBC 2008 Abstract Submission Template

Title:	**Tracking the distribution of gadolinium in early murine breast cancer with x-ray fluorescence microscopy and dynamic contrast enhanced MRI.**
Author(s):	Sanaz A. Jansen PhD[1], Tatjana Paunesku PhD[2], Gayle E Woloschak PhD[2], Stefan Vogt PhD[3], Suzanne D Conzen MD[4], Thomas Krausz MD[5], Xiaobing Fan PhD[1], Gillian M Newstead MD[1], and Gregory S Karczmar PhD[1].
Address:	[1] University of Chicago, Department of Radiology [2] Northwestern University, Department of Radiology, Department of Radiation Oncology [3] Argonne National Labs, X-ray Sciences Division [4] University of Chicago, Department of Hematology/Oncology [5] University of Chicago, Department of Pathology

Purpose: Ductal carcinoma *in situ* is a non-obligate precursor to invasive breast cancer in which cancer cells are still confined by the basement membrane of mammary ducts. Improving the targeted detection and treatment of DCIS, particularly those aggressive lesions that will rapidly turn invasive, is highly desirable to improve patient outcomes. Although dynamic contrast enhanced MR imaging (DCEMRI) can detect some DCIS lesions after injection of a gadolinium (Gd) chelate, the underlying physiological basis of Gd uptake is not clear. Our purpose was to use *ex vivo* x-ray fluorescence microscopy (XFM) and *in vivo* DCEMRI of transgenic mice to identify the spatial distribution of Gd following IV injection in mouse mammary glands with DCIS.

Methods:11 C3(1) Sv40 Tag transgenic mice, which develop mammary cancer similar to DCIS, were injected with Gd-DTPA, sacrificed after 2 minutes, and frozen sections containing ducts distended with DCIS were prepared for XFM at the Advanced Photon Source at Argonne National Laboratory. Elemental concentrations of Gd were determined in and around the ducts with DCIS. 12 additional mice were imaged with *in vivo* DCEMRI after injection of Gd-DTPA, and Gd concentration vs. time curves were obtained and fit to a two-compartment pharmacokinetic model(with parameters K_{trans} , v_e).

Results: DCEMRI demonstrated contrast uptake along the length of ducts with DCIS, with average $K_{trans}=0.21\pm0.14(min^{-1})$ and $v_e=0.40\pm0.16$. Interestingly, XFM demonstrated Gd uptake ***inside*** ducts with DCIS and accumulation within the duct lumen, with an average concentration of 0.475±0.380mM which is comparable to the *in vivo* DCEMRI value of 0.30±0.13mM.

Conclusion: Our results provide an important new insight into the mechanism of contrast enhancement of DCIS lesions on DCEMRI: leaky basement membranes of DCIS allow Gd diffusion into the ducts and collection in the lumen. This study provides baseline *in vivo* and *ex vivo* measurements of Gd-DTPA distribution on which targeted agents can be evaluated. Understanding the uptake of Gd in mammary ducts may lead to improvements in imaging methods, mathematical modeling of kinetic data and interpretation of DCEMRI.

Detection and Evaluation of Early Breast Cancer via Magnetic Resonance Imaging: Studies of Mouse Models and Clinical Implementation

Background and objectives

The early detection of breast cancer is a major prognostic factor in the management of the disease. In particular, detecting breast cancer in its pre-invasive form as ductal carcinoma *in situ* (DCIS) improves prognosis greatly compared with invasive tumors. However, because the natural history of DCIS is not well understood there is a clinical concern that DCIS may be overdiagnosed and overtreated. The goals of this project are to: (1) characterize the MR kinetic and morphologic findings of DCIS in women and compare with benign lesions and other malignant cancers, (2) develop techniques to detect early mammary cancer in mice, and (3) study the development and progression of early mammary cancer in mice by performing longitudinal MRI studies of development of DCIS and transition to invasive cancer.

Brief description of methodologies:

Clinical studies: The contrast media uptake and washout curves were mathematically analyzed. We analyzed the kinetic characteristics of 79 pure DCIS lesions by nuclear grade and mammographic presentation, and also compared the kinetic characteristics of DCIS with other malignant and benign lesions.
Murine studies: Twelve SV40 TAg transgenic mice were selected for imaging to determine whether MRI of early cancer, including DCIS, was feasible. MR images were compared with histopathology. To study the progression of DCIS, eight mice were selected for serial imaging every 2 weeks from ages 12-18 weeks.

Results to date:

Clinical studies: The variable kinetic characteristics of pure DCIS lesions were associated with mammographic presentation, but not nuclear grade. Invasive cancers exhibited significantly larger contrast uptake and stronger washout compared with DCIS lesions, which in turn showed considerable overlap with benign lesions.
Murine studies: MR images were able to detect 17/18 small (~1mm) tumors, and 13/16 ducts distended with DCIS greater than 300 microns in diameter (Figure 1). DCIS lesions developed at an average age of 14.5 weeks of age, and small tumors developed at an average age of 17.3 weeks. 4 of 8 mice not progress from DCIS to invasive cancer within the study period.

Conclusions, including the potential impact on breast cancer research and/or treatment

To our knowledge, this is the first demonstration that MRI can detect early murine mammary cancers, including DCIS, *in vivo*. We found that some DCIS lesions did not progress significantly during the study window, illustrating that this mouse model offers the opportunity to identify and influence factors that predict and affect DCIS progression. With the results presented here, MR imaging could be used to assess efficacy of therapies on cancers at all stages of disease (*in situ*, early and advanced), rather than only the

advanced, palpable tumors that are typically used in current murine therapy trials. In addition, the methods that prove optimal for image acquisition and analysis in early murine cancers can be adapted for use in humans in order to improve the accurate detection of early breast cancer.

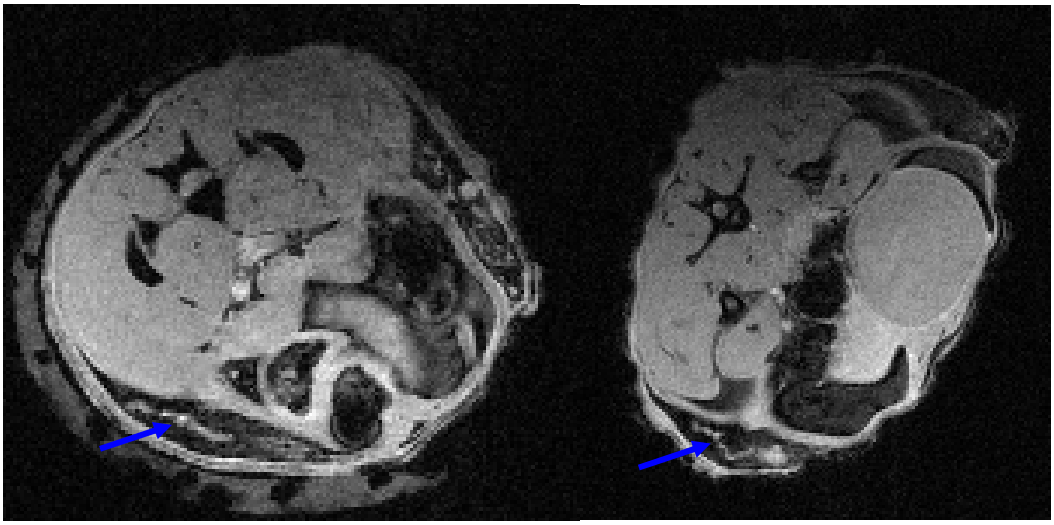

Parenchymal Enhancement on Breast MRI May be a Marker for Cancer Risk: Correlation of Parenchymal Enhancement with Breast Density

S. Arkani MSc, G. Newstead MD, V. Chen MD, C Cranford MD, L Zak, H Abe MD, G Karczmar MD, R Schmidt MD, O Olopade MD.
University of Chicago

Abstract

Purpose: To classify the parenchymal enhancement pattern at MR imaging and to correlate with breast density.

Methods: The study population consisted of 185 asymptomatic women who were imaged with a 3D bilateral dynamic MR sequence. Breast density was classified independently by one reader on digital x-ray mammograms according to the BI-RADS categories: 1=almost entirely fat, 2= scattered fibroglandular tissue, 3=heterogeneously dense, 4=extremely dense. The MR parenchymal pattern of enhancement for each case was classified by one reader as minimal, homogeneous, heterogeneous or nodular. Parenchymal signal intensity vs. time curves were generated by manually tracing a region of interest around the total parenchyma visible in a selected pre-contrast coronal slice. The peak magnitude of parenchymal enhancement relative to the pre-contrast signal intensity E_{peak}[%] was measured.

Results: The average E_{peak} was 45 4% overall. 60% of breasts with scattered fibroglandular tissue show minimal parenchymal enhancement while 25% show heterogeneous or nodular patterns. Conversely, 36 % of heterogeneously or extremely dense breasts show minimal enhancement. The average E_{peak} was 51% for heterogeneously and extremely dense breasts and 36% for breasts with scattered fibroglandular tissue.

Conclusions: A statistically significant correlation between breast density and magnitude (E_{peak}) and pattern (heterogeneous and nodular) of parenchymal enhancement was found ($p < 0.01$). Although further study is needed, this observation might lead to an improved reproducible quantification method of assessing breast cancer risk based on breast enhancement patterns.

Background

Parenchymal enhancement refers to the enhancement of normal breast tissue on dynamic contrast enhanced MRI, as shown below.

Parenchyma is dark on pre-contrast **Enhancement seen at 6 minutes**

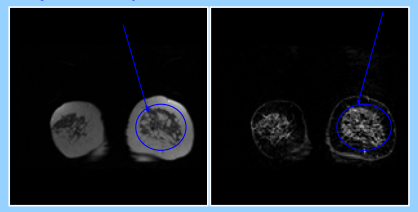

Parenchymal enhancement has not, as yet, been very well characterized. In prior studies of small numbers of patients (20-50), parenchymal enhancement has been shown to be greater in women who are between 35-50 years old[1], in weeks 1 and 4 of the menstrual cycle[2] and in women on hormone replacement therapy (HRT)[3]. Our goal here is to characterize the pattern and magnitude of parenchymal enhancement in a large group of asymptomatic women, and investigate the relationship of parenchymal enhancement with breast density.

Objective

a. To classify the parenchymal enhancement pattern and kinetics in a large group of asymptomatic women.

b. To explore the relationship between parenchymal enhancement and breast density, menopausal status, HRT and personal history of breast cancer.

Quantitative Measure of Parenchymal Enhancement Pattern (PEP): A classification system developed by Dr. Newstead that classifies the enhancement viewed on coronal slices as minimal, homogeneous, heterogeneous or nodular. Examples are shown below.

Minimal PEP **Homogeneous PEP**

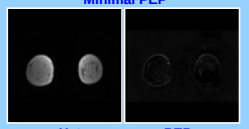

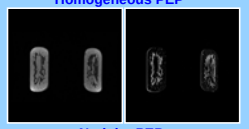

Heterogeneous PEP **Nodular PEP**

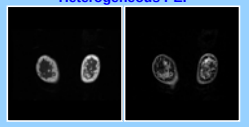

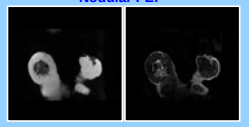

Quantitative Measure: We measure the magnitude of the parenchymal enhancement, $\mathbf{E_{peak}}$, by first tracing out the parenchyma on the pre-contrast image, as shown on the left. The kinetic curve on the right represents the signal intensity vs. time in the selected region.

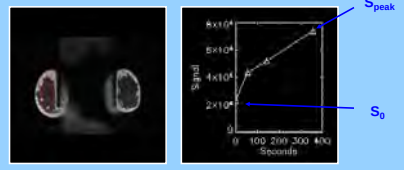

Peak Enhancement Percentage $E_{peak}=100 \times (S_{peak}-S_0)/S_0$

The more the curve rises, the larger E_{peak}

Materials & Methods

Patients: 185 patients selected in an IRB approved retrospective review. Average age 54 yr, range 20-84 yr. All have normal MRI.

Imaging: The dynamic MR protocol used was 1 pre and 5 post contrast T_1 weighted SPGR, 68 second time resolution, coronal plane. Digital mammograms acquired on GE Senograph 2000D.

Image Analysis: Breast density was classified on mammograms by one reader according to BI-RADS lexicon: 1=almost entirely fat, 2=scattered fibroglandular tissue, 3=heterogeneously dense and 4=extremely dense. MR PEP was assessed by one reader on 6 minute post contrast coronal images. The peak enhancement percentage $\mathbf{E_{peak}}$ was measured as shown above.

Statistical Analysis: The PEP, $\mathbf{E_{peak}}$ and breast density was determined for all cases. The population was then analyzed by menopausal status (postmenopausal n=111 and premenopausal n=74), by personal history of breast cancer status (with history n=55 and without history n=130) and HRT status in the postmenopausal group (on HRT =21 and not on HRT n=90). To test the significance of the distributions of PEP between these groups, the χ^2 test was used, with a p value < 0.05 indicating statistical significance.

Results

The overall distribution of PEP and breast density is shown below. The average $\mathbf{E_{peak}}$ was 45 4%. 58% of postmenopausal women showed minimal PEP, compared with only 30% of premenopausal women ($p<0.001$). There was no statistically significant difference in PEP or $\mathbf{E_{peak}}$ distribution based on personal history or HRT status.

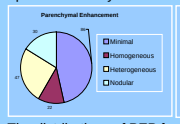

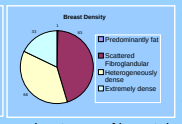

The average E_{peak} was 51% for heterogeneously and extremely dense breasts and 36% for breasts with scattered fibroglandular tissue.

The distributions of PEP for each category of breast density are shown on the left below. This graph implies that heterogeneously and extremely dense breasts are more likely to exhibit heterogeneous or nodular PEP ($p<0.001$). Similarly, the distributions of breast density for each category of PEP are shown on the right, demonstrating that breasts with heterogeneous and particularly nodular PEP are more likely heterogeneously or extremely dense ($p<0.001$).

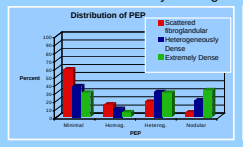

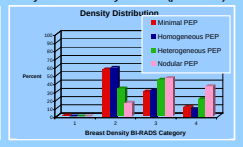

Discussion

We have presented a new classification system of parenchymal enhancement pattern (PEP) and documented the PEP and magnitude of enhancement (E_{peak}) in a group of 185 asymptomatic women. We have found that PEP and E_{peak} does not depend on having a personal history of breast cancer, nor does it change for women who are on HRT. Premenopausal women were more likely to exhibit heterogeneous or nodular PEP, than postmenopausal women. In addition, breasts with heterogeneous or nodular enhancement,and a larger E_{peak},are likely to be heterogeneously or extremely dense .

In some sense, these results aren't very surprising: the more dense the breast, the more capacity there is for heterogeneous or nodular enhancement. But it is perhaps the converse that is more interesting: 40% of breasts with only scattered fibroglandular tissue show non-minimal PEP, and 30% of extremely dense breasts show minimal enhancement, as shown below.

Dense breast with minimal parenchymal enhancement

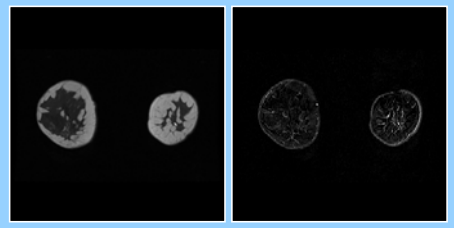

Increased breast density has been linked to an increased risk for breast cancer [4]. These results point to the possibility that parenchymal enhancement may provide a refined measure of breast cancer risk. This possibility has a physiological motivation: higher estrogen levels are a leading candidate theory for parenchymal enhancement and increased estrogen levels have also been linked to an increased risk for cancer[5]. These preliminary results may form the basis for a more detailed prospective study of the correlation of parenchymal enhancement and risk for breast cancer.

References

1. Effect of age and menstrual cycle on mammography and MR mammography, *Radiologe*
2. Healthy premenopausal breast parenchyma in dynamic contrast enhanced MR imaging of the breast: normal contrast medium enhancement and cyclical-phase dependency, *Radiology*
3. Hormone replacement therapy in postmenopausal women: breast tissue perfusion determined with MR imaging--initial observations, *Radiology*
4. Heritability of mammographic density, a risk factor for breast cancer, *New England Journal of Medicine*
5. The local hormonal environment and related biomarkers in the normal breast, *Endocr Relat Cancer.*

Printed by

Sanaz (Sunny) Arkani Jansen

CONTACT INFORMATION

Department of Radiology
Committee on Medical Physics
5841 S. Maryland Ave MC 2026
University of Chicago
Chicago, IL 60637 USA

Voice: (773) 834-8008
E-mail: sajansen@uchicago.edu
Website: http://home.uchicago.edu/~sarkani

RESEARCH INTERESTS

Imaging of ductal carcinoma *in situ* in women and mouse models of breast cancer towards improving detection of early breast cancer and understanding of tumorigenesis.

EDUCATION

University of Chicago, Chicago, Illinois USA

Ph.D. Medical Physics, 2008

- Thesis: Magnetic resonance imaging of ductal carcinoma *in situ* and early breast cancer
- Advisors: Gregory Karczmar and Gillian Newstead

M.S., Physics, 2003

University of Toronto, Toronto, Ontario Canada

B.Sc., Mathematics and Physics, 2001

PROFESSIONAL & ACADEMIC EXPERIENCE

University of Chicago, Chicago, Illinois USA

Postdoctoral Scholar **January 2009-present**

Graduate Student and Research Assistant (Medical Physics) **September 2004 - December 2008**
Includes Ph.D. research and graduate course work in medical physics.

Research Associate (Radiology) **January 2004 -August 2004**
Includes research under the supervision of Dr. Gillian Newstead and work on developing a clinical database of breast MRI examinations since 2002.

Graduate Student and Teaching Assistant (Physics) **September 2001 - December 2003**
Includes graduate course work and research in the department of Physics. Teaching assistant for five physics courses, duties included discussion section/lab leading, assignment preparation, grading, and tutoring.

University of Toronto, Toronto, Ontario Canada

Research Assistant **May 1999 - August 2001**
Summer research in the departments of mathematics and physics, using statistical methods to model mixing boundries of ozone in the stratosphere.

Teaching Course in Mammography Austin, TX USA
Finding Cancer in its Early Stages , Faculty: Laszlo Tabar, Ward Parsons, Ed Hendrick **October 2007**

HONORS AND AWARDS

Trainee Research Prize:
Radiological Society of North America (RSNA) 2006 and 2007

Department of Defense Breast Cancer Predoctoral Award:
Detection and Evaluation of Early Breast Cancer via Magnetic Resonance Imaging: Studies of Mouse Models and Clinical Implementation 2005-2008

Student Travel Stipend:
International Society for Magnetic Resonance in Medicine 2005, 2007 and 2008

University of Chicago:
Deans Fellowship Biological Sciences Division 2004

Carl J. Vyborny Award 2007

National Sciences and Engineering Research Council (NSERC):
Postgraduate Scholarship 2001

Undergraduate Student Research Award 1999, 2000 and 2001

University of Toronto:
Prince of Wales Award

3T0 M&P Associates Scholarship 1998 and 1999

University of Toronto Scholar 1998

Trinity College Chancellor Scholarship 1998-2001

RESEARCH SKILLS

Computer Languages: C, IDL, Matlab
Computer Applications: MS Office, Filemaker Pro
Animal work: Physiological monitoring set up, tail veins, dissections
Pahthology techniques: Microscopy, cryosectioning

PUBLICATIONS

1. Xiaobing Fan, Hiroyuki Abe, Milica Medved, Sean Foxley, Sanaz Arkani, Marta Zamora, Olopade OI, Gillian M Newstead, Gregory Karczmar. "Fat suppression with spectrally selective inversion vs. high spectral and spatial resolution MRI of breast lesions: qualitative and quantitative comparisons." J Magn Reson Imaging. 2006 Dec;24(6):1311-5.
2. Xiaobing Fan, Milica Medved, Gregory S. Karczmar Cheng Yang, Sean Foxley, Sanaz Arkani, Wendy Recant, Marta A. Zamora, Hiroyuki Abe, Gillian M. Newstead. "Diagnosis of suspicious breast lesions using an empirical mathematical model for dynamic contrast-enhanced MRI." J Magn Reson Imaging. 2007 25:593-603.
3. Sanaz A. Jansen, Hiroyuki Abe, Akiko Shimauchi, Gregory Karczmar, Robert Schmidt, Gillian Newsteadi. "Pure ductal carcinoma in situ: kinetic and morphologic MR characteristics compared with mammographic appearance and nuclear grade." Radiology. 2007 Dec;245(3):684-91.
4. Sanaz A. Jansen, Xiaobing Fan, Gregory S. Karczmar, Hiroyuki Abe, Robert A. Schmidt, and Gillian M. Newstead. "Differentiation between benign and malignant breast lesions detected by bilateral dynamic contrast enhanced MRI: A sensitivity and specificity study." Magnetic Resonance in Medicine. 2008 Apr; 59(4):747-54.
5. Sanaz A. Jansen, Xiaobing Fan, Gregory S. Karczmar, Hiroyuki Abe, Robert A. Schmidt, Maryellen Giger and Gillian M. Newstead."DCEMRI of breast lesions: Is kinetic analysis equally effective for both mass and non-mass-like enhancement?" Medical Physics. 2008 July;35(7):3102-3109.
6. Sean Foxley, Xiaobing Fan, Sanaz A. Jansen, Marta Zamora, Erica Markiewicz, Hikmat Al-Ahmadie and Gregory S. Karczmar. "High spectral and spatial resolution MRI of age related changes in murine prostate." Magnetic Resonance in Medicine. 2008 Sep; 60(3):575-81.
7. Sanaz A. Jansen, Suzanne Conzen, Xiaobing Fan, Thomas Krausz, Marta Zamora, Sean Foxley, Jonathan River, Gillian Newstead and Gregory Karczmar. "Detection of *in situ* mammary cancer in a transgenic mouse model:*in vitro* and *in vivo* MRI studies demonstrate histopathologic correlation." Physics in Medicine and Biology. 2008 Oct 7; 53(19): 5481-93.
8. Hui Li, Maryellen Giger, Yading Yuan, Weijie Chen, Li Lan, Anrew R. Jamieson, Charlene Sennett, Sanaz A. Jansen. "Evaluation of Coupter-aided Diagnosis on a Large Clinical Full-Field Digital Mammographic

Dataset." Academic Radiology. 2008 Nov; 15(11): 1437-45.

9. Sanaz A. Jansen, Tatjana Paunesku, Xiaobing Fan, Gayle E Woloschak, Stefan Vogt, Erica J Markiewicz, Suzanne D Conzen, Gillian M Newstead and Gregory S Karczmar. "X-Ray fluorescence microscopy and DCEMRI of murine ductal carcinoma *in situ* reveals gadolinium uptake within neoplastic mammary ducts." (in revisions, *Radiology*)
10. Sanaz A. Jansen, Akiko Shimacuhi, Lindsay Zak, Xiaobing Fan, Abbie M. Wood, Gregory Karczmar and Gillian M Newstead. "Kinetic curves of malignant lesions are not consistent across MR systems: The need for improved standardization of DCEMRI acquisitions of the breast" (in press, *American Journal of Roentgenology*)
11. Sanaz A. Jansen, Akiko Shimauchi, Lindsay Zak, Xiaobing Fan, Gregory Karczmar and Gillian Newstead. "Kinetic and pathologic findings of 457 breast lesions presenting as focus, mass and nonmass-like enhancement at MR imaging."(submitted, *American Journal of Roentgenology*)
12. Sanaz A. Jansen, Suzanne Conzen, Xiaobing Fan, Erica Markiewicz, Gillian Newstead and Gregory Karczmar. "Magnetic resonance imaging reveals the progression, regression and indolence of ductal carcinoma *in situ* in transgenic mice."(submitted, *Breast Cancer Research*)
13. Sanaz A. Jansen, Cheng Yang, Akiko Shimauchi, Lindsay Zak, Gregory Karczmar and Gillian Newstead. "Relating dose of contrast media administered to uptake and washout of malignant lesions on DCEMRI of the breast".(submitted, *Academic Radiology*)

FIRST AUTHOR ABSTRACTS

1. Sanaz A. Jansen, Xiaobing Fan, Erica Markiewicz, Gillian Newstead and Gregory S. Karczmar. "Short T2* components in the normal murine mammary gland and pre-invasive carcinoma may aid in detection of early breast cancer." in 17th Annual Meeting of the Society for Magnetic Resonance in Medicine, April 2009.
2. Sanaz A. Jansen, Suzanne D. Conzen, Xiaobing Fan, Erica Markiewicz, Gillian Newstead and Gregory S. Karczmar. "Magnetic resonance imaging reveals the progression, regression and indolence of in situ carcinoma in transgenic mice." in 17th Annual Meeting of the Society for Magnetic Resonance in Medicine, April 2009.
3. Sanaz A. Jansen, Akiko Shimauchi, Lindsay Zak, Xiaobing Fan, Abbie M. Wood, Gregory S. Karczmar and Gillian M. Newstead. "Kinetic curves of malignant lesions are not consistent across MR systems: The need for improved standardization of breast DCEMRI acquisitions." in 17th Annual Meeting of the Society for Magnetic Resonance in Medicine, April 2009.
4. Sanaz A. Jansen, Akiko Shimauchi, Lindsay Zak, Xiaobing Fan, Gregory S. Karczmar and Gillian M. Newstead. "Different MR systems yield variable kinetic characteristics of breast lesions." in 31st Annual San Antonio Breast Cancer Symposium, December 2008.
5. Sanaz A. Jansen, Suzanne Conzen, Xiaobing Fan, Gillian M. Newstead, Erica J Markiewicz and Gregory S. Karczmar. "In vivo magnetic resonance imaging of the progression of murine ductal carcinoma in situ: finding timescales and predictors of future invasion." in 31st Annual San Antonio Breast Cancer Symposium, December 2008.
6. Sanaz A. Jansen, Tatjana Paunesku, Xiaobing Fan, Gayle Woloschak, Stefan Vogt, Erica J Markiewicz, Suzanne Conzen, Gillian M. Newstead and Gregory S. Karczmar. "Why does Ductal Carcinoma in situ Enhance on Dynamic Contrast Enhanced MR Imaging of the Breast?" in 94th Annual Meeting of the Radiologic Society of North America, November 2008.
7. Sanaz A. Jansen, Tatjana Paunesku, Xiaobing Fan, Gayle Woloschak, Stefan Vogt, Erica J Marikiewicz, Suzanne Conzen, Gillian M. Newstead and Gregory S. Karczmar. "Tracking the distribution of gadolinium in early murine breast cancer with x-ray fluorescence microscopy and dynamic contrast enhanced MRI" in Frontiers of Molecular Imaging, Meeting of the Chicago Biomedical Consortium, October 2008.
8. Sanaz A. Jansen. "Detection and Evaluation of Early Breast Cancer via Magnetic Resonance Imaging: Studies of Mouse Models and Clinical Implementation." in DOD BCRP Era of Hope Meeting, June 2008.

9. Sanaz A. Jansen, Tatjana Paunesku, Xiaobing Fan, Gayle Woloschak, Stefan Vogt, Erica J Markiewicz, Suzanne Conzen, Gillian M. Newstead and Gregory S. Karczmar. "Why do Ductal Carcinoma in situ Lesions Enhance on Dynamic Contrast Enhance MRI of the Breast? Using X-Ray Fluorescence and MRI to Track the Spatial Distribution of Gd-DTPA in Murine DCIS." in 16th Annual Meeting of the Society for Magnetic Resonance in Medicine, May 2008.

10. Sanaz A. Jansen, Suzanne D. Conzen, Xiaobing Fan, Erica J Markiewicz, Thomas Krausz, Gillian Newstead and Gregory Karczmar. "Do all in situ cancers progress to invasive disease? A first look at progression of mammary cancer from in situ to invasive carcinoma in vivo." in 16th Annual Meeting of the Society for Magnetic Resonance in Medicine, May 2008.

11. Sanaz A. Jansen, Xiaobing Fan, Gregory Karczmar, Maryellen Giger, Hiroyuki Abe and Gillian M. Newstead. "Are Kinetic Parameters Diagnostically Useful for Breast Lesions Exhibiting Nonmass-like-Enhancement?" in 16th Annual Meeting of the Society for Magnetic Resonance in Medicine, May 2008.

12. Sanaz A. Jansen, Gregory Karczmar, Akiko Shimauchi, Hiroyuki Abe and Gillian M. Newstead. "Are Kinetic Parameters Related to Prognostic Indicators in ¡2.0 cm Invasive Ductal Carcinomas?" in 16th Annual Meeting of the Society for Magnetic Resonance in Medicine, May 2008.

13. Sanaz A. Jansen, Xiaobing Fan, Gregory S. Karczmar, Hiroyuki Abe, Akiko Shimauchi and Gillian M Newstead. "Non-mass vs. mass-like enhancement: Which kinetic parameters distinguish benign and malignant breast lesions?" in108th Annual Meeting of the American Roentgen Ray Society, April 2008.

14. Sanaz A. Jansen, Akiko Shimauchi, Hiroyuki Abe, Gregory S. Karczmar and Gillian M Newstead. "The kinetic and morphologic characteristics of mammographically occult, MR visible breast cancers: How different are the extra cancers found at MR imaging?" in 108th Annual Meeting of the American Roentgen Ray Society, April 2008.

15. Sanaz A Jansen, Suzanne Conzen, Marta Zamora, Thomas Krausz, Gillian M Newstead and Gregory S Karczmar. "A new approach to studying the progression of breast cancer in mice: High resolution MRI of early cancer and DCIS." in 30th Annual San Antonio Breast Cancer Symposium, December 2007.

16. Sanaz A Jansen, Hiroyuki Abe, Akiko Shimauchi, Gregory S Karczmar and Gillian M Newstead. "How does ER/PR and Her2/Neu status affect the MR characteristics of invasive ductal carcinoma?" in 30th Annual San Antonio Breast Cancer Symposium, December 2007.

17. Sanaz A Jansen, Hiroyuki Abe, Akiko Shimauchi, Gregory S Karczmar, Olufunmilayo Olopade, Lindsay Zak and Gillian M Newstead. "Are the MRI characteristics of malignant breast lesions different for African American women?" in 30th Annual San Antonio Breast Cancer Symposium, December 2007.

18. Sanaz A. Jansen, Xiaobing Fan, Gregory Karczmar, Hiroyuki Abe, Robert A. Schmidt and Gillian M. Newstead. "DCEMRI of Breast Lesions: Is Kinetic Analysis Equally Effective for Both Mass and Non-mass-like Enhancement?" in 93rd Scientific Assembly and Annual Meeting of the Radiological Society of North America, November 2007.

19. Sanaz A. Jansen, Cheng Yang, Hiroyuki Abe, Akiko Shimauchi, Gregory Karczmar and Gillian M. Newstead. "DCEMRI of Malignant Breast Lesions: Should a Fixed Volume of Contrast be Injected, or a Fixed Dose" in 93rd Scientific Assembly and Annual Meeting of the Radiological Society of North America, November 2007.

20. Sanaz Arkani, Hiroyuki Abe, Akiko Shimauchi, Robert A. Schmidt, Gregory Karczmar, and Gillian M. Newstead. "Dynamic MR Imaging of Invasive Ductal Carcinoma: Studying Kinetics by Estrogen Receptor, Progesterone Receptor and Her2/Neu Amplification Status Molecular Markers" in 107th Annual Meeting of the American Roentgen Ray Society, May 2007.

21. Sanaz Arkani, Xiaobing Fan, Hiroyuki Abe, Gregory Karczmar, Robert A. Schmidt, and Gillian M. Newstead. "Improving the Diagnostic Accuracy of 3D Breast DCEMRI Data Using an Empirical Mathematical Model" in 15th Annual Meeting of the Society for Magnetic Resonance in Medicine, May 2007.

22. Sanaz Arkani, Hiroyuki Abe, Akiko Shimauchi, Gregory Karczmar, and Gillian M. Newstead. "Molecular Markers and DCEMRI of Breast Cancer: Relationship with Kinetics in Invasive Ductal Carcinoma" in

15th Annual Meeting of the Society for Magnetic Resonance in Medicine, May 2007.

23. Sanaz Arkani, Suzanne Conzen, Thomas Krausz, Marta Zamora, Gillian M. Newstead, and Gregory Karczmar. "MRI of Ductal Carcinoma in situ and Other Early Mammary Cancers in Transgenic Mice" in 15th Annual Meeting of the Society for Magnetic Resonance in Medicine, May 2007.
24. Sanaz Arkani, Vicky Chen, Caroline Cranford, Lindsay Zak, Hiroyuki Abe, Gregory Karczmar, Robert A. Schmidt, Funmi Olopade and Gillian M. Newstead. "Parenchymal enhancement on breast MRI may be a marker for cancer risk: correlation of parenchymal enhancement with breast density" in 29th Annual San Antonio Breast Cancer Symposium, December 2006.
25. Sanaz Arkani, Hiroyuki Abe, Akiko Shimauchi, Gregory Karczmar, Robert A. Schmidt and Gillian M. Newstead. "MR Imaging of Pure Ductal Carcinoma in Situ: Kinetics, Morphology, and Correlation with Mammographic Presentation and Nuclear Grade" in 92nd Scientific Assembly and Annual Meeting of the Radiological Society of North America, November 2006.
26. Sanaz Arkani, Vicky Chen, Caroline Cranford, Lindsay Zak, Hiroyuki Abe, Gregory Karczmar, Robert A. Schmidt, Funmi Olopade and Gillian M. Newstead. "Women at High Risk for Breast Cancer: Classification of Parenchymal Enhancement on Breast MR Imaging and Correlation with Mammographic Density" in 106th Annual Meeting of the American Roentgen Ray Society, May 2006.
27. Sanaz Arkani, Hiroyuki Abe, Gregory Karczmar, Robert A. Schmidt and Gillian M. Newstead. "Ductal Carcinoma in Situ (DCIS): Kinetic and Morphologic Characteristics on Dynamic Contrast Enhanced Magnetic Resonance Imaging (DCEMRI)" in 105th Annual Meeting of the American Roentgen Ray Society, May 2005.
28. Sanaz Arkani, Hiroyuki Abe, Gregory Karczmar, Robert A. Schmidt and Gillian M. Newstead. "Characteristics of Ductal Carcinoma in Situ on Dynamic Contrast Enhanced Magnetic Resonance Imaging" in 13th Annual Meeting of the Society for Magnetic Resonance in Medicine, May 2005.

OTHER ABSTRACTS

1. Devkumar Mustafi, Jonathan River, Sean Foxley, Sanaz Jansen, Gillian Newstead and Gregory Karczmar. In Vitro MRI Identification and Characterization of Small Calcium Crystals for Probing Microcalcifications in Breast Cancer, in 94th Scientific Assembly and Annual Meeting of the Radiological Society of North America, November 2008.
2. Akiko Shimauchi, Sanaz Jansen, Lindsay Zak, Hiroyuki Abe, and Gillian Newstead. Can Assessment of Kinetic Heterogeneity of Breast Mass Lesion Enhancement Seen on MR Imaging Predict Malignancy?, in 94th Scientific Assembly and Annual Meeting of the Radiological Society of North America, November 2008.
3. Neha Bhooshan, Maryellen Giger, Weijie Chen, Sanaz Jansen, Hui Li, and Gillian Newstead. Prognosis of Breast Carcinoma Using Computer-extracted Morphological and Kinetic Features in DCE-MRI, in 94th Scientific Assembly and Annual Meeting of the Radiological Society of North America, November 2008.
4. Neha Bhooshan, Maryellen Giger, Weijie Chen, Sanaz Jansen, Hui Li, Li Lan and Gillian Newstead. Classification of Breast Carcinoma Subtypes Using Cmputer-Extracted Morphological and Kinetic Features in DCE-MRI, in 50th Annual Meeting of the American Association of Physicists in Medicine, July 2008.
5. Elizabeth Hipp, Neha Bhooshan, Maryellen Giger, Sanaz Jansen, Hui Liand Gillian Newstead. Preliminary Analysis of Morphological Features From T1 and T2 MR Images in the Diagnosis of Breast Cancer, in 50th Annual Meeting of the American Association of Physicists in Medicine, July 2008.
6. Xiaobing Fan, Sanaz Arkani, Gregory S Karczmar, Hiroyuki Abe, Robert A Schmidt, Gillian M Newstead. Using three-parameter empirical mathematical model to analyze breast DCEMRI data; comparison with conventional BI-RADS classification, in 30th Annual San Antonio Breast Cancer Symposium, December 2007.
7. Kirti Kulkarni, Gillian M Newstead, Sanaz A Jansen, Hiroyuki Abe, Akiko Shimauchi, Robert A Schmidt, Nora Jaskowiak. Does MRI improve chances of obtaining negative surgical margins after localized excision? A retrospective study. in 30th Annual San Antonio Breast Cancer Symposium, December 2007.

8. Gillian M Newstead, Hiroyuki Abe, Sanaz A Jansen, Akiko Shimauchi, Charlene A Sennett,, Robert A Schmidt, Lindsay Zak, Olufunmilayo Olopade, Nora Jaskowiak. Effect of magnetic resonance imaging on the clinical management of women with newly diagnosed breast cancer, in 30th Annual San Antonio Breast Cancer Symposium, December 2007.
9. Weijie Chen, Maryellen Giger, Gillian M. Newstead, Sanaz A. Jansen, Ken Chiang, Li Lan et al. Breast Cancer Diagnosis Using DCE-MRI: Role of Computer in Interpretation of 4D Data, in 93rd Scientific Assembly and Annual Meeting of the Radiological Society of North America, November 2007.
10. Steven Thiel, Rajshri Shah, Sanaz A. Jansen, Hiroyuki Abe, Akiko Shimauchi, Gillian M. Newstead. Evaluating the Extent of Disease with MRI in the Setting of Breast Calcifications Suggestive of DCIS, in 93rd Scientific Assembly and Annual Meeting of the Radiological Society of North America, November 2007.
11. Akiko Shimauchi, Sanaz A. Jansen, Hiroyuki Abe, Kirti Kulkarni, Robert A. Schmidt, Gillian M. Newstead et al. Cancers Not Detected at MR Imaging: Review of False-Negative Lesions, in 93rd Scientific Assembly and Annual Meeting of the Radiological Society of North America, November 2007.
12. Sean Foxley Sanaz Arkani, Xiaobing Fan, Marta Zamora, Erica Markiewicz, Gregory Karczmar. Serial Imaging of Transgenic Mice Prostate Tumors Using High-Resolution EPSI, in 92nd Scientific Assembly and Annual Meeting of the Radiological Society of North America, November 2006.
13. Hui Li, Maryellen Giger, Yading Yuan, Charlene Sennett, Li Lan , Andrew Jamieson et al. Conversion of Screen Film Mammographic CADx for FFDM, in 92nd Scientific Assembly and Annual Meeting of the Radiological Society of North America, November 2006.
14. Gillian M. Newstead, Hiroyuki Abe, Sanaz Arkani, Akiko Shimauchi, Charlene Sennett, Robert A. Schmidt. Magnetic Resonance-guided Vacuum-assisted Breast Biopsy: Diagnostic Utility in a Clinical Breast MR Program, in 92nd Scientific Assembly and Annual Meeting of the Radiological Society of North America, November 2006.
15. Weijie Chen, Maryellen Giger, Gillian M. Newstead, Ulrich Bick, Li Lan, Sanaz Arkani et al. Multicategory Feature Extraction in Computer-aided Diagnosis of Breast MRI, in 92nd Scientific Assembly and Annual Meeting of the Radiological Society of North America, November 2006.
16. Akiko Shimauchi, Hiroyuki Abe, Sanaz Arkani, Charlene Sennett, Robert A. Schmidt, Gillian M. Newstead. A Practical Approach to the Differential Diagnosis of Benign Lesions Detected at Breast MR Imaging, in 92nd Scientific Assembly and Annual Meeting of the Radiological Society of North America, November 2006.
17. Gillian M. Newstead, Sanaz Arkani, Hiroyuki Abe, Robert A. Schmidt, Charlene Sennett, Cheng Yang. Dynamic Breast MR Imaging: Comparison of Kinetic and Morphologic Characteristics of Malignant Lesions by Tumor Type and Grade. in 91st Scientific Assembly and Annual Meeting of the Radiological Society of North America, November 2005.
18. Hiroyuki Abe , Gillian M. Newstead, Sanaz Arkani , Charlene Sennett, Robert A. Schmidt, Gregory Karczmar et al . Effect of Magnetic Resonance Imaging on the Clinical Management of Women with Newly Diagnosed Breast Cancer, in 90th Scientific Assembly and Annual Meeting of the Radiological Society of North America, November 2004.
19. Bradbury AR, Newstead G, Li LS, Arkani S, Abe H, Cummings S, Olopade OI. Breast MRI surveillance in women at high risk for breast cancer, in 27th Annual San Antonio Breast Cancer Symposium, December 2004.